A THEORETICAL STUDY OF LEFT VENTRICULAR AND HEART MUSCLE DYNAMICS

by

PAUL TRAHAIR HADINGHAM

Submitted
in fulfilment of the requirements
for the degree of
Doctor of Philosophy in the
University of Cape Town
May, 1973.

To

CHERRY CAROLINE

ABSTRACT

The characteristics of the left ventricle of the human heart considered as a pump have been extensively analysed. Using a new approach relying heavily on the Tensor Calculus, a theoretical model describing the mechanical and dynamical operation of the left ventricle has been developed. This has considerably greater versatility than previously proposed models. In particular the physiological shape, both under normal as well as many abnormal situations, is realistically simulated. Further, the mechanical behaviour of the ventricular wall is synthesised from anatomical data concerning the cardiac muscle fibre structure of the wall. Its mechanical and dynamical properties are then, as in the physiological situation, dependent on those of the muscle fibre. These fibre properties have also been fully investigated and a simple new model for cardiac muscle dynamics, incorporating active state, proposed. This description of the ventricular behaviour in terms of muscle properties represents the first logically structured link between cardiac muscle fibre characteristics and ventricular performance.

ACKNOWLEDGEMENTS

The author is indebted to his research supervisor, Dr. Morris Milner, for his friendly and very rewarding guidance. He is also most grateful for the fruitful discussions held with Dr. R. Forman who also gave much of his time attempting to set up the author's experimental programme.

The interdisplinary nature of the research has resulted in the author obtaining valuable help from several more people:

Prof. H.O. Buhr who initiated the project;

Prof. J. de Wet whose most entertaining lectures on Tensor Calculus the author attended and

Mr. Tom Hennessy who advised the author in matters mathematical.

The author is also indebted to Mrs. Louise Whitcher who undertook the arduous task of typing this thesis.

Finally, the financial assistance of the South African Medical Research Council is gratefully acknowledged.

ACKNOWLEDGEMENTS FOR ILLUSTRATIONS

Figs 3.1, 3.3, 3.4 and 4.17 reproduced from Braunwald et al. (1968); Little Brown and Company, Boston; with the permission of the authors and publisher.

Figs 3.5, 3.6 and 3.7 reproduced from "Structure and Function of the Cardiovascular System" by R.F. Rushmer (1972); W.B. Saunders Company, Philadelphia; with the permission of the author and publisher.

Figs 3.2, 4.13 and 4.14 reproduced from "Calcium and the Heart" edited by P.Harris and L. Opie (1971); Academic Press, London; with the permission of the authors and publisher.

Figs 4.5, 4.6, 4.7 and 4.8 reproduced from Kaufmann et al. (1972); with the permission of the authors and the publishers, Springer-Verlag.

Figs 4.4, 4.7, 4.11 reproduced from Meiss and Sonnenblick (1972); with the permission of the authors and the American Physiological Society.

Fig. 4.10 reproduced from Brutsaert et al. (1971); with permission of the authors and the Physiological Society.

Fig. 4.12 reproduced from Brutsaert et al. (1972); with the permission of the authors and the American Heart Association.

CONTENTS

LIST OF FIGURES

TABLES

CHAPTER 1

INTRODUCTION

The left ventricle of the heart is basically a pump moving blood through the circulation in a pulsatile (non-continuous) manner. Pressure and flow are produced by the almost synchronous operation of the muscle fibres, which represent the major constituent of the chamber walls. The magnitudes of pressure and flow depend not only on the load imposed on the ventricle by the circulatory system, but also on the ability of the muscle fibres to produce force and to shorten. In this thesis, the properties of the ventrile as a pump will be fully investigated.

There is now little doubt regarding the efficacy of applying physical ideas and relations in biological systems. An advanced stage of development has been reached in the reconcileation of mathematical analysis with biological structure (Hoffman, 1973).

1.1 Statement of the Problem

Based on the ventricular structure, the investigation devolves into two distinct categories:

(a) the development of a left ventricular model which realistically simulates the geometry of the chamber This geometry is determined by the balance between mural forces and chamber pressure through the associated equilibrium equation. The kernel of the problem is therefore the derivation of the equilibrium equation for the geometry chosen.

(b) A synthesis of the stress-strain or elastic character of the ventricular wall from that of the wall substructure, the cardiac muscle fibre.

1.2 Main Contributions

Important and significant new advances have been made by the author in the first category. The equilibrium relation for a general geometry expressed in polar form has been derived: no assumption of axisymmetrical geometry is necessary, a restriction which has plagued previously published models. In the particular geometrical structure chosen by the author, the shape of the normal left ventricle is accurately described as well as any bulging caused by a ventricular wall weaknesses. This, in fact, is the first realistic simulation of a ventricular bulge (or aneurysm). As will be discussed later, such a simulation has the potential for considerable practical application.

Slightly revised forms of the left ventricular modelling literature survey and the theoretical development of the model, Chapters 5 and 6 respectively of this thesis, are being included in the book "Perspectives in Biomedical Engineering" to be published in America. This was by invitation from the editors, Professor D.N. Ghista and Dr. K.M. Patil.

With regard to the second category, the author has made some progress in developing a fairly rigorous mathematical structure to describe the elastic properties of the ventricular wall (myocardium) given the characteristics of the muscle fibre. More important progress has, however,

been made in describing the passive (unstimulated) and active (stimulated) character of the cardiac muscle fibre. A new muscle model describing the stress-strain dynamics of cardiac muscle based on a recognition of both its ultastructure as well as the mechanochemical events occurring during activity has been derived. It is simple and has been tailored to specifically suit the needs of the left ventricular model in providing the building block for the myocardial stress-strain relation.

Finally, a computer programme has been developed for calculating the pressure distribution in the left ventricle for the generalised shape discussed. The way this programme can be extended to simulate a ventricular cycle under normal conditions as well as in the presence of an aneurysm, has also been investigated.

1.3 Future Investigations Made Possible by this Study

The theoretical development and basis of the model is sound enough to warrant clinical application, particularly with regard to the investigation of all mechanical and dynamical factors associated with left ventricular aneurysms. Of special interest here is the stress analysis of the affected ventricle in order to help expedite decisions on the surgical removal of the aneurysm. If no significant areas of stress concentration occur, there would be little need for surgical intervention, but there is no way of quantitating such factors at present. †

† Personal communication with Dr. R. Forman, Cardiac Clinic, Groote Schuur Hospital, South Africa.

Other important developments are possible using the cardiac muscle model as the agent for ventricular contraction in the computer simulation of the left ventricular dynamics. Using routine techniques, pressure and volume data of the ventricle are obtainable (Yang et al., 1972). From this data, together with angiographic information regarding ventricular shape, the model could be used to quantitate the muscle parameters and so yield important information on the intrinsic state of the cardiac muscle. Moreover this information could be used to ascertain muscle work and power from which an index of myocardial efficiency could be extracted. Again, this would be a powerful aid in biochemical energy conversion studies of the intact "in vivo" myocardium.

The author's faith in these possibilities rests on his belief that the ventricular model is physiologically and anatomically sound. However, the cardiac muscle simulation requires closer examination in this regard: in particular, its link with Calcium kinetics in the fibre needs further theoretical and experimental investigation.

Finally, the field of optimal control theory will find fruitful application in the development of the computational aspects of this model (Jacobson and Mayne, 1970; Davis and Ottaway, 1972). For instance, the optimization of fibre distribution subject to a minimum energy criterion would be an interesting exercise.

1.4 Outline of Thesis

In Chapter 2 the development of the project is briefly chronicled. The reader is introduced to the relevant anatomy and physiology of the circulatory system in Chapter 3.

An extensive review of the results of cardiac muscle experimentation is provided in Chapter 4. This Chapter also includes the derivation and simulation of the muscle model.

Chapters 5 and 6 are the most significant ones of this Thesis. The former gives an extensive literature review of left ventricular modelling - a review of this scope has not previously been published. In the latter, the left ventricular model is derived. Observation on the computer simulation of the model are discribed in Chapter 7 and the general conclusions of the work are contained in Chapter 8.

Features of the Appendices are the reproduction of the ventricular model computer programme and rather extensive surveys of Tensor Calculus and the mathematical development of stress and strain theory. Further, the thesis also has a glossary of some medical terms defined in a simple way.

CHAPTER 2

SYNOPSIS OF THE PROJECT DEVELOPMENT

Based on an extensive literature review, many shortcomings in the state of development of left ventricular modelling were noted. The most obvious was the severe limitations imposed by the mathematics on the geometries available for representing the left ventricle. Successive improvements from spherical to ellipsoidal to general axisymmetric were made and the analyses became correspondingly more involved. It was clear that a completly new theoretical approach was required to overcome the endpoint of conventional analyses at axisymmetric geometry.

A way of expressing physical and geometrical quantities in a simple manner was needed. Futhermore, a means operating on equations so that, after having been set up with comparative ease in a rectangular cartesian co-ordinate system, they could be transformed to a complex geometry, was vitally necessary. The Tensor Calculus fulfills both these requirements. Accordingly, the author attended a formal post graduate course on Tensor Analysis: this provided an excellent background for tackling the problem of deriving a geometrically realistic left ventricular model. Further, because of its novelty in bio-engineering, it was felt appropriate to incorporate the basics of Tensor Analysis as an appendix (Appendix A).

In the theoretical development of the left ventricular model, the author was significantly influenced by the work of P.C. Voukydis (1969, 1970a, 1970b, 1972a, 1972b, 1972c). It provided the logical sequence for the mathematical structure

of the model. The derivation of the equilibrium equations for the left ventricle is modified from that given by Green and Zerna (1968) for a general shell-like object.

An extensive literature exists on the dynamics of isolated cardiac (and skeletal) muscle: the author was amazed by the lack of success in quantitatively linking this knowledge with the dynamics of the intact heart. No doubt the main reason is that, on the surface, it represents an exceptionally complex problem. Yet when one analyses the various facets of the problem as Voukydis did, then it becomes evident that there are two basic factors involved in the analysis; the geometry of the left ventricle and the elastic character of the ventricular wall. Much progress has been made in the latter consideration (and this will be carried a little further by the author) and so the geometric factor again emerges as the inhibiting one.

By providing the mathematical framework for a general shape simulation the author has therefore made an important breakthrough in left ventricular modelling.

This mathematical model relates stress produced by the muscle fibre with ventricular pressure and volume. The nature of the stress production in the cardiac muscle fibre provided a further fascinating study. It was aimed at developing a simple theoretical model for the stress-strain properties of cardiac muscle in terms of physiologically meaningful parameters. Many contoversial issues exist in the literature of experimental "in vitro" cardiac

muscle dynamics and the author attempted to rationalise these controversies by deriving his model from concepts different to those used by the experimentalists. This venture has, to a large extent, been successful.

Although much effort was expended in attempting to set up experimental "in vitro" cardiac muscle experiments, the author felt that the feedback he would eventually gain from them would not warrant the further considerable investment of time which would have been necessary to perfect the apparatus and techniques. The experience which nevertheless was gained (using frog muscle preparations) was sufficient to convince the author of the technical excellence of much of the published material.

Thus the project has developed along a logical sequence. All facets of left ventricular mechanics and dynamics have been analysed. Further, the author has an understanding of the cardiovascular system in general from his earlier studies on modelling the circulatory system (Hadingham and Buhr, 1970).

CHAPTER 3

CARDIOVASCULAR SYSTEM PHYSIOLOGY AND ANATOMY

A very brief account of the relevant physiology and anatomy of the cardiovascular system will be presented. Its purpose is to help orient the reader who has an engineering background, or alternatively, to provide the medical reader with an engineer's interpretation of the basics of the cardiovascular system.

The system studied will be synthesized: after starting with an account of the features of cardiac muscle, the building block of the heart wall, the heart itself (particularly the left ventricle) will be analysed and then finally the role of the heart in the circulatory system will be discussed.

3.1 Cardiac Muscle

Much of this Section is based on the excellent review by Braunwald *et al.* (1968).

3.1.1 Anatomy of Cardiac Muscle Fibre

Cardiac muscle, at the cellular level, comprises branching and interdigitating cylindrical fibres 10 to 15 μm in diameter and 30 to 60 μm in length. This is shown in Fig. 3.1A, a section of a typical light microscopical view of cardiac muscle. Each cell is transversely divided by a structure called an intercalated disc and its cylindrical surface membrane is known as the sarcolemma. The heart wall or myocardium is therefore a composite fibrous soft material from an engineering viewpoint.

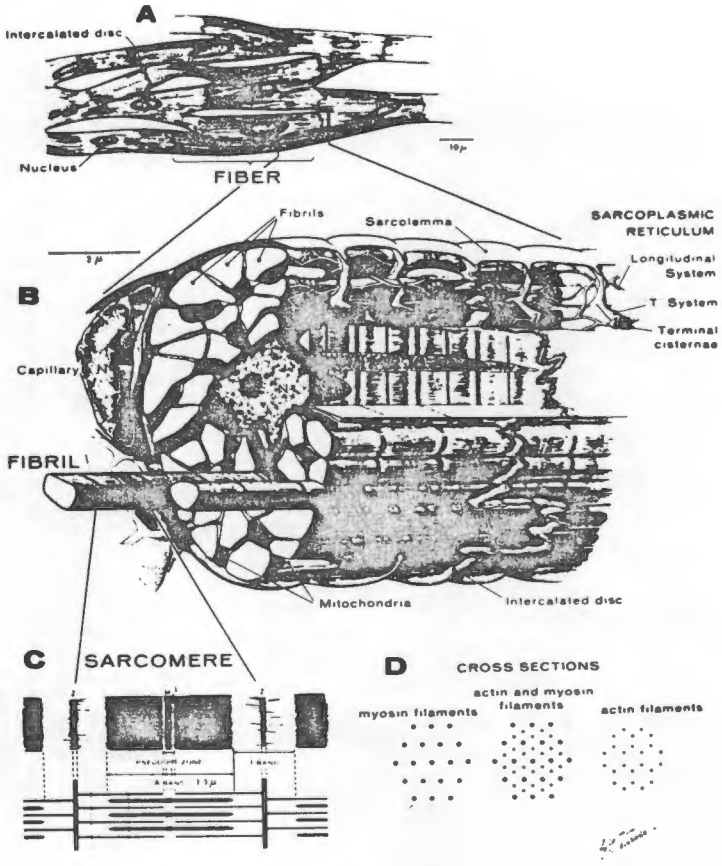

FIG. 3.1

ULTRASTRUCTURE OF CARDIAC MUSCLE

A - Cardiac muscle fibre showing the extensive cross-branching.

B - Myofibrils and the longitudinal and T - systems.

C - Sarcomere unit showing the various bands.

D - Representative cross-sections through the sarcomere

The prominent features of the fibre ultrastructure are the myofibrils which are axially oriented along the fibre as indicated in Fig. 3.1B. The myofibrils themselves possess a remarkable structure, the key to the mechanical manifestation of muscular activity. This is revealed in Fig. 3.1C which indicates each fibril has a serially repeating structure, each repeat unit being termed a sarcomere having a length of 2,2 μm. The sarcomere is defined by successive Z-lines which form the backbone for the actin filaments, each 1 μm long which project axially in each direction from the Z-line into the sarcomere. Myosin filaments, 1,5 μm long, are located centrally in the sarcomere and these overlap the thin actin filaments. The myosin filaments define the A-band as shown on Fig. 3.1C and the regions between the ends of the myosin filaments in successive sarcomeres (across the Z-lines) comprise the I-bands. Intriguing transverse order is possessed by the sarcomeres, the myosin (thick) filaments having an hexagonal arrangement. Where the actin and myosin filaments overlap, each myosin is surrounded by six actin filaments. Sections at representative positions along the sarcomere are shown in Fig. 3.1D.

When the muscle fibre changes length, the actin filaments move or slide in a direction parallel to the myosin (which remain in a fixed position in the sarcomere) and this relative motion or insertion changes the amount of overlap between the actin and myosin filaments. The mechanism of length change in muscle (both skeletal and cardiac) is therefore amazingly designed.

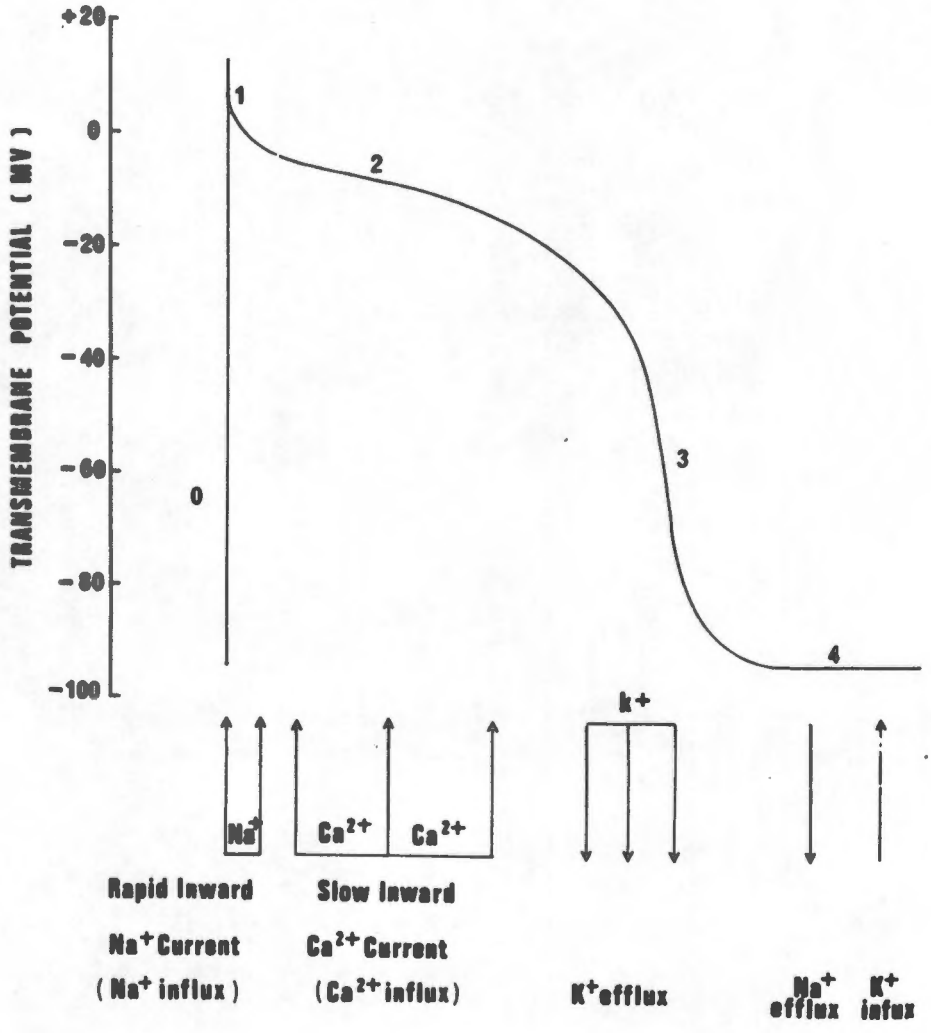

FIG. 3.2

CARDIAC MUSCLE ACTION POTENTIAL

Force generation arises from a mechanochemical interaction between actin and myosin in the overlap regions of the sarcomere induced by an electrochemical stimulus. These electro- and mechanochemical events will be further described.

3.1.2 Electrochemical Events: The Action Potential

Cardiac muscle possesses an inherent rhythmicity with regard to electrochemical events. Normally the inner surface of the muscle cell is at a resting potential of about -80 mV compared to the outer surface. This is maintained by the so called transmembrane "sodium pump" which actively pumps Na^+ out of the cell (thus using metabolic energy). The inside of the cell has a preponderance of K^+ and the extracellular (or interstitial) fluid a preponderance of Na^+. Since the concentration of intracellular K^+ is less than the concentration of extracellular Na^+ this electrical potential gradient exists.

In cardiac muscle there is a slow leakage of K^+ from the inside of the cell thus reducing the transmembrane potential until a level is reached (about -50 mV) at which an action potential is triggered (Langer, 1965). There is a sudden influx of Na^+ causing the transmembrane potential to reach zero or even go positive (inside with respect to outside). This rapid change is followed by a slower inward movement of Calcium ions (Ca^{2+}). The resting state is restored as K^+ and Na^+ are drawn back into the cell (Nayler and Merrillees, 1970). This sequence of events is shown in Fig. 3.2. The action

potential is self-propagated along the fibre at velocities of about 0,3 m/s and its typical duration at a point is 0,25 s.

There are minute transverse invaginations on the surface of the cell called the transverse tubular or T-system shown in Fig. 3.1B. These invaginations occur along the Z-lines of the myofibrils and it is on these invaginations that an internal tubular membrane system orientated axially along the surface of the fibril (called the longitudinal system) coalesce at the so-called terminal cisternae (see Fig. 3.1B). It is thought that the AP is transmitted down the T-system and its effect is then somehow transferred to the longitudinal system at the terminal cisternae at which stage the mechanochemical response of the muscle is elicited.

3.1.3 The Mechanochemical Response

Intracellular Calcium appears to be stored mainly in the internal longitudinal system of the muscle cell (Langer, 1965) and this Ca^{2+} is released when the effect of the AP is transferred across the terminal cisternae. The Ca^{2+} released is then free to cause cross-linking between actin and myosin in the overlap regions of the sarcomere and it is therefore the mechanochemical activating agent.

This actin and myosin cross-linking causes force to build up in the muscle which tends to shorten the muscle if the loading allows. The features of this force production as it relates to sarcomere length will now be analysed.

3.1.4 Active Tension and Sarcomere Length

The situation in the sarcomere for different degrees of stretch is shown in Fig. 3.3. Panel A shows electron micrographs of the sarcomere and these are sketched in panel B. As the muscle is lengthened so the I-band increases. In the shortest case, line 1, the actin filaments overlap one another in the centre of the sarcomere and this causes disruption of the cross-bridges which can only form in the actin and myosin overlap region.

As the muscle is progressively lengthened a stage is reached (intermediate between lines 2 and 3 of Fig. 3.3) at which maximum overlap between actin and myosin occurs and this overlap is decreased again at even greater lengths (lines 4 and 5).

The length of the sarcomere (measured between successive Z-lines) is about 2,2 μ (or about twice the length of the actin filament, as expected) for maximum overlap. Defining the corresponding muscle length at this stage to be L_{max} it is not surprising that the peak active tension occurs at this length. Either side of L_{max} the active tension (AT) decreases in sympathy with the decrease in muscle overlap as shown in Fig. 3.4A. The passive or resting tension (RT) of the muscle must be added to the AT to get the total tension (TT) of the muscle at any length. At L_{max} the RT contributes significantly to the TT in cardiac muscle and this fact will have important repercussions in later discussions. The same is not true of skeletal muscle as indicated in

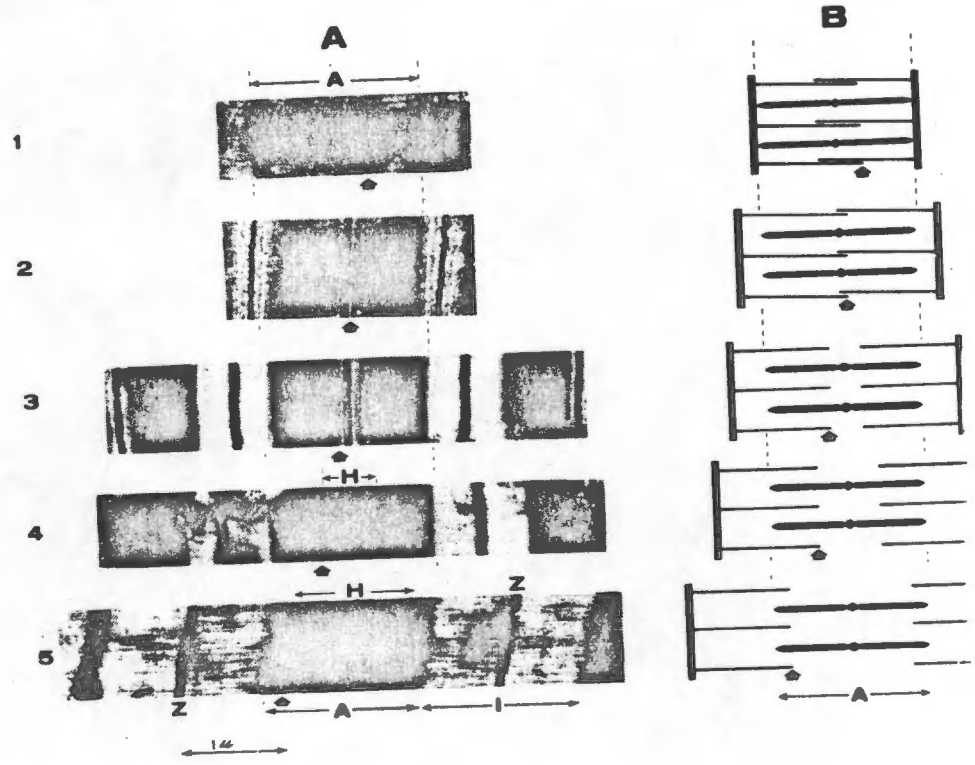

FIG. 3.3

EFFECT OF MUSCLE LENGTH CHANGE

ON SARCOMERE OVERLAP

A - Electron micrographs; B- Schematics of A

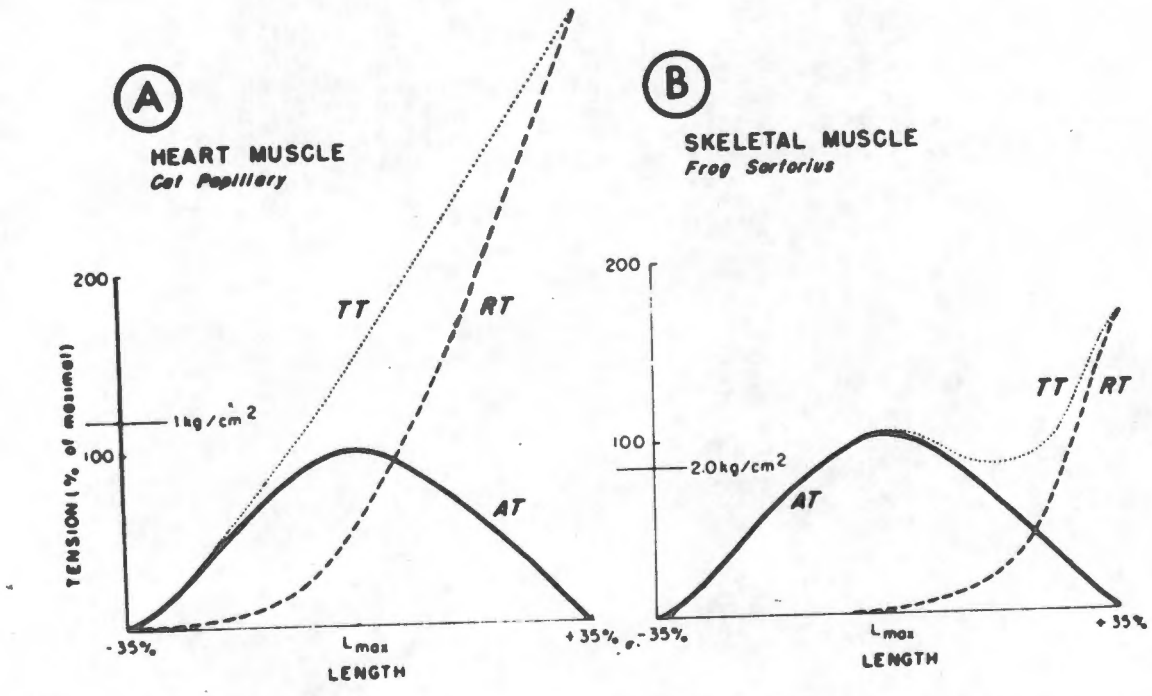

FIG. 3.4

RESTING AND ACTIVE TENSION IN CARDIAC AND SKELETAL MUSCLE

AT = Active tension; RT = Resting tension
TT = Total Tension

Fig 3.4B.

Irreversible muscle damage occurs in cardiac muscle if it is stretched beyond a sarcomere length of 2,2 μm so that the sarcomeres are seldom above this length in the physiological situation.

3.2 The Structure of the Heart

The heart is a four-chambered muscular organ responsible for providing the energy for distributing the blood within the body. It derives its energy from muscular activity (described in Section 3.1 above). A description of the way the fibres make up the ventricular wall is given in Chapter 5.

Its basic anatomy is revealed in Figs 3.5 and 3.6. The two conically shaped chambers are named the left and right ventricles: they are separated by the interventricular septum (Fig. 3.5). Capping these chambers are the left and right atria (also divided by a septum) and the junction between the ventricles and atria is formed by an inelastic fibrous structure which houses the heart valves: the mitral (M) between the left atrium and ventricle, the tricuspid (T) between the right atrium and ventricle, the aortic (A) at the exit of the left ventricle to the aorta and the pulmonary (P) at the exit of the right ventricle to the pulmonary artery. These are pictured in Fig. 3.6 and they are all one-way valves from the first- to the second- named structures in all cases. In each of the ventricles there are papillary muscles which are roughly cylindrical projections from the ventricular apex

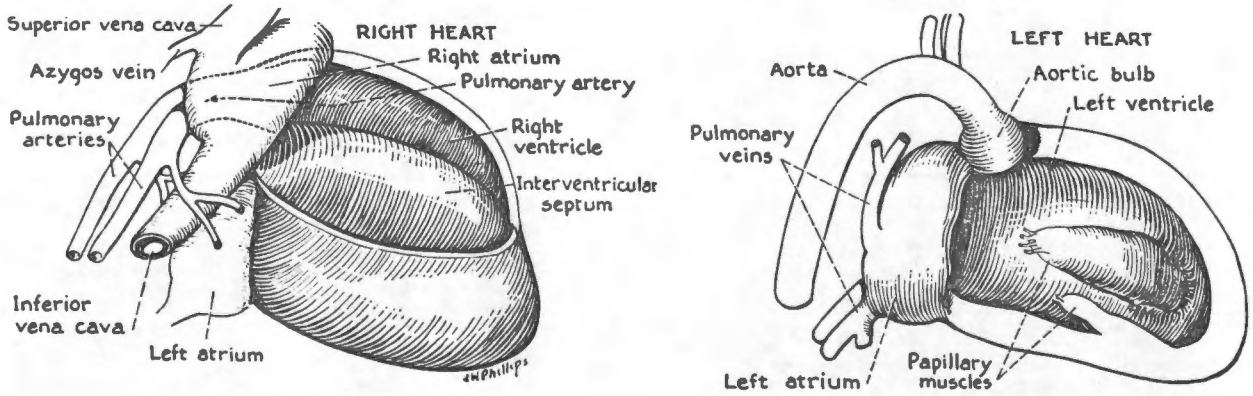

FIG. 3.5

HEART ANATOMY SHOWING PAPILLARY MUSCLES

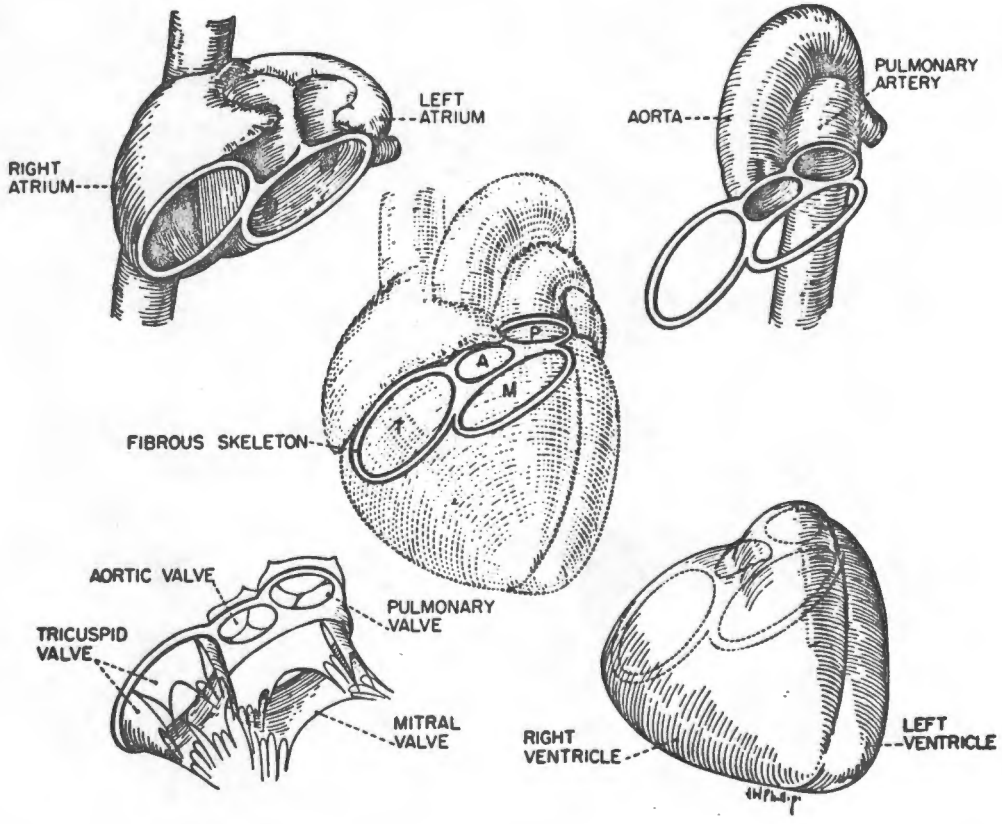

FIG. 3.6

HEART ANATOMY SHOWING THE POSITIONS
OF THE VALVES

to the atrioventricular valves. They are supporting struts for these valves (see Fig. 3.5).

Within the myocardium there are specialised pathways for the conduction of the AP throughout the heart. The AP is controlled by a pacemaker, the sino-atrial node, situated in right atrium as shown in Fig. 3.7. The atria are therefore first stimulated as the AP is delayed on its journey to the ventricles by a structure called the "bundle of His" in the basal area of the ventricular septum. After this delay, the AP is conducted down the two surfaces of the septum by the left and right bundle branches of the special conducting tissue, the Purkinje fibres (shown in Fig. 3.7). Thus the subendocardial (inside) layers of the ventricular septum are the first stimulated in the left ventricle (LV). Since the longitudinal AP propagation (along the Purkinje fibre branches) is much faster than the transverse propagation across the myocardium the excitation wave front tends to move transversely across the myocardium: the epicardial (outside) layers of the ventricle are the last activated.

Following this brief description of the heart, its role in the overall circulation can be examined.

3.3 The Circulation

It is evident from the heart anatomy that it comprises two parallel flow channels, the left and right sides of the heart. The left side supplies oxygenated blood to the body and the right sends de-oxygenated blood, which comes from the body, to the lungs to be oxygenated and

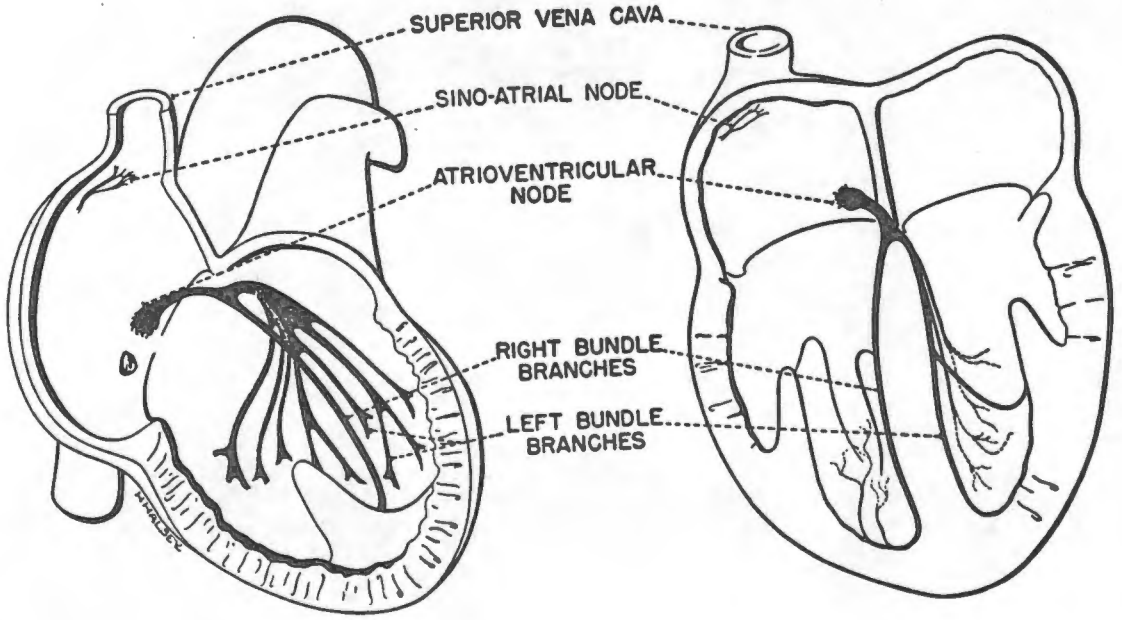

FIG. 3.7

CONDUCTION PATHWAYS IN THE HEART

subsequently fed to the left side for the cycle to be repeated.

This scheme is easily seen in the diagrammatic representation of the circulation, Fig. 3.8. The atria act as collecting chambers on each side of the heart and on stimulation ensure the ventricles are primed with blood (through the atrioventricular (AV) non-return valves). On the other hand, the ventricles are the main pumping chambers. The left ventricle supplies the whole body with oxygenated blood through the aorta and, as such, has the higher pumping load. Attention will be therefore focussed on its activity in this Thesis.

When the LV is stimulated, force builds up in the muscle fibres which increases the intraventricular pressure. The non-return action of the AV valve prevents regurgitation of blood into the left atrium and so muscle force (and ventricular pressure) rises isometrically (without any shortening) until the ventricular pressure is able to overcome the back pressure of the aorta (the only left ventricular outlet artery). At this stage the aortic valve is forced open and blood is ejected from the LV into the compliant aorta: as the aorta fills with blood so its pressure rises. When the LV contracts, the muscle fibres shorten and so the actin and myosin overlap decreases causing force production to drop. Coupled with this, the muscle activity starts decaying so enhancing the rate at which muscle force drops. Eventually the LV is no longer able to drive blood into the aorta and the aortic valve closes as soon as reverse

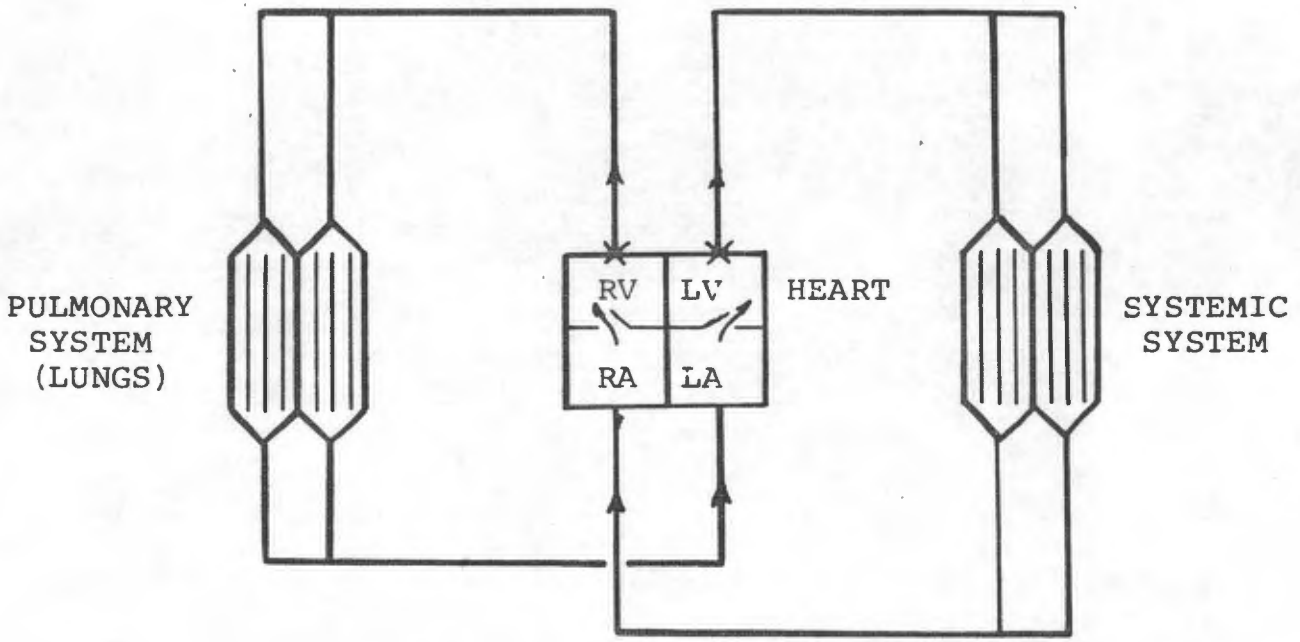

FIG. 3.8

SCHEMATIC OF THE CIRCULATION

RA,LA - Right and left atria
RV, LV - Right and left ventricles
Pulmonary circulation - Applies to lungs
Systemic circulation - Applies to the rest of the body.

flow begins.

The aorta has been pumped with blood: because of its compliance it acts as a volume reservoir which damps out the cyclic variations in LV activity and blood is more smoothly drained from the aorta and its branches to the rest of the body: so the aortic pressure slowly drops. In a separate study, the author has theoretically investigated the nature of this damping (Hadingham and Buhr, 1970).

LV pressure has meanwhile dropped rapidly allowing the AV valve to open and blood then starts filling the emptied LV again from the left atrium thus preparing the LV for the next contraction.

The sequence of events is shown in Fig. 3.9.

The filling phase of the LV is known as diastole. This is followed by systole on activation which comprises three phases: isovolumic contraction (before the aortic valve opens), systolic ejection and isovolumic relaxation (after the aortic valve closes and before the AV valve opens).

Typical parameters of the human circulation are now listed (in conventional units).

Left ventricular end diastolic volume (LVEDV) = 200 ml
Left ventricular stroke volume (SV) = 75 ml
Minimum aortic pressure (diastolic pressure) = 80 mmHg

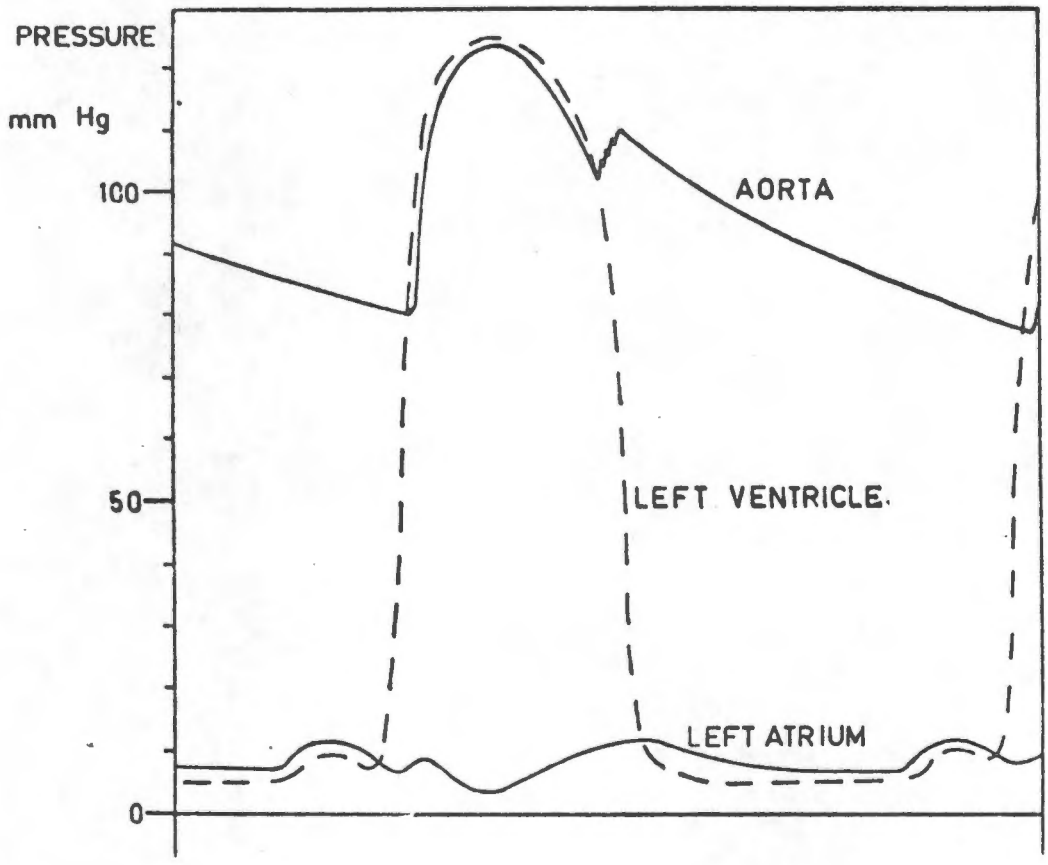

FIG. 3.9

LEFT VENTRICULAR AND AORTIC PRESSURE CYCLES

Peak aortic pressure = 120 mmHg

Heart rate = 70 beats/min

Systolic period = 0,25 s

Total volume of blood = 5.1

The considerable efforts made by many researchers in the study of cardiac muscle dynamics and also in the analysis of the mechanics of the left ventricle will now be extensively reviewed in the following three Chapters. Theoretical advances made by the author are presented in Chapter 4 (Section 4.3), for muscle dynamics, and in Chapter 6 with regard to left ventricular dynamics.

It will, it is earnestly hoped, become very clear to the reader the absolute necessity for a multi-disciplinary approach to these bio-engineering systems in order to find the "best" solutions: those which embody both scientific and medical perspective.

CHAPTER 4

CARDIAC MUSCLE DYNAMICS

What, at first glance, appears to be a rather straightforward process in purely mechanical terms, the contraction of an isolated heart muscle preparation, is on deeper investigation, a wonderfully complex process. A unified description of the processes occurring has thus far eluded both experimentalists and theorists.

In the introduction to this Thesis, reference was made to the advanced stage of development reached in the understanding of isolated "in vitro" cardiac muscle dynamics. A review is now presented of these advances (both experimental and theoretical) in the first two subsections of this Chapter. In the final subsection a new model for cardiac muscle dynamics is presented. Although this model is simple, being specifically tailored to suit the needs of a complex left ventricular model derived later in this Thesis (Chapter 6), it does incorporate significant new features such as the ability to simulate general muscle loading conditions. Previously proposed models are limited in this respect as will be seen.

4.1 Cardiac Muscle-Mechanical and Dynamical Characteristics

The elastic characteristics of cardiac muscle will be considered here. These fall into two categories, passive (unstimulated) and active (stimulated) properties and they will be considered using these categorizations in the ensuing two subsections, Sections 4.1.1 and 4.1.2.

4.1.1 The Elastic Properties of Passive Cardiac Muscle

Just as in the study of the elastic properties of laminated materials or crystals, so in the analysis of the stress-strain characteristics of passive cardiac muscle, the knowledge of the physical structure of the material considered plays a key role in the success of the analysis.

For cardiac muscle this structure has been described in Section 3.1. The myofibrils are roughly cylindrical features with the protein myofilaments (constituting about half the mass of the muscle) being directed axially in this cylinder. Connective tissue binds these myofibrils. It would appear that within the myofibril, there is little resistance to transverse stress, from a structural point of view, for the muscle in a passive state.

Studies on the passive elasticity of the sarcolemma and myoplasm of frog muscle indicate that the sarcolemma contributes negligibly to the elasticity at physiological muscle lengths (sarcomere lengths $\leq$ 2,2 μm) and that the major elastic character is due to the myoplasm (Rapoport, 1972). It is difficult to reconcile these findings with the qualitative conclusions drawn on structural grounds above.

Before the author's ideas on simulating the passive elasticity of cardiac muscle are presented, a brief review of the previously proposed formulations will be given.

4.1.1.1 Review of Passive Cardiac Muscle Characterisation

The procedures involved in obtaining the passive stress-strain characteristics of cardiac muscle are of two fundamentally different kinds. Either static experiments are performed where the muscle is allowed enough time to stabilise before stress and strain are measured, or dynamic tests are done to ascertain the "plastic" nature of the muscle.

For accurate analyses the latter method is obviously desirable. It has been used by Fung (1967; 1970) who showed the remarkable hysteresis character of passive muscle (which prompted the author to place plastic in inverted commas above). Contrary to normal inanimate material behaviour where the hysteresis effect is enhanced at higher rates of strain, the opposite is true of passive muscle. It would appear that there is a passive element involved in the muscle of the nature of a leaky capacitor (invoking an electrical analogue) whose leakage increases with increased rates of strain.

Fung presented the following relation describing passive stress-strain properties in muscle:

$$\sigma_{AA}(\varepsilon_{AA}) = (\sigma^*_{AA} + \beta) \exp\{\alpha(\varepsilon_{AA} - \varepsilon^*_{AA})\} - \beta, \quad (4.1.1.1:1)$$

$$\beta = \sigma^*_{AA} \exp(-\alpha\, \varepsilon^*_{AA})/\{1 - \exp(-\alpha\, \varepsilon^*_{AA})\} \ldots. \quad (4.1.1.1:2)$$

where σ_{AA} = the axial stress in the fibre (i.e. parallel to the sarcomeres),

ε_{AA} = the axial strain of the fibre,

σ^*_{AA} = the value of σ_{AA} when $\varepsilon_{AA} = \varepsilon^*_{AA}$

and α = the exponential constant.

The constant α, from the foregoing discussion, is clearly sensitive to both the sign of the strain (whether the muscle is being stretched or allowed to shorten) and the rate of strain (Fung, 1967).

For the majority of cases in the literature, the above-mentioned dependence of α is ignored and it is assumed to be a muscle constant independent of rate of strain (e.g. Sonnenblick, 1964). In the physiological situation, typical fibre shortening velocities are 0,5 lengths (or strain units) per second (Sonnenblick, 1962), well above the strain rates used by Fung (1967). Bearing in mind that the strain effect on α declines at increasing strain rates, it appears a very reasonable assumption to neglect this effect in the physiological situation.

A further assumption generally made is that the muscle is homogeneous and isotropic; i.e. the elastic properties are space and orientation independent muscle constants (see Appendix B, Section 5.3). Ultrastructural considerations given in Section 4.1.1 above reveal that this is probably untenable. Nevertheless Demiray (1972), using a homogeneous and isotropic model based on an assumed strain energy (or elastic potential) function for soft biological tissues (see Appendix B, Section 5.2), derived a formulation for the passive stress-strain relation yielding a remarkably close fit to experimental data.

To help facilitate the subsequent development of a model for active cardiac muscle (Section 4.3), in this analysis more store will be laid on structural considerations so

that the passive elastic properties of cardiac muscle will be assumed to be best describable when the muscle is viewed as a transversely isotropic material: i.e. the elastic properties in the axial fibre direction are different from those in the plane orthogonal to this direction.

4.1.1.2 Model for the Passive Elasticity of Cardiac Muscle.

As mentioned above, the muscle will be viewed as a transversely isotropic material. The structural uniqueness in the axial direction as shown above (Sections 3.1.1 and 4.1.1) dictates this choice.

A brief description of the theory of transversely isotropic materials is given in Section 5.4 of Appendix B. Reference to this Appendix is implied in much of this Section.

In a transversely isotropic material the stress-strain relation is given by equ. (B5.4:4):

$$\sigma_{\ell mn} = C \quad \varepsilon_{\ell mn} \quad \ldots\ldots\ldots\ldots\ldots\ldots \quad (4.1.1.2:1)$$

where, from equ. (B.4:2),

$$[C] = \begin{bmatrix} C^{11}_{11} & C^{11}_{22} & C^{11}_{22} & 0 & 0 & 0 \\ C^{11}_{22} & C^{22}_{22} & C^{22}_{33} & 0 & 0 & 0 \\ C^{11}_{22} & C^{22}_{33} & C^{22}_{22} & 0 & 0 & 0 \\ 0 & 0 & 0 & C^{11}_{33} & 0 & 0 \\ 0 & 0 & 0 & 0 & C^{11}_{33} & 0 \\ 0 & 0 & 0 & 0 & 0 & \tfrac{1}{2}(C^{22}_{22}-C^{11}_{22}) \end{bmatrix} \quad \ldots (4.1.1.2:2)$$

the C's being the five elastic constants of the material. The σ's and ε's are the components of the stresses and strains, ℓ, m and n each ranging over 1 to 3, the 1-axis being the anisotropic axis.

The matrix of elastic constants $[C]$ in this stress-strain relation can be written in terms of the well known "technical" or "engineering" constants (Janz and Grimm, 1972):

$$\left.\begin{aligned} C^{11}_{11} &= E' (1-\nu)/D \\ C^{11}_{22} &= \nu' E/D \\ C^{22}_{22} &= E (1-\nu'^2 E/E')/D(1+\nu) \\ C^{22}_{33} &= E (\nu+\nu'^2 E/E)/D(1+\nu) \\ C^{11}_{33} &= G', \\ \text{where} \quad D &= 1-\nu-2\nu'^2 E/E'. \end{aligned}\right\} \ldots (4.1.1.2:3)$$

The technical constants in the above equations are defined as:

E, E′ = Young's moduli in the isotropic plane and along anisotropic axis respectively,

G′ = shear modulus along the anisotropic axis

and ν, ν' = Poisson's ratios representing respectively

transverse reduction in the isotropic plane for strain as a result of tension in the same plane, and transverse reduction in the isotropic plane for strain along the anisotropic axis as a result of tension along that axis.

Using the relation proposed by Janz and Grimm (1972):

$$G' = \bar{E}/\{2(1+\nu')\}, \quad \ldots\ldots\ldots\ldots \quad (4.1.1.2:4)$$

where $$\bar{E} = (E+E')/2. \quad \ldots\ldots\ldots\ldots\ldots \quad (4.1.1.2:5)$$

In terms of technical constants, the stress-strain relation is usually expressed in the form (Lekhnitskii, 1963, p.25):

$$\begin{bmatrix} \varepsilon_{11} \\ \varepsilon_{22} \\ \varepsilon_{33} \\ \varepsilon_{12} \\ \varepsilon_{13} \\ \varepsilon_{23} \end{bmatrix} = \begin{bmatrix} 1/E' & -\nu/E & -\nu/E & 0 & 0 & 0 \\ -\nu'/E' & 1/E & -\nu/E & 0 & 0 & 0 \\ -\nu'/E' & -\nu/E & 1/E & 0 & 0 & 0 \\ 0 & 0 & 0 & 1/G' & 0 & 0 \\ 0 & 0 & 0 & 0 & 1/G' & 0 \\ 0 & 0 & 0 & 0 & 0 & 1/G \end{bmatrix} \cdot \begin{bmatrix} \sigma_{11} \\ \sigma_{22} \\ \sigma_{33} \\ \sigma_{12} \\ \sigma_{13} \\ \sigma_{23} \end{bmatrix}.$$

$$\ldots\ldots\ldots\ldots\ldots \quad (4.1.1.2:6)$$

The set of equations (4.1.1.2:3) arise from the inversion of the above equation.

No attempt is made here to analyse the intricacies of such an inversion which are caused by the peculiarities of the stress-strain relation particularly for the case

$\nu = \nu' = 0,5$. Such an attempt could considerably complicate the model, as revealed by Mirsky (1970) in his paper. This complication was also overlooked by Janz and Grimm (1972) who also postulated transverse isotropy for the myocardium, but on conceptually different grounds to those used herein.

In view of the assumption of transverse isotropy, the axial stress-strain relation is given by modifying equ. (4.1.1.2:1) in the light of equ. (4.1.1.1:1), the latter equation describing the stress as a result of axial strain: in this modification the term, $C^{11}_{11}\ \varepsilon^{11}_{11}$, in the expansion of equ. (4.1.1.2:1) is replaced. Accordingly, where the subscripts (1,2,3) are replaced by (A,B,3), A being the anisotropic axial co-ordinate, and the B-3 plane being the isotropic plane:

$$\sigma_{AA} = f\ (\varepsilon_{AA}) + C^{11}_{22}\ (\varepsilon_{BB} + \varepsilon_{33}), \quad \ldots\ldots \quad (4.1.1.2:7)$$

where $f\ (\varepsilon_{AA})$ is given by equ. (4.1.1.1:1).

For the physiological range of strains analysed, it is reasonable to replace the exponential function in equ. (4.1.1.1:1) by a second order polynomial so that equ. (4.1.1.2:7) becomes:

$$\sigma_{AA} = E_1(\varepsilon_{AA} - \varepsilon^*_{AA}) + E_2(\varepsilon_{AA} - \varepsilon^*_{AA})^2 +$$

$$C^{11}_{22}\ \{(\varepsilon_{BB} - \varepsilon^*_{BB}) + (\varepsilon_{33} - \varepsilon^*_{33})\} \ldots\ldots\ldots \quad (4.1.1.2:8)$$

where $\sigma_{AA} = 0$ for $\varepsilon_{AA} = \varepsilon^*_{AA}$ (at which stage $\varepsilon_{BB} = \varepsilon^*_{BB}$ and $\varepsilon_{33} = \varepsilon^*_{33}$) the strains being referred to the muscle length normalised with respect to a sarcomere length of 2,2 µm. E_1 and E_2 are the stress-strain polynomial constants.

Muscle is virtually incompressible so that $\nu = \nu' = 0,5$ (Baskin and Paolini, 1966) with the consequence, $\varepsilon_{BB} = \varepsilon_{33} = \varepsilon_{AA}/2$. Further, from the experimental stress-strain relation of passive cardiac muscle shown in Fig. 3.4A (based on the data of Spiro and Sonnenblick (1964)), it can be seen that:

$$d\sigma_{AA}/d\varepsilon_{AA} = 0 \text{ at } \varepsilon_{AA} = \varepsilon^*_{AA} = -0,35$$

and $\sigma_{AA} = 0,5$ kg/cm^2 when $\varepsilon_{AA} = 0$ i.e. at L_{max}.

It follows therefore that equ. (4.1.1.2:8) can be reduced to the form:

$$\sigma_{AA} = E_2 (\varepsilon_{AA} - \varepsilon^*_{AA})^2, \quad \ldots\ldots\ldots \quad (4.1.1.2:9)$$

where $$E_2 = \sigma_{AA} \text{ (at } L_{max})/\varepsilon^{*2}_{AA} \ldots\ldots\ldots \quad (4.1.1.2:10)$$

$$= 4,17 \text{ Kg/cm}^2 \text{ from the above data.}$$

Thus $C^{11}_{22} = 0$ or is close to it. This is interesting from the point of view of passive muscle stability: it has been shown that stretched passive muscle always returns to its normal length on release and so the transverse elasticity providing the restoring force cannot be totally neglected; but it is of second order importance compared to the axial case. The difficulty Forman et al. (1972) had in explaining the above phenomenon is readily reconciled by noting this transverse elastic component: there is no need to invoke the analogy of a spring in compression as Forman et al. did.

The fitted data is given in Fig. 4.1. This fit is quite adequate for use in the general muscle model to be developed in Section 3.3. Before this model can be described, a critical review of the properties of active (stimulated)

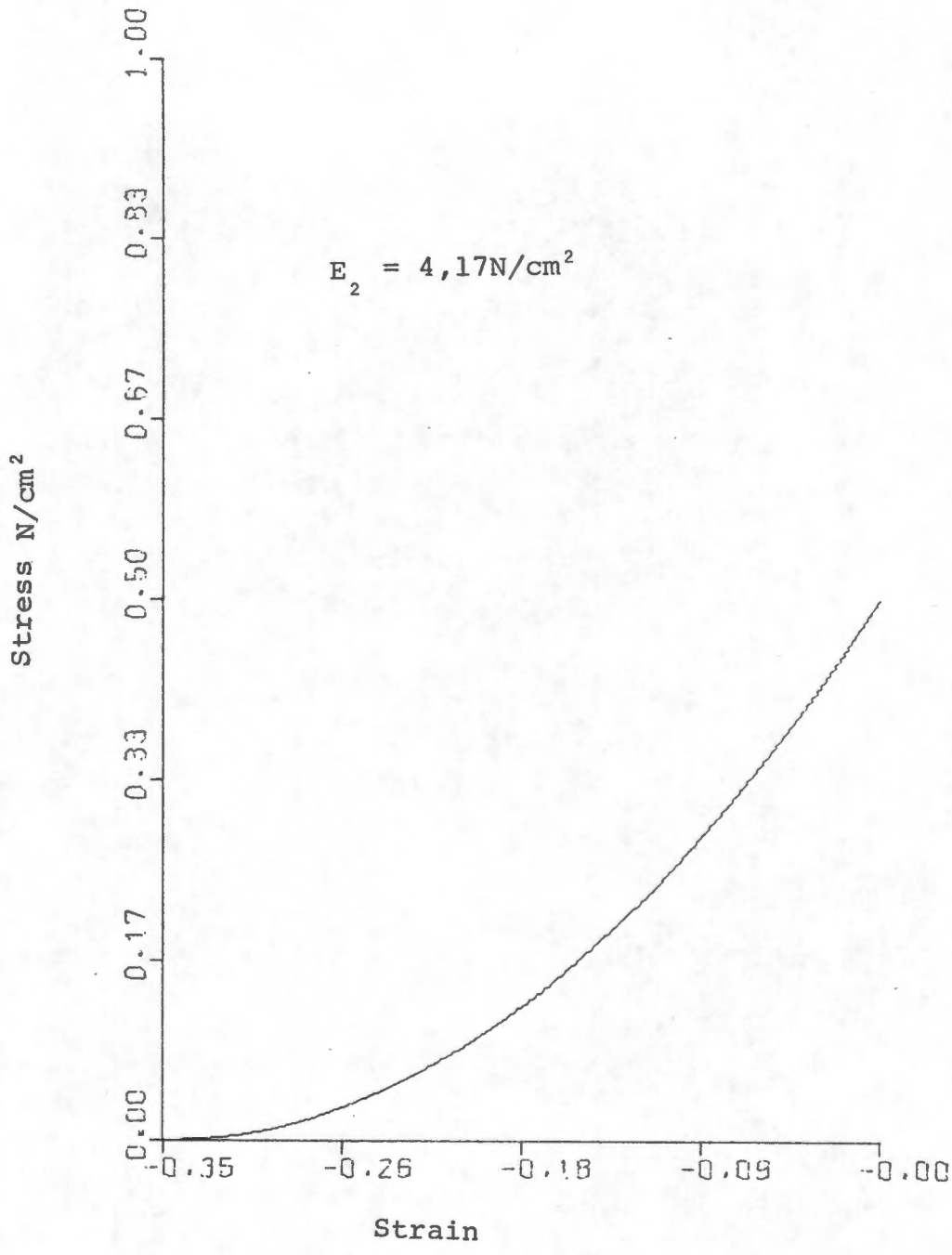

FIG. 4.1

PREDICTED PASSIVE PROPERTIES
OF CARDIAC MUSCLE

cardiac muscle will be presented.

4.1.2 Characteristics of Activated Cardiac Muscle

As explained in Section 3.1, once muscle is triggered the irreversible processes of electro- and mechanochemical activity occur in accordance with the "all or nothing" principle. The resultant mechanical response of the muscle depends on the load and the type of constraints imposed on the muscle. With a view towards expressing these loads and constraints in engineering parlance, the muscle is considered as a "black box" shown in Fig. 4.2.

There are two classes of input to the "black box"; firstly electrical stimulus (with its associated parameters such as frequency, waveform, voltage and so on) and secondly, the mechanical input constraints (independent or controlled variables). The output comprises the dependent or uncontrolled mechanical variables.

Muscle stress σ (force per unit cross-sectional area and strain ε (change in length per unit original length) are the mechanical variables considered and time modulation of the relationship between these variables is triggered by the stimulus. If strain (calculated with respect to a defined initial length here taken to be the length 2,2μm, at which maximum actin-myosin filament overlap occurs, from Section 3.1.1) is the controlled variable then:

$$\sigma = \sigma\ (\varepsilon, \tau)$$

and analogously, if stress is controlled:

$$\varepsilon = \varepsilon\ (\gamma, \tau).$$

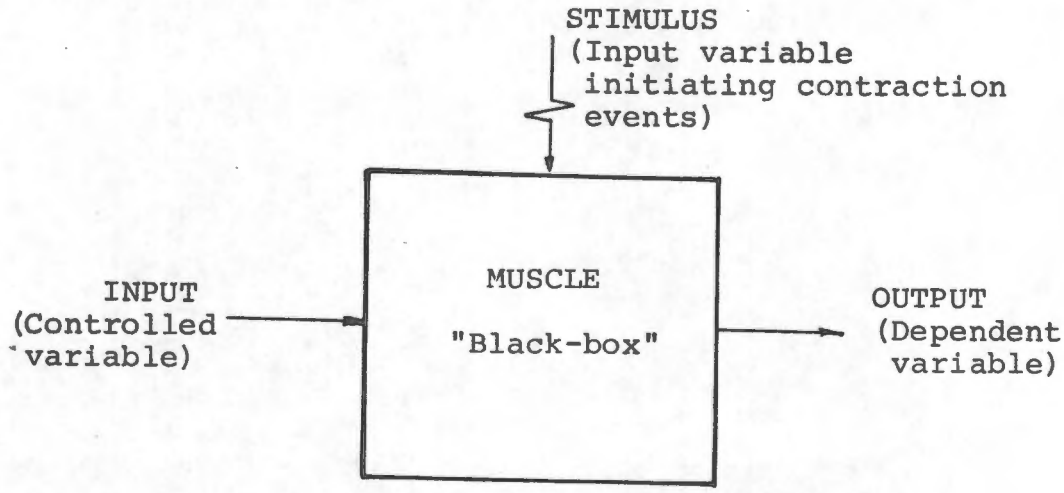

FIG. 4.2

ISOLATED MUSCLE AS A "BLACK BOX"

In order to help in the understanding of the way constraints are imposed in the range of cardiac muscle experimentation to be analysed, the principles influencing the basic design of the apparatus used in most of this experimental work will be briefly described.

4.1.2.1 Basics of Experimental Apparatus

Apparatus for studying the mechanical dynamics of isolated cardiac muscle must be designed with a view towards measuring and/or controlling force (from which σ can be obtained) and strain. Nearly all of the apparatus used for these measurements can be reduced to the simple form depicted in Fig. 4.3.

The muscle is attached between a fixed force transducer and the tip of a pivotted light (to minimize inertia) lever. A stretching load is imposed on the muscle by a torque applied about the fulcrum of the lever. This torque is produced electromagnetically by a galvanometer or by counterbalance weights (shown in Fig. 4.3). An upper level stop allows the distance H between the force transducer and the lever (and hence the initial muscle strain, assuming the connections to the muscle are inelastic) to be controlled if so desired. The load against which the muscle works is controlled by setting the torque on the lever.

Force and muscle strain are obtained as functions of time, the former with a fixed force transducer (strain gauge) and the latter by registering lever position for example with a photoelectric position transducer.

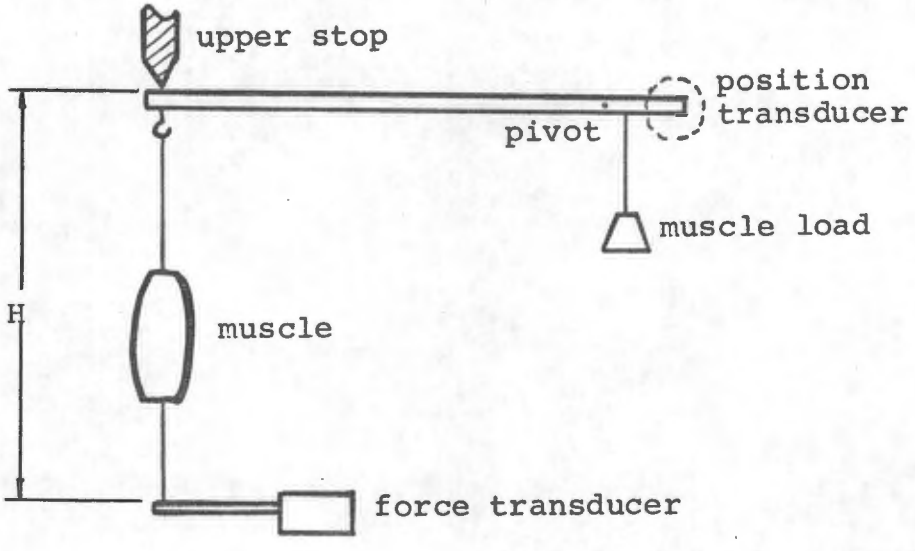

FIG. 4.3

BASIC ISOLATED MUSCLE APPARATUS

With the principles of this simple apparatus in mind, the conditions under which the following experiments were performed can be easily understood.

4.1.2.2 Range of Experiments Performed on Isolated Cardiac Muscle

The range of experiments performed on isolated cardiac muscle has been divided into distinct classes according to the type of constraint imposed upon the muscle. Each of these classes is treated separately and the main features of the responses of the different classes are carefully elucidated. These general responses are based on the wealth of published experimental results on isolated cardiac muscle.

4.1.2.2.1 Isometric Contractions

By applying a suitably large torque to the lever (see Fig. 4.3), the stimulated muscle will be unable to move the lever and so the muscle strain (hence length) will remain constant during the period of force production. This type of muscle response is referred to as an isometric contraction.

The features of an isometric contraction are shown in Fig. 4.4 (Sonnenblick, 1962) and are listed below.

a) The peak active force increases with increasing muscle strain in accordance with the effect of the passive stress-strain curve (Sections 3.1 and 4.1.1) and more importantly with the influence of increasing the actin-myosin overlap on active stress production

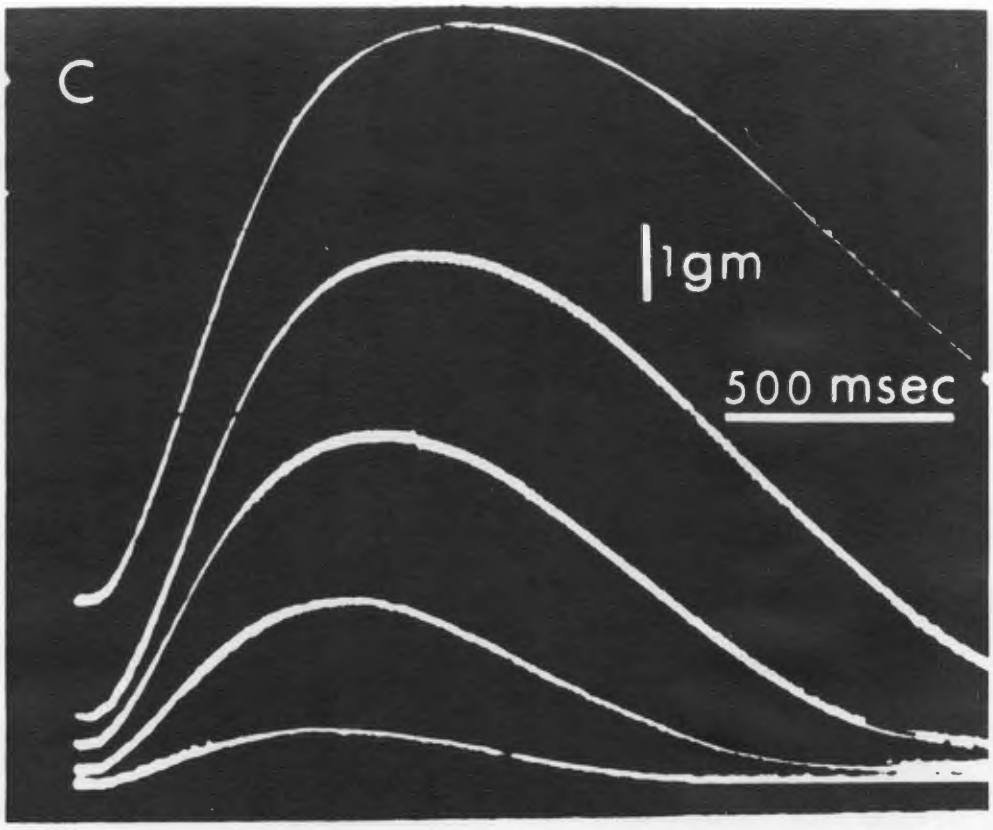

FIG. 4.4

EFFECT OF MUSCLE LENGTH ON ISOMETRIC CONTRACTIONS

(Section 3.1.4).

b) Phase characteristics of the muscle are sensitive to isometric muscle strain. Specifically, the period of the contraction and also the time to reach peak force are decreased with increasing strain (Blinks, 1970; Meiss and Sonnenblick, 1972).

4.1.2.2.2 Isotonic Contractions

An isotonic contraction is produced when the load experienced by the muscle is constant but less than the peak isometric force generated by the muscle for the given conditions so that the muscle is able to shorten. Isotonic contractions can be experimentally obtained in two ways:

a) by imposing an initial constant load (termed the preload) on the muscle, the resultant initial strain being controlled by the passive stress-strain relation of the muscle. Isotonic responses for this condition, (called preloaded isotonic contractions), in which the muscle initially shortens once the force produced overcomes the constant load and subsequently returns to its original state of strain as activity decays, is shown in Fig. 4.5D.

b) By setting the initial muscle strain (length) using the fixed upper stop (see Fig. 4.3) and imposing a constant load called the afterload on the muscle large enough to hold the muscle against the upper stop but, of course, less than the peak isometric force for this initial strain. On stimulation the muscle contracts isometrically until the force it

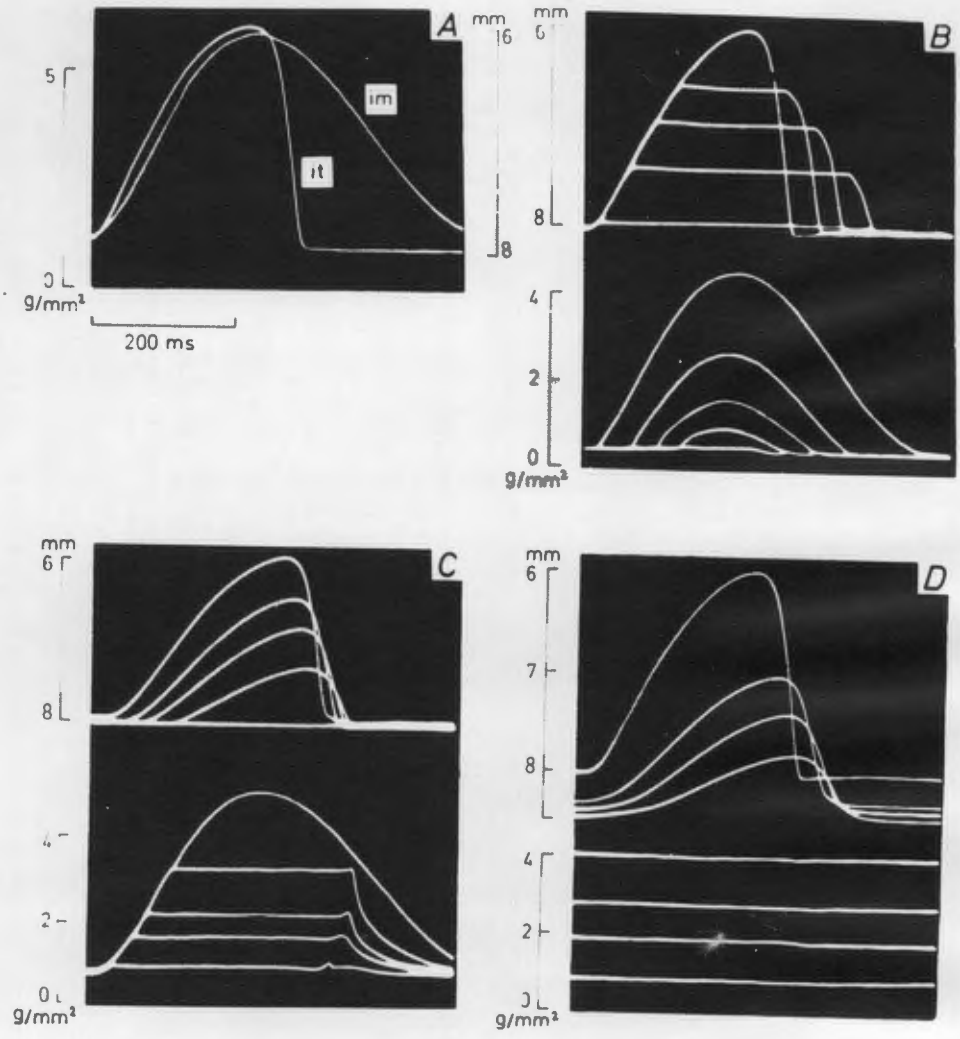

FIG. 4.5

ISOTONIC AND ISOMETRIC CONTRACTIONS

A - Isometric (im) and isotonic (it) contractions
B - Isotonic converted to isometric contractions
C - Afterloaded isotonic contractions
D - Preloaded isotonic contractions

produces matches the imposed total load. The muscle then shortens in such a way that the equality between the force generated and the load is maintained and subsequently stretches back to its original state of strain as the muscle activity decays. Muscle force then decays under isometric conditions. A set of isotonic stress and strain curves for different afterloads (but with the same preload) is shown in Fig. 4.5C.

Reference to Figs 4.5C and 4.5D reveals the following important characteristics of isotonically contracting muscle.

(i) A heavily (after-) loaded isotonic contration maintains its isotonic force level longer than would be expected from the isometric curve as shown in Fig. 4.6. The reverse is evident for lightly loaded contractions (Kaufmann et al., 1972) as shown in Fig. 4.5C.

(ii) The time after stimulation at which maximum shortening occurs increases and then decreases with increasing afterload. The peak appears to coincide with the cross-over point of the effect referred to in (i) above.

(iii) As expected, in preloaded isotonic contractions shown in Fig. 4.5D, the duration and extent of shortening are both decreased as preload is increased.

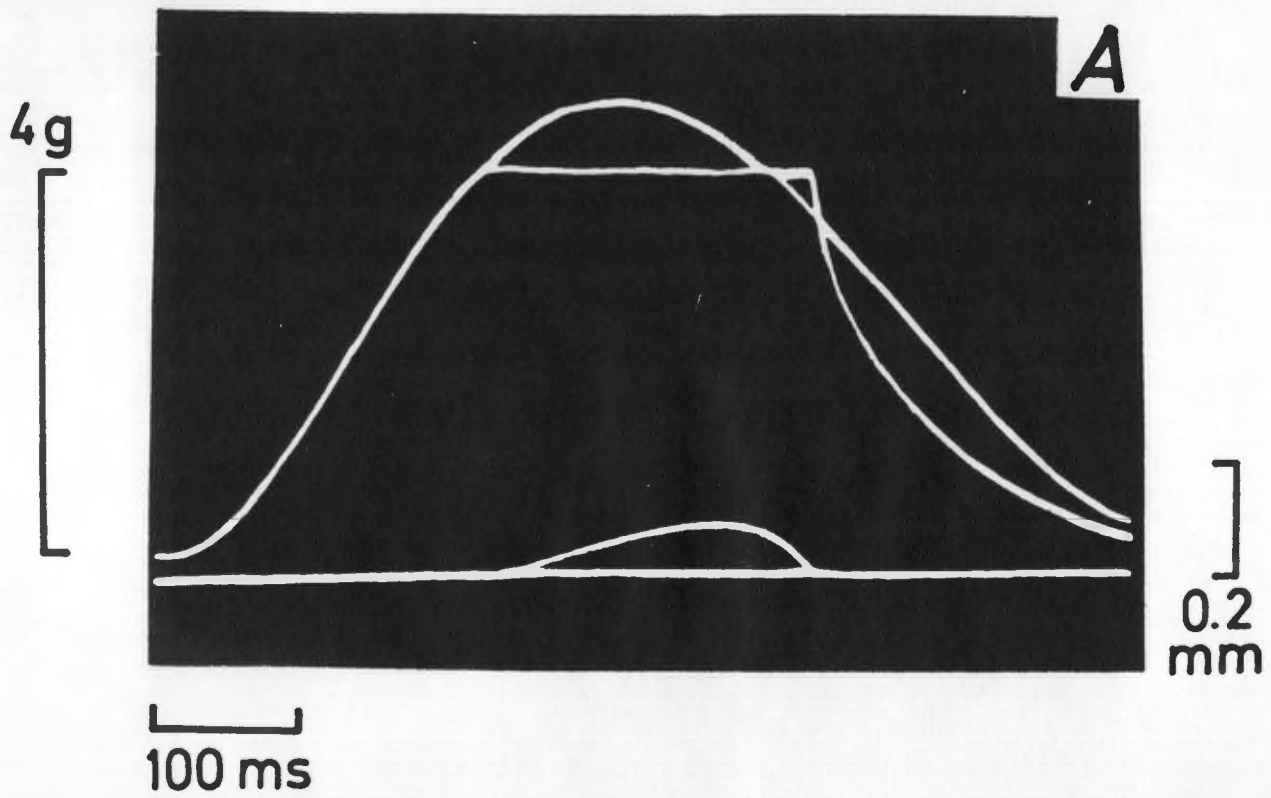

FIG. 4.6

HEAVILY AFTERLOADED ISOTONIC CONTRACTION

4.1.2.2.3 Quick Release and Quick Stretch Experiments

In contrast to isotonic and isometric contractions where no change is imposed on the muscle after stimulation, quick release (QR) and quick stretch (QS) experiments involve rapid changes in muscle length during the course of activation.

There are two types of QR experiments.

a) A step change in length is imposed on the muscle during an isometric contraction so that it is driven to its new shorter length (Brady, 1965; Meiss and Sonnenblick, 1972; Kaufmann et al., 1972).

b) The contraction is instantaneously converted from isometric to isotonic during activation by subjecting the muscle to a step reduction in load from the isometric value current at the time of step change (Parmley, 1967; Edman and Nilsson, 1968; Noble, et al., 1969; Henderson, et al., 1971; Kaufmann, et al., 1972; Meiss and Sonnenblick, 1972). Thus the muscle drives itself to the new length concomitant with the load change.

The fundamental difference between a) and b) is worthy of note: in method a) the muscle is driven whereas it drives itself in b).

In QS experiments a dichotomy of method in stretching is not possible for the muscle cannot actively stretch itself as would be required for case b) above. The only technique available is the same as in a) above except that the muscle

is stretched by the step change (Brady, 1965; Kaufmann, et al., 1972).

One can therefore classify these three types of experiments as follows:

a) QR or QS caused by length step changes, and

b) QR caused by a step decrease in force.

Features of these experiments will be discussed according to these classifications.

a) (i) When the QR is imposed at a given time after stimulation, the peak force reached decreases with decreasing length in accordance with the change in actin and myosin overlap but peak force is reached at the same time for all the length changes (Fig. 4.7A).

(ii) When QS's are imposed under the conditions in a)(i) above, the force peak increases with increasing stretch. However, in contrast to QR, the force peak is later for small increases in length, but decreases again to the time peak of the unstretched response as the length steps are increased. Further, for stretches applied even fairly early in the contraction, the force produced at the stretched length (for small stretches) becomes less than the corresponding isometric force produced at the new length without the QS intervention i.e. the normal isometric curve at the stretched length. This is illustrated in Fig. 4.8B. This phenomenon

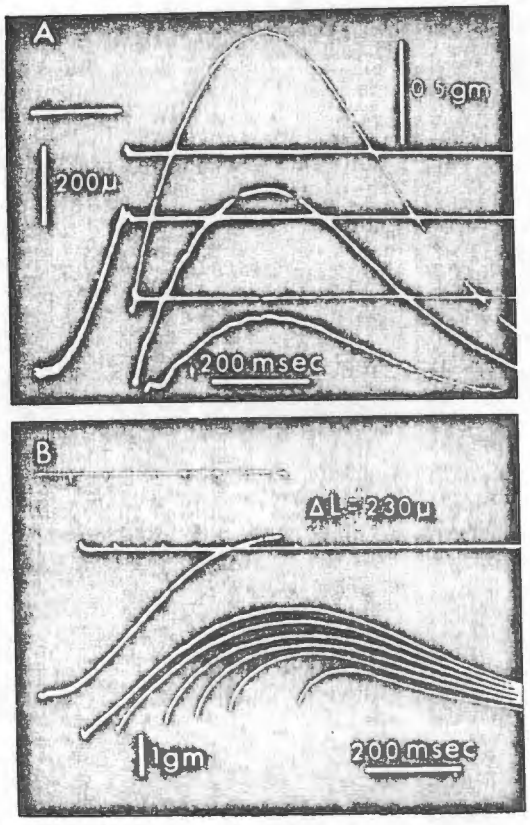

FIG. 4.7

QUICK RELEASE EXPERIMENTS

A - Quick releases of different magnitudes at the same time in the contraction

B - Quick releases of constant magnitude at different times in the contraction

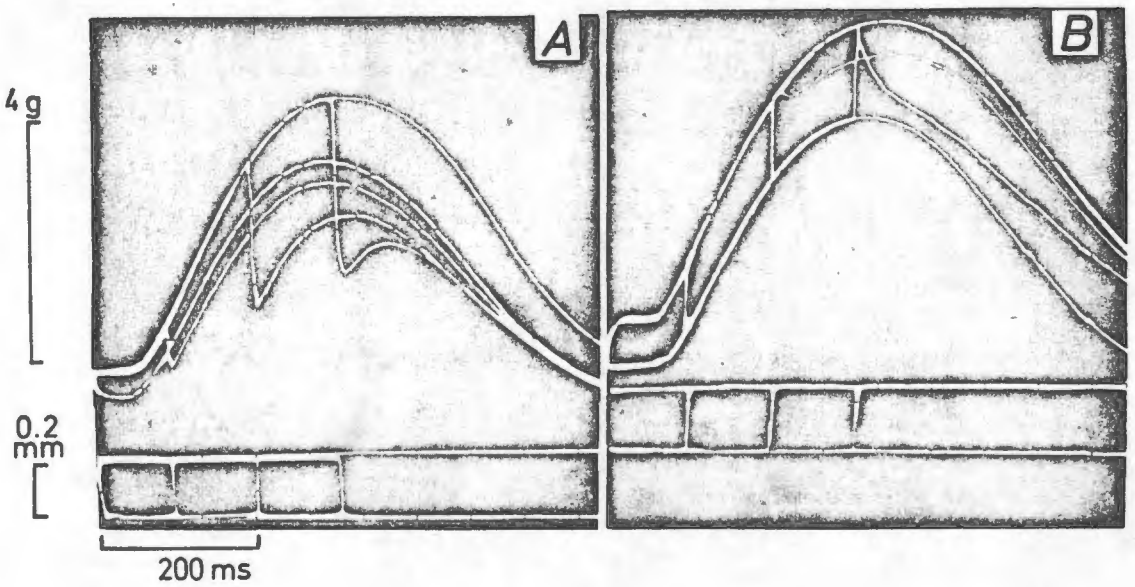

FIG. 4.8

QUICK RELEASES AND QUICK STRETCHES
AT VARIOUS TIMES DURING CONTRACTION

A - Quick releases; B - Quick stretches

is a result of the "uncoupling effect" (Brady, 1965).

b) (i) If a constant QR is applied but the time of its application after the stimulus is progressively increased, the force peak decreases and the time at which peak force is reached increases as shown in Fig. 4.7B.

(ii) Under the conditions in b)(i) but considering the case of the QS, as described in a)(i) above, the force generated in response to the QS is less than would be expected from the corresponding isometric curve obtained at the stretched length. In addition, this force decrement effect is enhanced the later after the stimulus the QS is applied. A further point to note is that this uncoupling effect for small QS's very late in the contraction elicits force responses less than those given by an isometric contraction at the unstretched length. The uncoupling effect is therefore greater than the difference between the isometric forces at the stretched and unstretched muscle for QS's late in the contraction.

4.1.2.2.4 Quick Release - Quick Stretch Experiments

In order to investigate whether the quick release experimental muscle loading is reversible in the sense that any uncoupling (Brady, 1965) caused during quick release in an isometric contraction is reversed during a subsequent very slightly delayed quick stretch, the release and stretch being of equal magnitude, Kaufmann

et al. (1972) performed just these experiments under a variety of conditions. The important findings are summarised as follows:

a) A quick length change intervention during an isometric contraction is irreversible. The force decrement (defined as the ration of the post-intervention force to the isometric force for the time at which the intervention took place) is always less than unity (except in the case when the intervention is applied very soon (within about 20% of the contraction period) after stimulation. This is illustrated in Fig. 4.9A. There exists in fact a reasonably linear relationship between force decrement and displacement for a given time after stimulation as well as between force decrement and time after stimulation for given displacements. (see Fig. 4.9C).

b) The effects in a) above are sensitive to external Calcium concentration, a higher concentration reducing the magnitude of the force decrements.

c) At a given time after stimulation, the force decrement is independent of preload (or correspondingly, initial muscle length).

d) Considering a quick release only, for a given displacement the force decrement increases as the velocity of release decreases from an upper limit (the releases terminating at the same time after stimulation). It must be noted that the lower velocity (0,5 strain units per second) used by Kaufmann et al. (1972, Fig. 4), falls well within

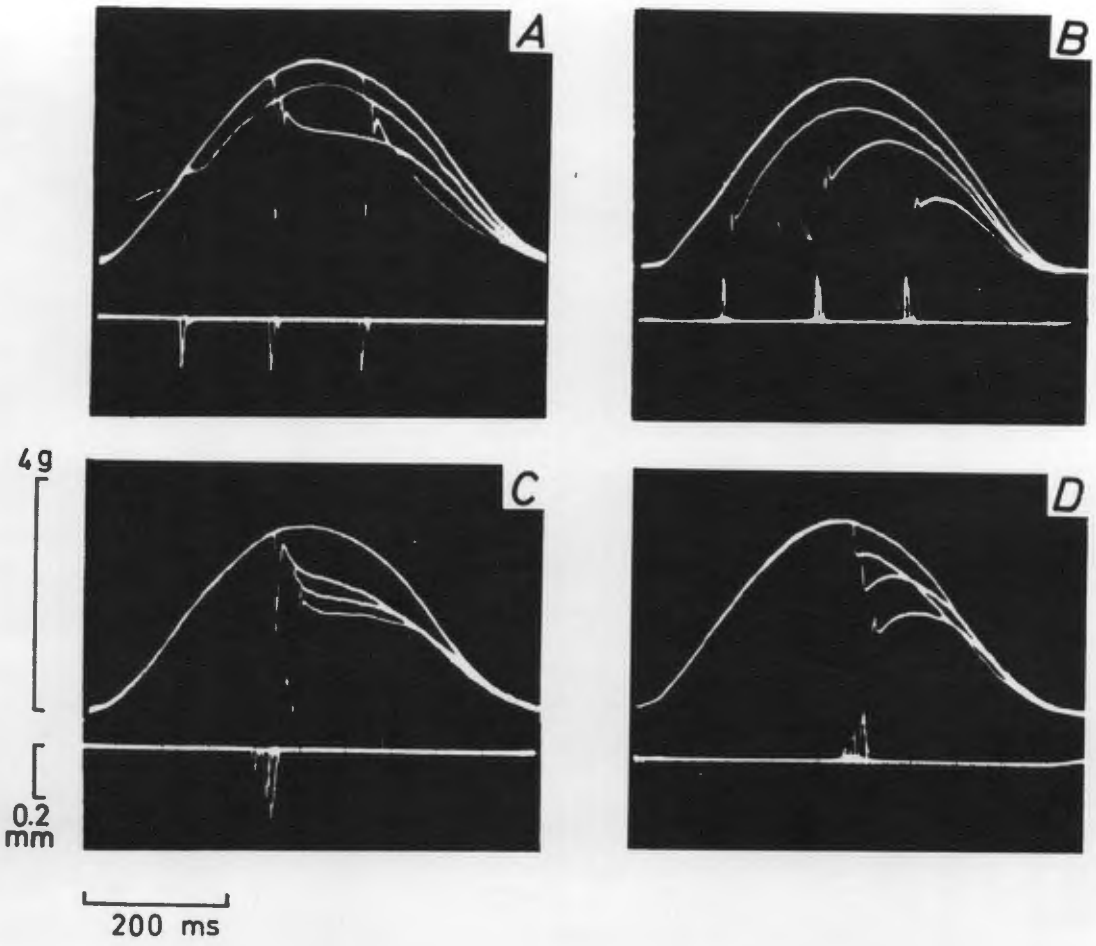

FIG. 4.9

QUICK RELEASE-QUICK STRETCH EXPERIMENTS

A - Quick release-quick stretch (QRQS) experiments
B - Quick stretch-quick release (QSQR) experiments
C - Effects of QRQS's of different magnitudes at the same time in the contraction
D - Effects of QSQR's of different magnitudes at the same time in the contraction

the range of physiologically occuring velocities in the intact left ventricle (Hugenholtz et al., 1970, Fig.2) so that this force decrement is of some import under "in vivo" conditions.

e) Increasing the delay interval between QR and QS from approximately 1% to 10% of isometric twitch duration had a negligible effect in the force decrement of the QRQS cycle.

4.1.2.2.5 Afterload Step Changes During Isotonic Contractions

An experimental technique has been developed by Brutsaert et al. (1971) in which abrupt afterload changes can be imposed on an isotonically contracting isolated cardiac muscle.

The sequence of events in this class of experiments is revealed in Fig. 4.10. In panel I, curves 1 and 2 are the isotonic curves for a light and a heavier afterload respectively (the preload being the same). Similar changes but with greater "clamps" are given in panels II to IV. The curves ABCDEF are given as follows:

a) at the point B in the lightly loaded isotonic contraction, the afterload is suddenly changed to the heavier case so that the seqment CD is a portion of an isotonic contraction at this heavier load.

b) At the point D, the afterload is suddenly released to the lighter case at which level it stays for the remainder of the contraction.

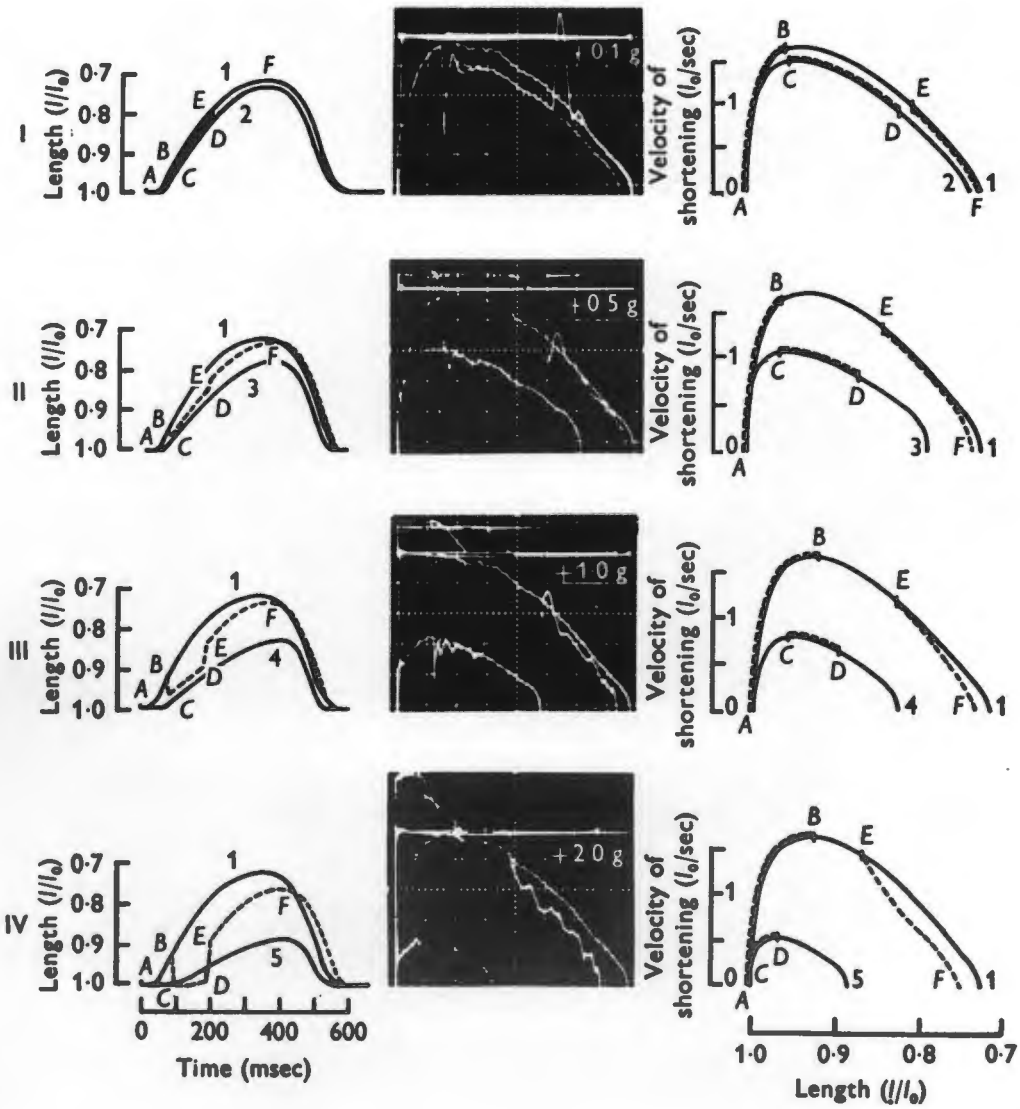

FIG. 4.10

LOAD CLAMPING EXPERIMENTS

Panels I through IV represent load clamps of increasing magnitude (see text for explanation)

The right hand side drawings in Fig. 4.10 are the velocity-strain plots of the experimental sequences described above. They reveal that the velocity of muscle shortening is determined by its instantaneous length only and is independent of the sequence of length changes by which this instantaneous length is attained. This state of affairs was shown to obtain, from just after the time of onset of shortening to just prior to the time at which peak shortening occurs (Brutsaert et al., 1971).

4.1.2.2.6 Controlled Constant Shortening Velocity Contractions

Controlled constant velocity of shortening experiments on isolated cardiac muscle similar to those described in part d) of Section 4.1.2.2.4 above were performed by Meiss and Sonnenblick (1972). A far wider range of velocities was, however, studied.

Two significant features emerge from these experiments:

a) at a given time after stimulation (in a given pre-loaded isometric contraction) a unique constant velocity of shortening existed at which the force response during this shortening remained constant for a short period. An example is shown in Fig. 4.11.

b) The shortening velocity giving the conditions above for a given time after stimulation is (approximately) equal to the initial velocity of shortening for the equivalent (with respect to preload and time after

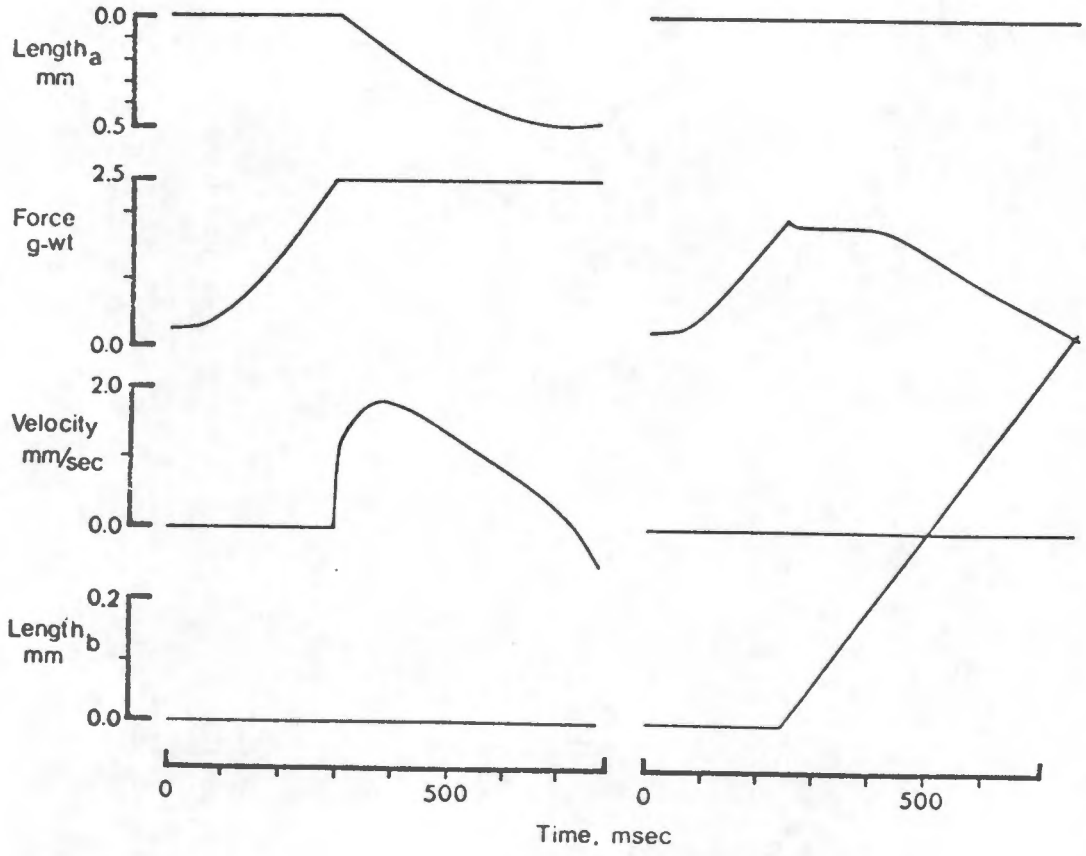

FIG. 4.11

VELOCITY-FORCE EXPERIMENTS

The left hand panel shows the conventional way of obtaining the force-velocity relation by quick release. The right hand panel shows the velocity - force method: ramp length changes giving force plateaux are sought.

stimulation) afterloaded isotonic contraction (see part b) of Section 4.1.2.2.2). This implies that the relation between force and velocity is insensitive to whether velocity is the dependent (uncontrolled) or independent (controlled) variable. This will be further discussed in Section 4.2.4 below.

Brutsaert et al. (1972) performed experiments conceptually different to those of Meiss and Sonnenblick. Instead of driving the muscle at a constant velocity, they clamped the contracting muscle at different velocities by controlling the muscle load. Typical results are shown in Fig. 4.12 which also has isotonic contractions for comparison.

4.1.3 Cardiac Muscle Experimentation - Discussion

In Section 4.1.2, the range of isolated cardiac muscle experimentation reported in the literature has been set out. These experiments have, in general been designed to test the hypotheses proposed by different researchers. An attempt is now made (in Sections 4.2 and 4.3) to dispassionately analyse these hypotheses in the light of the available experimental evidence as summarised in Section 4.1.2. A simple cardiac muscle model (explicitly incorporating the time variable) is then developed in Section 4.3. It will be seen that this model does not pretend to explain all the experimentally observed facts but rather is derived with the specific aim in mind of using it as the descriptor of cardiac muscle fibre stress-strain-time dynamics in the model of the left ventricle to be described in Chapter 6 of this Thesis.

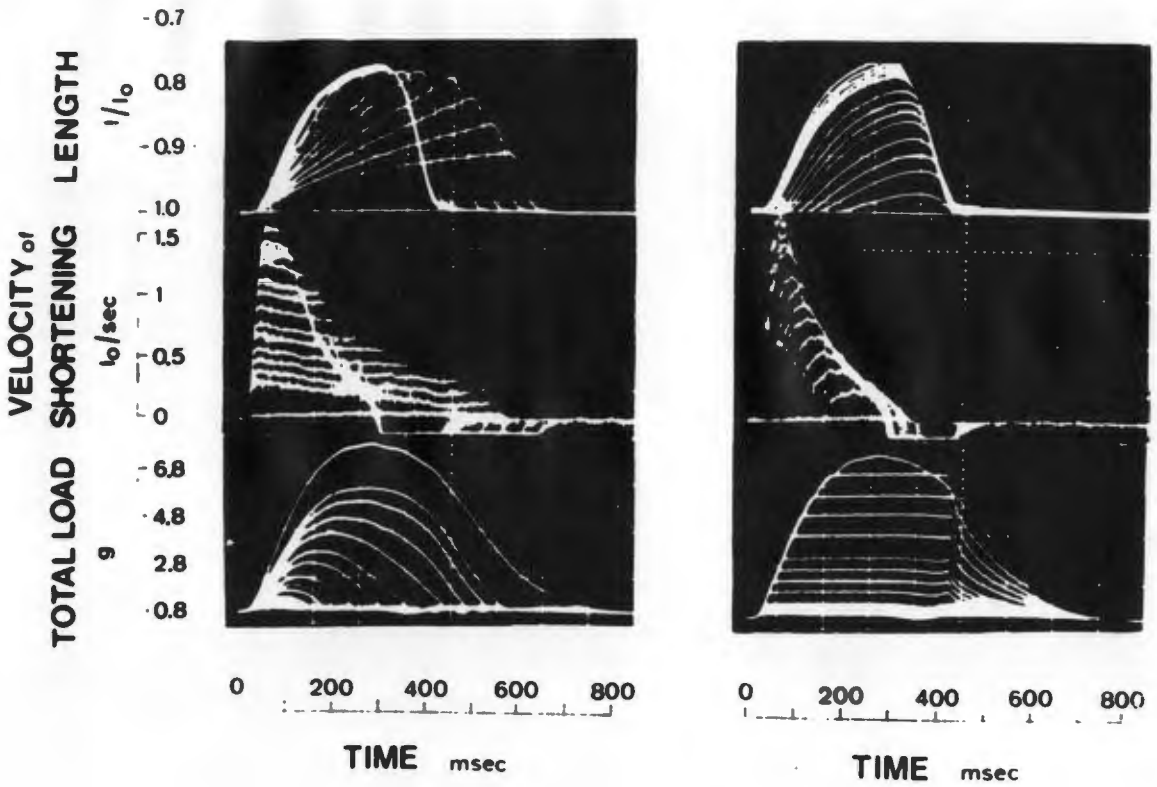

FIG. 4.12

LOAD CONTROLLED CONSTANT VELOCITY EXPERIMENTS

Left Hand Panel: Length and force responses for different controlled velocities.
Right Hand Panel: Conventional after-loaded isotonic contractions.

4.2 Muscle Modelling - A Review

A number of extensive reviews have been published on the subject of cardiac muscle dynamics incorporating both electrochemical and mechanochemical phenomena (Sandow, 1965; Braunwald et al., 1968; Brady, 1968; Sonnenblick and Stam, 1969; Katz, 1970a). Most of these reviews include sections on the modelling of the mechanical dynamics of muscle. In this review, much of this material will be repeated, but some conclusions will however be updated using the results of the recent experiments described above (Section 4.1.2). A few novel observations will be made and some old ones restated with regard to mechanochemical events in cardiac muscle, these observations being coloured by the author's chemical engineering background.

In order to put into perspective the factors to be discussed in this review, a brief account of the events occurring during a typical cardiac muscle contraction is now provided.

4.2.1 Relevant Mechanochemical Events Occuring During Cardiac Muscle Contraction

This description of mechanochemical events in cardiac muscle is based mainly on the exposition of Braunwald et al. (1968).

An action potential (AP) is triggered in cardiac muscle by electrical stimulation and/or in response to mechanical agencies. The AP is transferred from the outer fibre

surface (sarcolemma) to the Z-lines of the myofibrils by means of the extracellular T-system of the sarcoplasmic reticulum (see Fig. 3.1B and Section 3.1). The effect of the AP is, by a mechanism yet unknown, transferred to the terminal cisternae of the intracellular longitudinal (tubular) system of the sarcoplasmic reticulum. This triggers the apparently irreversible release of Calcium ions (Ca^{2+}) from sites in the terminal cisternae and/or along the longitudinal system: since this longitudinal system extensively ramifies the surfaces of the myofibrils (Section 3.1.1) the diffusion distances of the Ca^{2+} are small so that these ions rapidly reach the actin and myosin overlap region (Hill, 1948).

(Taking the diffusivity to typically be that of most metallic ions in water at 20^{0} C, 10^{-5} cm^2/s (Treybal, 1955, p25), since the maximum diffusion distance in cardiac muscle is about 0,5 µm, the maximum diffusion time is of the order of 50 ms which is typically 10% of the contraction period and consequently need not be considered.)

Once the free labile Calcium concentration reaches about 10^{-7} M, the Ca^{2+} starts combining with Troponin (a protein constituent of the actin fibres which in the Ca^{2+} - free state inhibits the reaction between actin and myosin) allowing the reversible reaction between actin and myosin to proceed (in the presence of Magnesium ions). The energy for the reaction is obtained by splitting the energy-rich compound, Adenosine Triphosphate (ATP) (Olson, 1971). Hence the sequential reactions are summarised as:

$$\text{Calcium} + \text{Troponin} \rightarrow \text{Actin}^*$$

$$\text{Actin}^* + \text{Myosin} + \text{ATP} \underset{\leftarrow}{\overset{Mg^{2+}}{\rightarrow}} \text{Actomyosin} + \text{ADP} + \text{iP}$$

..... (4.2.1:1)

where Actin* is the activated (or uninhibited) form of actin.

The portion of the myosin molecule implicated in the above reaction is the so-called globular head. These heads are the extremities of spatially ordered projections from the backbone of the composite myosin filament (Huxley, H.E., 1969; Olson, 1971). On reaction therefore, a cross-bridge is formed by the linkage of this projection with the spatially ordered activated sites, Actin*, on the actin filament. By means of processes not yet elucidated, the formation of cross-bridges produces an active tensional force in the muscle which may also shorten if the muscle loading so allows. Several theories have been presented in an attempt to explain the exact mechanism of force production and shortening (Huxley, H.E., 1969; Katz et al., 1971; Hatze, 1973). Subsequent analysis will not, however, depend on a direct knowledge of this mechanism.

By a further unknown process the Troponin-bound Calcium is, as a final stage of the contraction, resequestered by the longitudinal system of the myofibril causing relaxation and so completes the muscle contraction cycle.

The sequence of events just described is summarised in Fig. 4.13 and the movement of Calcium between the various

cellular compartments involved is shown in Fig. 4.14. Two further factors must be noted with regard to cardiac muscle Calcium kinetics.

a) As indicated in Figs 4.13 and 4.14, some of the labile Calcium released by the longitudinal system on activation is probably taken up by the mitochondria (the chemical factories of the cell) and so it is not all available for cross-bridge activation (Nayler and Merrillees, 1971).

b) In addition to the intracellular movement of Calcium there is also a transmembranous movement during activity (Section 3.1.2). This however appears to provide a negligibly small intracellular free Calcium contribution (Nayler and Merrillees, 1971).

4.2.2 Hill's Three-Element Muscle Model

It has been shown that muscle has passive elastic properties (Section 4.1.1) and, on stimulation, active properties (Section 4.1.2) which are markedly different from the passive.

For the purposes of quantitating muscle properties, A.V. Hill (1939) divided the passive and active muscle sites into two separate components acting in parallel. Passive elastic properties were described by one of these components, the parallel elastic (PE) element and the manifestation of active state properties was assumed to occur in the other component.

A clue to the nature of this latter component was provided

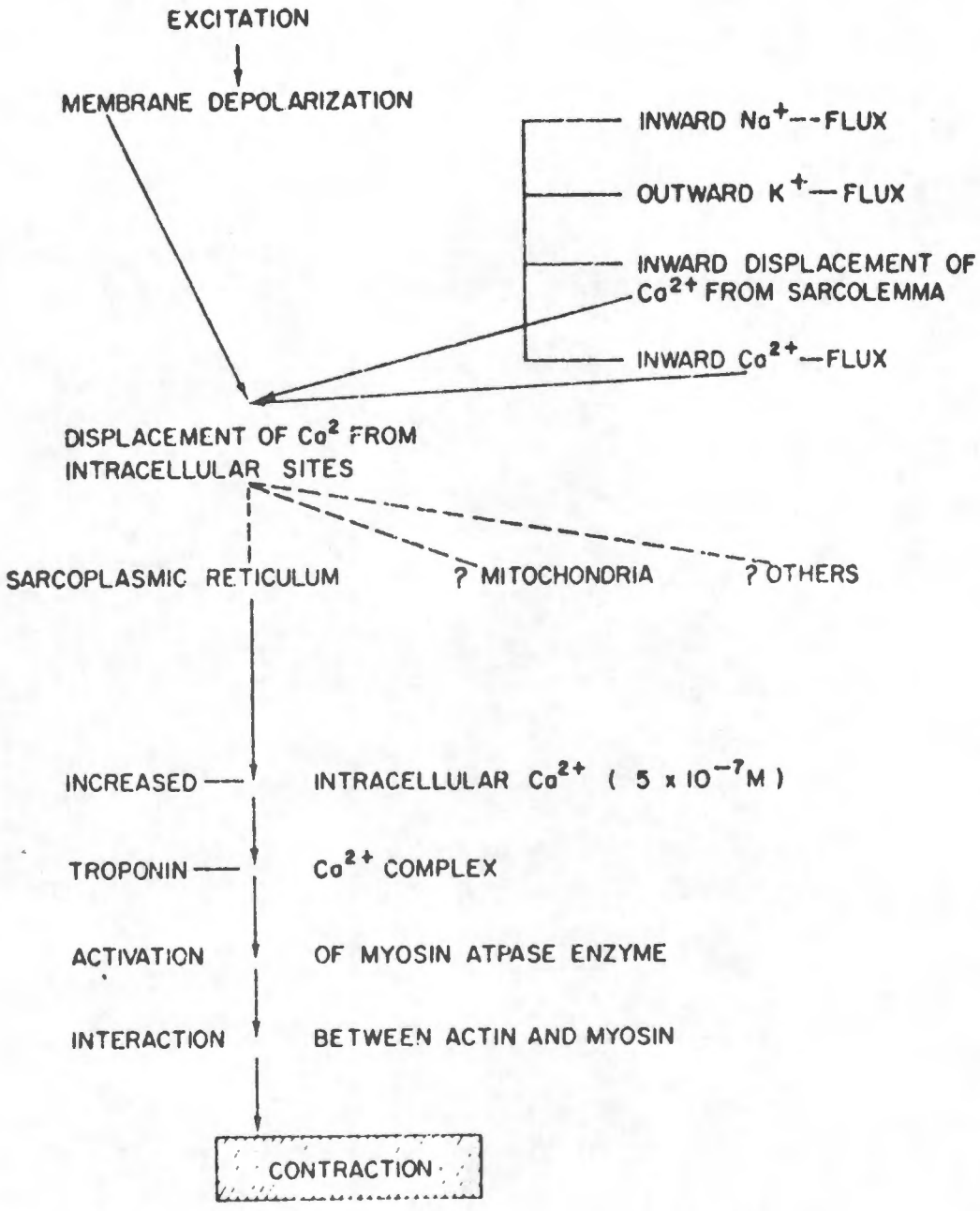

FIG. 4.13

MOVEMENT OF CALCIUM IN CARDIAC MUSCLE

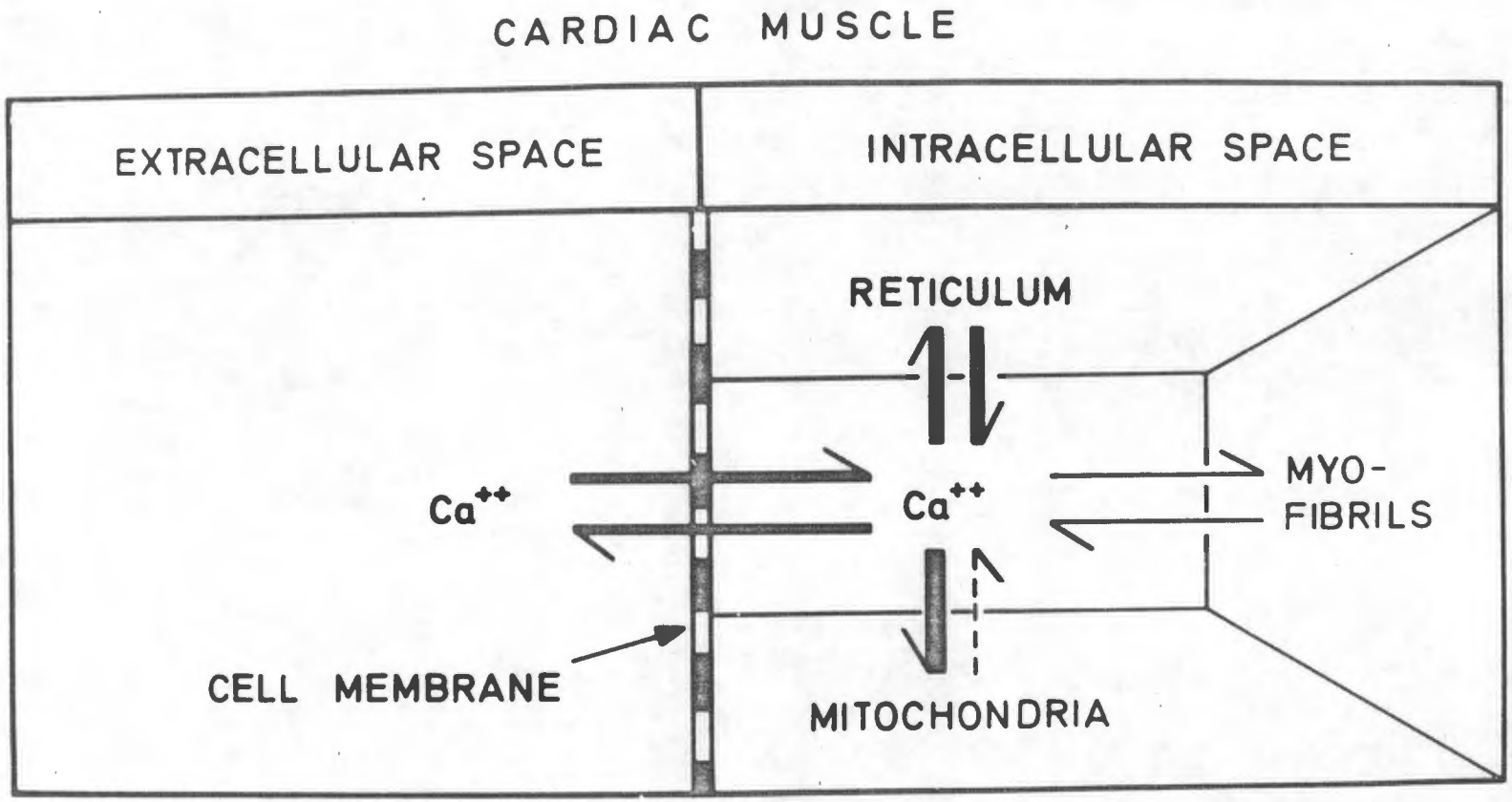

FIG. 4.14

COMPARTMENTAL MODEL FOR CARDIAC MUSCLE CALCIUM MOVEMENT.

by QR experiments where an isometric contraction was suddenly changed to isotonic (see part b) of Section 4.1.2.2.3): a virtually instantaneous muscle shortening was observed on this changeover followed by time-mediated shortening. These observations were most simply explained by assuming that the active parallel component comprised two elements in series, a series elastic (SE) element (giving the instantaneous shortening in QR) and a contractile element (CE), the seat of the active muscle properties. This model for muscle behaviour is shown in Fig. 4.15.

Alternative arrangements of the elastic elements have been postulated and evaluated: for instance the PE element and CE have been assumed to act in parallel with the resultant stress of the combination being transmitted through the SE element (Brady, 1967; Parmley and Sonnenblick, 1967; Parmley et al., 1969; Noble et al., 1969; Pollack, 1970). However, Fung (1971) has shown that these two models are equivalent: one can be transformed to the other provided one accepts that the model is in fact merely an aid in "curve-fitting" and rationalising experimental data. In this spirit Fung (1970) mathematically quantitated assumptions implied by the authors cited above who erred by assuming (unintentionally) a correspondence between the model elements (nonlinear springs) and the physical situtation pertaining in the muscle. Put another way, successful explanation of the data in terms of the model does not imply the model elements are structurally identifiable in the muscle. It is not however the intention here to delve too deeply into the

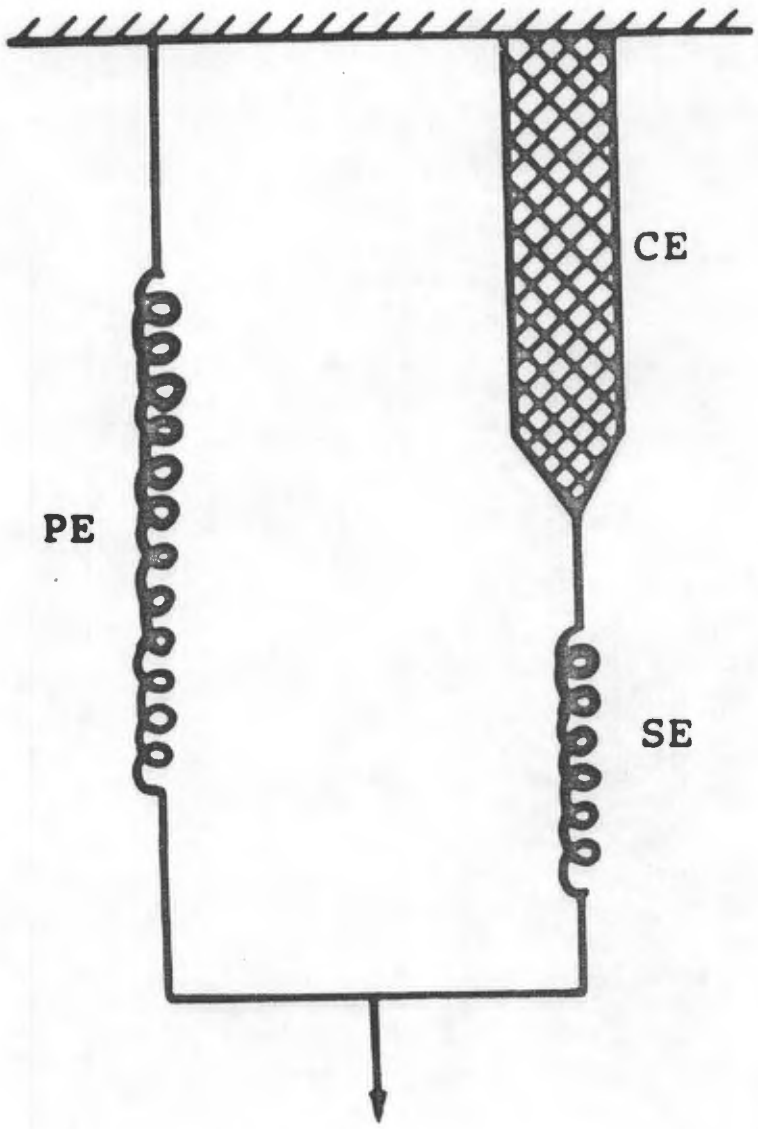

FIG. 4.15

HILL'S THREE-ELEMENT MODEL

CE - Contractile element
PE - Parallel elastic element
SE - Series elastic element

intricacies of muscle modelling, but rather to generate a simple model decribing cardiac muscle activity.

Guided by Fung's analysis and bounded by the demands of simplicity, not only because of the intrinsic desirability of such a model, but also because this is what is required for use in the left ventricular model (to be developed in Chapter 6), the author will base his muscle representation on what Fung has formally and unambiguously designated, "Hill's three-element model".

4.2.3 Analysis of Hill's Three-Element Model

The analysis in this Section is based almost entirely on Fung's (Fung, 1970). It is presented here to highlight remarks made above (Section 4.2.2) and because a simplified version of the analysis will be used as the framework of the model to be developed.

With reference to Fig. 4.15, it is easily seen that the stress balance of the elements of the muscle model is:

$$\sigma_{AA} = \sigma_p + \sigma_s \quad \ldots\ldots\ldots\ldots\ldots\ldots \quad (4.2.3:1)$$

and $$\sigma_c = \sigma_s \quad \ldots\ldots\ldots\ldots\ldots\ldots\ldots \quad (4.2.3:2)$$

where σ_{AA} = the axial fibre stress produced by the muscle,

σ_p, σ_s = the axial fibre stresses produced by the PE and SE elements respectively and

σ_c = CE stress.

For the case of passive elastic properties $\sigma_c = 0$ and so $\sigma_{AA} = \sigma_p$, and the equation describing these passive properties (equ. (4.1.1.2:9) is:

$$\sigma_p = E_2 (\varepsilon_{AA} - \varepsilon^*_{AA})^2 \quad \ldots\ldots\ldots\ldots\ldots\ldots \quad (4.2.3:3)$$

The axial muscle strain ε_{AA} is referred to the muscle length L_o at which maximum actin and myosin overlap occurs. The quantities E_1, E', E_2 and ε^*_{AA} are defined in Section 4.1.

In order to analyse the CE-SE element branch, reference must be made to Fig. 4.16. Following Fung's notation:

M = myosin filament length,

C = actin filament length,

Δ = insertion of actin filaments, i.e. the overlap between actin and myosin,

H = H-band width,

I = I-band width,

L = total length of the sarcomere,

L_o = length of sarcomere at maximum Δ,

l = length of the CE,

l_o = length of the CE at maximum Δ and

η = extension of the SE element in a sarcomere.

The following relations hold:

$$L = l + \eta, \quad \ldots\ldots\ldots\ldots\ldots\ldots\ldots \quad (4.2.3:4)$$

$$L_o = l_o + \eta, \quad \ldots\ldots\ldots\ldots\ldots\ldots\ldots \quad (4.2.3.5)$$

$$l_o = 2C \quad \ldots\ldots\ldots\ldots\ldots\ldots\ldots\ldots \quad (4.2.3.6)$$

$$\Delta = M + l_o - l, \quad l > l_o \quad \ldots\ldots\ldots\ldots \quad (4.2.3.7)$$

and $$\Delta = M - l_o + l, \quad l \leq l_o \quad \ldots\ldots\ldots\ldots \quad (4.2.3.8)$$

Since simulations under normal physiological end diastolic left ventricular pressures are to be performed, $l \leq l_o$ at

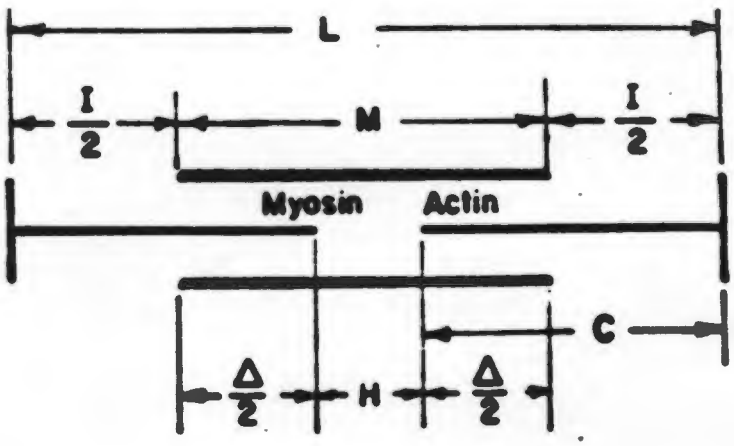

FIG. 4.16

LENGTH RELATIONSHIPS IN SARCOMERE
(See text for definitions of symbols)

all times (Sponitz et al., 1966) and so equ. (4.2.3:7) will not apply.

Further the quantities M and C can be considered constants. Thus the basic kinematic equation can be obtained as a function of Δ, L and η by substituting equ. (4.2.3:4) in (4.2.3:8) and differentiating the result:

$$\frac{d\Delta}{dt} = \frac{dL}{dt} - \frac{d\eta}{dt} \quad \ldots\ldots\ldots\ldots\ldots\ldots \quad (4.2.3:9)$$

The stress balance, equ. (4.2.3:1) can now be further analysed. The SE element stress-strain relation is, in its most general form (as explained by Fung):

$$\sigma_s = \sigma_s(\eta, \Delta) \quad \ldots\ldots\ldots\ldots\ldots\ldots \quad (4.2.3:10)$$

Substitution of this into the stress balance and then differentiation with respect to time yields:

$$\frac{d\sigma_{AA}}{dt} = \frac{d\sigma_p}{d\varepsilon_{AA}} \frac{d\varepsilon_{AA}}{dt} + \frac{\partial \sigma_s}{\partial \eta}\Big|_{\Delta} \frac{d\eta}{dt} + \frac{\partial \sigma_s}{\partial \Delta}\Big|_{\eta} \frac{d\Delta}{dt}, \quad (4.2.3:11)$$

where $\varepsilon_{AA} = (L - L_o)/L_o$. $\ldots\ldots\ldots\ldots\ldots\ldots (4.2.3:12)$

The quantity $d\eta/dt$ is related to $d\Delta/dt$ through equ. (4.2.3:9). Noting that $dL/dt = d\varepsilon_{AA}/dt$, substituting for $d\eta/dt$ in equ. (4.2.3:11) yields (after minor rearrangement):

$$\frac{d\sigma_{AA}}{dt} = \left(\frac{d\sigma_p}{d\varepsilon_{AA}} + \frac{\partial \sigma_s}{\partial \eta}\Big|_{\Delta} \right) \frac{d\varepsilon_{AA}}{dt}$$

$$+ \left(\frac{\partial \sigma_s}{\partial \Delta}\Big|_{\eta} - \frac{\partial \sigma_s}{\partial \eta}\Big|_{\Delta} \right) \frac{d\Delta}{dt} \quad \ldots\ldots\ldots\ldots\ldots\ldots (4.2.3:13)$$

Thus, the rate at which activated muscle generates stress can be simulated based on a knowledge of the velocity of muscle contraction and the velocity of insertion of the CE

myofilaments once the partial derivative factors in equ. (4.2.3:13) have been evaluated. Much of isolated muscle experimentation revolves around the determination of these (nonlinear) factors, explicitly defined for the first time by Fung (1970). These details will not be repeated here. Mindful of the errors implied but motivated by the demands of simplicity, it will be assumed that the SE element elastic character is independent of myofilament insertion so that equ. (4.2.3.10) is reduced to:

$$\sigma_s = \sigma_s(\eta), \quad \ldots\ldots\ldots\ldots\ldots\ldots\ldots\ldots \quad (4.2.3.14)$$

an exponential function of η (Parmley and Sonnenblick, 1967; Fung, 1970).

Having characterised the elastic properties of the PE and SE elements, attention is now focussed on the attempts made to analyse the CE.

4.2.4 The Force-Velocity Relation

A characterisation for the CE of skeletal muscle was provided by A.V. Hill (1939) from a study of the properties of contracting muscle.

From his experiments, Hill (1939, p.161) found that extra heat, over and above the maintenance heat (produced by the metabolic reactions) of an isometric contraction, was liberated if the muscle was allowed to shorten. This extra heat liberated (heat of shortening) was proportional to the muscle shortening (for isotonic contractions, where η = constant so that $d\Delta = dL$ from equ. (4.2.3:9), implying that CE shortening is the same as overall muscle

shortening). Letting the isotonic shortening be x (cm), the quantity of shortening heat liberated is a.x (g-cm). If P (g) is the total load lifted then the mechanical work done is P.x (g-cm) and so the total energy in excess of isometric is (P+a).x (g-cm). Hence the rate of extra energy liberation is (P+a).v (g-cm/s) if v is the shortening velocity in cm/s.

Hill further found that this rate of extra energy liberation was linearly related to the load lifted so that:

$$(P+a)v = b(P_o-P)$$

where P_o is the peak isometric load. Rearrangement of the above equation yields the familiar hyperbolic Hill force-velocity relation shown in Fig. 4.17B (for cat papillary muscle):

$$(P+a)(v+b) = (P+a)b = \text{constant}, \quad \ldots\ldots\ldots \quad (4.2.4:1)$$

where a (g) and b (cm/s) are muscle constants.

This hyperbolic force-velocity relation obtained from Hill's experiments outlined above, is a property of the CE only and not the muscle as a whole; for from equs (4.2.3:1) and (4.2.3:2), the relation between CE stress and muscle stress is (reverting to previously defined notations and units (Section 4.2.3)):

$$\sigma_{AA} = \sigma_p + \sigma_c \quad \ldots\ldots\ldots\ldots\ldots\ldots\ldots\ldots \quad (4.2.4:2)$$

and since σ_p the PE element stress is negligible at physiological lengths, (sarcomere lengths <2,2 μm: see Section 4.1), in skeletal muscle, $\sigma_{AA} \sim \sigma_c$. It was,

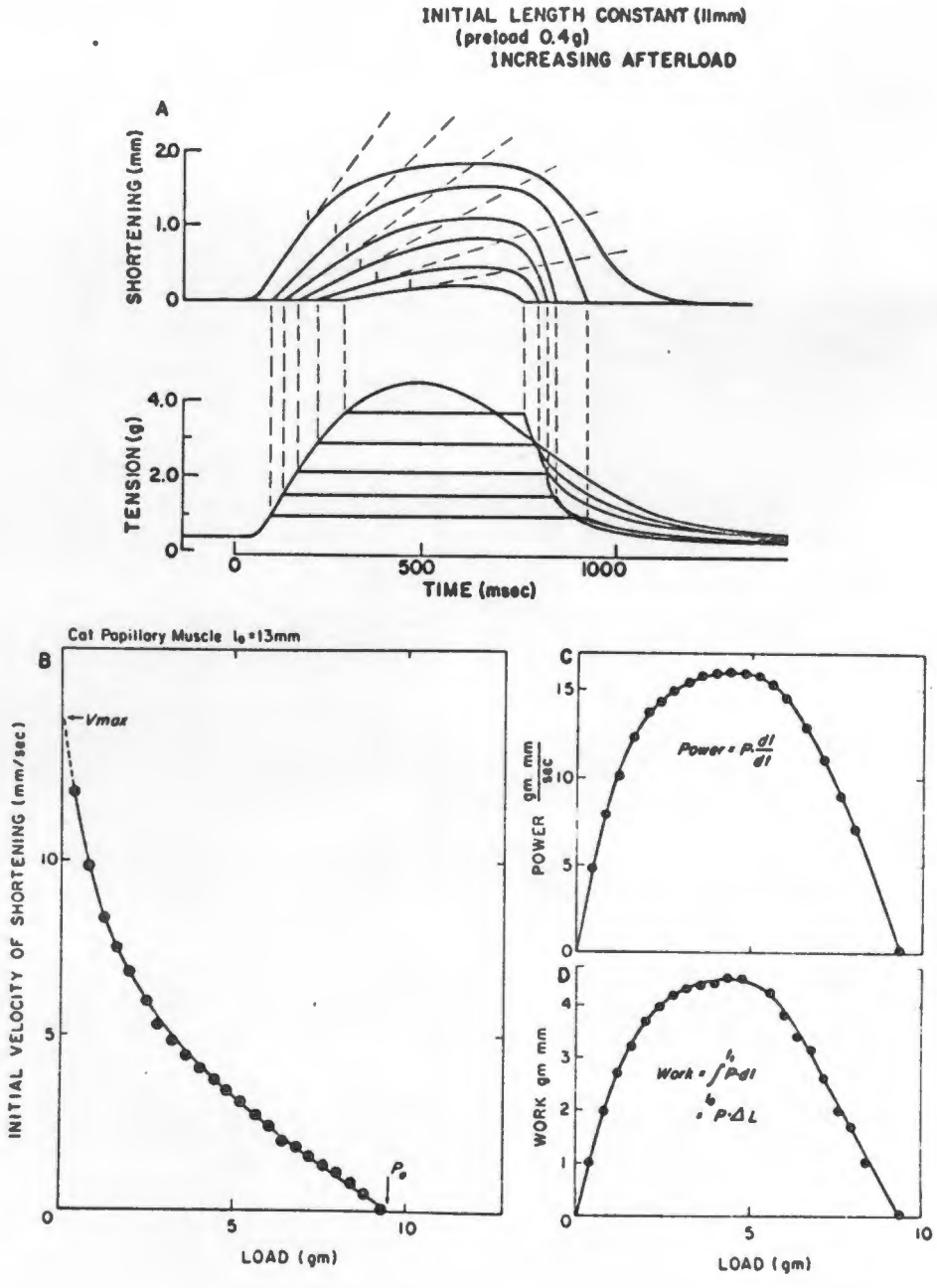

FIG. 4.17

HILL'S FORCE-VELOCITY RELATION

A - Afterloaded isotonic contractions using "in vitro" cat papillary muscle

B - Hill's Force-velocity relation obtained from the isotonic data

C,D - Power and work of the muscle vs. load

moreover, shown in the first paragraph of this Section that the overall muscle shortening velocity was the same as the velocity of shortening of the CE in isotonic contractions.

The above argument supports the assertion that the force-velocity relation describes, as Hill intended it to, the properties of the CE only.

The application of the force-velocity model of the CE to cardiac muscle is fraught with difficulties, the most striking and controversial of which is the role of the time course of the "active muscle potential" (AMP) herein defined to mean that quantity which the CE of the muscle manifests in response to the mechanical load imposed on it. Since skeletal muscle can be tetanised, (kept in a continuous state of tension) the AMP can be maintained at a constant level (for isometric loading). Further, even in a single isometric twitch, the AMP rises to a constant level very rapidly (relative to the period of contraction) and remains at this value for most of the rising phase of the isometric contraction. (Hill, 1970, Chapter 5).

This state of affairs does not obtain in cardiac muscle: firstly it cannot be tetanised (except under special conditions as recently shown (Forman et al., 1972)) and secondly the AMP exhibits a far slower rate of onset (measured relative to the contraction period). This latter factor greatly complicates the analysis of the CE in terms of the force-velocity relation. It is now propitious to summarize and briefly discuss the rationale

employed by researchers in this field to measure the analogue of the AMP and how they have interpreted the force-velocity relation in the light of their measurements.

4.2.4.1 Determination of the Force-Velocity Relation

Three methods have been employed to experimentally obtain the cardiac muscle force-velocity relation.

a) The method Hill (1939) used for skeletal muscle where, at a given preload, the initial velocity of shortening (dependent variable) is obtained for different after-loads. This velocity plotted against the total load yields an isotonic force-velocity relation (Sonnenblick, 1962). Also see Fig. 4.17.

b) By shortening the muscle at constant velocities at given times during an isometric contraction, the particular velocities yielding plateaux in the force (dependent variable) responses for each time after stimulation chosen are obtained (Section 4.1.2.2.6). These pairs of points yield a velocity-force curve (Meiss and Sonnenblick, 1972).

c) An isometric is "instantaneously" converted to an isotonic contraction at various times during the contraction (Section 4.1.2.2.3, part b)). The isometric force at this instant and the initial velocity (dependent variable) at which the muscle shortens after the change over define a point on the quick release force-velocity curve (Noble et al., 1969).

The curves obtained by all three methods are subject to the same serious limitations in interpretation based on the

strict force-velocity concept expounded by Hill and repeated above (Section 4.2.4).

4.2.4.2 Influence of the AMP on the Force-Velocity Constants

It is evident from equ. (4.2.2:1) that the constant, a, reflects the "velocity of shortening" ability of muscle since it has the dimensions of velocity. P_0 is the maximum isometric load the muscle is able to lift (for a given initial length). Now suppose that the AMP is defined by a time varying quantity A(t), say:

$$A(t) = A_p \sin(\pi t/t_p), \quad 0 \leq t/t_p \leq 1$$

where A_p is the peak activity and t_p is the period of the AMP. Early and late in the cycle the AMP is low and so the muscle's ability to lift a given load at these times is patently less than at times around the middle of cycle when $A \sim A_p$. An intuitive corollary would be (it is almost certainly a logical consequence) that the maximum velocity the muscle could lift the given load would also vary in sympathy with the AMP. As a result, the factors a and P_0 are not muscle constants, but depend on the time-mediated level of the AMP.

4.2.4.3 Interpretaion of the Force-Velocity Relation in Cardiac Muscle

It has been shown (Section 4.2.4) that the hyperbolic force-velocity relation defines the properties of the CE only and not the muscle as a whole. In cardiac muscle, the PE element contributes significantly to the muscle stress at physiological (normal) lengths and so cannot be neglected,

in sharp contrast to the assumption for skeletal muscle (Section 4.2.4). When the effect of the PE is accounted for (by substituting equ. (4.1.1.1;1) into (4.2.4;2)) in the data obtained from the experiments described above (Section 4.2.4.1) a hyperbolic relation is not obtained (Brady, 1965; Noble et al., 1969). But this does not necessarily mean that the physiological concepts surrounding the force-velocity relation are invalid for cardiac muscle. In fact for tetanised cardiac muscle where the AMP is constant, Forman et al. (1972) showed the hyperbolic relation is valid.

The cause of this dilemma is therefore rooted in the time variation of the AMP as discussed in Section 4.2.4.2 above. Although attempts have been made to show that the AMP remains at a constant level over most of the rising phase of the isometric contraction (Sonnenblick, 1965; Brutsaert and Sonnenblick, 1969; Brutsaert et al., 1971; Brutsaert et al., 1972) they remain unconvincing since the PE element correction is not made and no account is taken of SE element stretching prior to isotonic shortening (Pollack, 1970). The implication of this latter factor must be elucidated.

Well-founded evidence reveals that the number of actomyosin cross-bridges formed at a given time during a contraction is proportional to the overlap Δ of the actin and myosin filaments (see Sections 3.1 and 4.2.1). This follows from Huxley's sliding filament theory of muscle contraction (Huxley and Hanson, 1954). Making the reasonable assumption that the force per cross-bridge is constant at each time during a contraction, it follows that $\sigma_c|_t \propto \Delta$. The CE

length at the point of isometric to isotonic change over thus depends on the time at which the intervention occurs and this must be considered in generating the force velocity relation.

We are therefore brought back to a study of the nature of $\sigma_c(t)$ which must be related to the AMP. (Its relation to Δ has been discussed above). A model defining these relations is developed in Section 4.3.

Discussion of the force-velocity relation would be incomplete without some mention of the terms "contractility" and "active state", which are commonly used analogues of the AMP, as well as a look at attempts to verify the relation in terms of "mechanistic" postulates.

4.2.4.4 Contractility and Active State

Contractility is connected with the ability of cardiac muscle to shorten and it is conventionally obtained through the force-velocity relation (Sonnenblick, 1962) of the whole muscle (and not just the CE). It is quantitated by the factor V_{max} the maximum velocity of shortening (which occurs at zero total load, see Fig. 4.17). Owing to the significant contribution of the PE element to muscle force production (at physiological muscle lengths), it is not possible to experimentally measure V_{max}. It can however be inferred by extrapolating the force velocity curve to zero load (Sonnenblick, 1962).

From the foregoing discussions (Section 4.2.4.3) the method of obtaining v_{max} is unsatisfactory; it implies in

the first place that the AMP is time invariant and secondly that V_{max} has physiological meaning (bearing in mind the extrapolation required). However, there is some evidence of a direct physiological interpretation of V_{max} in that it correlates very well with the rate of splitting of ATP by the reaction between activated actin and myosin (Section 4.2.1)(Barany, 1967; Katz, 1970a): the rate of this reaction thus controls the contractility of muscle.

Whereas contractility is related to the ability to shorten, the active state of muscle is associated with its ability to generate force. It is defined as the force developed by the CE when it is prevented from shortening or lengthening (Noble et al., 1969). P_o has been used to quantitate active state (with the reservations regarding the effect of CE movement on this factor set out in Section 4.2.4.3). A different measure of active state over a contraction is the initial velocity of shortening in isometric to isotonic quick release experiments (Brady, 1965). But this measurement is clearly more closely related to V_{max} than to P_o based on the given definitions.

This anomaly is symptomatic of the confusion existing in the literature in some areas of cardiac muscle dynamics and it is the reason the author defined the new term, active muscle potential (Section 4.2.4) and avoided using the sometimes misleading terms, contractility and active state. The precise relation between these terms will be provided once the author has developed his muscle model (Section 4.3).

4.2.4.5 Mechanistic Interpretations of the Force-Velocity Relation

The way Hill derived the force-velocity relation is set out in Section 4.2.4. Researchers in this field began naturally to ask questions about the genesis of the relation, in particular how it arose from the known chemical reactions associated with muscle activity.

A.F. Huxley (1957) developed a widely respected theory explaining the force-velocity relation in skeletal muscle very convincingly. It was based on the properties of the rate constants of the reactions causing the actin and myosin cross-bridges to form (equ. 4.2.1:1) and to break up. By assigning space-dependent properties to these rate constants (i.e. the value of the rate constants were made to be dependent on the position of the myosin cross-bridge with respect to the backbone of the myosin filament), the number of activated bridges at any time could be calculated and from this, the force produced by the muscle computed. A theoretical force-velocity relation, which fitted Hill's experimental data remarkably well followed. This theory represented the first attempt to relate muscle mechanical properties to cross-bridge chemical activity.

Other theories followed. Podolsky (1959), by incorporating Huxley's sliding filament theory, rationalised the force-velocity relation from the analysis of the thermodynamics of the cross-bridge reactions. This approach was taken further when the theory behind the thermodynamics of direct energy converters (i.e. conversion directly from chemical to

mechanical energy) was applied to the muscle system which was viewed as a self-regulated linear energy converter incorporating feedback (Caplan, 1966). Hill's force-velocity relation followed from a restricted version of this theory which has been the subject of much theoretical interest (see, for instance Bornhorst and Minardi (1970)).

A more statistical tack was followed by McCrickerd (1969) who assigned a "reaction cross-section" to the activated actin site so that a certain probability of cross-bridge formation existed as myosin heads moved past these activated actin sites. The resulting equation was of the form of Hill's force-velocity relation.

The development of a theory explaining the exact mechano-chemical means by which actin and myosin insertion occurs as a result of the chemical reactions has been the subject of much recent interest (Davies, 1963; Huxley, 1969; Huxley and Simmons, 1971; Abbot, 1972; Hatze, 1973). These theories appear, at present, to be highly speculative; the development of the theory in this dissertation however, does not depend on any assumptions regarding the exact mechanical nature of muscle stress and motion production. This is indeed also true of the force-velocity theories alluded to above. It must further be noted that all theories proposed apply to skeletal muscle. The extension to cardiac muscle will be discussed later (Section 4.3).

4.2.6 Discussion of Muscle Experimental and Modelling Philosophy

The study of muscle mechanics is changing rapidly from

being empirical and semi-empirical to being fundamental. This inevitably has led to a feedback phenomenon; the philosophy behind former ideas and experiments can be recast in the light of present knowledge. Coloured by his engineering background, the author now presents some criticisms of conclusions drawn from various forms of experiments performed on isolated cardiac muscle.

It has been well established that virtually all the relationships so far derived to describe muscle dynamics (for example, equ. 4.1.1.1:1) are nonlinear. Data gained about a particular point cannot be extrapolated to any regions beyond a limited neighbourhood of the point considered if the functional relationship between the variables considered is not known.

With this in mind, the philosophy behind step-change muscle experiments (quick stretch and quick release for instance) is brought very much into question: for from them the properties of normally (physiologically) contracting muscle are inferred. This is particularly pertinent to any attempt to quantitate changes in the level of active state from QRQS experiments (Section 4.1.2.2.4). With these sudden changes, the contractile machinery is forced into quite different operating regimes from physiologically occurring (i.e. normal) conditions. It is not therefore valid to extrapolate these results to the physiological situation as has recently been done (Kaufmann et al., 1972). This must be particularly true of the analysis of the CE. For here the AMP is almost certainly nonlinear and further, nothing quantitative is known about the cross-bridge reaction

phenomena which almost certainly are nonlinear. Thus, with the probable exception of the QR experiments designed to measure SE element properties (since the CE is unaffected by this intervention), all experiments performed on activated cardiac muscle must be very carefully assessed before sweeping conclusions are drawn.

Simplicity is the essence of theoretical modelling and so the natural tendency is to linearise; the author will, in the development of his model, be found guilty of this despite the comments above. He will however not, without explicit mention, attempt to extend his model beyond reasonable physiological bounds (Section 4.3).

4.3 Generalised Cardiac Muscle Model

In Section 4.1.1 a relation describing the properties of passive cardiac muscle was derived (equ. (4.1.1.2:9)). The models developed to describe active skeletal muscle were critically reviewed in Sections 4.2.4.4 and 4.2.4.5. Drawbacks in the application of the force-velocity relation to cardiac muscle were enumerated.

There is no currently available cardiac muscle model able to simulate active properties (under arbitrary loading conditions such as isotonic) really convincingly. Attempts have been made along these lines using Huxley's theory (see Section 4.2.4.5). This theory was initially extended by Julian (1969) to account for the time varying AMP in skeletal muscle by allowing the cross-bridge formation rate constant to be time as well as space dependent. It was modified by Wong (1971, 1972) to describe cardiac muscle

dynamics. From the computational point of view, from the author's experience (unpublished), this model is too cumbersome for use in a complex left ventricular model (which is derived in Chapter 6). It was imperative, therefore that a new simple cardiac muscle model be developed. The author was able to invoke some recently expressed ideas to help formulate his model.

4.3.1 The Effect of Muscle Length Changes on the AMP

In Section 4.2.4 a new term, active muscle potential (AMP) was defined as "that quantity which the CE of the muscle manifests in response to the mechanical load imposed upon it". This important factor will now be investigated further.

It is obvious that an isometric contraction is of longer duration than an isotonic (see Fig. 4.5A). In fact, any muscle shortening tends to decrease the period of the contraction. The physiological interpretation for this is that the rate at which Calcium is resequestered from the vicinity of the cross-bridges is somehow increased by the shortening (Kaufmann et al., 1972; Bozler, 1972). As a direct consequence, the force producing ability of the muscle is diminished as Ca^{2+} is removed from the contractile machinery: this has been experimentally shown by Brady (1965), Brutsaert et al. (1971). Brutseart et al. (1972), Kaufmann et al. (1972) and Meiss and Sonnenblick (1972). Some of the data from these experiments are reproduced in Figs 4.8 and 4.9.

The foregoing reveals that the AMP is indeed sensitive to

the nature of the loading imposed on the muscle as was suspected by Wong (1972) in the development of his model. A simple quantitative interpretation of the AMP will now be given.

4.3.2 Derivation of the Muscle Model

The author's defintion of AMP will first be quantitated (equ. (4.2.3:1)). A formula relating CE stress, strain and time will then be derived (equ. (4.3.2:10)) followed by a similar relation for overall muscle stress, strain and time (eq. (4.3.2:11)).

Suppose the cross-bridge density (the number of cross-bridges formed per unit length of actin and myosin insertion) is n (a function of time after stimulation) and the sliding or axial stress generated by each cross-bridge is σ_s. The AMP can now be represented as:

$$\psi(t) = \sigma_s.n(t) \quad \ldots\ldots\ldots\ldots\ldots\ldots \quad (4.3.2:1)$$

and defines the active stress generated by the cross-bridges per unit insertion (or overlap). The total stress developed by the overlap region (the CE) is:

$$\sigma_c = \psi.\Delta \quad \ldots\ldots\ldots\ldots\ldots\ldots\ldots\ldots \quad (4.3.2:2)$$

where Δ is the insertion.

It has been noted in Section 4.3.1 that any change in Δ changes ψ in the same direction. The author has quantitatively demonstrated this. Using isotonic data for cat papillary muscle (Sonnenblick, 1962), $\psi(t)$ was calculated from the shortening trajectory at each different afterload using equ. (4.3.2:2). These $\psi(t)$ curves (in stress units)

are shown in Fig. 4.18.

Define $\Phi(t)$ to be the value of $\psi(t)$ for constant $\Delta = \Delta_o$ during a muscle contraction (where Δ_o is the insertion at a sarcomere length of 2,2 μm: this is in fact the definition of "active state" within the context of this model (see Section 4.2.4.4). Shortening of the muscle (active shortening only will be considered) from a length within the normal physiological range (sarcomere length $\leq$ 2,2 μm) will decrease Δ from equ. (4.2.3:8). The concomitant decrease in Φ, given by ϕ, to be called the shortening decrement, will be assumed to be proportional to the change in Δ, so that:

$$\phi = -k\ (\Delta - \Delta_i)$$
$$= -k.\delta\Delta \qquad \ldots\ldots\ldots\ldots\ldots\ldots\ldots\ldots \quad (4.3.2:3)$$

where k = shortening decrement constant,

Δ_i = the initial value of the insertion (not necessarily Δ_o)

and $\delta\Delta = \Delta - \Delta_i$, the CE change in insertion.

The AMP is, in view of the above definitions and equations, given by the difference between the active state and the shortening decrement as:

$$\psi = \Phi - \phi$$
$$= \Phi + k.\delta\Delta, \qquad \ldots\ldots\ldots\ldots\ldots\ldots\ldots \quad (4.3.2:4)$$

such that $\psi \leq 0$ and that $\psi = 0$ when $\Phi = 0$.

By substituting equ. (4.3.2:4) into equ. (4.3.2:2), the stress generated by the CE of the muscle in terms of this model is given as:

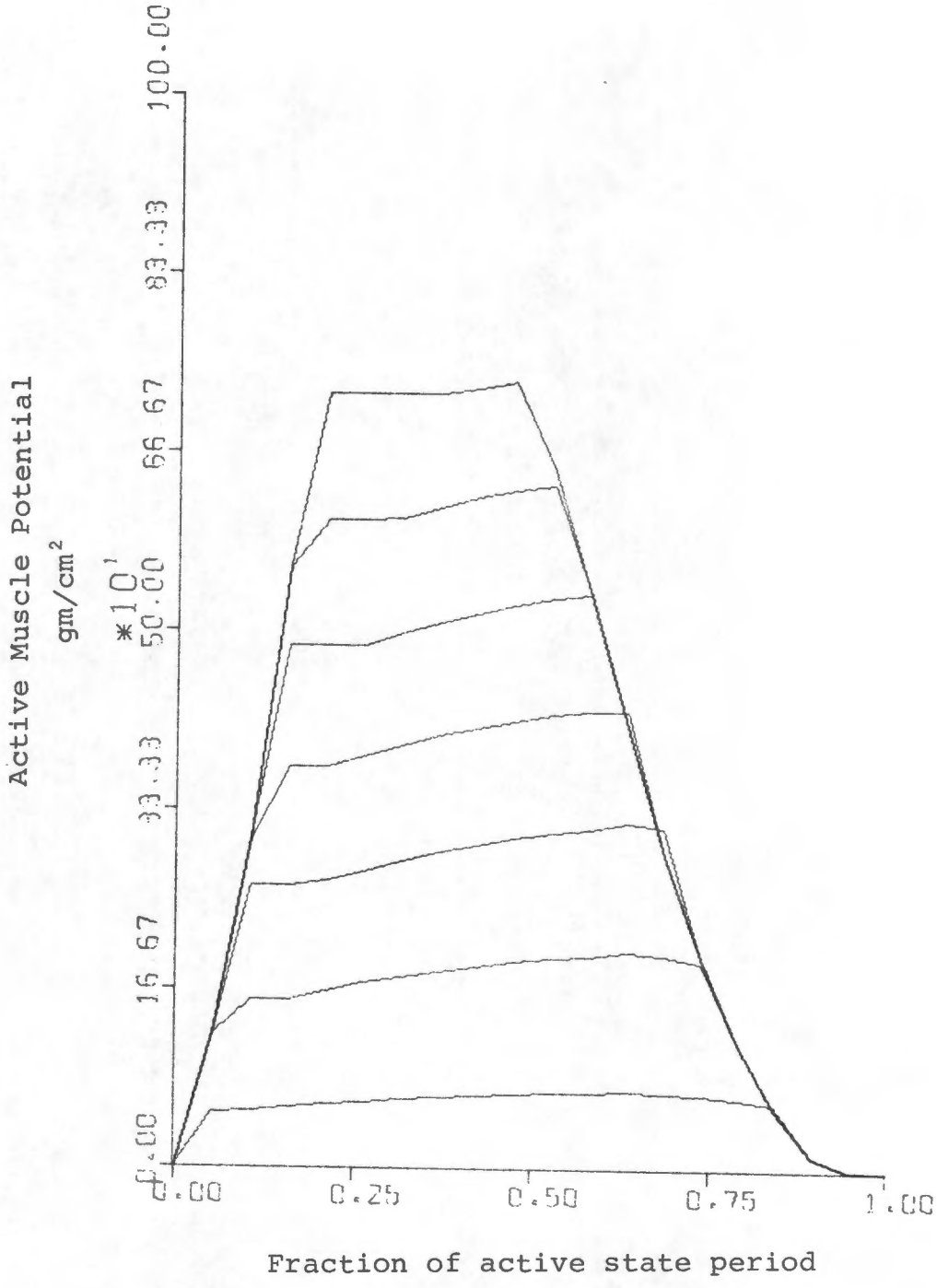

FIG. 4.18

THEORETICALLY GENERATED AMP
CURVES FOR ISOTONIC CONTRACTIONS

Based on data from Sonnenblick (1962)

$$\sigma_c = (\Phi + k.\delta\Delta).\Delta. \quad \text{..... (4.3.2:5)}$$

From the above equation, the active state Φ and the shortening decrement constant k have the units of stress (e.g. N/m^2) if the insertion Δ is given in length units normalised with respect to l_o, the CE length corresponding to a sarcomere length of 2,2 μm.

The stress σ_c developed by the CE stretches the SE which has an exponential stress-strain relation. To simplify the model, this will be linearised so that:

$$\sigma_s = E_s \eta \quad \text{..... (4.3.2:6)}$$

where E_s is the linear elastic modulus of the SE element.

The overall strain of the CE-SE element arm of the three-element model is the same as the overall muscle strain ε_{AA} (see Fig. 4.15) so that:

$$\varepsilon_{AA} = \eta + \delta\Delta + \delta\Delta_i \quad \text{..... (4.3.2:7)}$$

where $\delta\Delta_i = \Delta_i - \Delta_o$, and Δ_o is the insertion at l_o.

We also have, from the force balance for this arm (equ. 4.2.3:2)):

$$\sigma_s = \sigma_c. \quad \text{..... (4.3.2:8)}$$

Substituting for $\delta\Delta$ in equ. (4.3.2:5) using equ. (4.3.2:7) yields:

$$\sigma_c = \{\Phi + k(\varepsilon_{AA} - \eta - \delta\Delta_i)\}.\Delta.$$

By using equ. (4.3.2:8) in equ. (4.3.2:6) and then employing the result to substitute for η in terms of σ_c in the above

equation, the CE stress σ_c can be expressed in terms of the active state Φ, the muscle strain ε_{AA}, the insertion Δ and the constants k and E_s as follows:

$$\sigma_c = E_s \Delta\{\Phi + k(\varepsilon_{AA} - \delta\Delta_i)\}/(E_s + k\Delta) \quad \ldots \quad (4.3.2:9)$$

Remembering $\delta\Delta = \Delta - \Delta_i$ and $\delta\Delta_i = \Delta_i - \Delta_o$ it is possible to express Δ as a function of ε_{AA} and σ_c using equs (4.3.2:6), (4.3.2:7) and (4.3.2:8):

$$\Delta = \varepsilon_{AA} + \Delta_o - \sigma_c/E_s$$

The above equation can be substituted into equ. (4.3.2:9) yielding a quadratic in σ_c. This can be reduced to a linear equation by making the reasonable assumption that:

$$\eta = \sigma_c/E_s << \Delta_o,$$

since $\Delta_o \sim 1$ and $\eta \sim$ 0,05 strain units (Braunwald et al., 1968). Thus $\Delta = \varepsilon_{AA} + \Delta_o$ can justifiably be substituted into the denominator of equ. (4.3.2:9) in order to linearise it.

Making these substitutions and solving for σ_c yields:

$$\sigma_c = E_s(\Delta_o + \varepsilon_{AA})\{\Phi + k(\varepsilon_{AA} - \delta\Delta_i)\} /$$

$$\{E_s + \Phi + k(2\varepsilon_{AA} + 2\Delta_o - \Delta_i)\} \quad \ldots\ldots \quad (4.3.2:10)$$

This equation satisfies the condition $\sigma_c = 0$ for $\Phi = 0$, since $\delta\Delta_i = \varepsilon_{AA}$ when the CE is relaxed. $\delta\Delta_i$ actually sets the initial conditions for the CE at the instant of stimulation: it therefore is a CE constant during a particular stimulation.

From the assertion that $\Phi(t)$ is the analogue of the active state it follows that the stress-strain-time characteristics

are expressed by equ. (4.3.2:10) and that:

$$\sigma_c = \sigma_c \text{ (active state, } \varepsilon_{AA}) \quad \ldots\ldots\ldots \quad (4.3.2:11)$$

Active state (or its analogue in the context of this model) is therefore explicitly incorporated in describing the stress-strain-time properties of the CE.

The overall muscle stress production (active and passive), is given by substituting equs (4.3.2:10) and (4.1.1.2:9) into the stress balance for Hill's three-element model, equ. (4.2.3:1) so that:

$$\sigma_{AA}\ (\varepsilon_{AA},t) = \sigma_p(\varepsilon_{AA}) + \sigma_c(\varepsilon_{AA},t). \quad \ldots \quad (4.3.2:11)$$

Note that σ_{AA} in equ. (4.1.1.2:9) has been replaced by σ_p, the PE element stress with which the passive elasticity is now identified.

It is in the above form that the equation will be used in the ventricular model.

$\sigma_{AA}\ (\varepsilon_{AA},t)$ is a cubic function of ε_{AA} and so the equation can, in principle, be analytically cast in the form $\varepsilon_{AA}\ (\sigma_{AA},t)$. This will however be done numerically.

4.3.3 Properties of the Muscle Model

Firstly, the rationale used to obtain the active state will be given and this will be followed by a discussion of the means of estimating the shortening decrement constant, k. After computing these factors from published experimental data, the efficacy of this model in simulating isotonic contraction and ramp length change conditions will then be

analysed.

4.3.3.1 Quantitation of Active State

Under isometric conditions the CE shortens at most 5% of its overall length. This shortening represents about 25% of the maximum isotonic shortening of the CE (Braunwald et al., 1968). As initial approximation, it would therefore seem valid to neglect CE shortening in the calculation of Φ from an isometric (ε_{AA} = constant) contraction. Since Φ is defined for $\varepsilon_{AA} = 0$ (or $\Delta_i = \Delta_o$), equ. (4.3.2:5) becomes:

$$\sigma_c = \Phi\Delta$$

This is solved for Φ yielding:

$$\Phi = \sigma_c/\Delta \quad \ldots\ldots\ldots\ldots\ldots\ldots\ldots \quad (4.3.3.1:1)$$

$\Phi(t)$ can be estimated from this equation using isometric data. It is readily seen, from equ. (4.3.3.1:1), that Φ possesses the same phase characteristics as σ_c which is in direct conflict with the ideas of Sonnenblick and his co-workers who postulate an early rise of active state i.e. well before peak isometric force is reached (see Section 4.2.4:3). The model developed here suggests that this conflict arises through an inadequate quantitative definition of active state by Sonnenblick's group as will be discussed later (Section 4.3.4.3).

4.3.3.2 Estimation of the Shortening Decrement Constant

In order to estimate the shortening decrement constant, isotonic data is used. During the shortening phase ε_{AA}

is known and σ_{AA} is constant so, using the time varying values of Φ calculated above, k can be calculated from equ. (4.3.2:9) when it is solved for k i.e. in the form:

$$k = E_s(\sigma_c/\Delta - \Phi)/\{E_s\ (\varepsilon_{AA} - \delta\Delta_i) - \sigma_c\} \quad (4.3.3.2:1)$$

where $\Delta = \varepsilon_{AA} + \Delta_o - \sigma_c/E_s$

and where σ_c is easily obtained from equ. (4.3.2:11).

4.3.3.3 Computation of Model Active Constants

Using the isometric data of Sonnenblick (1962) in equ. (4.3.3.1:1) the active state curve shown in Fig. 4.19 is obtained and it strongly resembles a sine curve with an amplitude equal to the peak value of Φ. The fit is acceptably good as indicated on Fig. 4.19. Fung's active state simulation was also based on a sine function (Fung, 1970).

Based on this active state curve and on isotonic data the mean value of $k=-4$ N/cm^2 as calculated from equ. (4.3.3.2:1). Thus $|k\Delta/E_s| \sim 0{,}3$ † supporting the assumption in Section 4.3.3.1.

4.3.3.4 Isotonic and Constant Velocity Simulations

The prime motivation behind the development of this model for cardiac muscle dynamics is the realistic simulation of muscle behaviour under general loading conditions, particularly the case of muscle shortening.

In Fig. 4.20 the model predictions of Sonnenblick's isotonic shortening data are plotted and they show

† $E_s \sim 8{,}0$ N/cm^2

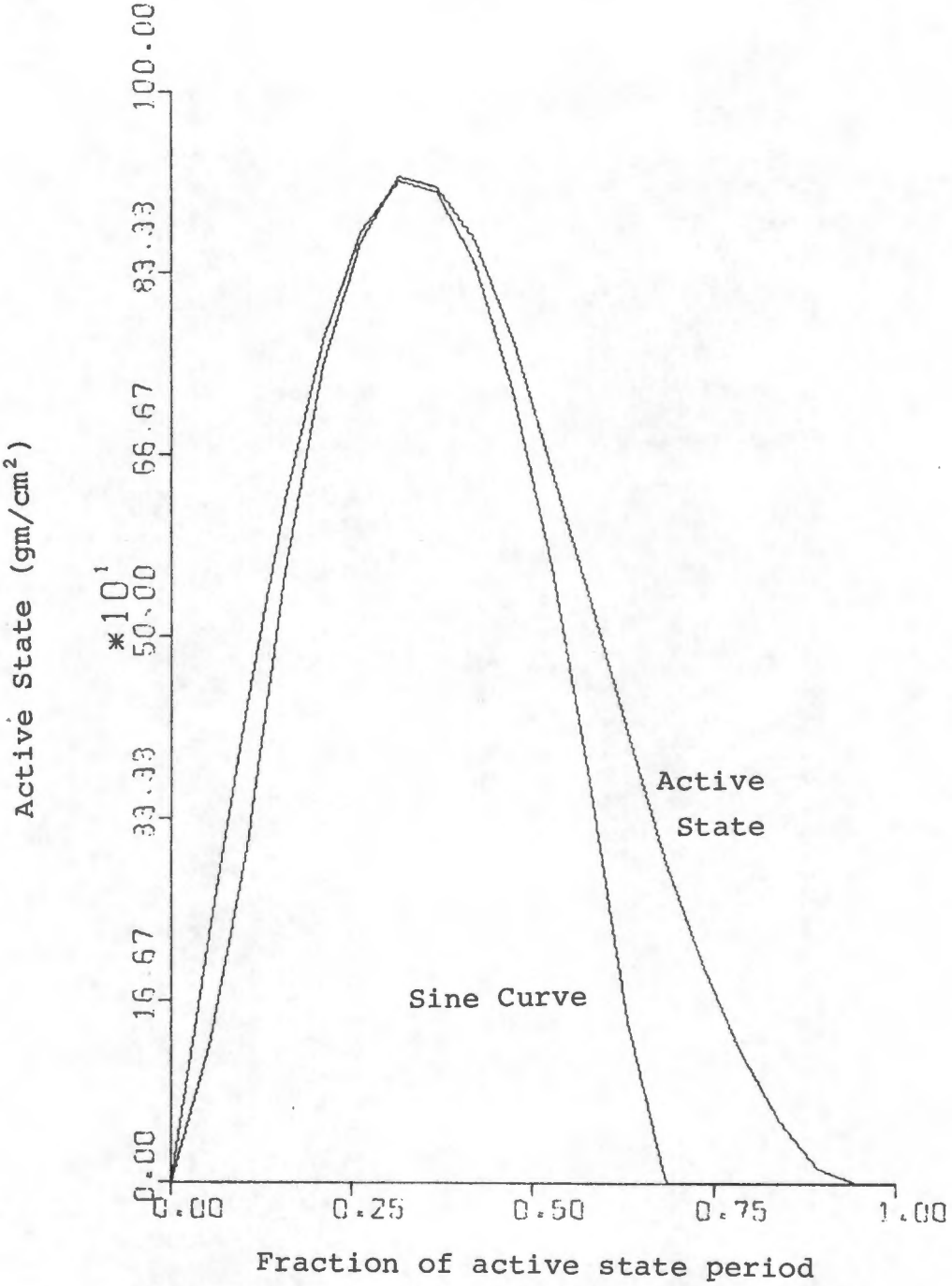

FIG. 4.19

THEORETICAL ACTIVE STATE CURVE
COMPARED WITH A SINE FUNCTION

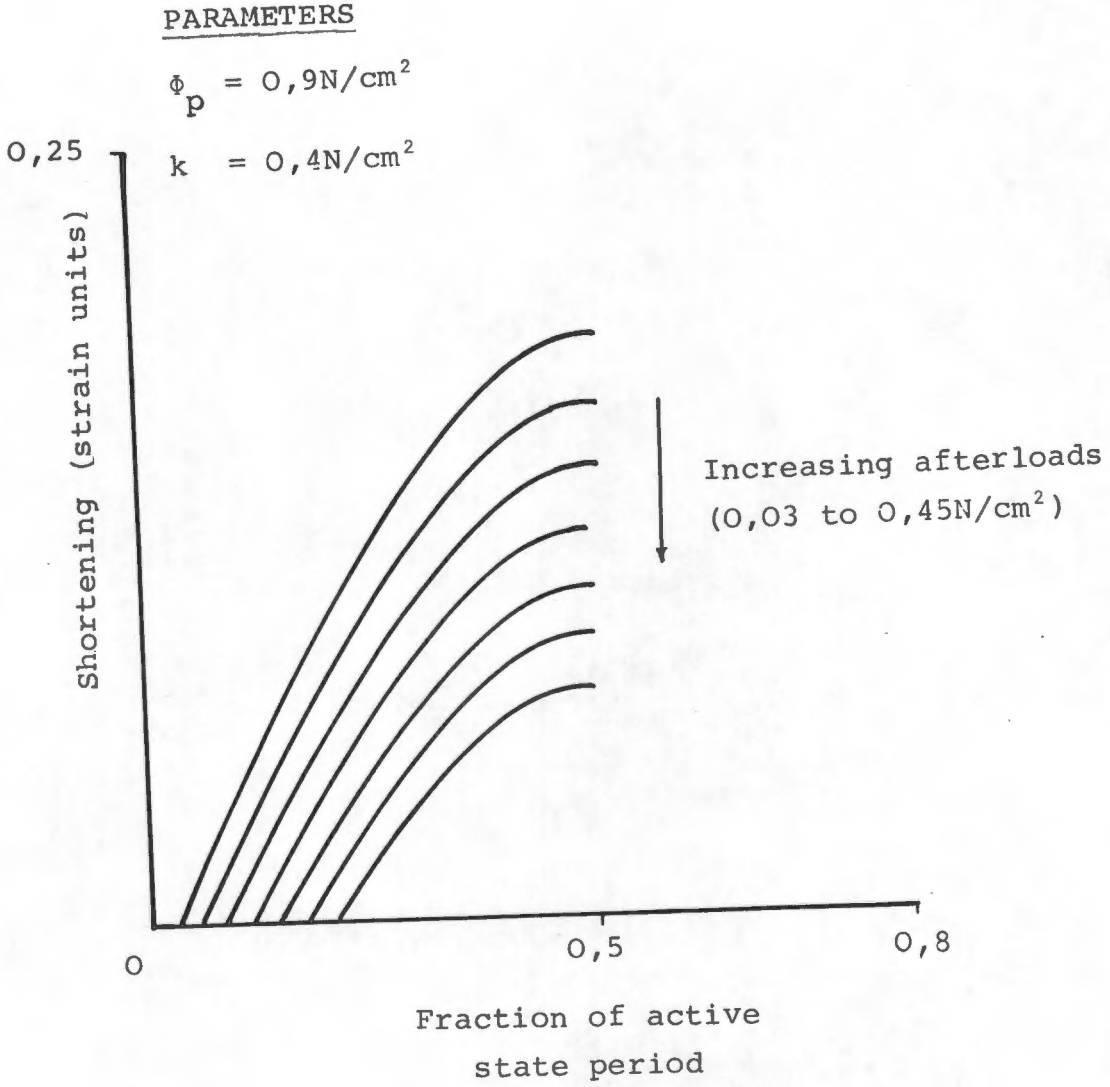

FIG. 4.20

ISOTONIC SHORTENING SIMULATIONS

reasonable agreement with the experimental data (for corresponding afterloads). These predictions are obtained by numerically solving equ. (4.3.2:11) for ε_{AA} at each time during the shortening phase of the contraction. No attempt is made to simulate the stretching phase as this does not occur in the left ventricle (except in the case of aortic valve incompetency).

Constant velocity shortenings are simulated in Fig. 4.21. These are obtained by setting the muscle at a given preload and allowing it to contract at a set velocity until the active state reaches its peak value. This constant velocity is simulated using equ. (4.3.2.10), ε_{AA} being computed as v.t where v is the velocity in strain units/second. These simulations in Fig. 4.21 reveal much the same characteristics as the experimentally obtained results in Fig. 4.12.

There are, however, two major failings in the model predictions involving muscle shortening. In a heavily afterloaded isotonic contraction shown in Fig. 4.6 the shortening tends to prolong the active state: the afterload is borne for a greater period than it would have been if the active state followed the isometric curve. Further, the peak shortening in isotonic contractions is reached after the peak force in an isometric contraction (see Section 4.1.2.2.1, parts (i) and (ii) for further discussion). Neither of these factors is predicted by this model since the active state is assumed to be in phase with the isometric contraction

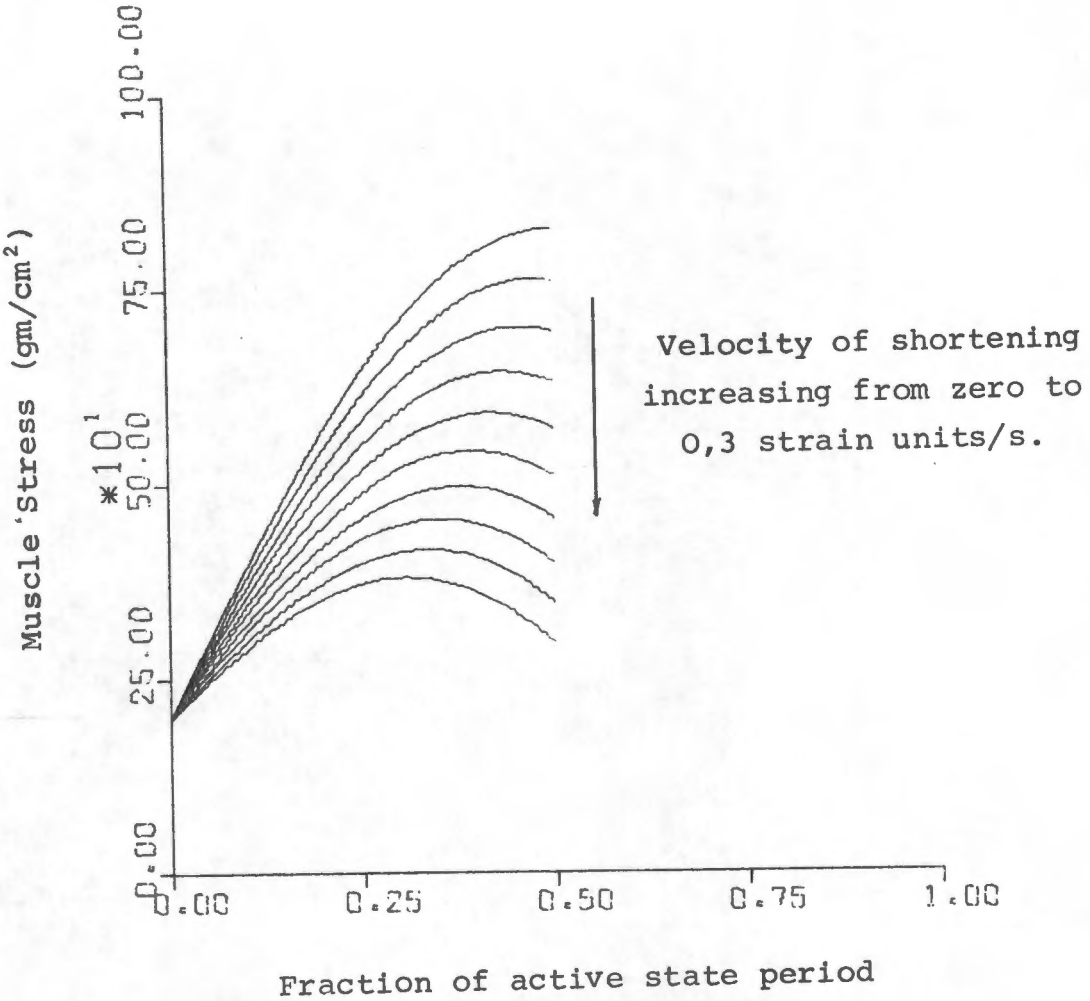

FIG. 4.21

CONSTANT VELOCITY OF SHORTENING
SIMULATIONS

Positive features of this model deserve further mention however.

4.3.4 Physiological Interpretation of the Model

Despite the shortcomings mentioned above in Section 4.3.3.4 the model does pose some considerable physiological possibilities which will now be discussed.

4.3.4.1 Relation to Calcium Kinetics

The basic proposition to be made is that the level of the AMP is proportional to the amount of the activating agent incorporated in cross-bridge formation in accordance with equ. (4.2.1:1): the concentration of bound Ca^{2+} is thus implicated in the "intensity" of the AMP.

This must be emphasised: in the classic experiments of Ridgway and Ashley (1967) the concentration of uncombined Calcium in the overlap region of the sarcomeres is monitored and not the concentration of combined Ca^{2+} (even if the reaction (4.2.1:1) is cyclic). The Ca^{2+} sensitive dye (aequorin) reacts with the Ca^{2+} as it diffuses from the longitudinal tubular system which surrounds the sarcomeres (Sections 3.1 and 4.2.1) to the cross-bridges and so naturally exhibits a peak before the isometric force peak. This helps solve the dilemma stated by Ridgway and Ashley: "..... the peak Calcium concentration occurs at a time when tension is no greater than 10% of its maximum value, hence there appears to be no simple relationship between ionized Calcium concentration and tension".

Expanding this proposition, the assumption is made that irreversible sequestration of the bound Ca^{2+} occurs when the muscle actively shortens so that it is no longer available for cross-bridge activation. If the muscle does not shorten the sequestration occurs in accordance with the decay of the active state.

These postulates are not without precedent. Kaufmann and his co-investigators have qualitatively proposed similar mechanisms regarding the effect of shortening on active state (Kaufmann et al., 1972; Tritthart et al., 1973). They were based on experimental evidence from QR, QS and QRQS experiments (see Sections 4.1.2.2.3 and 4.1.2.2.4). The model proposed herein does not simulate these experiments however, for reasons given in Section 4.2.6 - step changes are far removed from physiologically occurring conditions, which the model developed purports to simulate.

4.3.4.2 Relation to Muscle Energetics

A.V. Hill (1939) identified two components of heat production in activated muscle; maintenance heat (in an isometric contraction) and shortening heat (proportional to the extent of shortening) in an isotonic contraction (see Section 4.2.4).

Based on these observations it has been assumed that there is little ATP-ase activity, or splitting of ATP (the heat production being assumed proportional to ATP-ase activity), during isometric conditions and that excess ATP-ase activity occurs in proportion to the amount of shortening under

isotonic conditions. Interpreted in terms of the developed model, the ATP-ase activity occurs as a result of the sequestration of Ca^{2+} implying that there is an increased rate of cross-bridge formation (at which stage ATP-ase activity occurs in accordance with reaction (4.2.1:1)) under isotonic conditions. This is eminently reasonable as cross-bridges are cyclically formed and broken to allow contraction (the length of the cross-bridge << average isotonic shortening). There is limited experimental evidence for this (Takauji and Honig, 1972), but the propositions deserve further experimental study.

4.3.4.3 Examination of Hill's Force-Velocity Relation

If the effect of the PE element is for the moment ignored, the velocity of shortening is given by differentiating equ. (4.3.2:5) with respect to time and solving for CE shortening velocity $d\Delta/dt$ yielding:

$$\frac{d\Delta}{dt} = \frac{\Delta d\Phi/dt - d\sigma_c/dt}{2k\Delta - \Phi - k\Delta_i} \quad \ldots\ldots\ldots\ldots \quad (4.3.4.3:1)$$

Under isotonic conditions $d\sigma_c/dt = 0$ and so the CE velocity of shortening depends on the active state as well as its rate of change. This relation is not qualitatively obvious which explains the problems many researchers have faced in attempting to extract the meaning of active state from force-velocity relations. This does not mean to say that equ. (4.3.4.3:1) is correct; rather, the author has gleaned the meaning of active state from definitions in the literature, (Section 4.2.4.4) and then expressed them mathematically in a simple model (Section 4.3.2) which does not pretend to explain completely the

dynamics of cardiac muscle but which, for the first time, quantitatively incorporates newly expressed ideas.

It can readily be shown how V_{max}, the maximum velocity of shortening of the CE in isotonic contractions at zero load is affected by initial muscle length. Under these conditions $\sigma_c = 0$ and $\Delta = \Delta_i$ so equ. (4.3.4.3:1) becomes:

$$(d\Delta/dt)_{max} = (d\Phi/dt)/(k - \Phi/\Delta_i).$$

This equation reveals that V_{max} decreases as initial muscle length (or Δ_i) decreases: this agrees with the experimental findings on tetanised cardiac muscle (Forman et al., 1972).

A striking feature of equ. (4.3.4.3:1) is that the velocity of shortening is not explicitly dependent of the CE load σ_c but on its rate of change.

4.3.5 Cardiac Muscle Model Assessment

A model describing the behaviour of cardiac muscle under the general loading conditions occurring in the normal left ventricle has been developed. Its shortcomings (Section 4.3.3.3) result from the neglect of details of "second order importance" probably connected with the disruption of Ca^{2+} diffusion by sarcomere shortening. The model has also thrown new light on the concepts of active state and contractility: it has been shown that a newly defined term, "active muscle potential", becomes equal to the active state when the CE shortening is zero (equ. (4.3.2:4)). Further, the velocity of CE shortening has been shown to be related to rate of change of the AMP so that V_{max} is not a determinant of active state, but rather its rate of

change.

And most important, the muscle model is simple and so is readily applicable to a complex left ventricular model to be developed (Chapter 6). This development will forge what the author believes is the first really tenable link between cardiac muscle and left ventricular dynamics.

CHAPTER 5

SURVEY OF LEFT VENTRICULAR MODELLING

A hypothetical futuristic cardiac surgeon would be able, during the course of an operation, to interrogate an on-line computer-driven display for information on such factors as myocardial stress and the general tone (contractile or inotropic state) of the myocardium. The information would be based on continuously monitored left ventricular volume and pressure. This is the situation envisaged by Streeter (1970). It would, moreover be possible, based on this data, to gauge the degree and extent of myocardial damage as the result of disease.

What developments are necessary to achieve this futuristic state of affairs? The computer techniques and technology are available (Covvey et al., 1972; Andrews et al., 1972), but there is no currently accepted means of extracting the sort of information envisaged above from the measurements of left ventricular pressure (requiring catheterisation) and volume (which can be measured non-invasively).

The predictions of myocardial stress and contractile state depend on a theoretical relationship between left ventricular pressure and volume. It is the purpose of this Chapter to analyse the nature of the relationship required and to review the progress and improvements in its development. Shortcomings in the present stage of development will be discussed.

This review will bring into perspective the need for the development of a generalised and versatile left ventricular theoretical model.

5.1 STRESS IN THE LEFT VENTRICLE - ITS RELATION TO STRAIN AND GEOMETRY

Stress (force per unit area), strain (change in length per orginal length) and geometry are intimately linked through the stress-strain relation and the equilibrium equation of the system analysed. Considering the left ventricle, at a given time during a ventricular cycle it will have a certain shape, volume and internal pressure, these, for consistent conditions, being unique for that particular time.

To illustrate this uniqueness, suppose at this given time that a particular part of the ventricle had stretched slightly more than it should have (with a compensatory shortening elsewhere to maintain volume constant for the instant considered). The strain in the wall of the stretched section will consequently be greater; hence the wall stress will increase according to the stress-strain relation. But this disturbance will change the ventricular pressure of the fluid at this particular part of the wall. Since pressure should be the same in all parts of a fluid (Pascall's Law), the strain must decrease again to ensure equilibrium between the wall stresses and chamber pressure. The relation governing this interplay between wall stresses and strains and chamber pressure is the equilibrium equation.

The role of the equilibrium equation has been somewhat simplified above for it also incorporates the way wall curvature influences chamber pressure, a relation expressed in its basic form by Laplace's Law (see Section 5.3.1).

Thus the chamber shape and volume determines the strain distribution in the ventricular wall from which the stress distribution follows by use of the appropriate stress-strain relation. The equilibrium equation ensures that the shape is such that Pascall's Law is satisfied. However the equilibrium equation just described satisfies conditions only along a normal through the wall. The equations describing equilibrium in the two orthogonal directions in the plane of the wall must also be fulfilled.

So, in order to determine chamber shape the three equilibrium equations, describing conditions along three mutually perpendicular axes must be satisfied at each instant during the ventricular cycle. From the theoretical point of view, in order to be able to mathematically set up the equilibrium equations, assumptions must be made with regard to chamber shape (to reduce a complex geometry to a mathematically tractable one) and the ventricular wall stress-strain relation.

5.2 FACTORS IN LEFT VENTRICULAR MODELLING - DISCUSSION

Factors crucial in left ventricular modelling, namely chamber geometry and the stress-strain equation of the ventricular wall will now be discussed in more detail.

5.2.1 Ventricular Geometry

Single- and bi-plane angiocardiographic "in vivo" studies of both the human and canine left ventricle reveal that an ellipsoid of revolution is a good approximation to the shape of the cavity (Sandler, 1970). In man the shape can justifiably be further simplified to prolate spheroidal where the semi-minor

axes of the ellipsoid are equal (Greene et al., 1967; Sandler and Dodge, 1968).

The prolate spheroidal shape is truncated at the base by the presence of a fibrous, inelastic valvular ring which anchors the mitral (atrio-ventricular) valve and the aortic valve (Armour and Randall, 1970; Walls, 1972, p.851). This ring is assumed to be circular in shape.

Accurate "in vivo" measurement of ventricular wall thickness is difficult (Mitchell, et al., 1969; Sandler, 1970). Wall thickness varies both with time during a cardiac cycle and position in the ventricle. It is well known that the wall thickness is a minimum at the apex and increases towards the equator (Walls, 1972, p.849). The physical basis of this fact will become apparent later (Section 5.3.1).

The time variation of wall thickness depends on an additional factor, myocardial compressibility. Generally the myocardium can be regarded as incompressible (i.e. the total volume of ventricular muscle is constant) which is not surprising considering its high percentage water content (Baskin and Paolini, 1966).

Any disease causing impairment of muscle function will decrease stress production in the affected area and possibly cause a ventricular aneurysm. This term describes the bulging associated with the ventricular wall (Gould, 1960). The area of the aneurysm depends on its location and is usually smallest if situated at the ventricular apex. The diseased ventricle may therefore differ considerably in shape from the normal

prolate spheroidal (Gorlin et al., 1967).

A different condition may arise if the ventricle is overloaded which causes the wall to swell (hypertrophy) and there may be associated dilatation of the chamber (Gould, 1960). This condition is likely also to affect the shape of the ventricle as well as the dynamics of contraction (McDonald, 1972).

As outlined in Section 5.1, from the knowledge of ventricular geometry during a cardiac cycle, wall strain can be calculated.

5.2.2 Cardiac Muscle Fibre Elastic Properties

Inferences regarding the elastic properties of the myocardium can be made from the stress-strain relation (in both active and passive states, (see Chapter 4)) of isolated papillary muscle together with anatomical data on the fibre structure of the ventricular wall. Anatomically papillary muscles are cylindrically shaped projections from the apex region of the ventricular wall and functionally are strengthening struts for the atrio-ventricular valves (see Chapter 3).

Under passive conditions the muscle fibre is not Hookean, (stress is linearly related to strain in a Hookean material), but has been found to have a non-linear stress-strain relation which is exponential in form (Fung, 1967). Gou (1970) and Demiray (1972) have, by relating the strain energy density to the strain invariants, attempted to improve the theoretical basis of the non-linear relation. Demiray's model predictions are remarkably similar to the stress-strain relation of isolated papillary muscle (Sonnenblick, 1964).

There is some justification for assuming (as Fung, Gou and Demiray did) that relaxed papillary muscle is a homogeneous and isotropic elastic material if only that it simplifies the mathematical formulation. However, under active conditions (on stimulation of the muscle), the situation is completely transformed. The sliding filament theory of muscle (Huxley, 1957) which has been firmly established and applied to cardiac muscle, shows in effect that activated muscle fibre produces active force generating a stress vector in the axial direction parallel to actin and myosin filaments (Braunwald, et al., 1968). This swamps the stress contribution of the passive elasticity. Hence the elastic properties of the fibre become markedly anisotropic under active conditions and they are time-varying as shown by the stress-time relation of activated papillary muscle (Chapter 4).

These elastic characteristics of the myocardial fibre can be obtained from "in vitro" papillary muscles in which the muscle fibres are assumed to be parallel and elastically identical. It is now possible to assess the elastic character of the myocardial wall of which the muscle fibre is the building block.

5.2.3 The Elastic Properties of the Myocardium

Detailed anatomical investigation of the canine left ventricle has exposed a certain degree of order in the distribution of fibres in the ventricular wall. Streeter et al., (1969) found by measuring fibre directions with respect to a fixed axis in the canine left ventricle, the Left Aortic Valve Commissure-Apex axis, that the fibre angle of twist about a normal through the wall was roughly parabolic in distribtion varying from 60° to 70° at the endocardium (inner surface) to 0° (circumferential)

at the midwall and back to -60^{o} or -70^{o} at the epicardium (outer surface). Similar distributions were found at other points examined in the left ventricular free wall making mathematical fitting of ventricular fibre orientation data possible (Mirsky, 1970; Voukydis, 1972a). This was supported by subsequent work (Armour and Randall, 1970). The burrowing effect (Olsen, 1962, p.200) is considered negligible.

Strongly suggested by Streeter's investigations is the fact that the myocardium can be considered as a laminated material, the fibre direction and hence the direction of the "anisotropic axis" (discussed in Section 5.2.2; also see Apprendix B, Section 5.4) being fixed in any given lamina. Anatomically fibers are not single and continuous; they are discontinuous and may branch considerably (Grant, 1965). Nevertheless, it is analytically expedient to assume that the ventricular wall is made up from layers parallel to the epi- or endocardium, successive layers being connected by inert connective tissue and that fibres describe courses on each layer (or surface) in accordance with Streeter's data.

Thus the anisotropic character of the ventricular wall is clearly evident.

The question of nonhomogeneity in the myocardium is intriguing. There seems no reason to suppose that fibre to fibre elastic properties in the wall vary (ignoring for the moment the different state of activity of fibres during systole caused by the finite velocity of action potential propagation) implying that the myocardium is homogeneous (see Appendix B, Sections 5.3 and 5.4). However the presence of connective tissue

between layers and also between fibres on a given layer imposes the condition that discrete periodic variations in elastic properties occur as one moves from one layer to the next and similarly from one fibre to the next on a given layer. Hence the nonhomogeneity arises from structural considerations as illustrated in Fig. 5.1, a diagram of the idealised model described. But, as already mentioned, considerable fibre cross-branching occurs and this would tend to homogenise the structure.

Space-time variation of elastic properties of muscle fibres is imposed by the finite velocity of propagation of the action potential (which triggers contraction). This effect, a time dependent non-homogeneity, would be most marked at the early stages of contraction. It has been shown that excitation spreads from the ventricular apex, (th sub-endocardial layers of which are the first to be activated), more rapidly in the lateral than the transverse mural direction. The excitation wave front consequently tends to move transversely through the wall so that the epicardial layers are activated later than the endocardial, the basal epicardial portion of the wall being the last activated (Scher, 1962). The time taken to activate the whole ventricle is typically 15 to 20 per cent of left ventricular systole.

Further complications arise in the attempt to assess the initial conditions for the fibre-to-fibre strain distribution (such as at end diastole). Data provided by Sponitz et al. (1966) suggests that strain distribution tends to become uniform at low ventricular volume, though recent results have not corroborated this (Monroe et al., 1970).

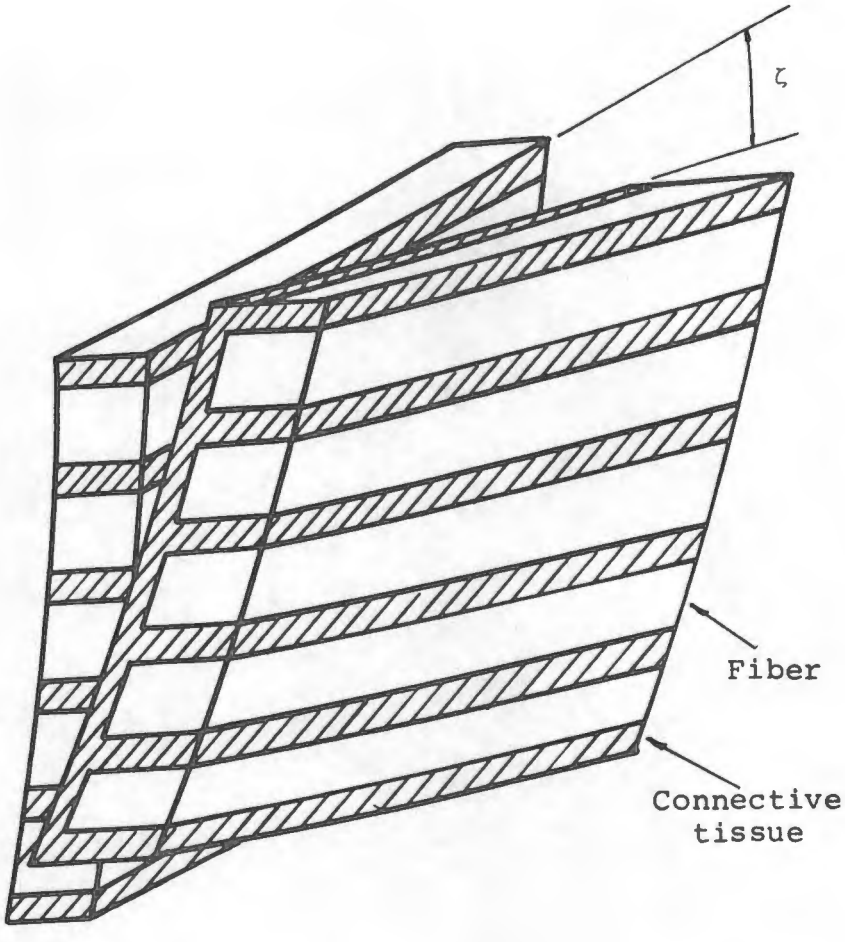

FIG. 5.1

ELEMENT OF MYOCARDIUM SHOWING FIBRE TWIST AND THE RELATION BETWEEN FIBRE AND CONNECTIVE TISSUE.

The myocardium is therefore anisotropic because of fibre properties and non-homogeneous on both structural and electro-mechanical grounds. Although the above observations were, in the main, made on the canine heart, the principles are also applicable to the human heart (Grant, 1965).

5.2.4 Myocardial Fibre Density

Active myocardial stress originates in the actin and myosin overlap regions of the sarcomeres (Braunwald et al., 1968) and so the potential for active stress production depends on the local sarcomere density (number of sarcomeres per unit area normal to sarcomere direction). The through-wall variation of this weighting factor is obviously important in analysing myocardial stress and has been only recently recognised (Hadingham, 1971). There is, however, no quantitative literature data available for this factor, though it is known that the outer layers of the ventricular wall comprise more densely packed fibres than the inner. The important point is that myocardial stress must be related to the number of fibres in the wall cross-section rather than the force per cross-sectional area (Burton, 1957; Falsetti et al., 1970).

Under conditions of ventricular wall swelling (hypertrophy) caused by overloading, the fibres swell initially with no increase in the quantity of contractile protein. After a delay (of the order of weeks) however, the concentration of contractile proteins is restored to normal (Meerson, 1969, pp. 115-117). Therefore, other conditions being equal, active myocardial stress first decreases (in sympathy with the decrease in the number of contractile proteins per unit area normal to the fibre direction) and then gradually returns

to normal.

5.2.5 Other Factors

Two further factors must be considered in left ventricular analysis.

(i) The loading of the ventricle: chamber pressure which acts normal to the surface is invariably considered the only internal loading factor. Epicardial loading is usually considered as a constant pressure, the pericardial pressure which is normally atmospheric. However in the ventricular septal area, the left ventricular external loading will be the time-varying right ventricular pressure. This time-varying factor is generally ignored.

(ii) The inertia of the ventricular wall: the force as a result of this is negligible compared to the wall and loading forces and so can be neglected. Hence, quasi-static analysis is justified.

5.3 LEFT VENTRICULAR MODELLING SURVEY

It was Woods (1892) who first used Laplace's Law to investigate the mechanical properties of the left ventricle. Since then, particularly within the last decade, this simple model has been found wanting as cardiologists come to seek more detailed, accurate and physiologically significant information from their measurements. This has stimulated theorists to evolve models of increasing complexity and versatility.

5.3.1 Development of Left Ventricular Modelling

Using Laplace's Law, Burton (1957) stated some important and persuasive facts regarding the left ventricle. In its general

form, Laplace's Law can be written:

$$P_v = T \left(\frac{1}{R_\theta} + \frac{1}{R_\phi}\right) \quad \ldots\ldots\ldots\ldots\ldots\ldots\ldots\ldots \quad (5.3.1:1)$$

where P_v = ventricular pressure,

R_θ, R_ϕ = the principal radii of curvature

and T = the wall tension.

At a given pressure, then, there is a proportional relation between wall tension and radius of curvature, so as the radius of curvature increases (as the ventricle dilates and also at the equatorial region compared to the apex), the wall tension increases. Burton was thus able to explain phenomena such as the thickening of the wall from apex to equator.

Better assumptions regarding the geometry of the ventricle were made by Wong and Rautaharju (1968). From their thick-walled ellipsoidal model (see Table 5.1, to which reference is implied for the remainder of this Section) they were able to generate stress profiles through the wall thus locating regions of maximum and minimum stress in the myocardium. Mirsky (1969) improved on Wong and Rautaharju's model by including transverse shear stresses in his formulation.

Important improvements were made by Mirsky (1970) and Streeter et al. (1970) who incorporated anatomical data on fibre orientation in the myocardium (Streeter, 1969) into their models (see Section 5.2.3). This was a major step in bringing ventricular modelling closer to physiological and anatomical reality. These models did not however incorporate transverse shear stresses and bending moments.

TABLE 5.1

COMPARISON OF PUBLISHED LEFT VENTRICULAR MODELS

AUTHORS	SHAPE	NORMAL WALL THICKNESS	ELASTIC CHARACTER	DISPLACEMENT	STRESS ASSUMPTIONS	DIASTOLE OR SYSTOLE	THEORY AND SOLUTION
Wong and Rautaharju (1968)	Prolate spheroid No AV ring.	Decreasing from Apex	Hooke's Law, Isotropic, homogeneous, incompressible.	Along radius of curvature.	Circumferential and meridional only. Shear and transverse ignored.	Both.	Only radial equilibrium. Analytic.
Mirsky (1969)	Prolate spheroid No AV ring.	Constant	Hooke's Law. Isotropic, homogeneous, incompressible.	Unrestricted.	Transverse shear, normal stresses as well as bending. Independent of circumferential co-ordinate.	Both.	Shell theory. Analytic approximate.
Vayo (1967 and 1970)	Prolate spheroid No AV ring.	Constant	Isotropic, homogeneous, incompressible layers, 3 differently oriented fiber layers. Used elastic potentials.	In planes normal to major axis.	Attempt to incorporate fiber distribution: 3 untethered concentric layers; applied Laplace's law to each. Ignored transverse shear, normal and bending stresses.	Both. Fourier series periodic representation.	Laplace's Law. Analytic.
Ghista and Sandler (1969), Ghista and Vayo(1969)	Resembles prolate spheroid No AV ring.	Increasing from Apex	Isotropic, homogeneous, incompressible, Hooke's law and visco-elastic formulations.	Uniform dilatation about a line.	Transverse normal, but not shear stresses. Shape defined by shear-free surfaces produced by line dilatation.	Diastole. (See Gould, et al.1972)	Analytic.
Mirsky (1970)	Prolate spheroid No AV ring.	Constant	Isotropic, homogeneous, incompressible. Stress equilibrium only. Incorporated fiber orientation data, (but see Hadingham (1971)).	Along radius of curvature.	Bending moments and shear stresses neglected. Independent of circumferential co-ordinate.	Both.	Only radial equilibrium. Analytical.
Streeter (1970)	Prolate spheroid AV ring.	Increasing from Apex	Incorporated fiber orientation data. Fiber properties used directly: diastole - constant across wall thickness, systole - used papillary muscle data.	Along radius of curvature.	Bending and transverse shearing stresses neglected.	Both (but only peak systolic pressure).	Numerical.

TABLE 5.1 (Continued)

AUTHORS	SHAPE	NORMAL WALL THICKNESS	ELASTIC CHARACTER	DISPLACEMENT	STRESS ASSUMPTIONS	DIASTOLE OR SYSTOLE	THEORY AND SOLUTION
Hadingham (1971)	Sphere. No AV ring.	Constant	Anisotropic, non-homogeneous, incompressible. Active elasticity given by suitably scaled (temporally and in magnitude) papillary muscle isotonic curves (Sonnenblick 1962). Fiber orientation data incorporated.	Along radius of curvature.	Circumferential and meridional only. Transverse shear ignored.	Systole.	Only radial equilibrium. Numerical.
Wong and Rautaharju (1971)	Prolate spheroid AV ring.	Increasing from Apex	Isotropic, homogeneous, incompressible. Fung's (1967) nonlinear stress-strain relation.	Along radius of curvature.	Circumferential and meridional only. Transverse shear ignored.	Diastole.	Similar to their (1968) model.
Voukydis (1969, 1970 and 1972)	Shell of revolution (axial symmetry). AV ring.	Increasing from Apex.	Anisotropic, non-homogeneous (orthotropic). Fiber orientation considered.	General, but axisymmetric.	All bending, shear and normal stresses considered.	Applicable to both.	Shell theory, Numerical: (nonlinear DE's).
Gould et al (1972)	General (but see text, Section 4.2). AV ring.	Constant	Not specified. Potential for inclusion of effect of fiber orientation.	General (see text).	All bending, shear and normal stresses considered.	Diastole (but, with fiber properties, also in systole).	Finite element analysis. Numerical.
Janz and Grimm (1972)	General, Axisymmetric. AV ring.	Increasing from Apex.	Hooke's law, non-homogeneous and Transversely isotropic. Also considered homogeneous case.	General, but axisymmetric.	All relevant stresses considered.	Diastole.	Finite element analysis. Numerical.

In a remarkably comprehensive series of papers, Voukydis (1969, 1970a, 1970b, 1972a, 1972b, 1972c) has mathematically investigated all major facets of left ventricular chamber geometry, fibre geometry and myocardial elastic characteristics. This has culminated in the formulation of equilibrium differential equations for the left ventricle, incorporating bending moments and normal as well as transverse shear stresses (Voukydis, 1972a). The midwall left ventricular shape is assumed to be an axisymmetric surface of revolution with wall thickness increasing from apex to equator. Anisotropic and non-homogeneous elastic characteristics are assigned to individual muscle fibres whose orientations, given by helices with pitch angles dependent on wall thickness, are mathematically related to spatial co-ordinates. Myocardial elastic characteristics are therefore described in a similar way to the method discussed in Section 5.2.3. No computer solutions for this model (Voukydis, 1972a) have yet been published, however.

A further generalisation of left ventricular shape was made by Gould et al. (1972) in his analysis. Cineangiographic left ventricular outlines were divided by a longitudinal axis into two portions and the axisymmetric shells of revolution formed by rotating the meridian or outline in each portion about this axis were separately analysed. Both Gould et al. (1972) and Janz and Grimm (1972) employed the finite element technique (Desai and Abel, 1972) for the development and solution of their models.

The progress made in left ventricular modelling has been presented. Despite the advances, shortcomings are still very

evident, principally:

(i) no model has the capability of using a generalised shape to simulate, for instance, a ventricular aneurysm.

(ii) The elastic character of the myocardium has not been rigorously formulated using the constitutive character of the muscle fibre as a basis, particulary under active state conditions.

(iii) No explicit account has been taken of the non-homogeneities introduced by the finite velocity of propagation of cardiac activity. The implications of this were qualitatively discussed in Section 5.2.3.

5.3.2 Features of Models

The most important predictions made by thick-walled ventricular models are the through-wall stress profiles. This data yields information about stress concentrations and the general distribution of stress within the myocardial wall. Provided the model is adequate, this knowledge represents an important diagnostic aid. Model adequacy depends on the efficacy of the assumptions made: these assumptions have been discussed above (Sections 5.2 and 5.3.1).

Pertinent features of through-wall stress profiles predicted by proposed models have been tabulated (Table 5.2). Two extreme geometrical locations, the equator and apex, have been considered for each proposed model. At each location, the variation of the three orthogonal normal stresses; radial, meridional (or longitudinal) and circumferential (or latitudinal) from endo- to epicardium have been tabulated (except in cases where the authors did not provide profiles).

TABLE 2 - VENTRICULAR STRESS PROFILE PREDICTIONS

PROFILE KEY

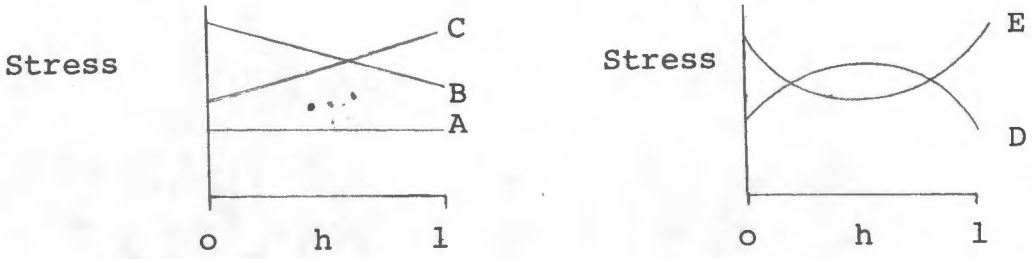

AUTHORS	σ_{rr}		σ_{circum}		σ_{merid}	
	Equ.	Apex	Equ.	Apex	Equ.	Apex
Wong and Rautaharju (1968)	B	B	B	B	A	B
Mirsky (1969)	B	B	B	B	C	B
Ghista and Sandler (1969) and Ghista and Vayo (1969).	-	-	B	B	B	B
Mirsky (1970) *	-	-	D	D	D	D
Streeter (1970)	B	B	D	D	E	E
Hadingham (1971)	B	B	D	D	E	E
Gould et al. (1972)	-	-	B/C†	B/C†	B/C†	B/C†
Voukydis (1972c)	See Text					

*see Hadingham (1971).

†B/C - for concave inward and convex inward ventricular wall curvature respectively.

Notes: (i) σ_{rr}, σ_{circum} and σ_{merid} are the radial, circumferential and meridional stresses respectively.

(ii) Equ. and Apex refer respectively to stresses at the equator and apex.

(iii) h is the fractional wall thickness from the endocardium.

The striking fact emerging (qualitatively) from Table 5.2 is that by including the anatomical fibre orientation data, the shapes of the circumferential and meridional stress distributions are completely changed; furthermore, the peak stresses are greater. (For instance, compare Mirsky (1969) with Streeter et al.(1970). This is direct and compelling evidence in favour of incorporating the anisotropic nature of the myocardium in any model, particularly during systole. Models such as those developed by Mirsky (1969) and Ghista and Sandler (1969) should therefore only be used during diastole. However, in the models of Gould et al. (1972) and Janz and Grimm (1972), it is possible to use an appropriate anisotropic constitutive relation for the myocardium in order to simulate left ventricular systole. (see Sections 5.2.2 and 5.2.3).

In an extension of an earlier paper (Voukydis, 1970b), Voukydis (1972c) presented diastolic stress profiles which accounted both for fibre orientation and for the increasing wall thickness from base to equator. An interesting finding was the peaking of stress at the apex in contrast to Voukydis' earlier predictions and those by Wong and Rautaharju (1968) as well as Mirsky (1969) where maximum stress was found to occur at the equator.

Employing a more accurate shape representation than the assumption of ellipsoidal geometry used by Voukydis, Gould et al. (1972) were able to demonstrate the effect of local shape on through-wall stress distribution. As the curvature changed from concave inward to convex inward, so the peak stress moved from the endocardial (inside) to the epicardial (outside)

surface as shown in Table 5.2. Fibre distribution data was not used in this model. Nevertheless, the same general shift of peak stress should result if the effects of fibre distribution were accounted for.

These two new quantitative results: the peaking of apical stress (Voukydis, 1972c) and the shift of peak stress with changes in curvature sign (Gould et al. 1972) lend powerful support to the principle of incorporating as much accepted anatomical, geometrical and physiological data as practicable in left ventricular model development. The benefits of such inclusions have been clearly demonstrated.

5.3.3 Comparison Between Predicted and Measured Ventricular Wall Stresses

Considerable practical difficulties are encountered in the direct measurement of ventricular wall stresses. Transmural auxotonic strain gauges were used for this purpose (Feigl et al., 1967). The principal difficulty was the assessment of the efficacy of the coupling between the gauge and the ventricular wall. Controlled experimentation by Burns et al. (1971) using isolated ventricular strips revealed their coupling to be adequate.

It is possible to measure and compare average wall stresses only, but based on their measurements, Burns et al. were able to show that ellipsoidal geometry yielded average stresses in closest agreement with measured values. Nevertheless, the thin-walled ellipsoidal model they employed generally over-estimated left ventricular stress (compared to experimentally measured stress). It has however been shown that a thin-walled

model predicts stresses greater than those given by the equivalent more complicated thick-walled representation, under the same conditions (Sandler and Ghista, 1969). This justifies the use of the more complex model which is supported by the close agreement Streeter found between stress predictions based on his thick-walled model and directly measured data (Streeter et al., 1970).

Comparison of experimentally measured intra-myocardial pressure (Johnson and Di Palma, 1939; Salisbury et al., 1962) with that predicted by ventricular models is hazardous. There is no certainty what the experimentalist is measuring; for if the pressure probe happens to lie between two fibres, the radial stress will be sensed as the detected pressure. On the other hand, if the pressure probe severs a fibre, the resultant fluid pressure it will sense will be the difference between the active fibre stress (the fibres pull and therefore produce negative pressure) and the radial stress. Since the fibre stresses are greater than the radial stresses, the resultant pressure sensed should be negative. These represent the two possible extremes or ideals and makes the interpretation of the finding that maximum intra-myocardial stress in excess of maximum left ventricular pressure occurs (Kreuzer and Schoeppe, 1963; Armour and Randall, 1971) very difficult. One suggested explanation has been that fibres with negative curvature exist either in the natural physiological state (Gay and Johnson, 1967) or because of the presence of the pressure sensor (Streeter et al., 1970).

However, despite the difficulties outlined, the experimental through-wall pressure distribution is nonlinear, decreasing

from endo- to epicardium, and so is in broad qualitative agreement with the radial stress distributions predicted by thick-walled models.

5.3.4 Use of Left Ventricular Models

From experimental measurements on isolated "in vitro" papillary muscle, a quantity, independent of the load on the muscle and therefore relating to its basic functional efficacy was determined. It was, in fact, the maximum velocity of shortening, V_{max}, of the contractile element (from Hill's three-component muscle model) of the muscle (Braunwald et al., 1968).

In order to extract this quantity for the intact "in vivo" left ventricle based on the available experimental measurements, (left ventricular pressure and volume) a relationship describing the interdependence of muscle fibre length, ventricular volume and shape and pressure was necessary. This, in effect, involved mathematically modelling the left ventricle.

Thin-walled (Fry et al., 1964) and thick-walled (Urschel et al., 1968) spheres have been used as models. Some limitations of these models (as discussed in Sections 5.3.1 and 5.3.2) have been obviated by using Mirsky's (1969) thick-walled ellipsoidal representation of the left ventricle (Hugenholtz et al., 1970; Mirsky et al., 1971). The clinical value of the results obtained using Mirsky's model is encouraging despite the effect on them of the inherent shortcomings of his analysis with regard to myocardial elasticity assumptions during systole.

The stage is therefore set for the clinical application of a physiologically sounder model based on known fibre geometry and

myocardial elasticity characteristics.

5.3.5 Evaluation of Left Ventricular Modelling

A model is no better than the assumptions made and implied in its derivation. This is the basic theme of Noble's critical and uninhibited editorial on the practical application of muscle and ventricular models (Noble, 1972). Recent developments in left ventricular modelling have removed the basis for some of Noble's criticisms but, as pointed out in Section 5.3.1, several complex problems remain to be solved.

The need for large computing facilities to handle the sophisticated models is in phase with the trend toward the computer orientation of hospital operation and so should not be an inhibitory factor in their use.

Perhaps the major obstacle to the use of left ventricular models is the uncertainty of the applicability of the data provided.

At present this data is almost invariably interpreted in terms of parameters associated with the dynamics of isolated muscle fibre and there is by no means unanimity as regards the meaning of these parameters (Pollack, 1970). Apart from their use for the calculation of myocardial stress, the application of mathematical left ventricular models as aids in diagnosis will therefore go hand in hand with improvements in the understanding of the mechanism of muscular contraction. (See Chapter 4).

CHAPTER 6

DEVELOPMENT OF A GENERALISED LEFT VENTRICULAR MODEL

In Section 5.3.1 the major shortcomings in ventricular modelling were listed. They involved the generalisation of ventricular shape, the formulation of the myocardial elastic character and the need to allow for the finite velocity of propagation of the action potential in the myocardium.

A model is now proposed in which all of these factors are explicity invoked.

The non-axisymmetric structure of the left ventricle is simulated by letting the semi-minor axis of the prolate spheroid (whose major axis is equal in length to that of the left ventricle) depend on position in such a way that the resultant shape possesses a plane of symmetry. Further, to allow for possible areas of myocardial weakness the associated bulging can be simulated by imposing a 3-dimensional normal distribution on the modified prolate spheroidal geometry. Although this scheme does not provide a complete generalisation of ventricular geometry, it certainly caters for most contingencies (Section 5.2.1).

The cardiac muscle fibre is regarded as being transversely isotropic (see Appendix B, Section 5.3). This means the elastic constants in one plane are independent of orientation in that plane but in a direction orthogonal to it (that is, the axial fibre direction), they are different. Time-varying fibre properties following stimulation

therefore manifest themselves as time-varying elastic constants in the anisotropic axis (Chapter 4). The use of anatomical data on fibre distribution in the myocardium together with these assumptions regarding fibre elasticity makes the description of myocardial elastic character possible in the manner described in Section 5.2.3. Furthermore, a space variation at a given time in the values of the anisotropic axis elastic constants can be used to simulate the space-time effect of the spread of action potential.

The mathematical development of the model is necessarily complex. The derivations rely heavily on concepts from tensor calculus and 3-dimensional differential geometry, subjects which provide remarkably succinct ways of expressing important physical and geometric relationships. Relevant theory is covered in Appendix A. Shell theory is used to set up the stress-strain relationship of the myocardium: the reference shell is the locus of the bisector of the normal myocardial wall thickness, which is fitted to the geometry described above.

Each aspect of the model derivation; geometry, fibre distribution, fibre and myocardial elastic properties, the myocardial stress-strain relation and the equilibrium equation will be presented in this Chapter.

6.1 Left Ventricular Geometry

Fig. 6.1 is a reproduction of a typical left ventricular angiogram. It is clear that the shape is not

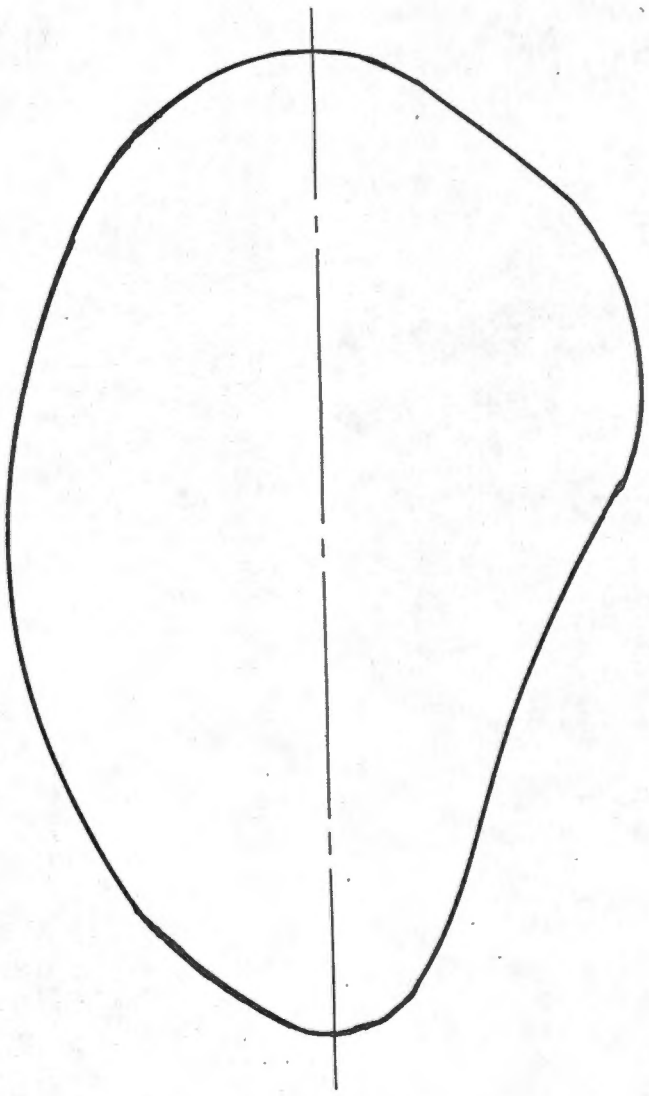

FIG. 6.1

NORMAL LEFT VENTRICULAR SHAPE

axisymmetric: on one side of the axis in the plane viewed, it is roughly elliptical, whereas on the other side there is a "tapering" effect towards the apex.

A shape representation accounting for these features, as well as possible bulges caused by areas of weakened myocardial wall is developed using prolate spheroidal geometry as a basis.

6.1.1 Non-Axisymmetric Shape Simulation

The polar representation (ρ,η,ξ) of a prolate spheroid is given by (see Mirsky (1969)):

$$\rho_o = \sqrt{(a^2 \cos^2\eta + b^2 \sin^2\eta)}, \quad \ldots\ldots\ldots\ldots \quad (6.1.1:1)$$

for $0 \leq \eta \leq \pi$

$0 \leq \xi \leq 2\pi$

where ρ_o = the magnitude of the position vector of the prolate spheroid,

a = the length of the semi-major and

b = the length of the semi-minor axis.

In order to simulate the elliptical left ventricular outline in the half-plane: $0 \leq \eta \leq \pi$; $\xi = 0$, and the tapered shape in the half-plane: $0 < \eta < \pi$; $\xi = \pi$, the semi-major a and semi-minor b axes are each allowed to be parabolic functions of η and ξ in such a way that the plane of symmetry is preserved.

The semi-minor axis variation will have the most marked influence of shape in the region of $\eta = \pi/2$ and the

variation in the semi-major axis towards the poles of the prolate spheroid. With these factors in mind and using the conditions (imposed by the plane of symmetry) for the a symmetrical outline (in the latter plane defined above):

for $\xi = \pi$; $\partial a/\partial \xi = \partial a/\partial \eta = \partial b/\partial \xi = \partial b/\partial \eta = 0$

and for $\eta = \pi$; $\partial a/\partial \eta = 0$,

the parabolic space variations in a and b are given by:

$$a(\xi,\eta) = a_o + (a_o - a_v)(\pi/2 - 2)(\xi/\pi) \ldots \quad (6.1.1:2)$$

where $a_v = (4a_1 - 3a_o) + 4(a_o - a_1)(2 - \eta/\pi)(\eta/\pi)$

$\ldots\ldots$ (6.1.1:3)

and

$$b(\eta,\xi) = b_o + \eta\xi\ (16/3\pi^2)(b_1 - b_o)(1 - \eta/2\pi) \times (1 - \xi/2\pi), \quad \ldots\ldots\ldots\ldots\ldots \quad (6.1.1:4)$$

where a_o = the value of a for $0<\eta<\pi/2$, $\xi=\pi$ and at $\eta=\pi$,

a_1 = the value of a at $\eta=\pi/2$, $\eta=\pi$,

b_o = the value of b in the half plane:

$\xi=0$, $0 \leq \eta \leq \pi$

and b_1 = the value of b at $\xi=\pi$, $\eta=\pi/2$.

Thus the space variation of a is effective only for $0<\eta<\pi/2$ and that of b in the region $\eta=\pi/2$. The simple derivations of equs (6.1.1:2) through (6.1.1:4) are given in Section 1 of Appendix C.

Substituting these values for a and b in equ. (6.1.1:1), the modified prolate spheroid becomes:

$$\rho_m = \sqrt{\{a(\eta,\xi)^2 \cos^2\eta + b(\eta,\xi)^2 \sin^2\eta\}} \ldots \quad (6.1.1:4)$$

and this shape representation possesses symmetry about the required plane.

An example of this shape simulation is shown in Fig. 6.2 and it compares very favourably with the angiographic outline of the normal left ventricle (Fig. 6.1; refer also to Section 5.2.1).

6.1.2 Simulation of Ventricular Aneurysm

A left ventricular aneurysm (or incipient aneurysm caused by wall weaknesses small in area) can be simulated by imposing a 3-dimensional normal distribution type function (representing a bulge) on the modified prolate spheroidal geometry. The bulge formula is accordingly given by a modified form of the normal distribution function:

$$\rho_b = H_b \exp\{-\tfrac{1}{2}(\tilde{\alpha}\sqrt{(2 \ln X)}/\pi C_2)\}^2 \times \exp\{-\tfrac{1}{2}(\tilde{\beta}\sqrt{(2 \ln X)}/\pi C_3)\}^2 \quad \ldots (6.1.2:1)$$

where H_b = the peak height of the bulge,

C_2, C_3 = parameters controlling the extent of the bulge in the η and ξ directions respectively,

$\tilde{\alpha} = (\tilde{\eta} - \pi/2)/C_2$

and $\tilde{\beta} = \xi/C_3$, the tildas referring to axes rotated from $\eta = 0$

by $\nu = (\pi/2 - \eta_b)$ in the symmetrical plane of the shape representation,

η_b = the position of the bulge (given as an angle from $\eta = 0$ in the symmetrical plane)

and X = the parameter controlling the height of the bulge as a fraction of H_b when $\tilde{\alpha}$ and $\tilde{\beta} = \pi$. It controls the rate of exponential decay.

PARAMETERS

$a = 1.0$

$b_0 = 0.7$

$b_1 = 0.6$

$H_b = 0.0$

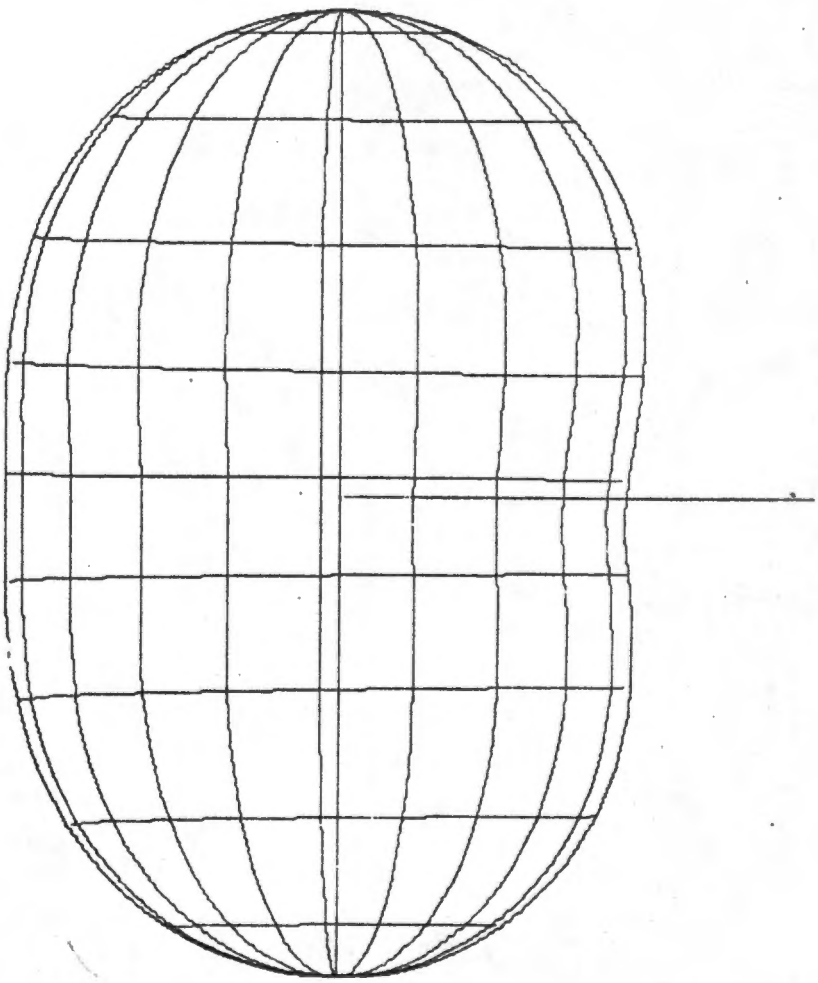

FIG. 6.2

SIMULATION OF NORMAL LEFT VENTRICULAR SHAPE

The transformation of surface co-ordinates from (η,ξ) to $(\tilde{\eta},\tilde{\xi})$ referred to above is necessary to minimise the effect of spherical distortion of the bulge in the circumferential direction. For instance, for values of η_b approaching 0 or π, the bulge would tend to become ridge-shaped if the transformation were not used.

The reason for this tendency is that arc length s_ξ on the surface in the ξ direction for a given $\Delta\xi$ depends on η:

$$s_\xi = \rho\Delta\xi \sin\eta$$

so that C_3 is not a constant but a function of η. This dependency is minimised by transforming the spherical co-ordinates in such a way that the peak bulge height is positioned at $\tilde{\eta} = \pi/2$, $\tilde{\xi} = 0$.

The required transformations are:

(i) from surface (ρ,η,ξ) to rectangular cartesian;

$$x = \rho \sin\eta \cos\xi$$
$$y = \rho \sin\eta \sin\xi$$
$$z = \rho \cos\eta, \quad \ldots\ldots\ldots\ldots\ldots\ldots \quad (6.1.2:2)$$

(ii) rotation in the plane of symmetry (i.e. about the y-axis) by an angle ν;

$$\tilde{x} = x \cos\nu + z \sin\nu$$
$$\tilde{y} = y$$
$$\tilde{z} = -x \sin\nu + z \cos\nu, \quad \ldots\ldots\ldots\ldots \quad (6.1.2:3)$$

(iii) from the rotated rectangular to the new surface co-ordinates;

$$\tilde{\xi} = \arctan(\tilde{y}/\tilde{x})$$
$$\tilde{\alpha} = \arccos(\tilde{z}/\rho) \quad \ldots\ldots\ldots\ldots\ldots\ldots \quad (6.1.2:4)$$

this transformation being independent of ρ since $\tilde{\rho} = \rho$.

(the ρ in the second equation above cancels with the ρ in $\tilde{z}$ from equs (6.1.2:3) and (6.1.2:2)).

6.1.3 General Shape Simulation

The shape simulation incorporating both prolate spheroidal distortion and possible ventricular bulging is now given from equs (6.1.1:4) and (6.1.2:1), by:

$$\rho = \rho_m + \rho_b \quad \ldots\ldots\ldots\ldots\ldots\ldots\ldots\ldots \quad (6.1.3:1)$$

where the ρ's are the magnitudes of the position vectors.

This representation is dependent on eight arbitrary parameters, four (a_0, a_1, b_0, b_1) associated with the modified prolate spheroid and the remainder (H_b, η_b, C_2, C_3) characterising the bulge position and shape. X is assumed to be fixed. Fig. 6.3 shows an example of an aneurysm simulation.

6.2 Discussion of Co-ordinate Systems Used

It is convenient in the theory to be presented to use, for reasons which will become evident later in this Chapter, three different but inter-related co-ordinate systems. These will be defined at this stage in order to help clarify the development of the theoretical model.

The spatial (3-dimensional) co-ordinate system (x,y,z) is used to describe the ventricular mid-surface (Section 6.1 above). From this rectangular cartesian co-ordinate system, the position vector of the mid-surface $\underset{\sim}{\rho}$ can be computed using the usual Pytharorean formula.

In order to express surface geometric parameters a surface

PARAMETERS

$a = 1.0$

$b_0 = 0.7$

$b_1 = 0.6$

$H_b = 0.5$

$\eta_b = 120^0$

$C_2 = C_3 = 50\%$

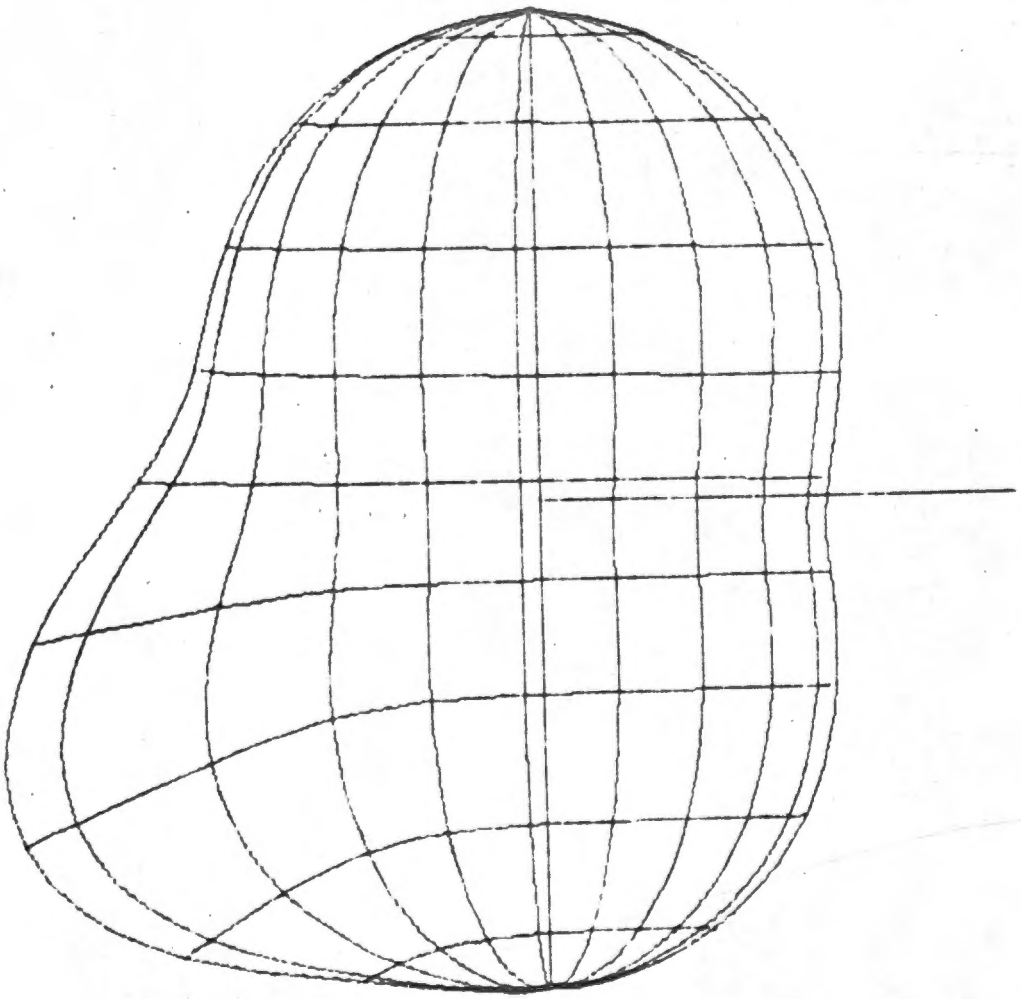

FIG. 6.3

SIMULATION OF A LEFT VENTRICULAR BULGE OR ANEURYSM

(2-dimensional) co-ordinate system (η,ξ) is defined. η is the meridional co-ordinate and ξ the circumferential. The relation between the spatial and surface co-ordinate systems is developed in Sections 7.3 and 7.4 of Appendix A.

Finally, another surface co-ordinate system, the fibre co.ordinate system (A,B), is defined. This system is required in order to express the stress-strain relation of each layer of myocardial fibres bearing in mind the fact that the fibre orientation varies with respect to the surface co-ordinates through the myocardial wall thickness. The A axis is taken to be in the direction of the fibre and the B axis in the orthogonal fibre surface co-ordinate direction.

6.3 Mathematical Description of Myocardial Fibre Orientation

From the evidence presented in Section 5.2.3 (based on the data provided by Streeter et al. (1969) and corroborated by Armour and Randall (1970)), the fibre orientation distribution along a normal through the ventricular wall is approximately parabolic and anti-symmetrical about the mid-wall and is therefore given by:

$$\zeta = -4\ \mathrm{sgn}|h/H|\,\zeta_s (h/H)^2 \quad \ldots\ldots\ldots\ldots\ldots\ (6.3:1)$$

where h/H = the fractional wall thickness ($h = -H/2$ at the endocardium and $+ H/2$ at the epicardium),

ζ = the fibre angle measured from the circumferential (ξ) co-ordinate direction

ζ_s = the value of ζ at $h = \pm H/2$

and sgn|h/H| is the positive sign when $h/H \geq 0$ and the negative sign when $h/H < 0$.

In contrast to Voukydis' assumption that the fibre orientation, ζ, remains constant at a given fractional wall thickness (or h/H) along a perpendicular to the major (or z) axis of the left ventricle (Voukydis, 1969), in this model this constancy will occur at a given h/H along a radius from the origin of the spatial co-ordinate system. Thus at a given h/H,

$$\tan \zeta = \text{constant} \quad \ldots\ldots\ldots\ldots\ldots\ldots \quad (6.3:2)$$

The assumption of constant fibre direction with respect to surface co-ordinates at a given radial fraction depth in the ventricular wall is more accurate than that of Voukydis, particularly near the apex. This is because Streeter's experimentally measured orientations are actually referred to the surface co-ordinate system and not spatial cylindrical co-ordinates. The assumption is nevertheless not entirely accurate since the surface normal and radial direction are not in general parallel.

It must be noted that the quantity ζ_s depends on any change which may occur from the initial (for instance and diastolic) ventricular configuration. Streeter's data shows this change to be small and it will therefore be neglected in this analysis (Streeter, 1969, Fig. 6).

In the next Section, the equation which describes the course of the fibre at a given h/H in the myocardium will be developed.

6.4 Geometric Parameters of the Shape Simulation

In order to mathematically express the slope (with respect to surface co-ordinates) of the fibre in the myocardium (which, as shown above in Section 6.3, is constant at a given fractional wall thickness) a relation giving arc length on the surface must be developed. Further, since the equilibrium relation of a shell involves wall curvature (see Sections 5.1 and 5.3.1) expressions incorporating this factor must be derived for the geometry in question. These factors are now considered. Much of the basic mathematics used is contained in Appendix A to which reference is implied in the following three sub-sections.

6.4.1 Surface Fundamental Forms

The surface metric in terms of spatial co-ordinates is given by equ. (A3:2):

$$ds^2 = g_{ij}\, dx^i\, dx^j, \quad \ldots\ldots\ldots\ldots\ldots\ldots \quad (6.4.1:1)$$

where ds = arc length

and g_{ij} = the metric or fundamental tensor.

In terms of surface co-ordinates this becomes (from equ. (A7.7:2)):

$$ds^2 = g_{\alpha\beta}\, du^\alpha\, du^\beta \quad \ldots\ldots\ldots\ldots\ldots\ldots \quad (6.4.1:2)$$

where $$g_{\alpha\beta} = a_{\alpha\beta} - 2u^3 b_{\alpha\beta} + (u^3)^2\, c_{\alpha\beta} \quad \ldots\ldots \quad (6.4.1:3)$$

in which $a_{\alpha\beta}$, $b_{\alpha\beta}$ and $c_{\alpha\beta}$ are the first, second and third surface fundamental forms respectively and where u^1 and u^2 are the surface co-ordinate variables and u^3 is the co-ordinate variable associated with the surface normal vector.

These fundamental forms are given by equs (A7.4:3), (A7.10:5) and (A7.8:5) which are rewritten here:

$$a_{\alpha\beta} = g_{ij}\, x^i_\alpha\, x^j_\beta, \quad \ldots\ldots\ldots\ldots\ldots\ldots \quad (6.4.1{:}4)$$

$$b_{\alpha\beta} = -\nu_i\, x^i_{\alpha,\beta} \quad \ldots\ldots\ldots\ldots\ldots\ldots \quad (6.4.1{:}5)$$

and $$c_{\alpha\beta} = b_{\alpha\mu}\, b^\mu_\beta, \quad \ldots\ldots\ldots\ldots\ldots\ldots \quad (6.4.1{:}6)$$

where $x^i_\alpha = \dfrac{\partial x^i}{\partial u^\alpha}$ are computed from the transformations:

$$\begin{aligned} x^1 &= \rho \sin\eta \cos\xi \\ x^2 &= \rho \sin\eta \sin\xi \quad \ldots\ldots\ldots\ldots\ldots\ldots \quad (6.4.1{:}7) \\ x^3 &= \rho \cos\eta \end{aligned}$$

(ρ being given by equ. (6.1.3:1)) and where ν_i (the space components of the unit surface normal) and $x^i_{\alpha,\beta}$ are given by equs (A7.10:1) and (A7.10:3) respectively. The components of the mixed second fundamental form are:

$$b^\mu_\beta = a^{\mu\nu}\, b_{\nu\beta} \quad \ldots\ldots\ldots\ldots\ldots\ldots \quad (6.4.1{:}8)$$

where (Green and Zerna, 1968, p. 33):

$$a^{\mu\nu} = a_{\mu\nu}/a, \quad \ldots\ldots\ldots\ldots\ldots\ldots \quad (6.4.1{:}8)$$

and $$a = \det(a_{\alpha\beta}). \quad \ldots\ldots\ldots\ldots\ldots\ldots \quad (6.4.1{:}9)$$

These are the contravariant components of the first fundamental surface form.

All the basic formulae necessary for the calculation of the surface fundamental forms have been pinpointed. These formulae for the specific surface geometry developed (Section 6.1 above) are provided in Section 2 of Appendix C.

6.4.2 Equation of the Fibre in the Myocardium

In Section 6.3, the variation of the slope of the fibre in the myocardium as a function of h/H with respect to the surface co-ordinate ξ was developed. Once arc length on the surface is given the slope of the fibre can be computed and so the equation of the fibre in terms of surface co-ordinates can be developed.

Taking $u^1 = \eta$ and $u^2 = \xi$, then from equ. (6.4.1:2),

$$\frac{ds_1}{d\eta} = \sqrt{g_{11}} \quad ; \quad \frac{ds_2}{d\xi} = \sqrt{g_{22}} \quad \ldots\ldots\ldots \quad (6.4.2:1)$$

where ds_1 and ds_2 are the differential arc lengths in the η and ξ co-ordinate directions respectively.

The fibre slope can now be expressed as:

$$\tan \xi = ds_1/ds_2$$
$$= \sqrt{(g_{11}/g_{22})}\, d\eta/d\xi$$

Thus: $$\eta = \int_{\xi_1}^{\xi_2} \tan \xi \sqrt{(g_{22}/g_{11})}\, d\xi, \quad \ldots\ldots \quad (6.4.2:2)$$

which represents the equation of the fibre in surface co-ordinates. All the quantities required for the computation of the g's in equ. (6.4.2:2) have been derived for the particular geometric formulation used.

6.4.3 Curvature and the Second Fundamental Form

The components of the second fundamental surface form are expressed in vector form in Appendix A (equ. (A7.7:3)). This vector equation reveals the geometric meaning of these components namely that they are a measure of the degree to which the surface unit base

vectors are directed along the unit surface normal. In this way, these components contain information with regard to surface curvature. The significance of this is revealed by the way the components of the second fundamental form feature in the stress equation of equilibrium now to be considered.

6.5 The Stress Equations of Equilibrium

The equations of stress equilibrium are easily set up for rectangular cartesian co-ordinates: since the resultant equations are tensor equations, they can be transformed to any other allowable co-ordinate system according to the rules of tensor transformation. (see Appendix A, Section 5.1)

The physical meaning of the stress tensor as well as the derivation of the general stress equations of equilibrium have been presented and discussed in Sections 3 and 4 of Appendix B.

Cauchy's equations of stress equilibrium in spatial co-ordinates for a deformed body, neglecting body and inertial forces can be written as shown in Section 4 of Appendix B (equ. (B4:1)):

$$\tau^{ij}||_i = 0 \quad \ldots\ldots\ldots\ldots\ldots\ldots\ldots \quad (6.5:1)$$

where τ^{ij} are the tensor components of stress and where the double vertical lines denote covariant differentiation with respect to the deformed body B. In expanded form the above equations become:

$$\frac{\partial \tau^{ij}}{\partial x^i} + \tau^{is} \left\{ \begin{matrix} j \\ s\ i \end{matrix} \right\} + \tau^{sj} \left\{ \begin{matrix} i \\ i\ s \end{matrix} \right\},$$

where the quanties $\left\{ \begin{matrix} i \\ j\ k \end{matrix} \right\}$ are the components of the Christoffel Symbols of the second kind (Section 5 of Appendix A).

As shown in Sections 4 and 5 of Appendix A, the covariant derivative in general co-ordinates is the operational equivalent to the partial derivative in rectangular cartesian co-ordinates.

These equilibrium equations can readily be transformed to their counterparts in surface co-ordinates.

For the cases $\alpha = 1,2,3$ and $\beta = 1,2$ equ. (6.5:1) becomes:

$$\tau^{\alpha\beta}||_\alpha + \tau^{3\gamma} \left\{ \begin{matrix} \beta \\ \gamma\ 3 \end{matrix} \right\} + \tau^{\gamma\beta} \left\{ \begin{matrix} 3 \\ \gamma\ 3 \end{matrix} \right\} + \frac{\partial \tau^{3\beta}}{\partial u^3} = 0$$

From equ. (A7.8:4) (Appendix A) and since the surface Christoffel symbol with two 3's is zero (Green and Zerna, 1968, p. 36), the above equation reduces to:

$$\tau^{\alpha\beta}||_\alpha - b^\beta_\gamma\ \tau^{\gamma 3} + \frac{\partial \tau^{3\beta}}{\partial u^3} = 0 \qquad \ldots\ldots\ldots\ldots \quad (6.5:2)$$

For the remaining cases where $\alpha = 1,2,3$ and $\beta = 3$, equ. (6.5:1) reduces to:

$$\tau^{\alpha 3}||_\alpha + \tau^{\alpha\gamma} \left\{ \begin{matrix} 3 \\ \gamma\ \alpha \end{matrix} \right\} + \frac{\partial \tau^{33}}{\partial u^3} = 0$$

which, using equ. (A7.8:3), becomes:

$$\tau^{\alpha 3}||_\alpha + b_{\alpha\beta}\ \tau^{\alpha\beta} + \frac{\partial \tau^{33}}{\partial u^3} = 0 \qquad \ldots\ldots\ldots\ldots \quad (6.5:3)$$

In equs (6.5:2) and (6.5:3):

$$\tau^{\alpha\beta}||_{\alpha} = \frac{\partial \tau^{\alpha\beta}}{\partial u^{\alpha}} + \tau^{\alpha\rho}\left\{ {\beta \atop \alpha\rho} \right\} + \tau^{\rho\beta}\left\{ {\alpha \atop \alpha\rho} \right\}, \quad .. \quad (6.5:4)$$

$$\tau^{\alpha 3}||_{\alpha} = \frac{\partial \tau^{\alpha 3}}{\partial u^{\alpha}} + \tau^{\beta 3}\left\{ {\alpha \atop \alpha\beta} \right\} \quad ..... \quad (6.5:5)$$

and $b^{\beta}_{\gamma} = a^{\beta\alpha}\, b_{\alpha\gamma}$ ..... (6.5:6)

from equ. (6.4.1:8).

The essence of shell theory is the reduction of the above equilibrium equations (6.5:2) and (6.5:3) in three dimensions to two dimensions by integrating them over the thickness of the shell thus yielding the equivalent "membrane equations" for a thick-walled shell.

Applying this technique to the ventricular shell, equs (6.5:2) and (6.5:3) are integrated through the thickness of the shell, $-H/2 \leq h \leq H/2$, where $h = u^3$ to give:

$$n^{\alpha\beta}||_{\alpha} - b^{\beta}_{\gamma}\, q^{\gamma} + p^{\beta} = 0 \quad ..... \quad (6.5:7)$$

$$b_{\alpha\beta}\, n^{\alpha\beta} + q^{\alpha}{}_{,\alpha} + n^{3} + p = 0 \quad ..... \quad (6.5:8)$$

where

$$n^{\alpha\beta} = \int_{-H/2}^{+H/2} \tau^{\alpha\beta}\, dh \quad ..... \quad (6.5:9)$$

= the stress resultants (forces per unit length) tangent to the surface,

$$q^{\alpha} = \int_{-H/2}^{+H/2} \tau^{\alpha 3}\, dh \quad ..... \quad (6.5.10)$$

= shearing force (per unit length) normal to the surface,

p^{β} = the resultant external loading forces per unit area tangent to the surface given by $\{\tau^{3\beta}$ (at $h = H/2$) $-\tau^{3\beta}$ (at $h = -H/2$)$\}$,

n^3 = the resultant normal force due to internal normal stresses, per unit area given by $\{\tau^{33}$ (at $h = H/2$) $- \tau^{33}$ (at $h = -H/2$)$\}$,

and p = the resultant normal external loading force per unit area given by $(p_+ - p_-)$ where

p_+ = the external normal loading pressure at $h = H/2$

and p_- = the external normal loading pressure at $h = -H/2$.

The meaning of some of these quantities is clarified in Fig. 6.4.

Except for the term arising from internal normal stress n^3 in equ. (6.5:8), equs (6.5:7) and (6.5:8) are the same as those derived by Green and Zerna (1968, p. 379). This inculsion of n^3 represents an important improvement for the case of left ventricular modelling since Mirsky (1969) has pointed out that normal stresses in the myocardium contribute significantly to the chamber pressure.

Meridional and circumferential equilibrium are described by equs (6.5:7) for $\beta = 1$ and $\beta = 2$ respectively: equ. (6.5:8) states the conditions necessary for equilibrium along the surface normal. Using well founded assumptions, it will be shown (in Section 6.10 below) how these equilibrium equations can be considerably modified

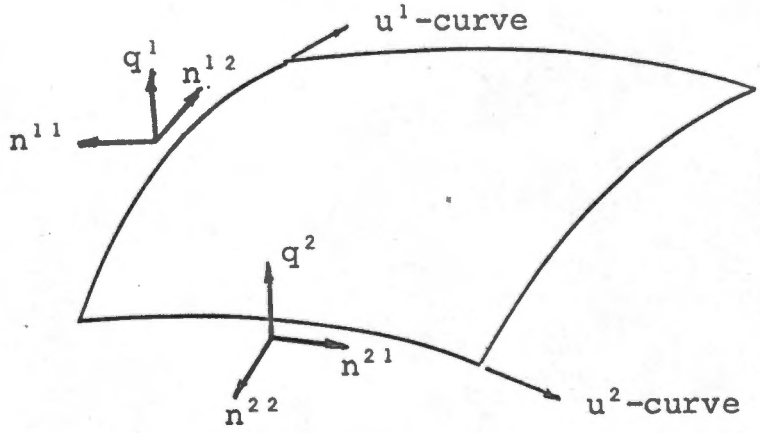

FIG. 6.4

STRESS RESULTANTS AND
SHEARING FORCES

for the simulation of left ventricular dynamics. Suffice it to say at this stage that the simplification yields a single equation (which is not a differential equation) which can be viewed as an advanced form of Laplace's Law, more general than the forms used by Mirsky (1969).

Having considered stress and stress equilibrium, it is now necessary to analyse strain in the ventricle within the context of the geometry prescribed (in Section 6.4 above).

6.6 Myocardial Strain Referred to Surface Co-ordinates

In Section 2 of Appendix B (to where reference is implied in most of this Section), the symmetric strain tensor in spatial co-ordinates was shown to be (equ. (B2:4)):

$$\tilde{\gamma}_{ij} = \tfrac{1}{2}(\tilde{G}_{ij} - \tilde{g}_{ij}) \quad \ldots\ldots\ldots\ldots\ldots \quad (6.6:1)$$

where the unstrained configuration B_o is given by the $\underset{\sim}{x}$ co-ordinate system and the strained configuration B by the $\underset{\sim}{X}$ co-ordinate system. The $\underset{\sim}{\tilde{x}}$ co-ordinate system (with reference to which the above strain tensor is given) is the so-called "convected" co-ordinate system in which the numerical values of the co-ordinates of given points in both B_o and B are the same (Fung, 1965). This co-ordinate system distorts with the material.

In order to compute left ventricular myocardial strain, equ. (6.6:1) must be converted to its counterpart in surface co-ordinates:

$$\tilde{\gamma}_{\alpha\beta} = \tfrac{1}{2}(\tilde{G}_{\alpha\beta} - \tilde{g}_{\alpha\beta}) \quad \ldots\ldots\ldots\ldots\ldots \quad (6.6:2)$$

where u^{α} are the co-ordinates of a given point P in B_o and U^{α} the co-ordinates of the same point P in B and where, in a manner analogous to the spatial case, $\tilde{u}^{\alpha}$ are the co-ordinates of P in both B_o and B in the surface "convected" co-ordinate system $\underset{\sim}{\tilde{u}}$.

Thus if the metric tensors in the undeformed and deformed configurations, $\tilde{g}_{\alpha\beta}$ and $\tilde{G}_{\alpha\beta}$ respectively are known, then the surface strain tensor $\gamma_{\alpha\beta}$ can be computed. However it is also necessary to be able to compute the components of the strain tensor in the normal direction, $\tilde{\gamma}_{\alpha 3}$ and $\tilde{\gamma}_{33}$.

Before these components can be formally related to the geomety in question, the nature of the displacements allowed must be discussed. It is obvious that "radial" displacements are the most important during a ventricular cycle if only because of the large volume changes accompanying the cycle. This is quantitatively revealed in the data used by Ghista and Sandler (1969, Fig.1) in the analysis of their model. In fact in many of the models developed "radial" displacements only have been considered (see Table 5.1). "Radial" has been placed in inverted commas here since it has the general meaning of a displacement along a vector with its origin at the origin of the spatial co-ordinate system (this origin being half-way along the major axis of the left ventricle).

It is therefore justifiable to ignore all but radial displacements in the model being developed.

Suppose at a given point P with convected co-ordinates $\tilde{u}^{\alpha}$, the magnitudes of the position vectors in B_Q and B are ρ_u and ρ_d respectively. In accordance with the assumption above, displacement takes place along the surface unit normal $\underset{\sim}{a}_3$ only and so the normal component of the displacement vector is:

$$\tilde{v}_3 = (\tilde{\underset{\sim}{\rho}}_d - \tilde{\underset{\sim}{\rho}}_u) . \underset{\sim}{a}_3 = \Delta\tilde{\underset{\sim}{\rho}} . \underset{\sim}{a}_3 . \quad \ldots\ldots\ldots \quad (6.6:3)$$

From equs (B5.1:1) the shear components of the infinitesimal strain tensor in terms of normal displacements for surface co-ordinates are:

$$\tilde{\gamma}_{\alpha 3} = \tfrac{1}{2}(\tilde{v}_{\alpha}|_3 + \tilde{v}_3|_{\alpha}) \quad \ldots\ldots\ldots\ldots\ldots \quad (6.6:4)$$

Using equ. (6.6:3),

$$\tilde{v}_3|_{\alpha} = \Delta\tilde{\underset{\sim}{\rho}}|_{\alpha} . \underset{\sim}{a}_3 = (\gamma\Delta\tilde{\underset{\sim}{\rho}}/\partial\tilde{u}^{\alpha}) . \underset{\sim}{a}_3$$

where the derivative $\underset{\sim}{a}_3|_{\alpha}$ is assumed to be negligible. Thus the above equation becomes:

$$\tilde{\gamma}_{\alpha 3} = (\gamma\Delta\tilde{\underset{\sim}{\rho}}/\partial\tilde{u}^{\alpha}) . \underset{\sim}{a}_3 \quad \ldots\ldots\ldots\ldots\ldots \quad (6.6:5)$$

The normal strain component γ_{33} of the strain tensor is calculated from the fact that the myocardium is incompressible (Section 5.2.1) so volume elements are conserved in deformation. Thus along a given surface normal

$$\int_{-H/2}^{+H/2} \sqrt{(g)}\, dh = \text{constant}$$

or, assuming $b_{\alpha\beta}$ to be small (i.e. minimal surface curvature),

$$H\sqrt{a} = \text{constant}. \quad \ldots\ldots\ldots \quad (6.6:6)$$

Differentiating the above equation,

$$dH/a + H\, d(1/a) = 0.$$

Normal strain γ_{33} is given by dH/H so that

$$\gamma_{33} = d\{\ln(1/a)\}/2 \quad \ldots\ldots\ldots\ldots\ldots\ldots \quad (6.6.7)$$

All the surface and normal components of the strain tensor have now been derived (equs (6.6:2), (6.6:5) and (6.6:7)). Now that the myocardial stress and strain tensors have been separately analysed and the stress equation of equilibrium derived, all that remains is to analyse the myocardial stress-strain relation and to develope a formula for computing ventricular volume in order to complete the theoretical development of the left ventricular model.

6.7 Synthesis of Myocardial Elastic Character

From previous discussions (Sections 5.2.2 and 5.2.3), it is clear that definition of the elastic characteristics of the myocardium is expedited by assigning an elastic character to cardiac muscle fibre. This elastic character in both the passive (unstimulated) and active (stimulated) conditions was extensively analysed in Chapter 4.

6.7.1 Elastic Character of Cardiac Muscle Fibre

Because of the nature of the ultrastructure of the cardiac muscle fibre, its elastic character was found to be best described as transversely isotropic (Sections 4.1.1.1 and 4.1.1.2). The general stress-strain relation was accordingly given by equs (4.1.1.2:1) and (4.1.1.2:2).

Based on published data, it was found possible to ignore the transverse elastic moduli in comparison with the axial fibre modulus so that transverse fibre stresses need not be taken into account. (Note that this is based on an additional assumption not specified in Section 4.1.1.2:2 i.e. that the transverse fibre elastic character is linear). Thus the fibre elasicity was described by the equation (based on Hill's three-element model):

$$\sigma_{AA}(\varepsilon_{AA},t) = \sigma_p(\varepsilon_{AA}) + \sigma_c(\varepsilon_{AA},t) \quad \ldots\ldots \quad (6.7.1:1)$$

where $\sigma_p(\varepsilon_{AA}) = E_2(\varepsilon_{AA} - \varepsilon^*_{AA})^2$ $\ldots\ldots\ldots$ (6.7.1:2)

= parallel elastic (passive) element elasticity

$$\sigma_c(\varepsilon_{AA},t) = E_s(\Delta_o + \varepsilon_{AA})\{\Phi + k(\varepsilon_{AA} - \delta\Delta_i)\}/$$
$$\{E_s + \Phi + k(2(\varepsilon_{AA} + \Delta_o) - \Delta_i)\}, \quad (6.7.1:3)$$

= contractile element (active) elasticity.

All other components of the fibre stress vector σ_{AB3} (i.e. σ_{BB}, σ_{33}, σ_{AB}, σ_{A3}, σ_{BB}) are zero (where (A,B,3) is the fibre co-ordinate, the A-axis being the anisotropic axis). The above equations, taken from Chapter 4, are respectively equs (4.3.2:12), (4.1.1.2:9) and (4.3.2:10) and the assumptions made in their development as well as the definitions of the symbols are given in that Chapter.

An interesting factor in the assumptions made, is worthy of restatement here, however. As the muscle activity rises, so the assumption of neglecting transverse stress improves i.e. the model becomes more accurate. Thus

this representation should therefore be quite adequate to describe myocardial elasticity under systolic conditions.

6.7.2 Simulation of Myocardial Elastic Character

The nature of the individual fibre elasticity has been analysed in Section 6.7.1 and in Chapter 4. Further, the fibre structure of the myocardium has been quantitated in Section 6.3. From this knowledge, the elastic character of the myocardium can be synthesised along the lines discussed in Section 5.2.3.

The fibres are embedded in surfaces described by equ. (A7.6:1) for different fixed values of $h = u^3$ (see Section 7.6 of Appendix A). In each layer, the stress-strain relation for the fibre is described by equ. (6.7.1:3) where the orthogonal surface fibre co-ordinate system is (A,B,3) and the A-axis is the anisotropic axis.

These fibre co-ordinates must be related to the surface co-ordinate system, $(\eta,\xi,3)$, in order that myocardial elastic characteristics can be generated. It must be noted that the surface co-ordinates are, in general (particularly for a bulge simulation), non-orthogonal as shown in Appendix C, Section 3. In order not to over-complicate the analysis, it will be assumed that the deviation from orthogonality is small enough to be negligble. This assumption deteriorates, however, as the shape becomes more axisymmetric.

If the positive rotation of the (A,B,3) co-ordinate system

about the $(\eta,\xi,3)$ system is given by ζ, the fibre twist angle referred to the circumferential ξ co-ordinate (where rotation is about the 3-axis), then the surface transformation tensor from the (A,B,3) to the $(\eta,\xi,3)$ co-ordinate system is given by (Voukydis, 1972a):

$$[T] = \begin{bmatrix} \cos^2\zeta & \sin^2\zeta & -\tfrac{1}{2}\sin 2\zeta & -\tfrac{1}{2}\sin 2\zeta \\ \sin^2\zeta & \cos^2\zeta & \tfrac{1}{2}\sin 2\zeta & \tfrac{1}{2}\sin 2\zeta \\ \tfrac{1}{2}\sin 2\zeta & -\tfrac{1}{2}\sin 2\zeta & \tfrac{1}{2}\cos 2\zeta & \tfrac{1}{2}\cos 2\zeta \\ \tfrac{1}{2}\sin 2\zeta & -\tfrac{1}{2}\sin 2\zeta & \tfrac{1}{2}\cos 2\zeta & \tfrac{1}{2}\cos 2\zeta \end{bmatrix} \quad \ldots (6.7.2{:}1)$$

Following Voukydis' analysis, and since the strain tensor is symmetric, the stress-strain relation referred to global surface co-ordinates can be written:

$$[\tau]_{\eta\xi} = [T]^{-1}\,[C]\,[T]\,[\gamma]_{\eta\xi} \quad \ldots\ldots\ldots (6.7.2{:}2)$$

where $[T]^{-1}$ is the inverse of simply the transpose of $[T]$ (since $[T]$ is orthogonal). Tensors involving the 3-axis are invariant under this surface transformation so, for example $\tau_{\eta 3} = \tau_{A3}$. The tensor components of stress and strain, $\tau_{\eta 3}$ and $\gamma_{\eta 3}$ are used above.

In view of the fact that only axial fibre stress need be considered (equ. 6.7.1:1), the transformation equations above can be greatly simplified. They have been included here for completeness so that if the orthogonal elastic constants are quantitated, the mathematical structure for incorporating them is available. At this stage such a move is impossible and in fact unnecessary, since the systolic (active) contractions are of prime interest here (see Section 6.7.1 above).

The trasformation of the tensor components of fibre stress in the fibre co-ordinate system to stress with reference to the surface co-ordinate system is given by (Streeter et al., 1970):

$$\tau^{\eta\eta} = \tau^{AA} \sin^2\zeta$$

$$\tau^{\xi\xi} = \tau^{AA} \cos^2\zeta \qquad \ldots\ldots\ldots\ldots \quad (6.7.2:3)$$

$$\tau^{\eta\xi} = \tfrac{1}{2}\, \tau^{AA} \sin 2\zeta$$

(Contravariant components of the stress tensor are used here as required by the stress transormation laws - see Section 3 of Appendix B).

In order to be in a position to compute γ_{AA}, the axial fibre strain, the transformation for the covariant tensor components of strain (see Section 2 of Appendix B) from the surface to the fibre co-ordinate systems is required since the $\gamma_{\eta\xi}$ components of strain are given by equ. (6.6:2). This transformation is:

$$\gamma_{AA} = \gamma_{\eta\eta} \cos^2(\zeta) + \gamma_{\xi\xi} \sin^2(\zeta) + \gamma_{\eta\xi} \sin(2\zeta)$$

$$\ldots\ldots\ldots \quad (6.7.2:4)$$

The general stress-strain relation of the myocardium has now been described in terms of the elastic characteristics of individual fibres together with the fibre structure of the ventricular wall. It remains to develope relations describing the way local wall thickness varies with strain in the ventricular wall and for the computation of ventricular volume.

6.8 Computation of Ventricular Wall Thickness and Volume

For any given configuration of the ventricle, within the framework of the shape simulation described in Section 6.1, it is necessary to be able to compute the wall thickness distribution (with reference to the surface co-ordinate system) and the ventricular volume.

Wall thickness at each point is easily obtained from the normal strain tensor γ_{33}, for from equ. (6.6:7):

$$\gamma_{33} = dH/H_o = d\{\ln(1/a)\}/2,$$

where a is the determinant of $a_{\alpha\beta}$ and H_o is the original wall thickness. Hence wall thickness H is given by rearranging the above equation:

$$H = \gamma_{33} + 1. \quad \ldots\ldots\ldots\ldots\ldots\ldots \quad (6.8:1)$$

This equation is valid only for small strains γ_{33}. It can be applied at each selected point in the wall to give the wall thickness distribution.

Ventricular volume, V, is obtained from the volume integral:

$$V = 2 \int_o^{\rho i} \int_o^{\pi} \int_{\eta o}^{\pi} \rho(\eta,\xi)\, d\eta\, d\xi\, d\rho + V_c$$

$$= \int_o^{\pi} \int_{\eta o}^{\pi} \rho_i(\eta,\xi)^2\, d\eta\, d\xi + V_c \quad \ldots\ldots\ldots \quad (6.8:2)$$

where $\underset{\sim}{\rho}_i(\eta,\xi) = \underset{\sim}{\rho}(\eta,\xi) - \underset{\sim}{a}_3\, H(\eta,\xi)/2$ is the position vector of the endocardial surface. The surface normal, $\underset{\sim}{a}_3$, is given by equ. (A7.10:1).

The existence of the initial angle η_0 and the volume V_c arise from the fact that account must be taken of the valvular ring which remains fixed in shape and area throughout the cardiac cycle (see Section 5.2.1). Assuming the ring to be circular it then has a fixed radius measured orthogonal to the $\eta = 0$ axis given by:

$$R = \bar{\rho} \sin \eta_0 \quad \ldots\ldots\ldots\ldots\ldots\ldots\ldots\ldots \quad (6.8:3)$$

where $\bar{\rho}$ is the average distance of the ring perimeter from $\rho = 0$. The situation is shown in Fig. 6.5. A trial and error method is used to give an estimate of η_0 for the initial conditions in the ventricular simulation. The first value of η_0 is guessed and the average value of ρ, $\bar{\rho}$, is calculated from equ. (6.1.3:1) using this value. Equ. (6.8:3) is then employed to give a new value of η_0 and the process is repeated until convergence to the correct value of η_0 is achieved.

In order to keep R constant during a ventricular cycle, $\bar{\rho}$ must change and this change, for the sake of simplicity is assumed to be proportional is the quantity $\sqrt{(a^2 + b^2)}$. This allows η_0 to be calculated during the cycle from the formula:

$$\eta_0 = \text{arc sin } \{R/k\sqrt{(a^2 + b^2)}\}. \quad \ldots\ldots\ldots \quad (6.8:4)$$

where k is the proportionality constant between $\bar{\rho}$ and a and is given by $\{\bar{\rho}/\sqrt{(a^2 + b^2)}\}_0$ where the subscript 0 refers to initial conditions. The effects of this change in $\bar{\rho}$ (or η_0) is also shown on Fig. 6.5.

The quantity V_c, is the volume of the cone subtended by the valvular ring a $\eta = 0$ which must be added to the

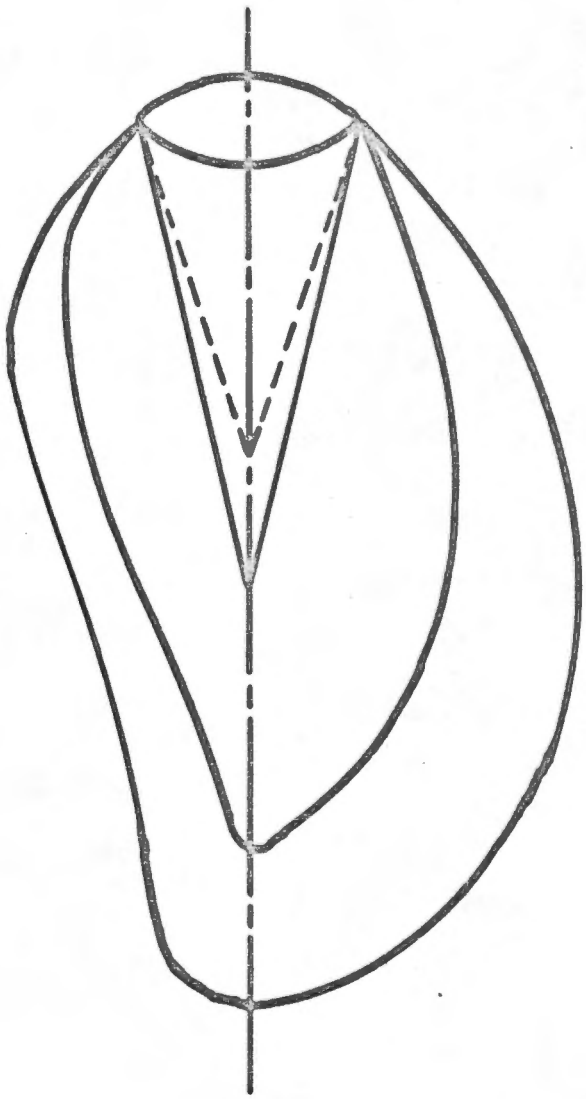

FIG. 6.5

EFFECT OF LEFT VENTRICULAR VOLUME CHANGES OF VALVULAR RING POSITION

Spatial co-ordinates fixed. Height of cone subtended by ring at origin decreases as volume decreases.

remainder of the ventricular volume as shown in equ. (6.8:2). V_c is given by:

$$V_c = \pi R^2 k \sqrt{(a^2 + b^2)} \cos \eta_o / 3 \quad \ldots\ldots\ldots \quad (6.8.5)$$

6.9 Left Ventricular Model Summary-Interplay of its Components

Each facet of the left ventricular model has now been discussed and mathematically described: it remains to summarise the interplay of the different facets.

The shape of the mid-wall of the left ventricle is given by equ. (6.1.3:1). This shape representation, which is the most general and accurate yet proposed, is controlled by eight shape parameters, defined in Section 6.1.3. Restrictions with regard to wall thickness (such as the necessity for it to be constant), are not necessary in this model. The variation of initial wall thickness is arbitrary.

For imposed ventricular shape changes, equations describing the resultant change in ventricular volume (6.8:2), wall thickness (6.8:1) and state of surface strain (6.6:2) have been developed. Myocardial stress developed as a consequence of the change in the state of strain is given by the stress-strain relation, equ. (6.7.1:1) which is based on the recognition of the properties of the cardiac muscle fibre. The relations between stress and strain in the surface and fibre co-ordinate systems are given by equs (6.7.2:3) and (6.7.2:4).

The optimal change in ventricular shape in response to a

change in volume (or internal pressure) is obtained by finding the a associated shape and volume parameters satisfying the equilibrium equations (6.5:7) and (6.5:8) at each point in the wall. This will be further discussed in Chapter 7.

This model is complex but nevertheless solvable in principle. Significant simplications can, however, be made thus making the solution more tractable.

6.10 Plausible Model Simplifications

The most fruitful simplifications to this model can be made by modifying the stress equilibrium equations (6.5:7) and (6.5:8). The differential equations (6.5:7) representing equilibrium in the η and ξ surface directions can be neglected completely as a first approximation. Further, since the shear stresses normal to the surface as well as the normal surface stresses are small compared to the fibre axial stresses during systole, the factors $q^{\alpha}{}_{,\alpha}$ and η^3 in equ. (6.5:8) can justifiably be neglected and so the final stress equilibrium equation is:

$$p = b_{\alpha\beta}\, n^{\alpha\beta} \quad \ldots\ldots\ldots\ldots\ldots\ldots\ldots \quad (6.10:1)$$

which is beautifully simple thus revealing the descriptive power of the Tensor Calculus. The resultant normal loading force per unit area is given by:

$$p = p_v - p_e \quad \ldots\ldots\ldots\ldots\ldots\ldots\ldots \quad (6.10:2)$$

where p_v = ventricular (internal) pressure

and p_e = the external loading pressure (generally taken to be zero, but see Section 5.2.5)

The second of the two assumptions is essentially the same as that used by Voukydis (1972a) in his analysis where he considered plane (surface) stress and strain only. It is ironic that this assumption improves in systole, the state which, on the face of it, appears to be the most difficult to simulate. With regard to the first assumption, the only real justification for itswuse is the marked increase in simplicity obtained which is computationally most desirable. This assumption is in fact made compulsory by allowing radial displacement only.

A further general simplification can be made. This involves neglecting the effect of h (or u^3) on the value of the metric $g_{\alpha\beta}$ given in equ. (6.4.1:3)

Hence, $g_{\alpha\beta}(h)$ can be replaced by $a_{\alpha\beta}$ (which is not a function of h) in all equations using this term. This assumption was, for example, made in computing normal strain γ_{33} (see Section 6.6).

This class of assumption deteriorates with increasing wall thickness and/or curvature (which affects the components $b_{\alpha\beta}$) but is nevertheless again made attractive by the increased ease in computational effort achieved through its incorporation.

6.11 Mathematical Development of the Left Ventricular Model - Conclusions

The model is now fully derived and is the most comprehensive and versatile yet proposed:

(i) fibre properties and elastic character are explicitly related. This was a prime objective of the research programme.

(ii) The ventricular model has been developed for a completely general shape or surface: the author has chosen to use prolate spheroidal modified by a 3-dimensional normal distribtion bulge as the shape best suited to simulating ventricular normal and abnormal conditions. But the model is not limited by this choice of geometry: any geometry suiting the needs of a particular situation can be invoked. As an important corollary, this is the first model proposed which is totally unhampered by the considerations of axisymmetric geometry (see Table 5.1).

(iii) In terms of the theoretical structure of the myocardium based on the muscle fibre, it is possible to incorporate space-time effects i.e. the spread of electrical activity on stimulation. This is not feasible in any of the proposed models in Table 5.1.

(iv) Wall thickness distribution is arbitrary.

(v) An inelastic valvular ring is incorporated in the model.

CHAPTER 7

COMPUTATIONAL ASPECTS OF THE MODEL

The derivation of the left ventricular model given in Chapter 6 is complex. Nevertheless, the final equilibrium relation to be solved is not explicitly a differential equation; it does however involve integration, to obtain the stress resultants in equ. (6.5:9), and differentiation in the computation of the second fundamental form (see Section 2 of Appendix C). This must be contrasted with the complex formulation of Voukydis (1972a) requiring the simultaneous solution of nonlinear differential equations.

Invoking the simplications described in Section 6.10, the equilibrium equation (equ. (6.10:1) is rewritten as:

$$p = b_{\alpha\beta}\, n^{\alpha\beta},$$

where $p = p_v - p_e$

and p_v = the ventricular pressure (N/m^2)

p_e = the external loading pressure (N/m^2).

Thus the ventricular pressure in terms of the myocardial stress resultants is:

$$p_v = p_e + b_{\alpha\beta}\, n^{\alpha\beta}, \quad \ldots\ldots\ldots\ldots\ldots\ldots \quad (7:1)$$

or, expanding the above equation,

$$p_v = p_e + b_{11}\, n^{11} + b_{12}\, (n^{12} + n^{21}) + b_{22}\, n^{22}. \quad \ldots\ldots\ldots \quad (7:2)$$

The quantities $b_{\alpha\beta}$ and $n^{\alpha\beta}$ are functions of the surface co-ordinates η and ξ. Further, they depend on geometry; $b_{\alpha\beta}$ directly and $n^{\alpha\beta}$ through the stress-strain relation (equ. (6.7.1:1)) since geometry controls strain (equ.

(6.6:2)). Thus $p_v = p_v(\rho,\eta,\xi)$ through equ. (7:1).

There is therefore a unique configuration for the left ventricle such that Pascall's Law is satisfied at a given time during the ventricular cycle. It is that configuration which gives the same value of p_v at each point on the endocardium. Thus, from a computational point of view the quantity:

$$S = \sum_m (p_j - \bar{p})^2 \quad \ldots\ldots\ldots\ldots\ldots\ldots\ldots \quad (7:3)$$

where m = the total number of points taken over the surface,

p_j = the value of the ventricular pressure P_v at the j-th point

and $\bar{p} = \sum_m (p_j)/m \quad \ldots\ldots\ldots\ldots\ldots\ldots\ldots \quad (7:4)$

= the average computed pressure must be minimized.

This is expedited by optimizing the shape parameters (Section 6:1) so that:

$$S \leq \varepsilon_s \quad \ldots\ldots\ldots\ldots\ldots\ldots\ldots \quad (7:5)$$

where ε is the error criterion set.

In the overall equilibrium of the ventricle, two variables are involved; ventricular pressure and volume. The pressure is related to the local equilibrium equation, equ. (7:1), through the stress-strain relation of the myocardium which in turn is given by the cardiac muscle model (derived in Section 4.3) and the equation describing myocardial fibre distribution, equ. (6.3:1). This fibre stress-strain relation can also be considered an independent factor.

Before discussing a possible simulation protocol for the left ventricular-cum-muscle fibre models, the properties of the muscle fibre model must be further investigated.

7.1 Muscle Fibre Model in Ventricular Simulation

Based on isolated cardiac muscle data, it was shown in Section 4.3 that the active and passive stress-strain characteristics of the cardiac muscle fibre could be adequately modelled in terms of four parameters:

E_s ; the series elastic modulus ($\sim 8 N/cm^2$)

E_2 ; the second order parallel elastic element ($\sim 4 N/cm^2$)

k ; the shortening decrement constant ($\sim -4 N/cm^2$)

Φ_p ; the peak active state ($\sim 9 N/cm^2$), assuming the sine variation of active state given in Section 4.2.4.2 to hold.

Since E_s and E_2 are passive moduli it is unlikely that they will differ much from the above values in the intact ventricle. However k and Φ_p, the parameters associated with the activated muscle, will be function of the state of the myocardium and it is not justified to assume the above values in the intact ventricle. Φ_p is obtainable from isometric contractions and k from shortening data.

Thus it is logical to quantitate Φ_p using pressure-volume data during the isovolumic contraction phase of the ventricular cycle (when k can be neglected) and to estimate k from ejection phase data.

The computational protocol for obtaining these parameters will now be discussed.

7.2 Computational Protocol For Solving Models

During isovolumic contraction, the ventricular volume V remains essentially constant at V_0. Let the pressure at the end of this phase be P_e.

An optimising procedure can then be used to obtain the value of Φ_p which satisfies the pressure requirement $\bar{p} = P_e$ in equ. (7:3) (this equation in turn expressing the criterion for optimizing geometry). This is also subject to the volume criterion:

$$|V_c - V_0| \leq \varepsilon_v \quad \ldots\ldots\ldots\ldots\ldots\ldots \quad (7.2:1)$$

where V_c is the computed ventricular volume for the optimized geometry.

The best value for $\Phi_p = \Phi_0$ is obtained when the pressure and volume criteria are simultaneously satisfied.

Using pressure and volume data during the ejection phase of the cycle the best value for k can be found in a manner essentially the same as that for the estimation of Φ_p already described. The value of peak active state Φ_0 obtained above is used.

At each time during this ejection phase, the pressure and volume are known, so that a value for k satisfying both the pressure and volume criteria can be computed. (Since the infinitesimal strain tensor is used, a time increment

giving small volume changes must be employed). As above for Φ_p, the value of k satisfying the pressure (and therefore geometric) criterion (equ. (7:5)) is first obtained by iteration; volume is calculated using this k and it is checked against the data value for volume. If the volume criterion (equ. 7.2:1) is not satisfied then a new value for k is estimated and the geometry rechecked, subject to the pressure criterion. The whole process must be repeated until the two criteria are simultaneously satisfied.

For the sake of clarity, the steps in the general parameter optimising procedure described above will be repeated:

(i) Set an initial value for the chosen parameter.

(ii) Obtain the required pressure-volume data point.

(iii) Optimise the shape parameters subject to the pressure criterion (equs (7.3) to (7.5)) and compute volume.

(iv) Check the colume criterion, equ. (7.2:1). If it is satisfied go to step (v). Otherwise, generate a new estimate for the parameter in question and go back to step (iii).

(v) Obtain the next pressure volume data point and go back to step (iii).

The computer simulation of the model reduces therefore to a problem in the field of dynamic programming (Jacobson and Mayne, 1970). A Fortran computer programme has been written which is able to compute the pressure distribution and volume for any given input shape parameters. It is reproduced in Appendix D and will be the core of any dynamic

programme of the ventricular and muscle models.

Some observations regarding the nature of the parameters will now be made as an aid in any future development of a dynamic programme.

7.3 Discussion of Ventricular and Cardiac Muscle Model Parameters

The shape parameters which are obtained by satisfying the pressure criterion (equ. 1:5) will first be considered.

A basically prolate spheroidal geometry has been chosen and deviations from this are under the control of the parameters connected with semi-major and semi-minor spatial variation and those connected with bulge position, magnitude and base area (Section 6.1).

7.3.1 Prolate Spheroidal Distortion Parameters

The meaning of the parameters a_0, b_0, a_1 and b_1 are defined in Section 6.1.1 Since the ventricle tapers towards the apex, $a_1 < a_0$ and $b_1 < b_0$. If $a_1 = a_0$ and $b_1 = b_0$ the geometry reduces to prolate spheroidal where a_0 and b_0 are its semi-major and semi-minor axes respectively. The effect of a variation in both a_1 and b_1 on the prolate spheroidal shape is shown in Fig. 7.1.

It is clear that the magnitude $b_0 - b_1$ affects the amount of reduction in the semi-minor axis in the region $\eta = \pi/2$. Similarly, the magnitude $a_0 - a_1$ controls the taper towards the base for $\pi/2 < \eta < \pi$. Its effect is zero at $\eta = \pi$.

PARAMETERS

$a_0 = 1.0$

$a_1 = 0.4$

$b_0 = 0.7$

$b_1 = 0.6$

$H_b = 0.0$

$C_2 = C_3 = 50\%$

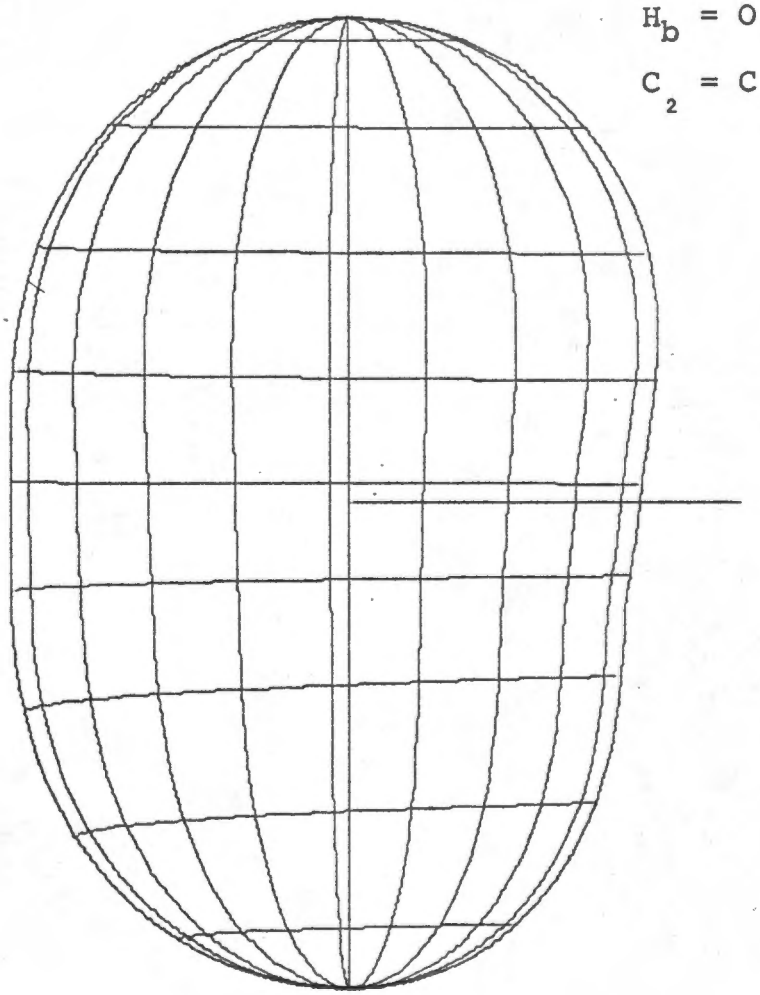

FIG. 7.1

SIMULATION OF TAPERING EFFECT
ON PROLATE SPHEROID

Both these effects are maximal at $\xi = \pi$ and zero for $\xi = 0$.

If the values for a_1 and b_1 are such that a change of sign of curvature from concave inwards to concave outwards occurs in the shape, the second fundamental form $b_{\alpha\beta}$ changes sign. Geometrically this is obvious from equ. (A7.7:3). This has important implications in the equilibrium equation, equ. (7:1). Since $n^{\alpha\beta} > 0$, p_v is positive only if $p_e > b_{\alpha\beta}\, n^{\alpha\beta}$.

Negative curvatures are likely to occur only in the ventricular septal region in the intact heart (Gould *et al.*, 1972) where the loading pressure is that of the right ventricle and is therefore not zero (relative to atmospheric). However, it must be noted that wall moments were not considered in the above equilibrium equation. They were included by Gould *et al.*, but it nevertheless is still very difficult to see how moments significant enough to cause this effect can occur except in early diastole where p_v is very low.

Thus the parameters a_1 and b_1 can initially be ignored in the simulation of the ventricular cycle (i.e. set equal to a_0 and b_0 respectively) unless the spread of the action potential is being considered. In this case the earlier build-up of stress in the septal region than in the rest of the ventricle will cause the magnitude of the curvature of the wall to decrease in this region.

7.3.2 Bulge Parameters

If there is no aneurysm based on angiographic evidence, then the bulge height is zero and the bulge parameters are not applicable. However, when an aneurysm does occur, the shape of the ventricle is fitted by ascertaining the extent of the aneurysm, thus defining the parameters C_2 and C_3 which are its base dimensions (expressed as percentages of the mid-wall circumferences in orthogonal directions).

The remaining parameter to be determined is the bulge height H_b. This can be done in two possible ways:

(i) if sequential angiographic data is available, then H_b can be extracted from it as a function of time. The passive elasticity coefficient of the bulge myocardium E_{2b} can then be obtained from the simulation programme if the rest of the myocardium is considered normal (i.e. the muscle constants are known).

(ii) Assume a value for E_{2b} and then simulate the ventricular shape changes during a contraction again using known muscle parameters.

The clinical implications of an aneurysm simulation are exciting. It appears that surgical removal of these bulges does not improve the condition of the patient significantly in the majority of cases. A stress analysis of the affected ventricle, as well as a measure of the work load on the healthy part of the myocardium obtained from

this model, could reveal an answer to this apparent anomaly.†

7.4 Initial Conditions for the Model

An important assumption which must be made is that for a defined configuration, the fibres are all in a specified state of strain. The easiest assumption is that strain is zero (i.e. $\varepsilon_{AA} = 0$) for all fibres at end diastole when the ventricle has been primed for a contraction. The volume giving zero strain is a constant for a given heart so that for different end diastolic volumes ε_{AA} is different.

The initial fibre length sets the initial actin-myosin insertion and so the stress the fibre can produce and ultimately the ventricular pressure. This is the basis of Starling's Law of the Heart (see Braunwald *et al.*, 1968).

The initial configuration chosen will not necessarily satisfy the pressure criterion and so the shape parameters must be optimized keeping strain zero. Note that although strain is zero, it has been defined relative to optimum fibre length L_{max} and passive elasticity is very significant at this length (see Fig. 3.4).

† Personal communication with Dr. R. Forman, Cardiac Clinic, Groote Schuur Hospital, South Africa.

7.5 Model Simulation Protocol - Conclusions

The way the model developed in Chapter 6 can be simulated has been discussed. Fairly sophisticated dynamic programming techniques appear to be needed in the simulation.

Although there are eight shape parameters involved, it has been shown how this number can be reduced according to the needs of the model. The possible types of simulation range from prolate spheroidal to the analysis of the effects of space variations in the elastic constants of the myocardium (caused by diseased muscle and/or the space-time effect of action potential spread).

CHAPTER 8

GENERAL CONCLUSIONS

Three main objectives have been attained by the reasearch described in this Thesis.

(i) A general model for describing the dynamical and mechanical properties of the left ventricle during systole and diastole has been formulated. It features both the ability to simulate a ventricular aneurysm and also non-axisymmetric shapes. No other published ventricular model has these capabilities.

(ii) The stress-strain-time properties of cardiac muscle under both active and passive conditions have been successfully described on the basis of a new model for cardiac muscle. This model incorporates novel ideas concerning the terms active state and contractility (as applied to cardiac muscle).

(iii) Myocardial elastic properties have been expressed in terms of those of the muscle fibre. Thus an explicit link is forged between cardiac muscle and ventricular dynamics when the muscle model is used as the "stress generator" (in terms of its stress-strain-time relation) in the left ventricular simulation.

Two extensive literature reviews are incorporated in this Thesis. The review on left ventricular modelling is the first ever written. It puts into perspective the valuable contribution the development of this model is in the field of theoretical left ventricular modelling.

The critical observations made concerning controversial issues in heart muscle dynamics are the prime features of the survey of this topic. Further, recently published experimental results have been carefully analysed.

Apart from improvements in the details of the ventricular and heart muscle models, the major development made possible by this study is the computer simulation of the ventricular cycle in the manner outlined in Chapter 7. Quantitative data concerning the intrinsic state of the heart muscle would then be obtainable using clinical data which is fairly easy to obtain. Attempts at quantitating this factor have, up till now, been hampered by both the restrictive nature of the assumptions used in the left ventricular model and also by the controversy concerning the description of the state of the heart muscle (Mirsky et al., 1970; Hugenholtz et al., 1971).

The author has considerably improved the basis of the ventricular model and has by-passed the controversies in heart muscle dynamics by proposing, analysing and simulating a new muscle model.

NOMENCLATURE

a	Semi-major axis of prolate spheroid or determinant of the first surface fundamental form (clear from context).
$\underset{\sim}{a}_3$	Unit surface normal.
$a_{\alpha\beta}$, $a^{\alpha\beta}$	Components of first surface fundamental form and its contravariant associate respectively.
b	Semi-minor axis of prolate spheroid.
b_o	Value of b in the half-plane $0 \leq \eta \leq \pi$, $\xi = 0$.
b_1	Value of b at $\eta = \pi/2$, $\xi = \pi$.
$b_{\alpha\beta}$	Components of second surface fundamental form.
$[C]$	Matrix of myocardial elastic constants.
C_2, C_3	Parameters controlling the extent of the bulge in the η and ξ surface co-ordinate directions respectively.
$c_{\alpha\beta}$	Components of third surface fundamental form.
ds	Differential arc length.
E_2	Second order polynomial constant of the parallel elastic element stress-strain relation.
E_s	Young's modulus of the series elastic element.
G_{ij}, $G_{\alpha\beta}$	Space and surface metric tensors respectively of the deformed ventricular configuration.

g_{ij}, $g_{\alpha\beta}$	Space and surface metric tensors respectively of the undeformed ventricular configuration.
H	Ventricular wall thickness.
H_b	Bulge height.
h	Wall thickness variable ($-H/2 \leq h \leq H/2$).
k	Shortening decrement constant.
L_o, L_{max}	Initial length of cardiac muscle fibres.
n	Density of cross-bridges (number per unit length of overlap).
$n^{\alpha\beta}$	Tensor components of the tangential surface resultant forces.
p_e	External loading pressure.
p_v	Ventricular pressure.
p^{β}	Tensor components of tangential loading forces.
q^{α}	Tensor components of normal shearing forces.
R	Radius of basal valvular ring.
R_{θ}, R_{ϕ}	Principal radii of curvature.
T	Ventricular wall tension.
$[T]$	Surface transformation matrix.
t	Time variable.
u^{α}, u^3	Surface co-ordinate variables and normal co-ordinate variable respectively.
V	Ventricular volume.

V_c	Volume of cone subtended by valvular ring at spatial co-ordinates origin.
v_m	Local myocardial muscle volume.
V_{max}	Maximum shortening velocity of the contractile element.
X	Parameter controlling the exponential decay of the bulge.
x^i	Rectangular cartesian co-ordinate variables.

Greek Symbols

$\tilde{\alpha}$, $\tilde{\beta}$	See text, Section 5.1.2.
γ_{ij}, $\gamma_{\alpha\beta}$	Space and surface components respectively of strain tensor.
γ	Array (column vector) of strain tensor components.
δ	Volume error criterion.
δ^{α}_{β}	Kronecker delta. (see Section 5.2.2).
Δ	Overlap of actin and myosin.
Δ_o, Δ_i	Maximum and initial overlaps respectively.
ε_{ijk}	Permutation tensor. (see Section 5.2.2).
ζ	Fibre orientation angle from the ξ surface co-ordinate.
ζ_s	Value of ζ at the endo- or epicardial ventricular surface.
η	Series elastic element extension
η_o	η position of valvular ring.

η_b	η position of venticular bulge.
ν	Rotation of surface co-ordinate system in the symmetrical plane of the left ventricle in the computation of the bulge.
ν_i	Space components of the unit surface normal.
ν_{AB}, ν_{B3}	Cardiac muscle fibre Poisson ratios.
$\underset{\sim}{\rho}$	Position vector of the left ventricular mid-surface.
$\bar{\rho}$	Average distance of the valvular ring perimeter from the origin of the space co-ordinate system.
$\underset{\sim}{\rho}_o$, $\underset{\sim}{\rho}_m$	Position vectors of the prolate and modified prolate spheroid respectively.
ρ_b	Bulge function variable.
$\underset{\sim}{\rho}_i$	Position vector of the left ventricular endocardial surface.
σ_C, σ_P, σ_S	Stresses in the contractile, parallel elastic and series elastic elements of the cardiac muscle fibre respectively.
τ^{ij}, $\tau^{\alpha\beta}$	Space and surface stress tensor components respectively.
Φ, Φ_o	Active state and peak active state respectively.
ψ	Active muscle potential.

Co-ordinate Systems

(A,B,3)	Fibre co-ordinate system.
(x,y,z)	Spatial cartesian co-ordinate system.
(η,ξ,3)	Ventricular mid-surface co-ordinate system.

SHORT GLOSSARY OF MEDICAL TERMS

Actin:	a rod-like fibrous protein constituent of muscle; projects into the sarcomere from the Z-line.
Action Potential:	wave of electrical excitation triggering a contraction in muscle.
Aneurysm:	area of dead muscle in the ventricular wall; often results in ventricular bulging during systole.
Aorta:	main artery of the body; situated at the exit to the left ventricle.
ATP:	adenosine triphosphate; energy-rich biochemical compound.
Diastole:	filling phase of the heart cycle; the myocardium is in a relaxed state during this period.
Endocardium:	inner surface of the ventricle.
Epicardium:	outer surface of the ventricle.
Fibre (muscle):	microscopical unit of a muscle bundle; roughly cylindrical and is branching in cardiac muscle.
"in vitro":	excised; out of natural state (with particular reference to muscle in this Thesis).
"in vivo":	in the natural state.
Isometric:	constant length.
Isotonic:	constant load.
Longitudinal System:	microtubules ramifying the muscle intracellular space in a longitudinal direction (parallel to the sarcomere).
Myocardium:	heart wall.
Myofibril:	striated substructure of the muscle fibre; comprises ordered sarcomeres.
Papillary Muscle:	cylindrical muscle bundles projecting from the apex region of the ventricles; act as strengtheners for supporting the atrio-ventricular valves.
Sarcolemma:	membrane of the myofibrils; the longitudinal system ramifies this membrane.

Sarcomere:	ultrastructural unit of muscle; has a banded appearance caused by the ordered arrays of contractile proteins (actin and myosin); bounded by successive Z-lines.
Sarcoplasmic Reticulum:	muscle cell surface membrane.
Skeletal Muscle:	striated muscle, excepting cardiac.
Systole:	phase during ventricular cycle when muscle is activated; comprises isovolumic contraction until the exit valves open, ejection while they remain open, isovolumic relaxation at the end of the cycle when the valves close as the muscle relaxes.
Transverse Tubular System:	extracellular microtubules which transversely invaginate the muscle fibre; responsible for transferring the action potential from the fibre surface to the Z-lines of the sarcomeres.
Ventricle:	the heart has two ventricles, left and right; the left is the main pumping chamber sending oxygenated blood through the arterial system of the body; the right pumps blood to the lungs for re-oxygenation.
Ventricular Cycle:	comprises diastole and systole.

REFERENCES

Abbot, R.H. 1972. "Comments on the Mechanism of Force Generation in Striated Muscles." Nature (New Biology), 239, 183-187.

Andrews, H.C., A.G. Tescher and R.P. Kruger. 1972. "Image processing by digital computer." IEEE Spectrum, 9, 20-32.

Apostol, T.M. 1957. "Mathematical Analysis." Reading, Massachusetts: Addison-Wesley.

Armour, J.A. and W.C. Randall. 1970. "Structure Basis for Cardiac Function." Amer.J. Physiol., 218, 1517-1523.

Armour, J.A. and W.C. Randall. 1971. "Canine Left Ventricular Intramyocardial Pressures." Amer. J. Physiol., 220, 1833-1839.

Barany, M. 1967. "ATPase Activity of Myosin Correlated with Speed of Muscle Shortening." J. Gen. Physiol., 50, 197.

Baskin, R.J. Paolini. 1966. "Muscle Volume Changes." J. Gen. Physiol., 49, 387-404.

Blinks, J.R. 1970. "Factors Influencing the Prolongation of the Active State by Stretch in Isolated Mammalion Heart Muscle (Abstract)". Federation Proc.,29,611.

Bornhorst, W.J. and J.E. Minardi. 1970. "A Phenomenological Theory of Muscular Contraction." Biophysical J., 10, 137-171.

Bozler, E. 1972. "Feedback in the Contractile Mechanism of the Frog Heart." J. Gen. Physiol.,60 239-247.

Brady, A.J. 1965. "Time and Displacement Dependence of Cardiac Contractility: Problems in Defining the Active State and Force-Velocity Relations." Fedn. Proc., 24, 1410-1420.

Brady, A.J. 1967. "The Three Element Model of Muscle Mechanics: Its Applicability to Cardiac Muscle." Physiologist, Wash., 10, 75-86.

Brady, A.J. 1968. "Active State in Cardiac Muscle". Physiological Rev., 48, 533-551.

Braunwald, E., J. Ross and E.H. Sonnenblick. 1968. "Mechanisms of Contraction of the Normal and Failing Heart". Boston: Little, Brown & Co.

Brutsaert, D.L. and E.H. Sonnenblick. 1969. "Force-Velocity-Length-Time Relations of the Contractile Elements in Heart Muscle of the Cat". Circ. Res., 24, 137-149.

Brutsaert, D.L., V.A. Claes and E.H. Sonnenblick. 1971. "Effects of Abrupt Load Alterations on Force-Velocity-Length and Time Relations During Isotonic Contractions of Heart Muscle: Load Clamping". J. Physiol. (Lond.), 216, 319-330.

Brutsaert, D.L., V.A. Claes and J.J.H. Donders. 1972. "Effects of Controlling the Velociy of Shortening on Force-Velocity-Length and Time Relations in Cat Papillary Muscle". Circ. Res., 30, 310-315.

Burns, J.W., J.W. Covell, R. Myers and J. Ross. 1971. "Comparison of Directly Measured Left Ventricular Wall Stress and Stress Calculated from Geometric Reference Figures". Circ. Res., 28, 611-621.

Burton, A.C. 1957. "The Importance of the Shape and Size of the Heart". Amer. Heart J., 54, 801-810.

Caplan, S.R. 1966. "A Characteristic of Self-Regulated Linear Energy Converters: The Hill Force-Velocity Relation for Muscle". J. Theoret. Biol., 11, 63-86.

Conroy, M.F. 1969. "Estimation of Aortic Distensibility and Instantaneous Left Ventricular Volume in Living Man". Bull. Math. Biophys., 31, 93-104.

Covvey, H.D.J., A.G. Adelman, C.H. Felderhof, K.W. Taylor and E.D. Wigle. 1972. "Television/Computer Dimensiolan Analysis Interface with Special Application to Left Ventricular Cineangiograms". Comput. Biol. Med., 2, 221-233.

Davies, R.E. 1963. "A Molecular Theory of Muscle Contraction: Calcium Dependent Contractions with Hydrogen Bond Formation Plus ATP-Dependent Extensions of the Myosin-Actin Cross-Bridges". Nature, 199, 1068-1074.

Demiray, H. 1972. "A Note on the Elasticity of Soft Biological Tissues". J. Biomechanics, 5, 309-311.

Davis, R.H. and J.H. Ottaway. 1972. "Application of Optimization Procedures to Tracer Kinetic Data". Math. Biosciences, 13, 265-282.

Desai, C.S. and J.F. Abel. 1972. "Introduction to the Finite Element Method". New York: Van Nostrand Reinhold Co.

Edman, K.A.P. and E. Nilsson. 1968. "The Mechanical Parameters of Myocardial Contraction Studied at a Constant Length of the Contractile Element". Acta. Physiol. Scand. 72, 205-219.

Ericksen, J.L. 1972. "Symmetry Transformations for Thin Elastic Shells". Arch. Rational Mech. Analysis, 47, 1-14.

Falsetti, H.L., R.E. Mates, C. Grant, D.G. Greene and I.L. Bunnel. 1970. "Left Ventricular Wall Stress Calculated From One Plane Cine-sngiography". Circ. Res., 26, 71-83.

Feigl, E.O., G.A. Simon and D.L. Fry. 1967. "Auxtonic and Isometric Cardiac Force Transducers". J. Appl. Physiol., 23, 597-600.

Forman, R., L.E. Ford and E.H. Sonnenblick. 1972. "Effect of Muscle Length on the Force-Velocity Relationship of Tetanized Cardiac Muscle". Circ. Res. 31, 195-206.

Fry, D.L., D.M. Griggs and J.C. Greenfield. 1964. "Myocardial Mechanics: Tension-Velocity-Length Relationships of Heart Muscle". Circ. Res., 14, 73-85.

Fung, Y.C. 1965. "Foundations of Solid Mechanics". Englewood Cliffs, N.J.: Prentice Hall.

Fung, Y.C. 1967. "Elasticity of Soft Tissues in Simple Elongation". Amer. J. Physiol., 213, 1532-1544.

Fung, Y.C. 1970. "Mathematical Representation of the Mechanical Properties of Heart Muscle". J. Biomechanics, 3, 381-404.

Fung, Y.C. 1971. "Comparison of Different Models of the Heart Muscle". J. Biomechanics., 4, 289-295.

Gaasch, W.H., W.E. Battle, A.A. Obeler, J.S. Banas and H.J. Levine. 1972. "Left Ventricular Stress and Compliance in Man: With Special Reference to Normalised Ventricular Function Curves". Circulation, 45, 746-762.

Gay, W.A. and E.A. Johnson. 1967. "An Anatomical Evaluation of the Myocardial Length-Tension Diagram". Circ. Res., 21, 33-42.

Ghista, D.N. and A.P. Rao. 1972. "Structural Mechanics of the Mitral Valve; Stresses Sustained by the Valve; Traumatic Determination of the Stiffness of the in vivo Valve". J. Biomechanics, 5, 295-307.

Ghista, D.N., K.M. Patil, K.B. Woo and C. Oliver. 1972. "A Human Left Ventricular Control System Model for Cardiac Diagnosis". J. Biomechanics, 5, 365-390.

Gorlin, R., M.D. Klein and J.M. Sullivan. 1967. "Pospective Correlative Study of Ventricular Aneurysm". Amer. J. Medicine, 42, 512-531.

Gou, P.F. 1970. "Strain Energy Function for Biological Tissues". J. Biomechanics, 3, 547-550.

Gould, P., D. Ghista, L. Brombolich and I. Mirsky. 1972. "In Vivo Stresses in the Human Left Ventricular Wall: Analysis Accounting for the Irregular 3-Dimensional Geometry and Comparison with Idealised Geometry Analyses". J. Biomechanics, 5, 521-539.

Gould, S.E. 1960. "Pathology of the Heart". 2nd ed. Springfield Ill: Charles C. Thomas.

Grant, R.P. 1965. "Notes on the Muscular Architecture of the Left Ventricle". Circulation, 32, 301-308.

Green, A.E. and W. Zerna. 1968. "Theoretical Elasticity". 2nd ed. Oxford: Oxford University Press.

Greene, D.G., R. Carlisle, C. Grant, et al. 1967. "Estimation of Left Ventricular Volume by one Plane Cine-angiography". Circulation, 35, 61-69.

Hadingham, P.T. and H.O. Buhr. 1970. "Simulation of the Heart and Arterial Blood Flow". Presented at the First National Meeting of the South African Institution of Chemical Engineers, 31 August-2 September.

Hadingham, P.T. 1971. "Left Ventricular Dynamics: Progress Report No.1 - A Left Ventricular Model Based on Cardiac Muscle Fibre". Laboratory Technical Report, LTR-BEMP-1/71, Department of Bio-Engineering and Medical Physics, University of Cape Town, Cape Town.

Hatze, H. 1973. "A Theory of Contraction and a Mathematical Model of Striated Model". Preprint; Author's address: Department of Physical Education, University of Stellenbosch, Stellenbosch, South Africa.

Henderson, A.H., R. Forman, D.L. Brutsaert and E.H. Sonnenblick. 1971. "Tetanic Contraction in Mammalian Cardiac Muscle". Cardiovascular Res., 5 Suppl. 1, 96-100.

Hill, A.V. 1938. "The Heat of Shortening and the Dynamic Constants of Muscle". Proc. Roy. Soc., Lond., B126, 136-195.

Hill, A.V. 1948. "On the Time Reguired for Diffusion and its Relation to Processes in Muscle". Proc. Roy. Soc., Lond., B135, 446-453.

Hill, A.V. 1970. "First and Last Experiments in Muscle Mechanics". Cambridge: Cambridge University Press.

Hoffman, W.C. 1973. "A System of Axioms for Mathematical Biology". Math. Biosciences, 16, 11-29.

Hugenholtz, P.G., R.C. Ellison, C.W. Urschel, I. Mirsky and E.H. Sonnenblick. 1970. "Myocardial Force-Velocity Relationships in Clinical Heart Disease". Circulation, 41, 191-202.

Huxley, A.F. 1957. "Muscle Structure and Theories of Contraction". Progr. Biophys. Chem., 7, 255-318.

Huxley, A.F. and R.M. Simmons. 1971. "Proposed Mechanism of Force Generation in Striated Muscle". Nature, 233, 533-538.

Huxley, H.E. 1969. "The Mechanism of Muscular Contraction". Science, 164, 1356-1365.

Huxley, H.E. and Hanson, J. 1954. "Changes in Cross-Striations of Muscle During Contraction and Stretch and their Structural Interpretation". Nature, 173, 973-976.

Jacobson, D.H. and D.Q. Mayne. 1970. "Differential Dynamic Programming". Elsevier.

Janz, R.F. and A.F. Grimm. 1972. "Finite Element Model for the Mechanical Behaviour of the Left Ventricle". Circ. Res., 30, 244-252.

Johnson, J.R. and J.R. Dipalma. 1939. "Intramyocardial and its Relation to Aortic Blood Pressure". Amer. J. Physiol., 125, 234-243.

Julian, F.J. 1969. "Activation in a Skeletal Muscle Contraction Model with a Modification for Insect Fibrillar Muscle". Biophys. J., 9, 547-570.

Katz, A.M. 1970a. "Contractile Proteins of the Heart". Physiological Rev., 50, 63-158.

Katz, A.M. 1970b. "Quantification of Myocardial Contractility". (Editorial). Amer. J. Cardiology, 26, 331-332.

Katz, A.M., P.J. Goodhart and H.L. Goodhart. 1971. "Calcium and the Cardiac Contractile Proteins", in "Calcium and the Heart", Harris, P. and L.H. Opie, Eds., pp 124-134. London: Academic Press.

Kaufmann, R.L., R.M. Bayer and C. Harnasch. 1972. "Autoregulation of Contractility in the Myocardial Cell: Displacement as a Controlling Parameter". Pflügers. Arch. Physiol., 332, 96-116.

Kreuzer, H. and W. Schoeppe. 1963. "Das Verhatten des Druckes in der Herzwand". Pflügers. Arch. Physiol., 278, 181-198.

Langer, G.A. 1968. "Ion Fluxes in Cardiac Excitation and Contraction and Their Relation to Myocardial Contractility". Phys. Rev., 48, 708-757.

Lekhnitskii, S.G. 1963. "Theory of Elasticity of an Anisotropic Elastic Body". San Francisco: Holden-Day,Inc.

Mason, D.T., J.F. Spann and R. Zelis. 1970. "Quantification of the Contractile State of the Intact Human Heart". Amer. J. Cardiol., 26, 248-257.

McCrickerd, J.T. 1969. IEEE Trans. on Bio-Med. Eng. BME-16 95-96.

McDonald, I.G. 1972. "Contraction of the Hypertrophied Left Ventricle in Man Studied by Cineradiography of Epicardial Markers". Amer. J. Cardiol., 30, 587-594.

Meiss, R.A. and E.H. Sonnenblick. 1972. "Controlled Shortening in Heart Muscle: Velocity-Force and Active-State Properties". Amer. J. Physiol., 222, 630-639.

Meerson, F.Z. 1969. "The Myocardium in Hyperfunction, Hypertrophy and Heart Failure". New York: American Heart Association Monograph Number 26.

Mirsky, I. 1969. "Left Ventricular Stresses in the Intact Human Heart". Biophysical J., 9, 189-208.

Mirsky, I. 1970. "Effects of Anisotropy and Nonhomogeneity of Left Ventricular Stresses in the Intact Human Heart". Bull. Math. Biophys., 32, 197-213.

Mirsky, I., R.C. Ellison and P.G. Hugenholtz. 1971. "Assesment of Myocardial Contractility in Children and Young Adults From Ventricular Pressure Recordings". Amer. J. Cardiol., 27, 359-367.

Mitchell, J.H., K. Wildenthal and C.B. Mullins. 1969. "Geometrical Studies of the Left Ventricle Using Biplane Cinefluorography". Fed. Proc., 28, 1334-1343.

Monroe, R.G., W.J. Gamble, C.G. Lafarge, K.A. Edalji and F.J. Hanasek. 1970. "Left Ventricular Performance at High End-Diastolic Pressure in Isolated Perfused Dog Hearts". Circ. Res., 26, 85-99.

Nayler, W.G. and N.C.R. Merrillees. 1971. "Cellular Exchange of Calcium", in "Calcium and the Heart", Harris, P. and L.H. Opie, Eds., pp24-65. London: Academic Press.

Noble, M.I.M. 1972. "Problems Concerning the Application of Concepts of Muscle Mechanics to the Determination of the Contractile State of the Heart". Circulation, 45, 252-255.

Noble, M.I.M., T.E. Bowen and L.L. Hefner. 1969. "Force-Velocity Relationship of Cat Cardiac Muscle Studied by Isotonic and Quick-Release Techniques". Circ. Res., 24, 821-834.

Olsen, R.E. 1960. "Physiology of Cardiac Muscle". In "Handbook of Physiology, Vol. 1, Circulation", W.F. Hamilton, Ed. Washington D.C. American Physiological Society.

Olson, R.E. 1971. "Introduction" in "Calcium and the Heart", Harris, P. and L.H. Opie, Eds. pp 1-23. London: Academic Press.

Parmley, W.W. and E.H. Sonnenblick. 1967. "Series Elasticity in Heart Muscle: Its Relation to Contractile Element Velocity and Proposed Muscle Models". Circ. Res., 20, 112-123.

Parmley, W.W., D.L. Brutsaert and E.H. Sonnenblick. 1969. "Effects of Altered Loading on Contractile EVents in Isolated Cat Papillary Muscle". Circ. Res., 24, 521-532.

Podolsky, R.J. 1959. "The Chemical Thermodynamics and Molecular Mechanism of Muscular Contraction". Ann. N.Y. Acad. Sci., 72, 522-537.

Pollack, G.H. 1970. "Maximum Velocity as an Index of Contractitity in Cardiac Muscle. A Critical Evaluation". Circ. Res., 26, 111-127.

Rapoport, S.I. 1972. "Mechanical Properties of the Sarcolemma and Myoplasm in Frog Muscle as a Function of Sarcomere Length". J. Gen. Physiol., 59, 559-585.

Reul, H., J. Schoenmackers and W. Starke. 1972. "Loss of Pressure, Energy and Performance at Simulated Steneses in Pulsatile Quasiphysiologic Flow". Med. Biol. Eng., 10, 711-718.

Ridgway, E.B. and C.C. Ashley. 1967. "Calcium Transients in Single Muscle Fibres". Biochem. Biophys. Res. Commun., 29, 229-234.

Salisbury, P.F., C.E. Cross and P.A. Rieben. 1962. "Intramyocardial Pressure and Strength of Left Ventricular Contraction". Circ. Res., 10, 608-623.

Sandler, H. 1970. "Dimensional Analysis of the Heart-A Rieview". Amer. J. Med. Sci., 260, 56-70.

Sandler, H. and H.T. Dodge. 1968. "The Use of Single Plane Angiocardiograms for the Calculation of Left Ventricular Volume in Man". Amer. Heart J., 75, 325-334.

Sandler, H. and D.H. Ghista. 1969. "Mechanical and Dynamical Implications of Dimensional Measurements of the Left Ventricle". Fed. Proc., 28, 1344-1350.

Sandow, A. 1965. "Excitation-Contraction Coupling in Skeletal Muscle". Pharmacol. Revies, 17, 265-320.

Scher, A.M. 1962. In "Handbook of Physiology, Volume I, Section 2 : Circulation". Ed. Hamilton, W.F. Washington, D.C.: American Physiological Society.

Sonnenblick, E.H. 1962. "Force-Velocity Relations in Mammalian Heart Muscle". Amer. J. Physiol., 202, 931-939.

Sonnenblick, E.H. 1964. "Series Elastic and Contractile Elements in Heart Muscle". Amer. J. Physiol., 207, 1330-1338.

Sonnenblick, E.H. 1965. "Determinants of Active State in Heart Muscle: Force Velocity Instantaneous Muscle Length, Time". Fed. Proc., 24, 1396-1409.

Sonnenblick, E.H. and A.C. Stam. 1969. "Cardiac Muscle: Activation and Contraction". Annual Review Physiology, 31, 647-674.

Spain, B. 1956. "Tensor Calculus". 2nd ed. Edinburgh: Oliver and Boyd.

Spiro, D. and E.H. Sonnenblick. 1964. "Comparison of Ultrastructural Basis of Contractile Process in Heart and Skeletal Muscle". Circ. Res., 15, (Supp.2), 14-37.

Sonitz, H.M., E.H. Sonnenblick and D. Spiro. 1966. "Relation of Ultrastructure to Function in the Intact Heart: Sarcomere Structure Relative to Pressure Volume Curves of Intact Left Ventricles of Dog and Cat". Circ. Res., 28, 49-66.

Stiles, R.N. and D.M. Alexander. 1972. "A Viscoelastic-Mass Model for Muscle". Math. Biosciences, 14, 343-354.

Streeter, D.D. 1970. "A New Law of the Heart Wall: Its Implications". Talk to the key campaign volunteers of the Washington State Heart Association on 12 December.

Streeter, D.D. and D.L. Bassett. 1966. "An Engineering Analysis of Myocardial Fibre Orientation in Pig's Left Ventricle in Systole". Anatomical Record, 155, 503-512.

Streeter, D.D., H.M. Sponitz, D.P. Patel, J. Ross and E.H. Sonnenblick. 1969. "Fibre Orientation in the Canine Left Ventricular During Diastole and Systole". Circ. Res., 24, 339-347.

Streeter, D.D., R.N. Vaishnay, D.J. Patel, H.M. Sponitz, J. Ross and E.H. Sonnenblick. 1970. "Stress Distribution in the Canine Left Ventricle During Diastole and Systole". Biophysical J., 10, 345-363.

Takauji, M. and C.R. Honig. 1972. "Shortening and ATPase Activities of Single Cardiac Fibrils of Normal Sarcomere Length". Amer. J. Physiol., 222, 1-9.

Treybal, R.E. 1955. "Mass Transfer Operations". New York: McGraw-Hill.

Tritthart, H., R. Kaufmann, H.P. Volkmer, R. Bayer and H. Krause. 1973. "Ca-Movement Controlling Myocardial Contractility I. Voltage-, Current- and Time-Dependence of Mechanical Activity under Voltage Clamp Conditions (Cat Papillary Muscles and Trabeculae)". Pflugers Arch., 338, 207-231.

Urschel, C.W, J.W. Covell, E.H. Sonnenblick, J. Ross and E. Braunwald. 1968. "Myocardial Mechanics in Aortic and Mitral Valvular Regurgitation: the Concept of Instantaneous Impedance as a Determinant of the Performance of the Intact Heart". J. Clin. Invest., 47, 867-883.

Vaishnav, R.N., J.T. Young, J.S. Janicki and D.J. Patel. 1972. "Nonlinear Anisotropic Elastic Properties of the Canine Aorta". Biophys. J., 12, 1008-1027.

Voukydis, P.C. 1969. "Physiological Significance of the Geometrical Shape of the Left Ventricle: Course and Curvature of the Individual Myocardial Fibres". Bull. Math. Biophys., 31, 383-393.

Voukydis, P.C. 1970a. "The effect of Distension of the left Ventricle of the Heart on the length of the Individual Myocardial Fibres". Bull. Math. Biophys., 32, 45-58.

Voukydis, P.C. 1970b. "The Preload of Individual Myocardial Fibres". Bull. Math. Biophys., 32, 323-335.

Voukydis, P.C. 1972a. "The Myocardium as a Composite Material: Analysis". Bull. Math. Biophys., 34, 173-204.

Voukydis, P.C. 1972b. "Geometrical Parameters of the Individual Myocardial Fibres". Bull. Math. Biophys., 34, 205-211.

Voukydis, P.C. 1972c. "Fibre Stress Profiles in the Left Ventricle of the Heart During Diastole: Effects of Distension and Hypertrophy". Bull. Math. Biophys., 34, 379-392.

Walls, E.W. 1972. In "Cunningham's Textbook of Anatomy"., G.J. Romanes, Ed., 11th Ed, London: Oxford University Press.

Wong, A.Y.K. 1971. "Mechanics of Cardiac Muscle, Based on Huxley's MOdel: Mathematical Simulation of Isometric Contraction". J. Biomechanics, 4, 529-540.

Wong, A.Y.K. 1972. "Mechanics of Cardiac Muscle, Based on Huxley's Model: Simulation of Active State and Force-Velocity Relation". J. Biomechanics, 5, 107-117.

Wong, A.Y.K. and P.M. Rautaharju. 1968. "Stress Distribution Within the Left Ventricular Wall Approximated as a Thick Ellipsoidal Shell". Amer. Heart J., 75, 649-662.

Wong, A.Y.K. and P.M. Rautaharju. 1971. "Relations of Sarcomere Lengths to Filling Pressures in Normal and Hypertrophied Hearts". Bull. Math. Biophysics, 33, 203-214.

Woods, R.H. 1892. "A few Application of a Physical Theorem to Membranes in the Human Body in a State of Tension". J. Anat. Physiol., 26, 362-370.

Yang, S.S., L.G. Bentivoglio, V. Maranhão and H. Goldberg. 1972. "From Cardiac Catheterisation Data to Hemodynamic Parameters". Philadelphia: F.A. Davis Co.

Zaret, B.L., B. Pitt and R.S. Ross. 1972. "Determination of the Site, Extent, and Significance of Regional Ventricular Dysfunction during Acute Myocardial Infarction". Circulation, 45, 441-456.

APPENDIX A

TENSOR CALCULUS AND SURFACE GEOMETRY

Basically Tensor Calculus arose from the premise that there should be no preferred co-ordinate system for describing physical quantities. So the form of a physical relationship obtained using a particular co-ordinate system (e.g. Cartesian) should hold in any co-ordinate system.

1. DEFINITIONS

1.1 Scalar Field

A scalar field is a collection of functions which are associated with each allowable co-ordinate system so that if:

$\phi(x_1, \ldots, x_n)$ is described by the $\underset{\sim}{x}$ co-ordinate system

and $\tilde{\phi}(\tilde{x}_1, \ldots, \tilde{x}_n)$ is described by the $\underset{\sim}{\tilde{x}}$ co-ordinate system

then $$\tilde{\phi}(\tilde{x}_1, \ldots, \tilde{x}_n) = \phi(x_1(\underset{\sim}{\tilde{x}}), \ldots, x_n(\underset{\sim}{\tilde{x}})) \quad \text{..... (A 1.1:1)}$$

e.g. a temperature field.

1.2 Contravariant Vector Field

A contravariant vector field is a set of n functions associated with each co-ordinate system with the property that if:

$A^{\mu}(\underset{\sim}{x})$ $(\mu = 1,2, \ldots, n)$ is set associated with the $\underset{\sim}{x}$ co-ordinate system

and $\tilde{A}^{i}(\underset{\sim}{\tilde{x}})$ $(i = 1,2, \ldots, n)$ is the set associated with the $\underset{\sim}{\tilde{x}}$ co-ordinate system

then $$A^{\mu}(x) = \tilde{A}^{i}(\tilde{x}) \frac{\partial x^{\mu}}{\partial \tilde{x}^{i}} \quad \text{..... (A 1.2:1)}$$

1.3 Covariant Vector Field

A covariant vector field is a set of n functions associated with each co-ordinate system with the property that if:

$A_{\mu}(x)$ $(\mu = 1, \ldots, n)$ is the set associated with the $\underset{\sim}{x}$ co-ordinate system

and $\tilde{A}_i(\tilde{x})$ $(i = 1, \ldots, n)$ is the set associated with the $\tilde{x}$ co-ordinate system

then $$A_\mu(x) = \tilde{A}_i(\tilde{x}) \frac{\partial \tilde{x}^i}{\partial x^\mu} \quad \ldots\ldots\ldots\ldots\ldots\ldots\ldots\ldots \text{(A 1.3:1)}$$

1.4 Vectors and Tensors

From the point of view of Tensor Calculus, vectors are considered to be tensors of order one and the transformations of Sections 1.2 and 1.3 can be generalised to tensors of any order. For instance the transformation law for the mixed second order tensor $\tilde{A}^i_j$ can be written:

$$A^\mu_\sigma = \tilde{A}^i_j \frac{\partial \tilde{x}^j}{\partial x^\sigma} \frac{\partial x^\mu}{\partial \tilde{x}^i} \quad \ldots\ldots\ldots\ldots\ldots\ldots\ldots\ldots \text{(A 1.4:1)}$$

1.5 Tensor Nature of the Differential and Gradient

It is well-known from partial differention theory that in order to convert the differential $d\tilde{x}$ to the x co-ordinate system, the formula:

$$dx^i = \frac{\partial x^i}{\partial \tilde{x}^\mu} d\tilde{x}^\mu \quad \ldots\ldots\ldots\ldots\ldots\ldots\ldots\ldots \text{(A 1.5:1)}$$

is used (Apostol, 1957, p109). This relation is equivalent to the transformation equation of a contravariant vector, equ. (A 1.2:1). Hence the co-ordinate differential transforms as a contravariant vector. This is not in general true for the co-ordinate variables x^i or $\tilde{x}^\mu$. But it is sufficient justification for using the contravariant index in their description.

From equ. (A 1.5:1) it follows that the gradient also transforms as a contravariant tensor:

$$\frac{dx^i}{ds} = \frac{\partial x^i}{\partial \tilde{x}^\mu} \frac{d\tilde{x}^\mu}{ds} \quad \ldots\ldots\ldots\ldots\ldots\ldots\ldots\ldots \text{(A 1.5:2)}$$

1.6 Tensor Nature of a Scalar Gradient

The gradient of a scalar function ϕ forms the prototype covariant transformation:

$$\frac{d\phi}{dx^i} = \frac{d\tilde{\phi}}{d\tilde{x}^\mu} \frac{d\tilde{x}^\mu}{\partial x^i} \quad \ldots\ldots\ldots\ldots\ldots\ldots\ldots\ldots \quad (A1.6:1)$$

2 SOME OPERATIONS WITH TENSORS

2.1 Process of Contraction

A particular case of a general process is considered. If the $A^{\mu\nu}$ and $B_{\sigma\tau}$ are the components of two tensor fields with respect to the $\underset{\sim}{x}$ co-ordinate system and if $\tilde{A}^{ij}$ and $\tilde{B}_{rs}$ are the components of the same tensor fields with respect to the $\underset{\sim}{\tilde{x}}$ co-ordinate system, then the set of n^2 functions,

$A^{\mu\nu} B_{\nu\tau}$ in the $\underset{\sim}{x}$ co-ordinate system and

$\tilde{A}^{ij} \tilde{B}_{js}$ in the $\underset{\sim}{\tilde{x}}$ co-ordinate system

and related by the transformation law of a mixed tensor of rank 2. This is one method of generating new tensors from old. An important theorem embodying this process will be given.

2.2 Quotient Theorem

Again a particular case of a general situation will be considered. This theorem essentially provides a means of establishing the tensorial nature of a quantity.
If:

a) one has a set of n^3 functions associated with each co-ordinate system, say

$A^{\mu\nu}{}_{\sigma}$ associated with the x co-ordinate system

$\tilde{A}^{ij}{}_{k}$ associated with the $\underset{\sim}{\tilde{x}}$ co-ordinate system,

and

b) if there exists an arbitrary contravariant vector field with components:

B^σ in the $\underset{\sim}{x}$ co-ordinate system and

$\tilde{B}^k$ in the $\underset{\sim}{\tilde{x}}$ co-ordinate system,

and

c) if the n^2 quantities $A^{\mu\nu}{}_\sigma B^\sigma$ ($\underset{\sim}{x}$ co-ords) and $\tilde{A}^{ij}{}_k \tilde{B}^k$ ($\underset{\sim}{\tilde{x}}$ co-ords) are related by the transformation law of a covariant tensor of rank 2,

then

the quantities $A^{\mu\nu}{}_\sigma$ and $\tilde{A}^{ij}{}_k$ are the components of a mixed tensor of rank 3.

Proof: From what is given:

$$A^{\mu\nu}{}_\sigma B^\sigma = \tilde{A}^{ij}{}_k \tilde{B}^k \frac{\partial x^\mu}{\partial \tilde{x}^i} \frac{\partial x^\nu}{\partial \tilde{x}^j}$$

$$= \tilde{A}^{ij}{}_k B^\sigma \frac{\partial \tilde{x}^k}{\partial x^\sigma} \frac{\partial x^\mu}{\partial \tilde{x}^i} \frac{\partial x^\nu}{\partial \tilde{x}^j}$$

Rearrange the above:

$$B^\sigma \; A^{\mu\nu}{}_\sigma - \tilde{A}^{ij}{}_k \frac{\partial \tilde{x}^k}{\partial x^\sigma} \frac{\partial x^\mu}{\partial \tilde{x}^i} \frac{\partial x^\nu}{\partial \tilde{x}^j} = 0$$

Now B^σ is arbitrary and so we can choose $B^1 \neq 0$ and all other B^σ's = 0. This implies that - - - - = 0 and this can be done for any component of B^σ. Hence the quantities A are related by the transformation law of a mixed tensor of rank 3.

As inferred, this proof can be generalised.

3 METRIC OR FUNDAMENTAL TENSOR

Consider a co-ordinate transformation from the $\tilde{x}$ - to the x - co-ordinate system as follows:

$$x^\nu = x^\nu (\underset{\sim}{\tilde{x}}^i).$$

Provided the Jacobian of the transformation, $|\partial x^\mu / \partial \tilde{x}^j|$, does

not vanish, the inverse transformation,

$$\tilde{x}^i = \tilde{x}^i \ (\underset{\sim}{x}^\nu)$$

is defined.

Now suppose the x - co-ordinate system is rectangular cartesian. Then the length, ds, of a differential line element is given by:

$$ds^2 = dx^\nu \, dx^\nu = \delta_{\mu\nu} \, dx^\mu \, dx^\nu \quad \ldots\ldots\ldots\ldots\ldots\ldots \text{(A 3:1)}$$

where the kronecker delta is defined as:

$$\delta_{\mu\nu} = \delta^{\mu\nu} = \delta_\nu{}^\mu = 1 \text{ if } \mu = \nu$$
$$= 0 \text{ if } \mu \neq \nu \ .$$

Based on the premise that the line element defined in equ. (A 3:1) is invariant under all admissible co-ordinate transformations and since:

$$dx^\mu = \frac{\partial x^\mu}{\partial x^j} \, d\tilde{x}^j,$$

by substitution of this in equ. (A 3:1) we get:

$$ds^2 = \delta_{\mu\nu} \, dx^\mu \, dx^\nu$$
$$= \delta_{\mu\nu} \frac{\partial x^\mu}{\partial \tilde{x}^i} \frac{\partial x^\nu}{\partial \tilde{x}^j} \, d\tilde{x}^i \, d\tilde{x}^j.$$

Hence, in general co-ordinates,

$$ds^2 = \tilde{g}_{ij} \, d\tilde{x}^i \, d\tilde{x}^j \quad \ldots\ldots\ldots\ldots\ldots\ldots\ldots\ldots \text{(A 3:2)}$$

where $\tilde{g}_{ij} = \delta_{\mu\nu} \frac{\partial x^\mu}{\partial \tilde{x}^i} \frac{\partial x^\nu}{\partial \tilde{x}^j}$.

The components g_{ij} are those of the fundamental tensor which is covariant, rank 2 and the tensor is defined to be symmetric.

A set of n^2 functions g^{ij} can be defined as follows:

$$g^{ij} = \frac{\text{co-factor of } g_{ij} \text{ in the matrix } g_{ij}}{\text{determinant of } g_{ij}}$$

From the theory of determinants it follows that

$$g^{ij}\, g_{is} = \delta^{j}_{s}$$

and $$g^{ij} = g^{ji}.$$

The following theorem gives the expected tensor nature of g^{ij}.

Theorem: The components g^{ij} are those of a symmetric contravariant tensor of rank 2 (called the contravariant associate of g_{ij}).

Proof: Let b^{i} be an arbitrary contravariant vector field and let

$$a_{s} = g_{si}\, b^{i}$$

so that a_{s} are the components of an arbitary covariant vector field.

Then: $g^{ls}\, a_{s} = g^{ls}\, g_{si}\, b^{i} = \delta^{l}_{i}\, b^{i} = b^{l}$

Hence $g^{ls}\, a_{s}$ is a contravariant vector field and since a_{s} is an arbitary covariant vector, by the Quotient Theorem, g^{ls} is a contravariant tensor of rank 2.

4. COVARIANT DIFFERENTIATION

Consider a vector

$$\underset{\sim}{r} = \underset{\sim}{g}_{i}\, x^{i}$$

where $\underset{\sim}{g}_{i}$ are the base vectors and x^{i} are the components. Its differential can be formed as follows:

$$d\underset{\sim}{r} = \underset{\sim}{g}_{i}\, dx^{i} + x^{i}\, d\underset{\sim}{g}_{i}.$$

This shows that, in general case, the differential of a vector depends on, not only the change in its components, but also the change of the base vector. It becomes important therefore to formulate a rule for differentiating a tensor which remains invariant under co-ordinate transformations.

The transformation of a contravariant vector is given by:

$$\tilde{A}^i = \frac{\partial \tilde{x}^i}{\partial x^\mu} A^\mu$$

Differentiate both sides of the equation:

$$\frac{\partial \tilde{A}^i}{\partial \tilde{x}^j} = \frac{\partial A^\mu}{\partial x^\nu} \frac{\partial x^\nu}{\partial \tilde{x}^j} \frac{\partial \tilde{x}^i}{\partial x^\mu} + A^\mu \frac{\partial^2 \tilde{x}^i}{\partial x^\mu \partial x^\nu} \frac{\partial x^\nu}{\partial \tilde{x}^j} \quad \ldots\ldots\ldots\ldots \text{(A 4:1)}$$

The last term on the right in the above equation shows that the rules of ordinary differentiation do not remain invariant under co-ordinate transformation.

4.1 Affine Connection

It is clear that the structure of the space (characterised by the metric, for instance) must play a part in governing relationships defined in the given space. Further it is intuitively plausable that the quantity representing the structure of the space, the affine connection, is dependent only on the way the co-ordinates change from one co-ordinate system to the next under co-ordinate transformation and not on any quantity (tensor) described by the co-ordinate systems.

This affine connection is formally defined as follows:

Definition: Let a set of n^3 function be denoted by:

$\Gamma^\mu_{\nu\sigma}$ associated with the $\underset{\sim}{x}$ - co-ordinate system

and $\tilde{\Gamma}^i_{jk}$ associated with the $\underset{\sim}{\tilde{x}}$ - co-ordinate system .

then if:

$$\tilde{\Gamma}^i_{jk} = \Gamma^\mu_{\nu\sigma} \frac{\partial \tilde{x}^i}{\partial x^\mu} \frac{\partial x^\nu}{\partial \tilde{x}^j} \frac{\partial x^\sigma}{\partial \tilde{x}^k} + \frac{\partial^2 x^\tau}{\partial \tilde{x}^j \partial \tilde{x}^k} \frac{\partial \tilde{x}^i}{\partial x^\tau} \quad \ldots\ldots\ldots\ldots \text{(A4.1:1)}$$

the abstract thing determined by these sets of n^3 functions associated with each co-ordinate system is called on affine connection in the space.

4.2 Covariant Derivative - Formulation

In attempting to develop a rule for differentiating a tensor which remains unchanged under co-ordinate transformation, it seems natural to include a term expressing the way the tensor is affected by the space structure. For example, consider the differentiating rule (of a contravariant tensor) as follows:

$$\frac{\partial A^{\mu}}{\partial x^{\nu}} + A^{\sigma}\Gamma_{\nu\sigma}^{\ \mu}$$

Compared to ordinary partial differentiation, the term $A^{\sigma}\Gamma_{\nu\sigma}^{\ \mu}$ has been added in the hope of obtaining a differentiating formula invariant under co-ordinate transformations.
Rewrite equ. (A 4.1:1) interchanging the roles of x and $\tilde{x}$

$$\Gamma_{\nu\sigma}^{\ \mu} = \tilde{\Gamma}_{jk}^{\ i}\frac{\partial x^{\mu}}{\partial \tilde{x}^{i}}\frac{\partial \tilde{x}^{j}}{\partial x^{\nu}}\frac{\partial \tilde{x}^{k}}{\partial x^{\sigma}} + \frac{\partial^{2}\tilde{x}^{l}}{\partial x^{\nu}\,\partial x^{\sigma}}\frac{\partial x^{\mu}}{\partial \tilde{x}^{l}}$$

Multiply by $\partial\tilde{x}^{l}/\partial x^{\mu}$ and rearrange to give:

$$\frac{\partial^{2}\tilde{x}^{l}}{\partial \tilde{x}^{\nu}\,\partial x^{\sigma}} = \frac{\partial \tilde{x}^{l}}{\partial x^{\mu}}\Gamma_{\nu\sigma}^{\ \mu} - \frac{\partial \tilde{x}^{l}}{\partial x^{\mu}}\tilde{\Gamma}_{jk}^{\ i}\frac{\partial x^{\mu}}{\partial \tilde{x}^{i}}\frac{\partial \tilde{x}^{j}}{\partial x^{\nu}}\frac{\partial \tilde{x}^{k}}{\partial x^{\sigma}}$$

Substitute this into equ. (A 4.1:1) yielding:

$$\frac{\partial \tilde{A}^{i}}{\partial \tilde{x}^{j}} = \frac{\partial A^{\mu}}{\partial x^{\nu}}\frac{\partial x^{\nu}}{\partial \tilde{x}^{j}}\frac{\partial \tilde{x}^{i}}{\partial x^{\mu}} + A^{\tau}\frac{\partial x^{\nu}}{\partial \tilde{x}^{j}}\left[\frac{\partial \tilde{x}^{i}}{\partial x^{\mu}}\Gamma_{\tau\nu}^{\ \mu} - \tilde{\Gamma}_{jk}^{\ i}\frac{\partial \tilde{x}^{j}}{\partial x^{\mu}}\frac{\partial \tilde{x}^{k}}{\partial x^{\nu}}\right]$$

This can be reduced to:

$$\frac{\partial \tilde{A}^{i}}{\partial \tilde{x}^{j}} + \tilde{A}^{k}\tilde{\Gamma}_{jk}^{\ i} = \left[\frac{\partial A^{\mu}}{\partial x^{\nu}} + A^{\tau}\Gamma_{\nu\tau}^{\mu}\right]\frac{\partial x^{\nu}}{\partial \tilde{x}^{j}}\frac{\partial \tilde{x}^{i}}{\partial x^{\mu}}$$

Hence the quantity:

$$\frac{\partial A^{\mu}}{\partial x^{\nu}} + A^{\tau}\Gamma_{\nu\tau}^{\mu} = A^{\mu}{}_{,\nu}$$

transforms as a mixed tensor of rank 2. It is the rule for differentiating a tensor we were looking for and is called the covariant derivative of a contravariant vector.

Using a parallel argument the covariant derivative of a covariant vector is found to be:

$$\frac{\partial A_\mu}{\partial x^\nu} - A_\tau \Gamma^\tau_{\nu\mu} = A_{\mu,\nu}$$

Extensions to tensors of higher order and mixed tensors is obvious. For instance, the covariant derivative of the mixed tensor $A^\mu_{\rho\nu}$ is:

$$A^\mu_{\rho\nu,\sigma} = \frac{\partial A^\mu_{\rho\nu}}{\partial x^\sigma} + A^\tau_{\rho\nu}\Gamma^\mu_{\tau\sigma} - A^\mu_{\tau\nu}\Gamma^\tau_{\rho\sigma} - A^\mu_{\rho\tau}\Gamma^\tau_{\nu\sigma} \quad \ldots\ldots\ldots \text{(A 4:3)}$$

5 CHRISTOFFEL SYMBOLS

It was pointed out in Section 4.1 that the structure of the space is in some way dependent on the metric tensor g_{ij}. Alternatively the affine connection can be described in terms of the fundamental tensor g_{ij}.

Definition: In a space with a fundamental covariant tensor of rank 2, g_{ij} one defines the Christoffel Symbol of the First Kind as follows:

$$[ij,k] = \tfrac{1}{2}\left(\frac{\partial g_{ik}}{\partial x^j} + \frac{\partial g_{jk}}{\partial x^i} - \frac{\partial g_{ik}}{\partial x^k}\right) \quad \ldots\ldots\ldots\ldots\ldots\ldots \text{(A 5:1)}$$

One can now define the Christoffel Symbol of the Second Kind as follows:

$$\left\{ \begin{matrix} k \\ i\ j \end{matrix} \right\} = [ij,s]\ g^{sk} \quad \ldots\ldots\ldots\ldots\ldots\ldots\ldots\ldots\ldots\ldots \text{(A 5:2)}$$

It can be shown that the components of the Christoffel symbol of the second kind transform in the same manner as those of an affine connection. This leads to the formulation of the covariant derivative in terms of the Christoffel symbols.

5.1 Covariant Derivative in Terms of Christoffel Symbols

Instead of using the components of the affine connection in equ. (A 4:3), substitute the components of the Christoffel

symbol of the second kind giving:

$$A^{\mu}_{\rho\nu,\sigma} = \frac{\partial A^{\mu}_{\rho\nu}}{\partial x^{\sigma}} + A^{\tau}_{\rho\nu}\left\{ \begin{matrix} \mu \\ \tau\ \sigma \end{matrix} \right\} - A^{\mu}_{\tau\nu}\left\{ \begin{matrix} \tau \\ \rho\ \sigma \end{matrix} \right\} - A^{\mu}_{\rho\tau}\left\{ \begin{matrix} \tau \\ \nu\ \sigma \end{matrix} \right\} \quad \ldots\ldots \text{(A 5.1:1)}$$

Now, if the components of the Fundamental Tensor, g_{ij}, defined in equ. (A 3:2) are known, the Christoffel symbols can be evaluated using equations (A 5:1) and (A 5:2). Thus the components of the covariant derivative can be computed using the above equation.

The Christofel symbols are defined only in terms of the derivatives of the g's. Now in rectangular Cartesian co-ordinates, the $g_{ij} = 1$ for all $i = j$. Hence the derivatives and consequently the Christoffel symbols are zero. Thus from the above equation, the covariant derivative reduces to the ordinary partial derivative.

The implication of this is that if a tensor relationship is set up in rectangular Cartesian co-ordinates in terms of ordinary partial derivatives (generally the easiest co-ordinate system), the equation can be transformed into any other admissible co-ordinates. The only stipulation is that the g's for this new system are known.

The theorem embodying this principle and some of its implications is now formally stated and proved.

5.2 Locally Cartesian Co-ordinate Systems

Theorem: Given a space with an affine connection and a point P in the space, then there exists a co-ordinate system x, such that, in this co-ordinate system, all the components of the affine connection at the point P vanish. Such a co-ordinate system is called locally cartesian at the point P.

Proof: Let $\tilde{\Gamma}^{i}_{jk}$ be the affine connection in $\tilde{x}$ and let $\tilde{x}^{i}$ be the co-ordinates of P.

Suppose:

$$x^\mu = (\tilde{x}^\mu - \tilde{x}^\mu_0) - \tfrac{1}{2}\,\tilde{\Gamma}^\mu_{\sigma\nu}\,(\tilde{x}^\sigma - \tilde{x}^\sigma_0)\,(\tilde{x}^\nu - \tilde{x}^\nu_0) \quad \ldots\ldots \quad (1)$$

is the required relation between the co-ordinate systems which makes the affine connection vanish in $\underset{\sim}{x}$. The co-ordinates of P in $\underset{\sim}{x}$ are (0,0...,0). The affine connection at this point is by equ. (A 4.1:1)

$$\left(\Gamma^i_{jk}\right)_0 = \left(\Gamma^\lambda_{\alpha\beta}\right)_P \left(\frac{\partial x^i}{\partial \tilde{x}^\lambda}\right)_P \left(\frac{\partial \tilde{x}^\alpha}{\partial x^j}\right)_0 \left(\frac{\partial \tilde{x}^\beta}{\partial x^k}\right)_0$$

$$+ \left(\frac{\partial^2 \tilde{x}^\tau}{\partial x^j\, \partial x^k}\right)_0 \left(\frac{\partial x^i}{\partial \tilde{x}^\tau}\right)_P \quad \ldots\ldots\ldots\ldots\ldots\ldots (2)$$

Now from equ. (1) by differentiation:

$$\frac{\partial x^\mu}{\partial \tilde{x}^\nu} = \delta^\mu_\nu - \tfrac{1}{2}\,\tilde{\Gamma}^\mu_{\sigma\nu}\,(\tilde{x}^\sigma - \tilde{x}^\sigma_0)\,\delta^\nu_\nu$$

$$\therefore \left(\frac{\partial x^\mu}{\partial \tilde{x}^\nu}\right)_P = \delta^\mu_\nu \text{ since } \tilde{x}^\sigma - \tilde{x}^\sigma_0 = 0 \text{ at P.}$$

Invert equ. (1) (a power series) to give:

$$\tilde{x}^\mu - \tilde{x}^\mu_0 = x^\mu - \tfrac{1}{2}\,\tilde{\Gamma}^\mu_{st} x^s\, x^t \quad \ldots\ldots\ldots\ldots\ldots\ldots (3)$$

Hence: $\left(\frac{\partial \tilde{x}^\mu}{\partial x^\nu}\right)_0 = \delta^\mu_\nu$ as above

and: $\frac{\partial \tilde{x}^\mu}{\partial x^j} = \delta^\mu_j - \tfrac{1}{2}\,\tilde{\Gamma}^\mu_{st}\, x^t\, \delta^s_j - \tfrac{1}{2}\,\tilde{\Gamma}^\mu_{st}\, x^s\, \delta^t_j$

so: $\frac{\partial^2 \tilde{x}^\mu}{\partial x^j\, \partial x^k} = -\,\tilde{\Gamma}^\mu_{jk}$ after contraction.

When all these derived relations are substituted in equ. (2) we get:

$$\left(\Gamma^i_{jk}\right)_0 = \left(\tilde{\Gamma}^\lambda_{\alpha\beta}\right)_P \delta^i_\lambda\, \delta^\alpha_j\, \delta^\beta_k + \left(-\tilde{\Gamma}^\tau_{jk}\, \delta^i_\tau\right)$$

$$= 0$$

Hence the affine connection vanishes at P.

5.3 Some Implications of Locally Cartesian Co-ordinates

1) In a locally cartesian system

$$\left\{ {i \atop j\ k} \right\}_P = 0 \quad \text{if and only if} \quad \left(\frac{\partial g_{ij}}{\partial x^k} \right)_P = 0 \text{ for all i,j,and k.}$$

Proof: Clearly from equ. (A 5:1), if all the derivatives of g_{ij} are zero at P, $\left\{ {i \atop j\ k} \right\}$ at P is zero.

Also since $\frac{\partial g_{ik}}{\partial x^j} = [ij,k] + [kj,i]$, if $\left\{ {i \atop j\ k} \right\}_P = 0$,

then $\left(\frac{\partial g_{ij}}{\partial x^k} \right)_P = 0$, for all i,j and k.

2) In a locally cartesian co-ordinate system

$$g_{ij,k} = g^{ij},_k = 0, \text{ for all i,j and k.}$$

Proof:

$$g_{ij,k} = \frac{\partial g_{ij}}{\partial x^k} - g_{sj}\left\{ {s \atop k\ i} \right\} - g_{is}\left\{ {s \atop j\ k} \right\}$$

$$= 0 \text{ in a locally cartesian system at P by 1) above.}$$

6 GEOMETRIC INTERPRETATION OF TENSOR COMPONENTS

We can represent the vector $d\underset{\sim}{R}$ joining the points P and Q in rectangular Cartesian co-ordinates as:

$$d\underset{\sim}{R} = dx^r \underset{\sim}{i}_r = dx_r \underset{\sim}{i}^r$$

where the dx's are the vector components and the $\underset{\sim}{i}$'s are the unit base vectors along the co-ordinate axes. Let $\underset{\sim}{\tilde{x}}$ be general co-ordinate system so that:

$$d\tilde{x}^\mu = \frac{\partial \tilde{x}^\mu}{\partial x^i} dx^i \qquad dx^i = \frac{\partial x^i}{\partial \tilde{x}^\mu} d\tilde{x}^\mu$$

$$d\tilde{x}_\mu = \frac{\partial x^i}{\partial \tilde{x}^\mu} dx_i \qquad dx_i = \frac{\partial \tilde{x}^\mu}{\partial x^i} d\tilde{x}_\mu$$

Substitute these in the above equation getting:

$$d\underset{\sim}{R} = \underset{\sim}{g}_{\mu}\, d\tilde{x}^{\mu} = \underset{\sim}{g}^{\mu}\, d\tilde{x}_{\mu}$$

where $\underset{\sim}{g}_{\mu} = \dfrac{\partial x^{s}}{\partial \tilde{x}^{\mu}}\ \underset{\sim}{i}_{s}$ and $\underset{\sim}{g}^{\mu} = \dfrac{\partial \tilde{x}^{\mu}}{\partial x^{s}}\ \underset{\sim}{i}^{s}$ ..... (A 6:1)

Also from equ. (A 6:1)

$$g = \frac{\partial \underset{\sim}{R}}{\partial \tilde{x}^{\mu}} \qquad \text{..... (A 6:2)}$$

which shows that $\underset{\sim}{g}_{\mu}$ is directed tangentially along the co-ordinate curve $\tilde{x}^{\mu}$. This is shown in Fig. A6.1 where the vector $\underset{\sim}{v}$ has been resolved into contravariant components v^1 and v^2 along the $\tilde{x}^1$ and $\tilde{x}^2$ co-ordinate curves with the corresponding base vectors $\underset{\sim}{g}_1$ and $\underset{\sim}{g}_2$. If the reciprocal base vectors, $\underset{\sim}{g}^1$ and $\underset{\sim}{g}^2$ are used (respectively perpendicular to $\underset{\sim}{g}_1$ and $\underset{\sim}{g}_2$), the covariant components, v_1 and v_2 are obtained. It can be seen that in rectangular Cartesian co-ordinates, the distinction between co- and contravariant vectors disappears.

6.1 Physical Components of a Tensor

The base vectors $\underset{\sim}{g}_r$ are, in general, not unit vectors. Hence the dimensions of the tensor quantities v^r in:

$$\underset{\sim}{v} = v^r\, \underset{\sim}{g}_r = v_r\, \underset{\sim}{g}^r\ , \qquad \text{..... (A 6.1:1)}$$

depend on the co-ordinate system chosen. To give them physical meaning, these quantities v^r must be related to unit base vectors. These unit base vectors along the $\underset{\sim}{g}_r$ co-ordinate curves are:

$$\underset{\sim}{g}_r \,/\, |\underset{\sim}{g}_r| = \underset{\sim}{g}_r \,/\, \sqrt{g_{rr}}.$$

Substitute this in equ. (A6.1:1) yielding:

$$\underset{\sim}{v} = v^r\, \sqrt{(g_{rr})}\, \underset{\sim}{g}_r \,/\, \sqrt{g_{rr}} = v_r\, \sqrt{(g^{rr})}\ g^r \,/\, \sqrt{g^{rr}} \quad \text{.. (A6.1:2)}$$

where r is summed over 1,3.

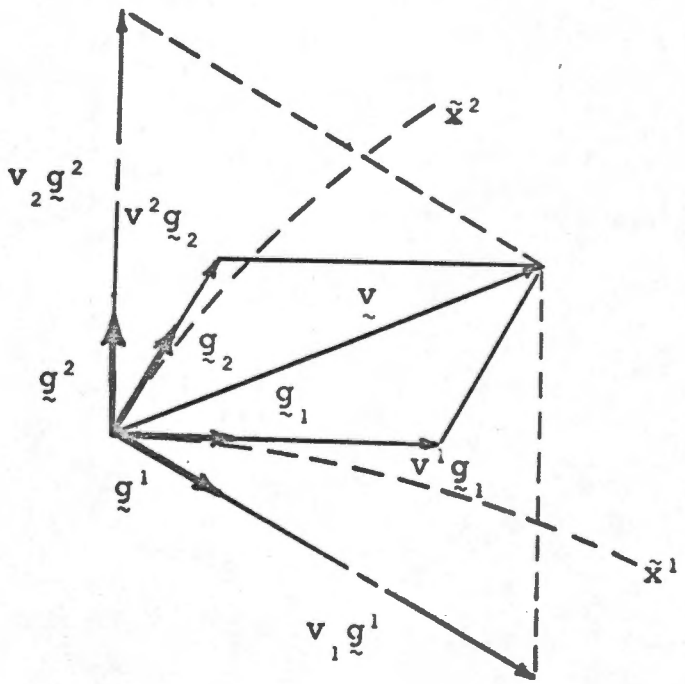

FIG. A6.1

COVARIANT AND CONTRAVARIANT VECTORS IN 2-D NON-ORTHOGONAL CO-ORDINATES

The quantities $v^r \sqrt{g_{rr}}$ and $v_r \sqrt{g^{rr}}$ now have the same physical dimensions and are called the physical components of the vector $\underset{\sim}{v}$. Note, they do not transform as a tensor.

7 SURFACE GEOMETRY - RELEVANT ASPECTS

Application of the Tensor Calculus to 3-dimensional surface geometry (where, in fact, the concept of a tensor had its origin), enables important geometric parameters to be succinctly expressed. The importance of this simplicity of expression in revealing the complex interplay between, on the one hand stress and strain and on the other the geometry of a shell-like structure is exemplified by the elegance of the final stress equilibrium equations for the structure. Its significance in left ventricular modelling is consequently obvious.

Aspects of surface geometry relevant to left ventricular modelling will be developed in a semi-rigorous manner. Essentially, it will be a hybridisation of the presentation by Green and Zerna (1968) and that of Spain (1956): The former's derivations are streamlined using the latter's techniques.

7.1 Permutation Tensors

In rectangular Cartesian co-ordinates, x, the permutation tensor is defined as:

$$e_{ijk} = e^{ijk} \quad \begin{cases} = 0 \text{ when any two indices are equal} \\ = 1 \text{ for even permutations of i,j and k} \\ = -1 \text{ for odd pertutations of i,j and k.} \end{cases}$$

Working with the covariant symbol, its transformation to a general $\underset{\sim}{\tilde{x}}$ co-ordinate is given by:

$$\tilde{\varepsilon}_{\alpha\beta\gamma} = \frac{\partial x^i}{\partial \tilde{x}^\alpha} \frac{\partial x^j}{\partial \tilde{x}^\beta} \frac{\partial x^k}{\partial \tilde{x}^\gamma} e_{ijk}$$

$$= e_{\alpha\beta\gamma} \left| \frac{\partial x^p}{\partial \tilde{x}^\rho} \right| \qquad \ldots\ldots\ldots\ldots\ldots\ldots\ldots\ldots \text{(A7.1:1)}$$

from the theory of determinants where $|\partial x^p/\partial \tilde{x}^\rho|$ is the Jacobian determinant. In Section 3 it was shown that:

$$\tilde{g}_{\mu\nu} = \delta_{ij} \frac{\partial x^i}{\partial \tilde{x}^\mu} \frac{\partial x^j}{\partial x^\nu}$$

Hence the determinant of $\tilde{g}$ is given by:

$$\tilde{g} = |\tilde{g}_{\mu\nu}| = |\frac{\partial x^i}{\partial \tilde{x}^\mu}|^2 .$$

Substituting this in equ. (A 7.1:1) yields the result:

$$\tilde{\varepsilon}_{\alpha\beta\gamma} = e_{\alpha\beta\gamma} \sqrt{\tilde{g}} \ . \quad \ldots\ldots\ldots\ldots\ldots\ldots\ldots\ldots \quad (A\ 7.1{:}2)$$

The quantity ε_{ijk} is defined as the permutation tensor, its tensor character being evident from equ. (A 7.1:1).

The contravariant permutation tensor, $\tilde{\varepsilon}^{\alpha\beta\gamma}$, can be similarly shown to be given by:

$$\tilde{\varepsilon}^{\alpha\beta\gamma} = e^{\alpha\beta\gamma} / \sqrt{\tilde{g}} \ . \quad \ldots\ldots\ldots\ldots\ldots\ldots\ldots\ldots (A\ 7.1{:}3)$$

7.2 Vector Product

The contravariant vector:

$$C^i = \varepsilon^{ijk} A_j B_k \quad \ldots\ldots\ldots\ldots\ldots\ldots\ldots\ldots (A\ 7.2{:}1)$$

can be formed from the two covariant vectors A_j and B_j (the quotient theorem, section 2.2, ensuring the tensorial character of C^i). In the rectangular Cartesian co-ordinate system where the distinction between co- and contravariance disappears, expansion of the above reveals that the C^i are the components of the vector product of A_i and B_i.

Hence C^i is a vector normal to A_i and B_i and of magnitude AB sin θ (where θ is the angle between A_i and B_i) its direction being uniquely determined by the fact that A_i, B_i and C^i form a right-handed system.

7.3 Notation for Surface Geometry

Conventions adopted by Spain (1956) will be used. Namely:

a) surface variables are denoted by u^{α}.

b) Greek indices will have the range 1,2 whereas Latin indices, the range 1,2,3.

An unambiguous distinction between space and surface variables is therefore provided. Unless explicitly stated, these conventions will be adhered to for the remainder of Section 7.

7.4 Relation between space and surface variables

A surface can be parametrically represented by:

$$x^i = x^i(u^{\alpha}) \quad \ldots\ldots\ldots\ldots\ldots\ldots\ldots\ldots\ldots \quad (A\ 7.4{:}1)$$

where x^i are three functions of u^1 and u^2 which are real and continuous. Each pair of values u^{α} determines a point on the surface so that u^{α} form a co-ordinate system on it. The curves u^1 = constant are called the u^2 - curves and vice-versa. Positive directions along the curves correspond to increasing u^{α}.

The contravariant vectors dx^i and du^{α} representing the same displacement in space and on the surface respectively are connected by the equations:

$$dx^i = \frac{\partial x^i}{\partial u^{\alpha}}\, du^{\alpha}. \quad \ldots\ldots\ldots\ldots\ldots\ldots\ldots\ldots\ldots \quad (A\ 7.4{:}2)$$

Thus the line element, ds, on the surface is given by equ. (A 3:2) as:

$$ds^2 = g_{ij}\, dx^i\, dx^j$$

$$= g_{ij}\, \frac{\partial x^i}{\partial u^{\alpha}}\, \frac{\partial x^j}{\partial u^{\beta}}\, du^{\alpha}\, du^{\beta}.$$

setting

$$a_{\alpha\beta} = g_{ij}\, \frac{\partial x^i}{\partial u^{\alpha}}\, \frac{\partial x^j}{\partial u^{\beta}} = a_{\beta\alpha}, \quad \ldots\ldots\ldots\ldots\ldots\ldots\ldots\ldots (A\ 7.4{:}3)$$

the surface metric can be written:

$$ds^2 = d_{\alpha\beta}\, du^\alpha\, du^\beta. \qquad \text{(A 7.4:4)}$$

where $a_{\alpha\beta}$ is the fundamental surface tensor.

Since in the transformation of co-ordinates in space, dx^i is a contravariant vector and du^α an invariant and for the transformation of surface co-ordinates, dx^i is an invariant and du^α a contravariant vector, equ. (A 7.4:2) indicates that $\partial x^i/\partial u^\alpha$ and be regarded as both a contravariant space vector and covariant surface vector. This justifies the notation:

$$x^i_\alpha \equiv \frac{\partial x^i}{\partial u^\alpha}. \qquad \text{(A 7.4;5)}$$

7.5 Permutation Surface Tensor

In the same way the space permutation tensor was introduced (equs (A 7.1:2) and (A 7.1:3)), the surface permutation tensors can be shown to be given by:

$$\varepsilon_{\alpha\beta} = \sqrt{a}\, e_{\alpha\beta} \qquad \text{(A 7.5:1)}$$

$$\varepsilon^{\alpha\beta} = e_{\alpha\beta}/\sqrt{a} \qquad \text{(A 7.5:2)}$$

where $a = |a_{\alpha\beta}|$.

They are related by:

$$\varepsilon_{\alpha\beta} = a_{\alpha\gamma}\, a_{\beta\rho}\, \varepsilon^{\gamma\rho}.$$

Now the angle between the two unit vectors A^α and B^α is given by:

$$\cos\theta = a_{\alpha\beta}\, A^\alpha\, B^\beta$$

Hence $\sin^2\theta = 1 - a_{\alpha\beta}\, A^\alpha\, B^\beta\, a_{\gamma\rho}\, A^\gamma\, B^\rho$

$$= (\varepsilon_{\alpha\rho}\, A^\alpha\, B^\rho)^2.$$

choosing θ such that:

$$\sin\theta = + \varepsilon_{\alpha\beta}\, A^\alpha\, B^\beta \qquad \text{(A7.5:3)}$$

implies that rotation from A^α to B^α is positive if the invariant $\varepsilon_{\alpha\beta}\, A^\alpha\, B^\beta$ is positive (i.e. $0 \leq \theta \leq \pi$).

The angle ω between the co-ordinate curves can now be calculated. By differentiating equ. (A 7.4:4) with respect to u^α, the unit tangent vectors to the u^1 - and u^2 - curves are:

$$\frac{1}{\sqrt{a_{11}}}\ \delta^\alpha_1 \text{ and } \frac{1}{\sqrt{a_{22}}}\ \delta^\alpha_2 \quad \text{respectively.}$$

Thus from equ. (A 7.5:3), the angle ω satisfies:

$$\sin\omega = \sqrt{\left(\frac{1}{a_{11}\, a_{22}}\right)}\ \varepsilon_{\alpha\beta}\ \delta^\alpha_1\ \delta^\beta_2 = \sqrt{\left(\frac{1}{a_{11}\, a_{22}}\right)}\ \varepsilon_{12}$$

$$= \sqrt{(a/a_{11}\, a_{22})} \qquad \text{(A 7.5:4)}$$

Note that the condition that the co-ordinate curves are orthogonal if, and only if, a_{12} vanishes everywhere follows from the relation:

$$a = a_{11}\, a_{22} - (a_{12})^2.$$

7.6 The Position Vector

A surface can be described in terms of the surface co-ordinates u^α (Section 7.4). Hence:

$$\underset{\sim}{r} = \underset{\sim}{r}\ (u^\alpha) \qquad (\alpha = 1,2).$$

Using Fig. A 7.1, any point in the space can be expressed in terms of surface co-ordinates as follows. (Green and Zerna, 1968, pp 31-33):

$$\underset{\sim}{R}(u^1, u^2, u^3) = \underset{\sim}{r}\ (u^1, u^2) + u^3\, \underset{\sim}{a}_3\ (u_1, u_2) \qquad \text{(A 7.6:1)}$$

where $\underset{\sim}{R}$ is the general position vector and where $\underset{\sim}{a}_3$ is the unit normal to the surface at (u^1, u^2) and is a function of u^1 and u^2 only.

In the same manner that equ. (A 6:2) was derived for space base vectors $\underset{\sim}{g}_i$, the surface base vectors are shown, (from

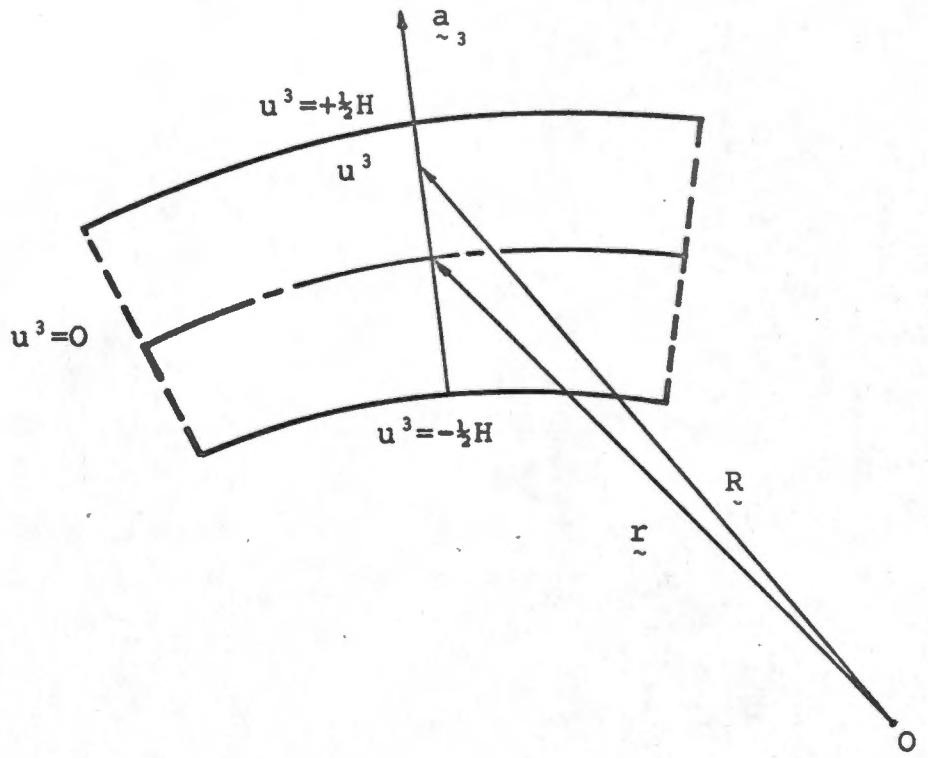

FIG. A7.1

POSITION VECTOR OF A POINT
IN A SHELL

equ. (A 7.6:1)) to be:

$$\underset{\sim}{g}_\alpha = \underset{\sim}{a}_\alpha + u^3 \underset{\sim}{a}_{3,\alpha} \quad \ldots\ldots\ldots\ldots\ldots\ldots\ldots \text{(A 7.6:2)}$$

$$\underset{\sim}{g}_3 = \underset{\sim}{a}_3$$

where: $\underset{\sim}{a}_\alpha = \underset{\sim}{r}_{,\alpha}$ $\quad \ldots\ldots\ldots\ldots\ldots\ldots\ldots\ldots \text{(A 7.6:3)}$

Note that the comma here represents normal partial differentiation. Also, equ. (A 7.6:3) reveals that $\underset{\sim}{a}_\alpha$ is a covariant tensor under surface variable transformation.

Further, the following relationships hold:

$$\underset{\sim}{a}_\alpha \cdot \underset{\sim}{a}_\beta = a_{\alpha\beta} \quad ; \quad \underset{\sim}{a}_3 \cdot \underset{\sim}{a}_\alpha = 0$$
$$\underset{\sim}{a}_3 \cdot \underset{\sim}{a}_3 = 1 \quad ; \quad \underset{\sim}{a}_3 \cdot \underset{\sim}{a}_{3,\alpha} = 0 \quad \ldots\ldots\ldots\ldots\ldots\ldots \text{(A 7.6:4)}$$

When $u_3 = 0$ in equs (A 7.6:2), $\underset{\sim}{a}_\alpha = \underset{\sim}{g}_\alpha$ and $a_{\alpha\beta}$ assumes the role for surface operations of the space metric tensor g_{ij}. Thus, for example:

$$a_{\alpha\beta}\, a^{\beta\gamma} = \delta_\alpha^\gamma \quad ; \quad \underset{\sim}{a}^\alpha = a^{\alpha\beta}\, \underset{\sim}{a}_\beta .$$

7.7 Metric Tensor in Surface Co-ordinates

For a point in space referred to surface co-ordinates given by equ. (A 7.6:1), the metric tensor becomes, using equs (A 7.6:2),

$$g_{\alpha\beta} = \underset{\sim}{g}_\alpha \cdot \underset{\sim}{g}_\beta$$

$$= a_{\alpha\beta} + 2\, u^3\, \underset{\sim}{a}_{3,\alpha} \cdot \underset{\sim}{a}_\beta + (u^3)^2\, \underset{\sim}{a}_{3,\alpha} \cdot \underset{\sim}{a}_{3,\beta} \quad \text{(A 7.7:1)}$$

This can be written in the form:

$$g_{\alpha\beta} = a_{\alpha\beta} - 2\, u^3\, b_{\alpha\beta} + (u^3)^2\, c_{\alpha\beta} \quad \ldots\ldots\ldots\ldots \text{(A 7.7:2)}$$

where $b_{\alpha\beta}$ and $c_{\alpha\beta}$ are defined as:

$$b_{\alpha\beta} = - \underset{\sim}{a}_{3,\alpha} \cdot \underset{\sim}{a}_\beta \quad \ldots\ldots\ldots\ldots\ldots\ldots\ldots\ldots \text{(A 7.7:3)}$$

and $c_{\alpha\beta} = \underset{\sim}{a}_{3,\alpha} \cdot \underset{\sim}{a}_{3,\beta}$ $\quad \ldots\ldots\ldots\ldots\ldots\ldots\ldots\ldots \text{(A 7.7:4)}$

In the following section, it will be shown how $b_{\alpha\beta}$ and $c_{\alpha\beta}$ are related to the surface covariant derivative and then that $b_{\alpha\beta}$ are the components of a tensor (Section 7.10).

7.8 Covariant Derivative with Respect to Surface Co-ordinates

In exactly the same manner as for space co-ordinates (Section 5), Christoffel Symbols referred to surface co-ordinates can be shown to be:

$$\left[\alpha\beta,\gamma\right] = \tfrac{1}{2}\left(\frac{\partial g_{\alpha\gamma}}{\partial u^{\beta}} + \frac{\partial g_{\beta\gamma}}{\partial u^{\alpha}} - \frac{\partial g_{\alpha\beta}}{\partial u^{\gamma}}\right) \quad \text{..... (A 7.8:1)}$$

$$\left\{ {\gamma \atop \alpha\ \beta} \right\} = g^{\gamma\rho}\left[\alpha\beta,\rho\right] \quad \text{..... (A 7.8:2)}$$

where the Greek symbols have the range 1,2.

Note that these symbols are functions of u^3, the distance along the surface normal, (see Fig. A 7.1) by virtue of equ. (A 7.7:1). Hence the symbols involving this normal must also be evaluated.

Using equs (A 7.6:4), (A 7.7:2) and (A7.8:1):

$$\left[\alpha\beta,3\right] = -\tfrac{1}{2}\frac{\partial g_{\alpha\beta}}{\partial u^{3}} = b_{\alpha\beta} - c_{\alpha\beta}u^{3}$$

Hence, at the surface ($u^3 = 0$):

$$\left[\alpha\beta,3\right] = b_{\alpha\beta}$$

and

$$\left\{ {3 \atop \alpha\ \beta} \right\} = a^{33}\left[\alpha\beta,3\right] = b_{\alpha\beta}. \quad \text{.....(A 7.8:3)}$$

A similar derivation reveals that:

$$\left\{ {\beta \atop \alpha\ 3} \right\} = a^{\beta\gamma}\left[\alpha 3,\gamma\right] = -\,b_{\alpha\gamma}a^{\beta\gamma} = -\,b_{\alpha}^{\beta} \quad \text{..... (A 7.8:4)}$$

Further, the quantities $c_{\alpha\beta}$ can be related to $b_{\alpha\beta}$ as follows using equs (A 7.7:3) and (A 7.7:4):

$$b_{\alpha\beta}\, b_{\mu\nu} = \underset{\sim}{a}_{3,\alpha} \cdot \underset{\sim}{a}_{3,\mu}\, a_{\beta\nu}$$

Hence $b_{\alpha\beta}\, b^{\beta}_{\mu} = a^{\beta\nu}\, b_{\alpha\beta}\, b_{\mu\nu} = \underset{\sim}{a}_{3,\alpha} \cdot \underset{\sim}{a}_{3,\mu}$

Thus $b_{\alpha\beta}\, b^{\beta}_{\mu} = c_{\alpha\mu}$ . .....(A 7.8:5)

7.9 Surface Fundamental Forms

The quantities

$$a_{\alpha\beta}\, du^{\alpha}\, du^{\beta}$$
$$b_{\alpha\beta}\, du^{\alpha}\, du^{\beta}$$
$$c_{\alpha\beta}\, du^{\alpha}\, du^{\beta}$$

are called the first, second and third fundamental forms of the surface respectively. Equ. (A 7.8:5) shows that the second and third forms are related. It can be proved that specifying the first and second fundamental forms of the surface uniquely determines the surface in space (except for rotation and/or translation).

7.10 Computation of $b_{\alpha\beta}$

In order to compute the components of $b_{\alpha\beta}$, it is necessary to relate the surface unit vectors $\underset{\sim}{a}_{\alpha}$ and the surface normal $\underset{\approx}{a}_{3}$ to the global spatial co-ordinates. This is revealed by equ. (A 7.7:3).

To derive an expression for the unit normal vector ν^i at any point on a surface, choose its direction such that the u^1 - curve, u^2 - curve and ν^i form a right-handed co-ordinate system on the surface. In Section 7, the unit tangent vectors to the co-ordinate curves were derived:

$$\frac{1}{\sqrt{a_{11}}}\, \delta^{2}_{1} \text{ and } \frac{1}{\sqrt{a_{22}}}\, \delta^{\alpha}_{2} \ .$$

The corresponding space components are (from equ. (A 7.4:5)):

$$\frac{1}{\sqrt{a_{11}}}\, x^{i}_{\alpha}\, \delta^{\alpha}_{2} = \frac{1}{\sqrt{a_{11}}}\, x^{i}_{1}$$

and $\sqrt{\frac{1}{a_{22}}}\ x^i_\alpha\ \delta^\alpha_2 = \sqrt{\frac{1}{a_{22}}}\ x^i_2$.

Now from equ. (A 7.5:4) and the covariant form of equ. (A 7.2:1):

$$\sqrt{(a/a_{11}\ a_{22})}\,\nu_i = \varepsilon_{ijk}\ \sqrt{\frac{1}{(a_{11}\ a_{22})}}\ x^j_1\ x^k_2 ,$$

$$\text{so } \nu_i = \sqrt{\frac{1}{a}}\,\varepsilon_{ijk}\ x^j_1\ x^k_2 \qquad \text{.....(A 7.10:1)}$$

and the covariant character of ν_i is revealed in the equivalent expression:

$$\nu_i = \tfrac{1}{2}\ \varepsilon^{\alpha\beta}\ \varepsilon_{ijk}\ x^j_\alpha\ x^k_\beta \ .$$

In order to generate the second fundamental form, perform the tensor differentiation of (A 7.4:3), noting the substitution of equ. (A 7.4:5);

$$g_{ij}\ x^i_{\alpha,\gamma}\ x^j_\beta + g_{ij}\ x^i_\alpha\ x^j_{\beta,\gamma} = 0 \qquad \text{.....(A 7.10:2)}$$

where the tensor derivative is shown to be (Spain, 1956, pp. 74-76):

$$x^i_{\alpha,\beta} = \frac{\partial^2 x^i}{\partial u^\alpha\ \partial u^\beta} + \left\{ \begin{matrix} i \\ j\ k \end{matrix} \right\} x^j_\alpha\ x^k_\beta - \left\{ \begin{matrix} \gamma \\ \alpha\ \beta \end{matrix} \right\} x^i_\gamma \qquad \text{.....(A 7.10:3)}$$

Thus $x^i_{\alpha,\beta}$ is symmetric in α and β.

Now subtract equ. (A 7.10:2) from the sum of the two formed by cyclic interchange of the indices α,β and γ giving:

$$g_{ij}\ x^i_{\alpha,\beta}\ x^i_\gamma = 0. \qquad \text{.....(A 7.10:4)}$$

Hence $x^i_{\alpha,\beta}$ is a contravariant space vector orthogonal to all vectors x^i_γ lying in the surface. It is then co-directional with the normal vector ν^i and so the quantities $b_{\alpha\beta}$ must exist such that:

$$x^i_{\alpha,\beta} = -\ b_{\alpha\beta}\ \nu^i \qquad \text{.....(A 7.10:5)}$$

which shows, according to the quotient theorem, Section 2.2,

that $b_{\alpha\beta}$ form the components of a covariant symmetric surface tensor.

Contraction of equ. (A 7.10:5) with ν_i (a unit vector) and subsequent substitution of equ. (A 7.10:1) provides a suitable computational formula for $b_{\alpha\beta}$,

$$b_{\alpha\beta} = -\sqrt{\frac{1}{a}}\,\varepsilon_{ijk}\,x^i_{\alpha,\beta}\,x^j_1\,x^k_2\,. \qquad \text{.....(A 7.10:6)}$$

The negative sign is to ensure that the $b_{\alpha\beta}$ have positive values for shell-like structures whose origin is within the shell.

It can readily be shown that equ. (A 7.10:1) for the unit normal vector ν_i, and consequently equ. (A 7.10:6) above for the second fundamental form are the same if the surface co-ordinate curves, u^1 and u^2 are non-orthogonal.

APPENDIX B

BASIC ELASTICITY THEORY

1 INTRODUCTION

Despite the discrete structure of all matter on a molecular scale, this structure need not "per se" influence the macroscopic behaviour of a given material. An analysis of its elastic properties, for instance, can proceed without regard for the molecular nature of the material in the sense that it can be postulated that the elastic character of a differential volume element containing a given point is independent of the volume of the element, even in the limit. This idea is the basic precept of Continuum Mechanics.

The development of the theory in this Appendix is based on that given by Green and Zerna (1968). Firstly the strain and stress tensors are defined followed by the derivation of the stress equations of equilibrium and a discussion of stress-strain relations.

2 THE STRAIN TENSOR

As a given body is strained from its initial undeformed (at time t = 0) configuration, B_0, to a deformed state, B, (at time t = t) so the material points in the body move with respect to one another.

Let x^i be the co-ordinates of a given point, P_0, in the material in B_0,

X^i be the co-ordinates of the same material point which has moved to P in B.

If X^i are referred to the same general curvilinear co-ordinate system as x^i, then the displacement vector, v^i, of the point between the deformed and undeformed states is given by:

$$v^i = X^i - x^i \quad \ldots\ldots\ldots\ldots\ldots\ldots\ldots\ldots\ldots\ldots \quad (B2:1)$$

Suppose, on the other hand, that x^i and X^i are related to a general curvilinear co-ordinate system $\tilde{x}$, in which the numerical values of the co-ordinate variables specifying the same point P in both B and B_o, i.e. $\tilde{x}^i$, are identical. (The co-ordinate system may be thought of as distorting with the body). Hence:

$$\text{in } B_o \quad x^i = x^i\ (\tilde{x}^k) \qquad \ldots\ldots\ldots\ldots\ldots\ldots\ldots \text{(B2:2)}$$

$$\text{and in } B \quad X^i = X^i\ (\tilde{x}^k). \qquad \ldots\ldots\ldots\ldots\ldots\ldots\ldots \text{(B2:3)}$$

From equ. (A3:2), the line elements in the original and final configurations with respect to the $\tilde{x}$ co-ordinate system are given by:

$$\text{in } B_o; \quad ds_o^2 = \tilde{g}_{ij}\, d\tilde{x}^i\, d\tilde{x}^j$$

$$\text{in } B\ ; \quad ds^2 = \tilde{G}_{ij}\, d\tilde{x}^i\, d\tilde{x}^j$$

The change in the line elements caused by the deformation is thus:

$$ds^2 - ds_o^2 = (\tilde{G}_{ij} - \tilde{g}_{ij})\, d\tilde{x}^i\, d\tilde{x}^j,$$

and the quantity:

$$\tilde{\gamma}_{ij} = \tfrac{1}{2}(\tilde{G}_{ij} - \tilde{g}_{ij}) \qquad \ldots\ldots\ldots\ldots\ldots\ldots\ldots \text{(B2:4)}$$

is defined as the strain tensor which is symmetric: (see Section 3 of Appendix A).

The strain tensor can also be expressed in terms of the covariant components of the displacement vector, $\tilde{v}$, given by equ. (B2:1). Express this in vector form using equ. (A6.1:2) yielding:

$$\underset{\sim}{\tilde{v}} = \tilde{v}_m\, \underset{\sim}{\tilde{g}}^m = \tilde{V}_m\, \underset{\sim}{\tilde{G}}^m \qquad \ldots\ldots\ldots\ldots\ldots\ldots\ldots \text{(B2:5)}$$

for the unstrained and strained configurations respectively.

The rate at which this vector changes with respect to $\tilde{x}^i$ is given from the above equation by:

$$\underset{\sim}{\tilde{v}}_{,i} = \tilde{v}_m|_i \, \underset{\sim}{\tilde{g}}^m = \tilde{v}_m||_i \, \underset{\sim}{\tilde{G}}^m , \qquad \text{..... (B2:6)}$$

where $\tilde{v}_m|_i$ and $\tilde{v}_m||_i$ are the covariant derivatives of the displacement vector components with respect to $\tilde{x}^i$ in the undeformed and deformed configuations respectively. (See Section 4 in Appendix A).

Using equs (B2:6) in equ. (B2:4) and also employing equ. (A6:2), following some manipulation, the following expressions for the strain tensor are obtainable (Green and Zerna, 1968, p.57):

$$\tilde{\gamma}_{ij} = \tfrac{1}{2} \left(\tilde{v}_i|_j + \tilde{v}_j|_i + \tilde{v}^r|_i \, \tilde{v}_r|_j\right)$$

$$= \tfrac{1}{2} \left(\tilde{v}_i||_j + \tilde{v}_j||_i + \tilde{v}^r||_i \, \tilde{v}_r||_j\right) , \qquad \text{..... (B2:7)}$$

depending on whether the undeformed or deformed configurations are referred to. The former description of the strain tensor is known as the Eulerian or spatial description whilst the latter is the Lagrangian or material description.

3 THE STRESS TENSOR

Two classes of force can act on a body:

a) body force $\underset{\sim}{F}$ per unit mass which effectively act on units of volume (e.g. gravitational or electromagnetic force) and

b) surface force $\underset{\sim}{P}$ per unit area which act on surface elements (e.g. the contact pressure of colliding bodies).

Suppose that the body B_0 is moved to its strained position B by the action of the body and surface forces $\underset{\sim}{F}$ (per unit mass) and $\underset{\sim}{P}$ (per unit area) respectively. Consider an element ΔS of a surface situated in the strained body B and which contains within its area a point O.

Now let $\underset{\sim}{\nu}$ be the unit vector at O normal to ΔS with a direction outwards from the surface ΔS. The force exerted across the area ΔS can be considered statically equivalent to a force $\Delta \underset{\sim}{Z}$ at O and a couple $\Delta \underset{\sim}{G}$. By letting the area ΔS tend to zero (always keeping the point O within it), the vector $\Delta \underset{\sim}{Z}/\Delta S$ tends to a definite limit:

$$\overset{\nu}{\underset{\sim}{T}} = \lim_{\Delta S \to O} \frac{\Delta \underset{\sim}{Z}}{\Delta S} .$$

$\overset{\nu}{\underset{\sim}{T}}$ is known as the stress vector and, in general, is not in the direction $\underset{\sim}{\nu}$. It represents the force, per unit area of surface in the deformed body, exerted by material lying on the positive side of the area on material lying on the negative side (the sign being given by the unit normal at O). It can easily be shown that the force, per unit area of surface in the deformed body, exerted by material lying on the negative side of the area, on material lying on the positive side is $- \overset{\nu}{\underset{\sim}{T}}$. (Fung, 1965, p. 63).

The acceleration of each point of the body B is denoted by $\underset{\sim}{f}$. Consider an arbitrary volume V in the body B bounded by a closed surface S. Cauchy's equation of motion (conservation of force) is:

$$\int_S \overset{\nu}{\underset{\sim}{T}} \, ds + \int_V \rho(\underset{\sim}{F} - \underset{\sim}{f}) \, dV = O \quad \ldots\ldots\ldots\ldots\ldots\ldots \quad (B3:1)$$

for the volume V and Cauchy's equation of moments (conservation of the rate of change of the moment of the momentum) is:

$$\int_S (\underset{\sim}{R} \times \overset{\nu}{\underset{\sim}{T}}) \, ds + \int_V \rho \, \underset{\sim}{R} \times (\underset{\sim}{F} - \underset{\sim}{f}) \, dV = O \quad \ldots\ldots\ldots \quad (B3:2)$$

where ρ is the density of the body B.

At any point P of the strained body B a parallelepiped bounded by the surfaces x^i = constant, $x^i + dx^i$ = constant and a tetrahedron whose edges are formed by the co-ordinate curves PP_i of lengths ds^i, and the curves P_1P_2, P_2P_3, P_3P_1 (see

Fig. B3:1), which in the limit are defined by the vectors:

$$d\underset{\sim}{s}^j - d\underset{\sim}{s}^i = \underset{\sim}{G}_j \, dx^j - \underset{\sim}{G}_i \, dx^i \quad \ldots\ldots\ldots\ldots\ldots\ldots \quad (B3:3)$$

is constructed, where i and j are not summed and $i \neq j$ in the above equation.

The surfaces x^i = constant of the tetrahedron have areas dS_i and may be represented vetorially as:

$$dS_i \, \underset{\sim}{G}^i \sqrt{|G^{ii}|}. \quad \ldots\ldots\ldots\ldots\ldots\ldots\ldots\ldots\ldots \quad (B3:4)$$

Also, the area of $P_1 P_2 P_3$ is denoted by dS and is represented vectorially by:

$$\underset{\sim}{\nu} \, dS, \quad \ldots\ldots\ldots\ldots\ldots\ldots\ldots\ldots\ldots\ldots \quad (B3:5)$$

where $\underset{\sim}{\nu}$ is the unit normal to the surface. Hence, since the area $P_1 P_2 P_3$ is vectorially equivalent to the surfaces x^i = constant of the tetrahedron, it follows from equs (B3:4) and (B3:5) that:

$$\underset{\sim}{\nu} \, dS = \sum_{i=1}^{3} dS_i \, \underset{\sim}{G}^i \sqrt{|G^{ii}|},$$

or $$\nu_i \sqrt{(G^{ii})} \, dS = dS_i, \quad \ldots\ldots\ldots\ldots\ldots\ldots\ldots \quad (B3:6)$$

since $\underset{\sim}{\nu} = \nu_i \, \underset{\sim}{G}^i$.

By applying the equation of motion, equ. (B3:1), to the infinitesimal tetrahedron $PP_1 P_2 P_3$, in the limit, keeping the direction of $\underset{\sim}{\nu}$ fixed, the following result is obtained:

$$\underset{\sim}{T}^{\nu} \, dS = \underset{\sim}{T}^{i} \, dS_i, \quad \ldots\ldots\ldots\ldots\ldots\ldots\ldots\ldots \quad (B3:7)$$

where $\underset{\sim}{T}^{i}$ are the stress vector, $\underset{\sim}{T}^{\nu}$, components acting on the surfaces dS_i. Volume forces and mass-accelerations acting on the tetrahedron do not appear in this equation since they are of higher order of smallness (being taken over volume) than the surface forces.

From equs (B3:6) and (B3:7),

$$\underset{\sim}{T}^{\nu} = \sum_{i=1}^{3} \nu_i \, \underset{\sim}{T}^{i} \sqrt{G^{ii}}. \qquad \text{..... (B3:8)}$$

Since, under general transformations of co-ordinates, $\underset{\sim}{T}^{\nu}$ is an invariant, (i.e. the stress vector does not depend on the co-ordinate system used to describe it), and ν_i is a covariant vector, it follows from equ. (B3:8) that $\underset{\sim}{T}^{i}\sqrt{G^{ii}}$ transforms according to a contravariant type of transformation (Quotient Theorem, Section 2.2 of Appendix A).

Resolving these vectors $\underset{\sim}{T}^{i}\sqrt{G^{ii}}$ into their components with respect to the base vectors $\underset{\sim}{G}_j$ and $\underset{\sim}{G}^j$, then:

$$\underset{\sim}{T}^{i}\sqrt{G^{ii}} = \tau^{ij} \, \underset{\sim}{G}_j = \tau^{i}_{j} \, \underset{\sim}{G}^j \qquad \text{..... (B3:9)}$$

On the other hand, using the base vector components of $\underset{\sim}{T}^{\nu}$,

$$\underset{\sim}{T}^{\nu} = T^{\nu}_{j} \, \underset{\sim}{g}_j = T^{\nu}_{j} \, \underset{\sim}{g}^j,$$

and equs (B3:8) and (B3:9) yield:

$$T^{\nu}_{j} = \tau^{ij} \, \nu_i = \tau^{j}_{i} \, \nu^i. \qquad \text{..... (B3:10)}$$

The tensorial character of both τ^{ij} and τ^{i}_{j} is revealed by equ. (B3:9) or (B3:10) by using the Quotient Theorem.

In the contravariant form of the stress tensor, τ^{ij}, for example:

- i refers to the direction of the normal to the surface being considered and
- j refers to the direction of the component of the stress vector,

so that normal stresses are given by i=j and shearing stresses by $i \neq j$.

3.1 Physical Components of a Second Order Tensor

The stress tensor τ^{ij} will be considered, but this analysis applies equally well to the strain tensor γ_{ij}.

Equ. (B3:9) can be rewritten as:

$$\underset{\sim}{T}^{i} = \sum_{j=1}^{3} \sqrt{(G_{jj}/G^{ii})}\ \tau^{ij}\ \underset{\sim}{G}_{j}/\sqrt{G_{jj}}\ , \quad \text{i not summed}$$

In a similar manner to that given in Section 6.1 of Appendix A, the quantities:

$$\sigma^{ij} = \tau^{ij}\sqrt{(G_{jj}/G^{ii})}, \quad \text{.....(B3.1:1)}$$

have physical units and are the physical components of the stress tensor. The physical components of the strain tensor are correspondingly (Fung, 1965, p 112) given by:

$$\varepsilon_{ij} = \gamma_{ij}\sqrt{(G^{ii}\ G^{jj})}. \quad \text{.....(B3.1:2)}$$

3.2 Sign Convention for Stress Tensor Components

An example will suffice to explain the sign convention for stress tensor components.

Suppose that the outer normal of the surface considered in the body points in the positive direction along the x^1 axis and also that τ^{12} is negative. Then the vector representing τ^{12} will point in the negative direction of the x^2 axis.

3.3 Gauss' (Divergence) Theorem

This theorem is required in the following two Sub-sections. It will merely be stated here as the proof is well-known (e.g. Apostol, 1956, pp 339-341).

In words: the covariant divergence of a well-behaved tensor field $A_{jkl...}$ taken over a volume V is the same as integrating the flux of $A_{jkl...}$ over the surface S bounding the volume.

$$\int_V (A_{jkl\ldots})\, dV = \int_S (A_{jkl\ldots})\nu_i\, dS \quad \ldots\ldots\ldots\ldots \quad (B3.3:1)$$

where ν_i are the components of the surface normal.

3.4 Symmetry of the Stress Tensor

Expressing equ. (B3:2) in tensor form (using the deformed configuration B with the $\underset{\sim}{X}$ co-ordinate system):

$$\int_S (e_{ijk}\, X^j\, \overset{\nu}{T}{}^k)\, dS + \int_V \rho\, e_{ijk}\, X^j\, (F^k - f^k)\, dV = 0$$

Substitute equ. (B3:10) into the above equation and then apply Gauss' Theorem yielding:

$$\int_V (e_{ijk}\, X^j\, \tau^{lk})||_l\, dV + \int_V \rho\, e_{ijk}\, X^j\, (F^k - f^k)\, dV = 0$$

Carry out the covariant differentiation in (---) in the first term of the above equation, and rearrange:

$$\int_V e_{ijk}\, X^j\, \{\rho(F^k - f^k) + \tau^{lk}||_l\}\, dV + \int_V e_{ijk}\, \tau^{jk}\, dV = 0$$

Now since the body is in equilibrium, the first term vanishes (from equ. (B4:1) in Section 4 below). Thus, for the arbitary volume V,

$$e_{ijk}\, \tau^{jk} = 0 \text{ and so } \tau^{jk} = \tau^{kj}.$$

4 EQUATION OF STRESS EQUILIBRIUM

Consider the equilibrium of the deformed body B (with the associated $\underset{\sim}{\tilde{X}}$ co-ordinate system). Cauchy's equation of motion, equ. (B3:1) can be expressed in tensor form as follows:

$$\int_S \overset{\nu}{T}{}^k\, dS + \int_V \rho\, (F^k - f^k)\, dV = 0.$$

Substituting equ. (B3:10) this becomes:

$$\int_S \tau^{jk}\, \nu_j\, dS + \int_V \rho\, (F^k - f^k)\, dV = 0.$$

Using Gauss' theorem equ. (B3.3:1) in the first term of the above equation yields:

$$\int_V \{\tau^{jk}||_j + \rho\ (F^k - f^k)\}\ dV = 0,$$

and since the volume V is arbitrary,

$$\tau^{jk}||_j + \rho\ (F^k - f^k) = 0. \quad \ldots\ldots\ldots\ldots\ldots\ldots \quad (B4:1)$$

This is the equation of equilibrium (expressed with reference to the deformed configuration B).

5 THE INFINITESIMAL STRESS-STRAIN RELATIONSHIP

In this section a very brief account of the general infinitesimal stress-strain relation will be presented.

Firstly the meaning of infinitesimal deformation and the definition of elastic potential are stated and the general stress-strain relation is derived from the elastic potential. After discussing the meaning of the terms anisotropic and non-homogeneous, the influence of symmetry considerations on the matrix of elastic constants in the general infinitesimal stress-strain relation is analysed. In particular, the transversely isotropic as well as the isotropic and homogeneous cases are studied. Finally, the stress-strain relation in terms of the elastic potential and the strain invariants is considered.

5.1 Infinitesimal Deformation

Infinitesimal deformation implies that the components, v^i, of the displacement vector and their derivatives with respect to $\tilde{x}^i$ are infinitesimals of the first order and so the squares and products of these infinitesimals can be neglected in comparison to their first powers.

Thus the strain tensor, equ. (B2:7) becomes:

$$\gamma_{ij} = \tfrac{1}{2}\ (v^i|_j + v^j|_i) \quad \ldots\ldots\ldots\ldots\ldots\ldots \quad (B5.1:1)$$

and the distinction between Lagrangian and Eulerian co-ordinates disappears (See Section 2). However, if a finite strain is computed as a trajectory of successive infinitesimal displacements, then this distinction reappears in considering the finite displacement.

5.2 Elastic Potential and the General Stress-Strain Relation

It can be shown, by considering the difference between the rate of work of the surfaces forces over the surface S plus the rate of work of the body forces throughout the volume V and the rate of increase of kinetic energy of the mass in S, that (Green and Zerna, 1968, pp 62-63):

$$\tau^{ij} = \tfrac{1}{2}\,\rho\left(\frac{\partial E}{\partial \gamma_{ij}} + \frac{\partial E}{\partial \gamma_{ji}}\right) \qquad \text{.....(B5.2:1)}$$

where E is the elastic potential of the body per unit mass. It is convenient to express equ. (B5.2:1) in terms of an elastic potential W per unit volume of the unstrained body B_0. Since mass elements are conserved under deformation:

$$\rho_0 \sqrt{g} = \rho \sqrt{G}$$

where ρ_0 is the density of B_0. Hence:

$$\tau^{ij} = \left(\frac{\partial W}{\partial \gamma_{ij}} + \frac{\partial W}{\partial \gamma_{ji}}\right)/2\sqrt{I_3} \qquad \text{.....(B5.2:2)}$$

where $W = \rho_0 E$, $W = W(\gamma_{ij})$ and $I_3 = G/g$, the third strain invariant.

For infinitesimal strain g = G and so equ.(B5.2:2) becomes:

$$\tau^{ij} = \tfrac{1}{2}\left(\frac{\partial W}{\partial \gamma_{ij}} + \frac{\partial W}{\partial \gamma_{ji}}\right). \qquad \text{.....(B5.2:3)}$$

The elastic potential W is invariant under all co-ordinate transformations (Green and Zerna, 1968, p 64) and a suitable form to assume for $W(\gamma_{ij})$ consistent with the approximations associated with infinitesimal strain is:

$$W = \text{constant} + E^{ij}\,\gamma_{ij} + \tfrac{1}{2}\,E^{ijrs}\,\gamma_{ij}\,\gamma_{rs}. \qquad \text{.....(B5.2:5)}$$

Substituting equ. (B5.2:4) into equ. (B5.2:3) and taking W to be zero when the body is in the initial state B_0 when $\gamma_{ij} = 0$ also assuming that the body is unstressed in the state B_0 yields:

$$\tau^{ij} = E^{ijrs} \gamma_{rs} , \quad \text{.....(B5.2:5)}$$

where E^{ijrs} are tensor components (by the Quotient theorem) known as the elastic coefficients of the body. Without loss of generality it can be assumed E^{ijrs} has the symmetric properties:

$$E^{ijrs} = E^{jirs} = E^{ijrs} = F^{rsij}. \quad \text{.....(B5.2:6)}$$

The expression (B5.2:5) represents a general relation between stress and (infinitesimal) strain. It will be convenient to consider the form of this equation in the rectangular cartesian co-ordinate system:

$$t_{ij} = C_{ij}^{rs} e_{rs} \quad \text{..... (B5.2:7)}$$

where t_{ij} and e_{rs} are the rectangular cartesian stress end strain tensors respectively and C_{ij}^{rs} the associated 2-dimensional matrix of elastic coefficients.

5.3 Homogeneity and Isotropy

The meaning of these two terms, homogeneity and isotropy is embodied in the properties of the elastic coefficients C_{ij}^{rs}. If the density of the orginal body B_0 is constant and if the coefficients are constant (the same at all points in the body) then the body is elastically homogeneous. As an aside it should be indicated that in such a body the covariant derivative of the general elastic coefficients E_{ij}^{rs} is zero, but this is not so in a nonhomogeneous body.

At a particular point in the body, the magnitude of the

coefficients C_{ij}^{rs} may depend on orientation in the body in which case the material is anisotropic. In an isotropic body, on the other hand, these constants are independent of orientation.

Homogeneity and isotropy are therefore associated with translational and rotational symmetry within the body respectively.

5.4 Elastic Coefficients for a Transversely Isotropic Body

In order to obtain the elastic coeffieients for a transversely isotropic body the form of the elastic potential (or strain energy) function, equ. (B5.2:5), is analysed under co-ordinate transformations allowed within the framework of this imposed symmetry. The transformations which maintain this symmetry are accordingly:

a) about a plane, the symmetric isotropic plane and

b) about an axis, the anisotropic axis, orthogonal to this plane.

It can be shown that the number of independent elastic coefficients for a transversely isotropic body reduces to five (Green and Zerna 1968, pp 153-156; Leknitskii, 1963, pp 15-24). If the components of the stress and strain tensors are written as column vectors $[t]_{lmn}$ and $[e]_{lmn}$ respectively, then equ. (B5.2:7) can be expressed as:

$$[t]_{lmn} = [c][e]_{lmn}, \qquad \text{..... (5.4:1)}$$

where the matrix of elastic coefficients is:

$$[c] = \begin{bmatrix} C_{11}^{11} & C_{22}^{11} & C_{22}^{11} & 0 & 0 & 0 \\ C_{22}^{11} & C_{22}^{22} & C_{33}^{22} & 0 & 0 & 0 \\ C_{22}^{11} & C_{33}^{22} & C_{22}^{22} & 0 & 0 & 0 \\ 0 & 0 & 0 & C_{33}^{11} & 0 & 0 \\ 0 & 0 & 0 & 0 & C_{33}^{11} & 0 \\ 0 & 0 & 0 & 0 & 0 & \tfrac{1}{2}(C_{22}^{22}-C_{22}^{11}) \end{bmatrix} \qquad \text{..... (B5.4:2)}$$

and the stress and strain vectors are:

$$[t]_{lmn} = \begin{bmatrix} t_{11} \\ t_{22} \\ t_{33} \\ t_{12} \\ t_{13} \\ t_{23} \end{bmatrix} \quad \text{and} \quad [e]_{lmn} = \begin{bmatrix} e_{11} \\ e_{22} \\ e_{33} \\ e_{12} \\ e_{13} \\ e_{23} \end{bmatrix} . \qquad \text{..... (B5.4:3)}$$

In this formulation, the 1-axis is the anisotropic axis and the 2,3- plane is the plane of isotropy.

If the physical components of strain are given (having been obtained from a general curvilinear co-ordinate system by using equ. (B3.1:2)), the physical components of stress may be generated from a modification of equ. (B5.4:1):

$$[\sigma]_{lmn} = [C]\,[\varepsilon]_{lmn} \qquad \text{..... (B5.4:4)}$$

For the isotropic case there are only two independent elastic "engineering" coefficients and the general elastic coefficients are given by (Green and Zerna, 1968, p 157):

$$E^{ij}_{rs} = \lambda\, g^{ij}\, g_{rs} + \mu\,(\delta^i_r\,\delta^j_s + \delta^i_s\,\delta^j_r) \qquad \text{..... (B5.4:4)}$$

where λ and μ are the "engineering" coefficients or constants of Lamé. These are related to the Young's modulus E and Poisson's ratio ν by:

$$\lambda = \frac{E\nu}{(1+\nu)(1-2\nu)} \quad ; \quad \mu = \frac{E}{2(1+\nu)} \qquad \text{..... (B5.4:5)}$$

$$\text{thus} \quad \lambda = \frac{2\nu\mu}{1-2\nu} \qquad \text{..... (B5.4:6)}$$

and substituting equ. (B5.4:6) in (B5.4:4) and the result in the general stress-strain relation equ. (B5.2:5) yields (Green and Zerna, 1968, p 158):

$$\tau^{ij} = \mu \{g^{ir} g^{js} + g^{is} g^{ir} + 2\nu g^{ij} g^{rs}(1-2\nu)\} \gamma_{rs} \quad ..(B5.4:7)$$

Thus stress and strain are related in terms of two elastic "engineering" constants (this term being used to distinguish them from the elastic coefficients E^{ij}_{rs}).

6 STRESS-STRAIN RELATION IN TERMS OF STRAIN INVARIANTS

In a isotropic body, the elastic potential W depends only on three strain invariants I_1, I_2 and I_3 and on scalar functions of the co-ordinates $\tilde{x}^i$. Since the strain tensor equ. (B2:4) is symmetric, these three invariants may be formed from it (Green and Zerna, 1968, p 57):

$$\begin{aligned} I_1 &= g^{rs} G_{rs} \\ I_2 &= G^{rs} g_{rs} I_3 \qquad \ldots\ldots\ldots\ldots\ldots\ldots\ldots\ldots \quad (B6:1) \\ I_3 &= G/g \qquad , \end{aligned}$$

The tildas being ignored (i.e. the $\tilde{\underset{\sim}{x}}$ co-ordinate system is changed to the $\underset{\sim}{x}$ for convenience).

It can now be shown that the stress-strain equation (B5.2:2) can be expressed in the form (Green and Zerna, 1968, pp 63-65):

$$\tau^{ij} = \Phi g^{ij} + \Psi B^{ij} + p G^{ij} \quad \ldots\ldots\ldots\ldots\ldots \quad (B6:2)$$

where $\Phi = \frac{2}{\sqrt{I_3}} \frac{\partial W}{\partial I_1}$; $\Psi = \frac{2}{\sqrt{I_3}} \frac{\partial W}{\partial I_2}$; $p = 2\sqrt{I_3} \frac{\partial W}{\partial I_3}$ ..(B6:3)

and $B^{ij} = I\ g^{ij} - g^{ir} g^{js} G_{rs}$ .....(B6:4)

The three functions Φ, Ψ and p depend only on I_1, I_2 and I_3 and are therefore scalar invariant functions.

If, in addition to being homogeneous and isotropic, the body is incompressible, then volume elements are conserved under

deformation so that G = g and $I_3 = 1$ (equ. B6:1)). The stress-strain equations (B6:2) still retain their same form but now:

$$\Phi = 2\frac{\partial W}{\partial I_1} \quad ; \quad \Psi = 2\frac{\partial W}{\partial I_2} \quad . \qquad \text{..... (B6:5)}$$

The quantity p cannot be evaluated from equ. (B6:3). It is an unknown function representing a hydrostatic pressure which must be found from the equations of equilibrium equ. (B4:1) together with the associated boundary conditions.

APPENDIX C

SUNDRY DERIVATIONS

1 Prolate Spheroidal Distortions

The space variations of the major and minor axes will be separately considered.

1.1 Major Axis

The space variation of the major axis, a, occurs for $\pi/2 \leq \eta \leq \pi$ and $0 \leq \xi \leq \pi$. The ξ boundary conditions are:

at $\xi = 0$ $\quad a = a_0$ $\quad$ for all allowable η

at $\xi = \pi$ $\quad a = a_1$ $\quad$ for $\eta = \pi/2$.

Using these, the general parabolic relation:

$$a = A + B\,\xi + C\,\xi^2$$

becomes:

$$a = a_0 + \xi\,(a_0 - a_\eta)/\{(\xi/\pi - 2)\pi\} \quad \ldots\ldots\ldots \text{(C1.1:1)}$$

where a_η is the η -varying coefficient. This coefficient is made a parabolic function :

$$a_v = D + E\,\eta + F\,\eta^2$$

subject to the following boundary conditions at $\xi = \pi$:

at $\eta = \pi/2$, $a_v = a_1$

at $\eta = \pi$, $a_v = a_0$

at $\eta = \pi$, $\partial a_v/\partial\eta = 0$.

These boundary conditions arise as a result of the assumed plane of symmetry.

The final form for a_v is then:

$$a_v = (4a_1 - 3a_0) + 8\eta(a_0 - a_1)/\pi - 4\eta^2(a_0 - a_1)/\pi^2 \quad \ldots\ldots\ldots\ldots\ldots\ldots \text{(C1.1:2)}$$

This equation together with equ. (C1.1:1) gives the (η,ξ) variation of the major axis.

1.2 Minor Axis

In a manner analogous to the space variation of the major axis the variation of the minor axis the variation of the minor axis will be assumed to be a parabolic function of both η and ξ. The boundary conditions for the ξ variation are:

$$b = b_o \text{ at } \xi = 0 \quad \text{for} \quad 0 \leq \eta \leq \pi$$

$$\partial b/\partial \xi = 0 \quad \text{at} \quad \xi = \pi$$

and for the η variation:

$$b = b_o \text{ at } \eta = \pi$$

$$\partial b/\partial \eta = 0 \text{ at } \eta = \pi.$$

Using an analysis similar to that in Section 1.1 above, the final equation:

$$b = b_o + (16/3\pi^2)\eta\xi(b_1 - b_o) \times (1 - \eta/2\pi)(1 - \xi/2\pi) \quad \ldots\ldots\ldots\ldots\ldots \text{(C1.2:1)}$$

is obtained.

2 Computation of the Surface Fundamental Forms

2.1 The First Fundamental Form

The first fundamental form is given by equ. (6.4.1:4):

$$a_{\alpha\beta} = g_{ij} \frac{\partial x^i}{\partial u^\alpha} \frac{\partial x^j}{\partial u^\beta}$$

the relation between the space and surface variables being given by equ. (6.4.1:7):

$$\left.\begin{aligned} x &= \rho \sin\eta \cos\xi \\ y &= \rho \sin\eta \sin\xi \\ z &= \rho \cos\eta \end{aligned}\right\} \quad \ldots\ldots\ldots\ldots\ldots\ldots\ldots \text{(C2.1:1)}$$

where $x = x^1$, $y = x^2$, $z = x^3$ are rectangular cartesian so that $g_{ij} = 1$ for $i = j$ and $= 0$ for $i \neq j$. The surface variables are $u^1 = \eta$, $u^2 = \xi$. The components of the first fundamental form are given, using the above relations, by the symmetrical matrix:

$$a_{\alpha\beta} = \begin{bmatrix} \{\rho^2 + D_\eta^2\} & \{D_\eta\ D_\xi\} \\ \{D_\eta\ D_\xi\} & \{\rho^2 \sin^2 \eta + D_\xi^2\} \end{bmatrix} \quad \ldots\ldots \text{(C2.1:2)}$$

and so $a = |a_{\alpha\beta}| = \rho^4 \sin^2 \eta + \rho^2 (D_\xi^2 + D_\eta^2 \sin_\eta^2)$ .. (C2.1:3)

where $D_\eta = \partial\rho/\partial\eta$

and $D_\xi = \partial\rho/\partial\xi$.

Though in principle analytically obtainable from equ. (6.1.3:1), it is easier to compute these partial derivatives using numerical techniques.

Note also that since $a_{12} \neq 0$, η and ξ do not form an orthogonal surface co-ordinate system (Spain 1956, p. 69).

2.2 The Second Fundamental Form:

The components of the unit surface normal are given by the expanded form of equ. (A7.10:1):

$$\begin{aligned} \nu_1 &= (x^2_1\ x^3_2 - x^3_1\ x^2_2)/\sqrt{a} \\ \nu_2 &= (x^3_1\ x^1_2 - x^1_1\ x^3_2)/\sqrt{a} \qquad \ldots\ldots\ldots\ldots \text{(C2.2:1)} \\ \nu_3 &= (x^1_1\ x^2_2 - x^2_1\ x^1_2)/\sqrt{a} \end{aligned}$$

where:

$$x_\alpha = \frac{\partial x^i}{\partial u^\alpha} \qquad \ldots\ldots\ldots\ldots\ldots\ldots\ldots\ldots \text{(C2.2:2)}$$

and where a is the determinant of the first fundamental form.

The components of the second fundamental form are now given by equ. (6.4.1:5) as:

$$b_{\alpha\beta} = -\left(\nu_1 x^1_{\alpha,\beta} + \nu_2 x^2_{\alpha,\beta} + \nu_3 x^3_{\alpha,\beta}\right) \quad \ldots\ldots \text{(C2.2:3)}$$

where, from equ. (A7.10:3),

$$x^i_{\alpha;\beta} = \frac{\partial^2 x^i}{\partial u^\alpha \partial u^\beta} - \left\{ {\gamma \atop \alpha\ \beta} \right\} x^i_\gamma \quad \ldots\ldots\ldots \text{(C2.2:4)}$$

The Christoffel symbols of the symbols of the second kind required in equ. (C2.2;4) are computed from equs (A7.8:1) and (A7.8:2).

In order to compute the above factors, the quantities: $\frac{\partial x^i}{\partial u^\alpha}$, $\frac{\partial^2 x^i}{\partial u^\alpha \partial u^\beta}$ and $\frac{\partial a_{\alpha\beta}}{\partial u^\rho}$ need to be quantified in terms of of the chosen surface co-ordinates (equ. (C2.1:1)),

(i) "Space-surface" mixed tensor components:

$$\frac{\partial x^1}{\partial u^1} = \frac{\partial x^1}{\partial \eta} = \cos\xi(\rho\cos\eta + D_\eta \sin\eta)$$

$$\frac{\partial x^1}{\partial u^2} = \frac{\partial x^1}{\partial \xi} = \sin\eta(D_\xi \cos\xi - \rho\sin\xi)$$

$$\frac{\partial x^2}{\partial u^1} = \frac{\partial x^2}{\partial \eta} = \sin\xi(\rho\cos\eta + D_\eta \sin\eta)$$

$$\frac{\partial x^2}{\partial u^2} = \frac{\partial x^2}{\partial \xi} = \sin\eta(\rho\cos\xi + D_\xi \sin\xi)$$

$$\frac{\partial x^3}{\partial u^1} = \frac{\partial x^3}{\partial \eta} = -\rho\sin\eta + D_\eta \cos\eta$$

$$\frac{\partial x^3}{\partial u^2} = \frac{\partial x^3}{\partial \xi} = D_\xi \cos\eta$$

(ii) Surface partial derivatives of "space-surface" mixed tensor:

$$\frac{\partial^2 x^1}{\partial u^1 \partial u^1} = \frac{\partial^2 x^1}{\partial \eta \partial \eta} = 2D_\eta \cos\eta\cos\xi + \sin\eta\cos\xi(D_{\eta\eta} - \rho)$$

$$\frac{\partial^2 x^1}{\partial u^1\ \partial u^2} = \frac{\partial^2 x^1}{\partial \eta\ \partial \xi} = \cos\eta(D_\xi \cos\xi - \rho \sin\xi) + \sin\eta(D_{\xi\xi} \cos\xi - D_\eta \sin\xi)$$

$$\frac{\partial^2 x^1}{\partial u^2\ \partial u^2} = \frac{\partial^2 x^1}{\partial \xi\ \partial \xi} = -2D_\xi \sin\eta \sin\xi + \sin\eta \cos\xi(D_{\xi\xi}-\rho)$$

$$\frac{\partial^2 x^2}{\partial u^1\ \partial u^1} = \frac{\partial^2 x^2}{\partial \eta\ \partial \eta} = 2D_\eta \sin\xi \cos\eta + \sin\eta \sin\xi(D_{\eta\eta}-\rho)$$

$$\frac{\partial^2 x^2}{\partial u^1\ \partial u^2} = \frac{\partial^2 x^2}{\partial \eta\ \partial \xi} = \cos\eta(D_\xi \sin\xi + \rho \cos\xi) + \sin\eta(D_{\eta\xi} \sin\xi + D_\eta \cos\xi)$$

$$\frac{\partial^2 x^2}{\partial u^2\ \partial u^2} = \frac{\partial^2 x^2}{\partial \xi\ \partial \xi} = 2D_\xi \sin\eta \cos\xi + \sin\eta \sin\xi(D_{\xi\xi}-\rho)$$

$$\frac{\partial^2 x^3}{\partial u^1\ \partial u^1} = \frac{\partial^2 x^3}{\partial \eta\ \partial \eta} = -2D_\eta \sin\eta + \cos\eta(D_{\eta\eta}-\rho)$$

$$\frac{\partial^2 x^3}{\partial u^1\ \partial u^2} = \frac{\partial^2 x^3}{\partial \eta\ \partial \xi} = D_{\eta\xi} \cos\eta - D_\xi \sin\eta$$

$$\frac{\partial^2 x^3}{\partial u^2\ \partial u^2} = \frac{\partial^2 x^3}{\partial \xi\ \partial \xi} = D_{\xi\xi} \cos\eta$$

(iii) Surface derivative of first fundamental form:

$$\frac{\partial a_{11}}{\partial u^1} = \frac{\partial a_{11}}{\partial \eta} = 2D_\eta(\rho + D_{\eta\eta})$$

$$\frac{\partial a_{11}}{\partial u^2} = \frac{\partial a_{11}}{\partial \xi} = 2(\rho D_\xi + D_\eta\ D_{\eta\xi})$$

$$\frac{\partial a_{12}}{\partial u^1} = \frac{\partial a_{12}}{\partial \eta} = D_\xi\ D_{\eta\eta} + D_\eta\ D_{\eta\xi}$$

$$\frac{\partial a_{12}}{\partial u^2} = \frac{\partial a_{12}}{\partial \xi} = D_\eta\ D_{\xi\xi} + D_\xi\ D_{\eta\xi}$$

$$\frac{\partial a_{22}}{\partial u^1} = \frac{\partial a_{22}}{\partial \eta} = 2(\rho D_\eta \sin^2\eta + D_\xi\ D_{\eta\xi}) + \rho^2 \sin 2\eta$$

$$\frac{\partial a_{22}}{\partial u^2} = \frac{\partial a_{22}}{\partial \xi} = 2D_{\xi}(\rho \sin^2\eta + D_{\xi\xi})$$

All the formulae necessary for computing the surface normal and the second fundamental form have been presented.

The double suffix notations represent the second partial derivatives of the position vector:

e.g. $D_{\eta\xi} = \frac{\partial^2 \rho}{\partial\eta\ \partial\xi}$.

These must also be numerically computed.

2.3 The Third Fundamental Form

Using the second fundamental form, the third fundamental form can be computed using equs (6.4.1:6) and (6.4.1:8):

$$c_{\alpha\beta} = a^{\mu\rho}\ b_{\alpha\rho}\ b_{\mu\beta}\ .$$

3 Variation of Wall thickness from Apex to Equator in the Ventricle

It is anatomical fact that the left ventricle is not shell of constant wall thickness: it increases with position from the apex to equator and then decreases towards the base. This variation is therefore adequately described by the relation:

$$H = M + N\ |\cos\ \eta|$$

with the boundary conditions:

$$H = H_1 \text{ at } \eta = \pi$$

$$H = H_2 \text{ at } \eta = \pi/2.$$

Thus the wall thickness variation becomes:

$$H = H_2 + (H_1 - H_2)|\cos\ \eta|. \quad \ldots\ldots\ldots\ldots\ldots \text{(C3:1)}$$

APPENDIX D

COMPUTER PROGRAMME

A listing of the computer programme which, for any given ventricular configuration, computes the pressure distribution on the endocardial surface using the model developed in Chapter 6, is included in this Appendix. The simplified flow diagram for the programme is also included as well as a typical example of the model predictions.

The shape parameters and elastic constants are given on the first page of print-out and this is followed by tables of the ventricular dimensions (including wall thickness distribution), the magnitudes of the components of the first and second fundamental forms and finally the pressure distribution and stress resultants.

It can be seen how geometry influences pressure. Since an initial condition of zero strain has been used throughout the surface, the stress resultant magnitudes are independent of position. However the components of the second fundamental form are surface position dependent and so cause a non-uniform pressure distribution through the equilibrium equation. (Note that spurious negative values in the pressure distribution arise through a singularity in the bulge transformation in the vicinity of $\eta = \pi - \eta_b$, $\xi = \pi$: this can be avoided if the programme is to be used for more sophisticated simulations).

The need for dynamic programme techniques to obtain the geometry satisfying the criterion of uniform pressure distribution is thus demonstrated.

SIMPLIFIED FLOW DIAGRAM

OF MAINLINE PROGRAMME

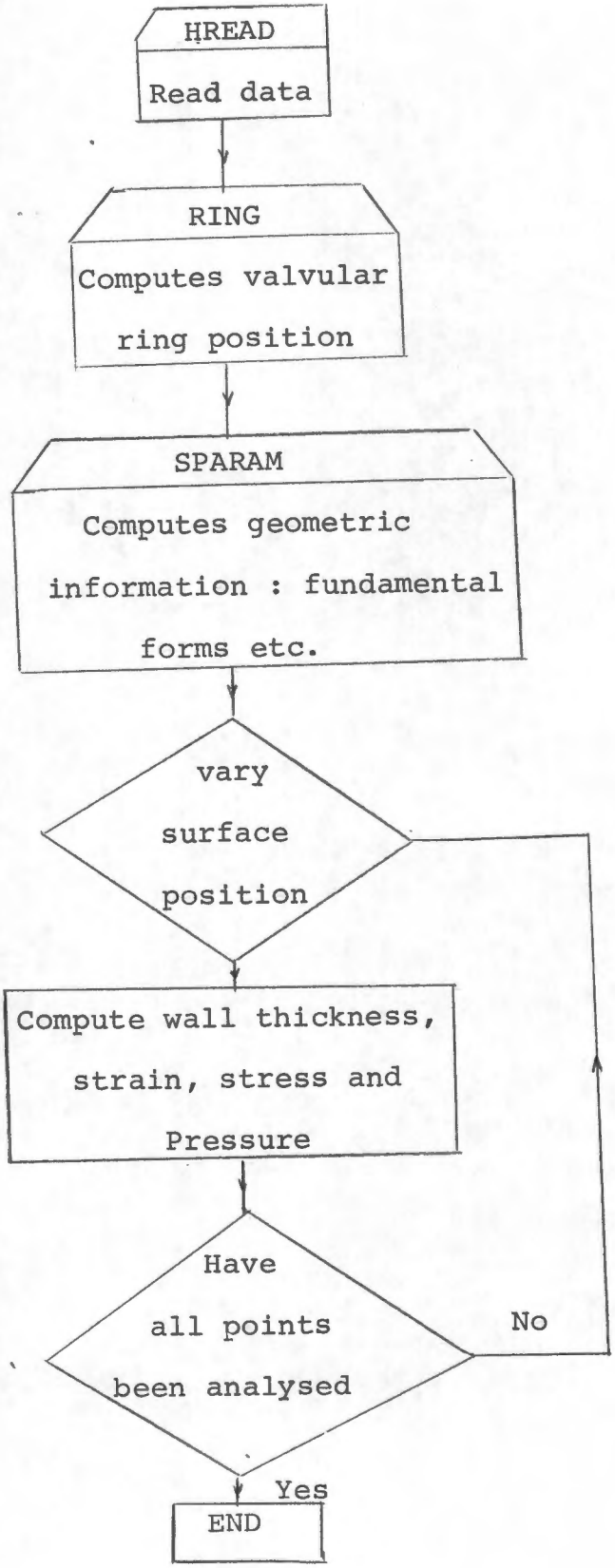

CONTROL SWITCHES: 2=ON; 1=OFF

1 THIRD FUNDAMENTAL FORM
1 LOCAL SURFACE METRIC, G(ALPHA,BETA), IN STRAIN EVALUATION
1 SURFACE NORMAL FOR FINDING ENDO- & EPICARDIAL LOCI

NUMBER OF DATA POINTS ANALYSED

5 NUMBER OF POINTS SURFACE COORDINATE VARIABLES DIVIDED INTO
10 NUMBER OF POINTS TAKEN THROUGH WALL THICKNESS
0 NUMBER OF TIME INTERVALS

MODIFIED PROLATE SPHEROID MIDWALL DIMENSIONS(CM)

5.00 SEMI-MAJOR AXIS
2.50 SEMI-MINOR AXIS (ELLIPSOIDAL HALF-PLANE)
2.00 SEMI-MINOR AXIS (TAPERED HALF-PLANE)

VALVE RADIUS & BULGE PARAMETERS

1.00 VALVULAR RING RADIUS(CM)
120.00 BULGE POSITION (DEGREES FROM BASE)
1.50 BULGE HEIGHT(CM)
50.00 PERCENTAGE EXTENT OF BULGE IN MERIDIONAL DIRECTION
50.00 PERCENTAGE EXTENT OF BULGE IN CIRCUMFERENTIAL DIRECTION

WALL THICKNESS PARAMETERS & SURFACE FIBER ANGLE

.75 WALL THICKNESS AT APEX(CM)
1.00 WALL THICKNESS AT BASE(CM)
70.00 FIBER ANGLE WRT CIRCUMFERENTIAL COORDINATE AT SURFACE

MYOCARDIAL TIME INDEPENDENT ELASTIC CONSTANTS

.00 PE ELEMENT FIRST ORDER CONSTANT(GM/CM**2)
41.70 PE ELEMENT SECOND ORDER CONSTANT(GM/CM**2)
8000.00 MODULUS OF SERIES ELASTIC ELEMENT(GM/CM**2)
-.35 STRAIN FOR ZERO STRESS
.50 POISSONS RATIO

TIME DURATION OF SIMULATION & DERIVATIVE FACTOR

1.00 TIME DURATION OF SIMULATION (SECS)
2.50 DERIVATIVE PERTURBATION (DEGREES)

MERIDIONAL ANGLES: COLUMNS

9.31	43.45	77.58	111.72	145.86	179.71

CIRCUMFERENTIAL ANGLES: ROWS

.00	36.00	72.00	108.00	144.00	179.71

MIDSURFACE DIMENSIONS; ENDOCARDIAL DIMENSIONS;
EPICARDIAL DIMENSIONS; WALL THICKNESS (IN CM)

4.95	4.95	4.95	4.95	4.95	4.95
4.02	3.99	3.96	3.95	3.94	3.94
2.85	2.56	2.41	2.33	2.29	2.27
4.34	3.25	2.73	2.64	2.59	2.58
5.07	4.65	4.33	4.29	4.27	4.27
5.03	5.03	5.03	5.03	5.02	5.02
4.57	4.54	4.48	4.50	4.55	4.57
3.64	3.58	3.49	3.50	3.54	3.56
2.47	2.15	1.94	1.88	1.89	1.90
3.96	2.84	2.25	2.18	2.20	2.20
4.69	4.24	3.86	3.83	3.88	3.90
4.65	4.62	4.55	4.57	4.63	4.65
5.33	5.36	5.42	5.40	5.35	5.32
4.39	4.40	4.44	4.40	4.34	4.31
3.22	2.97	2.89	2.79	2.68	2.65
4.72	3.66	3.20	3.09	2.99	2.95
5.44	5.06	4.81	4.74	4.67	4.65
5.40	5.44	5.50	5.48	5.42	5.40
.75	.82	.95	.91	.79	.75
.75	.82	.95	.91	.79	.75
.75	.82	.95	.91	.79	.75
.75	.82	.95	.91	.79	.75
.75	.82	.95	.91	.79	.75
.75	.82	.95	.91	.79	.75

FIRST FUNDAMENTAL FORM: A11, A22, A12=0

24.87	24.52	24.52	24.52	24.52	24.52
16.34	16.13	15.98	15.86	15.80	15.78
8.12	6.68	6.04	5.70	5.50	5.44
20.48	11.97	8.52	8.18	8.06	8.02
25.68	21.81	19.37	19.00	18.93	18.91
25.27	25.27	25.26	25.25	25.25	25.25
.64	.64	.64	.64	.64	.64
7.63	7.52	7.44	7.38	7.34	252.37
7.75	6.27	5.55	5.19	4.99	5.49
16.29	9.62	6.43	6.00	5.80	5.85
8.06	6.88	5.91	5.77	5.73	5.73
.00	.00	.00	.00	.00	.01

SECOND FUNDAMENTAL FORM: B11, B22, B12=0

8.70	5.10	5.10	5.11	5.11	5.11
4.15	4.15	4.15	4.14	4.14	.71
2.24	2.19	2.17	2.11	2.08	1.96
5.55	3.62	2.77	2.75	2.75	2.73
5.06	4.90	4.87	4.86	4.88	4.83
5.50	5.64	5.87	6.02	6.11	.97
.22	-.47	-.29	-.38	-.47	-.38
2.21	2.09	2.09	2.09	2.09	-130.94
2.96	2.40	2.34	2.27	2.22	.55
5.03	2.72	2.42	2.44	2.39	-3.68
1.72	1.58	1.59	1.68	1.69	1.67
-.00	-.00	-.00	-.00	-.00	.36

PRESSURE AND STRESS RESULTANTS:
P (GM/CM**2), N11, N22, N12=0 (GM/CM)

166.44	94.55	95.49	95.09	94.67	95.12
89.94	89.33	89.21	89.12	89.07	-641.18
57.34	53.61	52.95	51.46	50.58	40.03
130.63	82.31	64.77	64.35	64.26	33.54
104.76	101.10	100.47	100.72	101.05	101.04
104.44	107.23	111.46	114.39	116.05	20.17

19.77	19.77	19.77	19.77	19.77	19.77
19.77	19.77	19.77	19.77	19.77	19.77
19.77	19.77	19.77	19.77	19.77	19.77
19.77	19.77	19.77	19.77	19.77	19.77
19.77	19.77	19.77	19.77	19.77	19.77
19.77	19.77	19.77	19.77	19.77	19.77

5.77	5.77	5.77	5.77	5.77	5.77
5.77	5.77	5.77	5.77	5.77	5.77
5.77	5.77	5.77	5.77	5.77	5.77
5.77	5.77	5.77	5.77	5.77	5.77
5.77	5.77	5.77	5.77	5.77	5.77
5.77	5.77	5.77	5.77	5.77	5.77

VENTRICULAR VOLUME
112.93

```
      REAL N11,N12,N21,N22
C        TIME DIMENSIONS
      DIMENSION APDATA(11),AVDATA(11),AVCAL(11),ATIME(11)
C        SPACE DIMENSIONS
      DIMENSION APCAL(11,11)
      DIMENSION AA11(11,11),AA12(11,11),AA22(11,11)
      DIMENSION AB11(11,11),AB12(11,11),AB22(11,11)
      DIMENSION AC11(11,11),AC12(11,11),AC22(11,11)
      DIMENSION AAI11(11,11),AAI12(11,11),AAI22(11,11)
      DIMENSION AADET(11,11),AADDET(11,11),ADRHOP(11,11),ADRHOT(11,11)
      DIMENSION ANORM1(11,11),ANORM2(11,11),ANORM3(11,11)
      DIMENSION AAH11(11,11),AAH12(11,11),AAH22(11,11),AADETH(11,11)
      DIMENSION AGH11(11,11),AGH12(11,11),AGH22(11,11)
      DIMENSION AN11(11,11),AN12(11,11),AN21(11,11)
      DIMENSION ADP(11,11),ADT(11,11)
      DIMENSION APHI(11),ATHETA(11),AH(11,11),AN22(11,11)
      DIMENSION ADPH(11,11),ADTH(11,11)
      DIMENSION ARHO(11,11),AHD(11,11)
      DIMENSION ARHOIN(11,11),ARHOUT(11,11)
      DIMENSION ANG1(11),ANG2(11)
C        WALL THICKNESS
      DIMENSION AZETA(11),ASZSQ(11),ASZQU(11),AS2Z(11),AS2ZSQ(11)
      DIMENSION ACZSQ(11),ACZQU(11),AC2Z(11),AC2ZSQ(11)
      DIMENSION ASP11(11),ASP22(11),          ASP12(11),ASP21(11)
      DIMENSION AFWT(11)
      DATA/IWR/5/IN/8/
      DATA/LA1/11/LA2/11/ LA3/11/
      PI = 22./7.
C        READ IN DATA
      CALL HREAD(PI,LA3,
     1           KPLT,KS3FF,KSTRAN,KSURF,NDATA,NLAYER,NTIME,
     2   A,B0,B1,BPHI,HB,D2,D3,PTAIL,R,HPI,HPI2,ZETAS,EP1,EP2,
     3   ESE,VNUAB,VNUB3,PETURB,TTOT,APDATA,AVDATA,GAMAAS)
C        CIRCUMFERENTIAL ANGLE INCREMENT
      TINC = PI/(NDATA-1)
C        EVALUATE CONSTANTS ASSOCIATED WITH FIBER WALL THICKNESS
C          VARIATION
      CALL FCONST(LA2,NLAYER,ZETAS,KPLT,
     1   NZIT,DFWT,AZETA,ASZSQ,ASZQU,AS2Z,AS2ZSQ,
     2   ACZSQ,ACZQU,AC2Z,AC2ZSQ,AFWT)
C        FIND INITIAL RING POSITION
      CALL RING(R,A,B0,B1,BPHI,HB,D2,D3,PTAIL,NDATA,TINC,PI,
     1   PINC,RPROP,PHI0)
C        ANGLE VARIABLES CONVERTED TO DEGREES
      DPHI0 = 180*PHI0/PI
      DPINC = 180*PINC/PI
      DTINC = 180*TINC/PI
C        COMPUTE NORMALISED TIME INCREMENT, HTIMEN
      HTIMEN = 1./FLOAT(NTIME)
C        ENTRY FOR NEW ITERATION
C        TIME LOOP
      DO 10 K=1,NTIME
       P = APDATA(K)
       V = AVDATA(K)
```

```
      T = HTIMEN*(K-1)
      ATIME(K) = T*TTOT
C           STORE DP ADT FROM PREVIOUS OPTIMIZED CONFIGURATION BEFORE
C           NEXT OPTIMIZING PROCEDORE
      DO 25 I=1,NDATA
      DO 25 J=1,NDATA
      ADPH(J,I) = ADP(J,I)
      ADTH(J,I) = ADT(J,I)
   25 CONTINUE
C          ENTRY AFTER PARAMETER PERTURBATION
   15 CONTINUE
C          COMPUTE ALL GEOMETRIC INFORMATION
      CALL SPARAM(KS3FF,LA1,NDATA,A,BC,B1,BPHI,HB,D2,D3,PTAIL,
     1    PINC,TINC,RPROP,PI,
     2    PETURB,APHI,ATHETA,AA11,AA12,AA22,AADET,AACDET,
     3    AAI11,AAI12,AAI22,AB11,AB12,AB22,AC11,AC12,AC22,
     4    ANORM1,ANORM2,ANORM3,ARHO,ADP,ADT,PHID)
C          INITIAL WALL THICKNESS DISTRIBUTION
      CALL WTDIST(LA1,NDATA,PI,HPI,HPI2,APHI,
     1    AHO)
C          THETA (XI) ANGLE LOOP
      DO 20 I=1,NDATA
      THETA = ATHETA(I)
C          PHI (ETA) LOOP
      DO 20 J=1, NDATA
      PHI = APHI(J)
C          CHANGE DIMENSIONED TO UNDIMENSIONED VARIABLES
      A11 = AA11(J,I)
      A12 = AA12(J,I)
      A22 = AA22(J,I)
      B11 = AB11(J,I)
      B12 = AB12(J,I)
      B22 = AB22(J,I)
      C11 = AC11(J,I)
      C12 = AC12(J,I)
      C22 = AC22(J,I)
      ADET = AADET(J,I)
      ACDET = AACDET(J,I)
      AI11 = AAI11(J,I)
      AI12 = AAI12(J,I)
      AI22 = AAI22(J,I)
      RHO = ARHO(J,I)
      DRHOP = ADRHOP(J,I)
      DRHOT = ADRHOT(J,I)
      DP = ADP(J,I)
      DT = ADT(J,I)
      DPH = ADPH(J,I)
      DTH = ADTH(J,I)
      HO = AHO(J,I)
C          COMPUTE PRESENT WALL THICKNESS
      H = HO*SQRT(ADET/ACDET)
      AH(J,I) = H
C          COMPUTE & ETORE FACTORS NECESSARY FOR CALCULATING NORMAL
C            STRAIN
      DRHOP = DP-DPH
      DRHOT = DT-DTH
      ADRHOP(J,I) = DRHOP
```

```
      ADRHOT(J,I) = DRHOT
C        COMPUTE BASE VECTOR MAGNITUDES
      VM11 = SQRT(A11*AI11)
      VM12 = SQRT(A11*AI22)
      VM21 = SQRT(A22*AI11)
      VM22 = SQRT(A22*AI22)
C        PREVIOUS VALUES OF METIC
      AH11 = AAH11(J,I)
      AH12 = AAH12(J,I)
      AH22 = AAH22(J,I)
      ADETH = AADETH(J,I)
      GH11 = AGH11(J,I)
      GH12 = AGH12(J,I)
      GH22 = AGH22(J,I)
C        FOR FIRST TIME THROUGH, HOLD PRESENT VALUES OF METRIC
      IF (K-1) ,,50
      AH11 = A11
      AH12 = A12
      AH22 = A22
      ADETH = ADET
      GH11 = G11
      GH12 = G12
      GH22 = G22
   50 CONTINUE
C        VARY FRACTIONAL WALL THICKNESS FROM ENDO- TO EPICARDIUM
      DO 30 L=1,NZIT
      FWT = (L-1)*DFWT-0.5
      ZETA = AZETA(L)
C        CHANGE WALL THICKNESS PARAMETERS FROM DIMENSIONED TO
C          UNDIMENSIONED VARIABLES
      SZSQ = ASZSQ(L)
      SZQU = ASZQU(L)
      S2Z = AS2Z(L)
      S2ZSQ = AS2ZSQ(L)
      CZSQ = ACZSQ(L)
      CZQU = ACZQU(L)
      C2Z = AC2Z(L)
      C2ZSQ = AC2ZSQ(L)
C        ONLY NEED ENTER SUB. STRAIN ON FIRST ENTRY
      GO TO (31,32), KSTRAN
   31 CONTINUE
      IF (L-1) ,,33
   32 CONTINUE
C          COMPUTE STRAIN
      CALL STRAIN(KSTRAN,FWT,DP,DT,DRHOP,DRHOT,ADET,
     1   A11,A12,A22,AI11,AI12,AI22,B11,B12,B22,C11,C12,C22,
     2   AH11,AH12,AH22,ADETH ,GH11,GH12,GH22,
     2   G11,G12,G22,GAM11,GAM12,GAM21,GAM22,GAM13,GAM31,GAM23,
     3   GAM32,GAM33)
   33 CONTINUE
C        HOLD PRESENT VALUES OF METRIC
      AAH11(J,I) = A11
      AAH12(J,I) = A12
      AAH22(J,I) = A22
      AADETH(J,I) = ADET
      AGH11(J,I) = G11
      AGH12(J,I) = G12
```

```
      AGH22(J,I) = G22
C        COMPUTE FIBRE AXIAL STRAIN
      GAMAA = GAM11*CZSQ+GAM22*SZSQ+0.5*(GAM12+GAM21)*S2Z
C        COMPUTE FIBRE STRESS
      SDC = 0.0
      CALL FIBRE(T,EP1,EP2,ESE,SDC,AS,GAMAA,GAMAAS,
     1   SAA)
C        COMPUTE PHYSICAL COMPOMENTS OF STRESS
      S11 = SAA*CZSQ
      S22 = SAA*SZSQ
      S12 = 0.5*SAA*S2Z
      S21 = S12
C        STORE THROUGH WALL STRESS VARIATIONS
      ASP11(L) = S11
      ASP22(L) = S22
      ASP12(L) = S12
      ASP21(L) = S21
C        END WALL THICKNESS VARIATION LOOP
   30 CONTINUE
C        COMPUTE STRESS RESULTANTS & SHEARING FORCES
      CALL STRESR(LA2,NZIT,FWT,ASP11,ASP12,ASP21,ASP22,
     3   N11,N22,N12,N21)
C        COMPUTE TENSOR COMPONENTS OF RESULTANTS & SHEARS
      NT11 = N11/VM11
      NT12 = N12/VM11
      NT21 = N21/VM11
      NT22 = N22/VM11
C        COMPUTE & STORE PRESSURE
      P =    B11*NT11+B12*(NT12+NT21)+B22*NT22
      APCAL(J,I) = P
C
C        STORE SPATIAL VALUES OF RESULTANTS & SHEARS
      AN11(J,I) = N11
      AN22(J,I) = N22
      AN12(J,I) = N12
      AN21(J,I) = N21
C        END ANGLE VARIATION LOOP
   20 CONTINUE
C        COMPUTE LOCI OF ENDO- & EPICARDIAL SURFACES
      CALL LVSURF(KSURF,LA1,NDATA,PINC,TINC,APHI,ATHETA,ARHO,
     1   AH,ANORM1,ANORM2,ANORM3,
     3    ARHOIN,ARHOUT)
C        COMPUTE LV VOLUME
      BAV = (B0+B1)/2
      PVECT = SQRT(A*A+BAV*BAV)
      CALL LVVOL(LA1,NDATA,PINC,TINC,ARHOIN,PHIC,RPROP,R,PI,PVECT,
     1   VC)
      AVCAL(K) = VC
C        PRINT ANGLE VARIABLES
      DO 40 I=1,NDATA
      ANG1(I) = 180*APHI(I)/PI
      ANG2(I) = 180*ATHETA(I)/PI
   40 CONTINUE
      WRITE (IWR,120)
      WRITE (IWR,130)
      WRITE (IWR,150) (ANG1(I),I=1,NDATA)
      WRITE (IWR,140)
```

```
      WRITE (IWR,150) (ANG2(I),I=1,NDATA)
      WRITE (IWR,110)
C        PRINT ARRAYS
      WRITE (IWR,160)
      CALL HPRT2(LA1,NDATA,ARHO)
      CALL HPRT2(LA1,NDATA,ARHOIN)
      CALL HPRT2(LA1,NDATA,ARHOUT)
      CALL HPRT2(LA1,NDATA,AHO)
      WRITE (IWR,120)
      WRITE (IWR,170)
      CALL HPRT2(LA1,NDATA,AA11)
      CALL HPRT2(LA1,NDATA,AA22)
      WRITE (IWR,180)
      CALL HPRT2(LA1,NDATA,AB11)
      CALL HPRT2(LA1,NDATA,AB22)
      WRITE (IWR,120)
      WRITE (IWR,190)
      CALL HPRT2(LA1,NDATA,APCAL)
      CALL HPRT2(LA1,NDATA,AN11)
      CALL HPRT2(LA1,NDATA,AN22)
      WRITE (IWR,200)
      WRITE (IWR,100) VC.
C        COMPUTE PRESSURE ERROR
      NPPTS = (NDATA-1)*(NDATA-1)
C        COMPUTE MEAN PRESSURE
      PSUM = 0.0
      DO 60 I=1,NDATA
      DO 60 J=1,NDATA
        PSUM = PSUM+APCAL(J,I)
   60 CONTINUE
       PAV = PSUM/NPPTS
C        COMPUTE SUM OF SQUARES OF ERROR
      PSIGSQ = 0.0
       DO 65 I=1,NDATA
       DO 65 J=1,NDATA
      PSIGSQ = (APCAL(J,I)-PAV) *(APCAL(J,I)-PAV)
   65 CONTINUE
      PSTD = SQRT(PSIGSQ/NPPTS)
      WRITE (IWR,110)
      WRITE (IWR,100) PAV,PSTD,NPPTS
CC       WRITE DATA INTO PLOT FILE
C        END TIME LOOP
   10 CONTINUE
      CALL EXIT
  100 FORMAT()
  110 FORMAT(//)
  120 FORMAT (1H1)
  130 FORMAT (' MERIDIONAL ANGLES: COLUMNS')
  140 FORMAT (//' CIRCUMFERENTIAL ANGLES: ROWS')
  150 FORMAT (6(2X,F8.2))
  160 FORMAT (//' MIDSURFACE DIMENSIONS; ENDOCARDIAL DIMENSIONS;'/
     1'  EPICARDIAL DIMENSIONS; WALL THICKNESS (IN CM)')
  170 FORMAT (////' FIRST FUNDAMENTAL FORM: A11, A22, A12=0')
  180 FORMAT (////' SECOND FUNDAMENTAL FORM: B11, B22, B12=0')
  190 FORMAT (' PRESSURE AND STRESS RESULTANTS:'/
     1'     P (GM/CM**2), N11, N22, N12=0 (GM/CM)')
  200 FORMAT (////' VENTRICULAR VOLUME')
```

```
      SUBROUTINE HREAD(PI,LA3,
     1                 KPLT,KS3FF,KSTRAN,KSURF,NDATA,NLAYER,NTIME,
     2   A,B0,B1,BPHI,HB,D2,D3,PTAIL,R,HPI,HPI2,ZETAS,EP1,EP2,
     3   ESE,VNUAB,VNUB3,PETURB,TTOT,APDATA,AVDATA,GAMAAS)
      DIMENSION APDATA(LA3),AVDATA(LA3)
      DATA/IWR/5/IN/3/
C        READS & WRITES INITIALIZATION DATA
C     ***************************************************************
C        INITIALIZATION DATA PRINTED IF KPRINT=2
C        PRINT-PLOT INVOKED IF KPLT=2
      READ(IN,100) KPRINT,KPLT
C        READ IN DATA
C
C                 CONTROL SWITCHES (2=ON; 1=OFF)
      READ (IN,100) KS3FF,KSTRAN,KSURF
C        NUMBER OF POINTS ANALYSED IN SPACE & TIME
      READ (IN,100) LDATA,NLAYER,LTIME
C                 INITIAL SHAPE SETTINGS
C        MIDWALL DIMENSIONS OF MODIFIED PROLATE SPHEROID
      READ (IN,100) A,B0,B1
C        BULGE PARAMETERS
      READ (IN,100) DBPHI,HB,D2,D3
C        VALVE RADIUS
      READ (IN,100) R
C              MYOCARDIAL PARAMETERSN
C        WALL THICKNESS
      READ (IN,100) HPI,HPI2
C        FIBER ANGLE AT SURFACE
      READ (IN,100) DZETAS
C        ELASTIC CONSTANTS
      READ (IN,100) EP1,EP2,ESE,GAMAAS,VNUAB,VNUB3
C                 DERIVATIVE DISPLACEMENT & TOTAL TIME OF SIMULATION
      READ (IN,100) DPETRB,TTOT
      NDATA = LDATA+1
      NTIME = LTIME+1
C        READ TIME DATA
      READ (IN,100) (APDATA(I), I=1,NTIME)
      READ (IN,100) (AVDATA(I), I=1,NTIME)
      PTAIL = 10.0
      PETURB = PI*DPETRB/180
      ZETAS  = PI*DZETAS/180
      BPHI = PI*DBPHI/180
      GO TO (11,12), KPRINT
   11 CONTINUE
      RETURN
   12 CONTINUE
C                 WRITE DATA
      WRITE (IWR,110)
      WRITE (IWR,120) KS3FF,KSTRAN,KSURF
      WRITE (IWR,130) LDATA,NLAYER,LTIME
      WRITE (IWR,140) A,B0,B1
      WRITE (IWR,150) R,DBPHI,HB,D2,D3
      WRITE (IWR,160) HPI,HPI2,DZETAS
      WRITE (IWR,170) EP1,EP2,ESE,GAMAAS,VNUAB
```

```
      WRITE (IWR,180) TTOT,DPETRB
C        WRITE TIME DATA
C                  FORMAT STATEMENTS
  100 FORMAT()
  110 FORMAT(1H1)
  120 FORMAT(// 15X,'CONTROL SWITCHES: 2=ON; 1=OFF'/
     1 8X,I2,' THIRD FUNDAMENTAL FORM'/
     2 8X,I2,' LOCAL SURFACE METRIC, G(ALPHA,BETA), IN STRAIN EVALUATIO
     3'/8X,I2,' SURFACE NORMAL FOR FINDING ENDO- & EPICARDIAL LOCI')
  130 FORMAT(//15X,'NUMBER OF DATA POINTS ANALYSED'/
     1 7X,I3,' NUMBER OF POINTS SURFACE COORDINATE VARIABLES DIVIDED IN
     20'/7X,I3,' NUMBER OF POINTS TAKEN THROUGH WALL THICKNESS'/
     3 7X,I3,' NUMBER OF TIME INTERVALS')
  140 FORMAT(//15X,' MODIFIED PROLATE SPHEROID MIDWALL DIMENSIONS(CM)'/
     1 F10.2,' SEMI-MAJOR AXIS'/
     2 F10.2,' SEMI-MINOR AXIS (ELLIPSOIDAL HALF-PLANE)'/
     3 F10.2,' SEMI-MINOR AXIS ( TAPERED  HALF-PLANE)')
  150 FORMAT(//15X,'VALVE RADIUS & BULGE PARAMETERS'/
     1 F10.2,' VALVULAR RING RADIUS(CM)'/
     2 F10.2,' BULGE POSITION (DEGREES FROM BASE)'/
     3 F10.2,' BULGE HEIGHT(CM)'/
     3 F10.2,' PERCENTAGE EXTENT OF BULGE IN MERIDIONAL DIRECTION'/
     4 F10.2,' PERCENTAGE EXTENT OF BULGE IN CIRCUMFERENTIAL DIRECTION'
  160 FORMAT(//15X,'WALL THICKNESS PARAMETERS & SURFACE FIBER ANGLE'/
     1 F10.2,' WALL THICKNESS AT APEX(CM)'/
     2 F10.2,' WALL THICKNESS AT BASE(CM)'/
     3 F10.2,' FIBER ANGLE WRT CIRCUMFERENTIAL COORDINATE AT SURFACE')
  170 FORMAT(//15X,' MYOCARDIAL TIME INDEPENDENT ELASTIC CONSTANTS'/
     1 F10.2 ,' PE ELEMENT FIRST ORDER CONSTANT(GM/CM**2)'/
     2 F10.2 ,' PE ELEMENT SECOND ORDER CONSTANT(GM/CM**2)'/
     4 F10.2 ,' MODULUS OF SERIES ELASTIC ELEMENT(GM/CM**2)'/
     3 F10.2, ' STRAIN FOR ZERO STRESS'/
     5 F10.2 ,' POISSONS  RATIO')
  180 FORMAT(//15X,'TIME DURATION OF SIMULATION & DERIVATIVE FACTOR'/
     1 F10.2,' TIME DURATION OF SIMULATION (SECS)'/
     2 F10.2,' DERIVATIVE PERTURBATION (DEGREES)')
  190 FORMAT (////10X,'PRESSURE DATA')
  200 FORMAT (//10X,'VOLUME DATA')
      RETURN
      END
```

```
      SUBROUTINE RING(R,A,B0,B1,BPHI,HB,D2,D3,PTAIL,
     1  NDATA,TINC,PI,
     2   PINC,RPROP,PHIO)
C        COMPUTES THE INITIAL PHI (ETA) POSITION OF THE VALVULAR
C          RING & THE THE PROPORTIONALITY CONSTANT FOR COMPUTING FUTURE
C         .VALUES.
C     ***************************************************************
C        NOMENCLATURE:
C            R; RADIUS OF VALVULAR RING
C            TRHO; POSITION VECTOR OF LV SURFACE AT RING
C            PHIO; POSITION OF VALVULAR RING
C            RPROP; PROPORTIONALITY CONSTANT OF RING POSITION
C     ***************************************************************
      EXTERNAL BCALC,FLVS
C        CONVERGENCE CRITERION
      CFACTR  = R/20
C        INITIAL VALUES
      DTHETA = PI/4
      PHIO = PI/8
   30 CONTINUE
      PINC = (PI-PHIO)/(NDATA-1)
      SRHO = 0.0
C        REPRESENTATIVE POSITION VECTORS
      DO 10 I=1,5
       THETA = (I-1)*DTHETA
      B = BCALC(B0,B1,PHIO,THETA,PI)
      TRHO = FLVS(PHIO,THETA,PINC,TINC,BPHI,HB,A,B,D2,D3,PTAIL,PI)
      SRHO = TRHO+SRHO
   10 CONTINUE
C        AVERAGE POSITION VECTOR
      AVRHO = SRHO/4
      TRHO = AVRHO*SIN(PHIO)
C     CHECK ON CONVERGENCE
      DEL = ABS(R-TRHO)
      IF (DEL-CFACTR ) 20,,
      PHIO = ASIN(R/AVRHO)
      GO TO 30
   20 CONTINUE
C        FINAL VALUES
      PHIO = ASIN(R/AVRHO)
      BAV = (B0+B1)/2
      RPROP = PHIO/SQRT(A*A+BAV*BAV)
      RETURN
      END
```

```
      SUBROUTINE FCONST(LA2,NLAYER,ZETAS,KPLT,
     1   NZIT,DFWT,AZETA,ASZSQ,ASZQU,AS2Z,AS2ZSQ,
     2   ACZSQ,ACZQU,AC2Z,AC2ZSQ,AFWT)
C        EVALUATES ARRAYS OF CONSTANTS ASSOCIATED WITH FIBER ORIENTATION
C     ******************************************************************
C        NOMENCLATURE:
C          Z/ZETA= ORIENTATION ANGLE WRT THETA (XI)
C          SQ=SQUARED; 2=MULTIPLIED BY 2; A=ARRAY; S=SIN; C=COS
C          NLAYER=NUMBER OF LATERS; FWT=FRACTIONAL WALL THICKNESS
C          DFWT=INCREMENT IN FRACTIONAL WALL THICKNESS
C          ZETAS=BOUNDARY VALUE OF ZETA (AT ENDO- & EPICARDIUM)
C          LA2=LENGTH OF ARRAY
C     ******************************************************************
      DIMENSION AZETA(LA2),AS2Z(LA2),ASZSQ(LA2),ASZQU(LA2),AS2ZSQ(LA2)
      DIMENSION ACZSQ(LA2),AC2Z(LA2),AC2ZSQ(LA2),ACZQU(LA2),AFWT(LA2)
      DIMENSION YEXP(2),XEXP(24)
      DATA/YEXP/'ANGLE:RADIAN'/
      DATA/XEXP/'FRACTIONAL WALL THICKNESS     ',19*'      '/
      DATA/IWR/5/
      DFWT = 1./FLOAT(NLAYER)
      NZIT = NLAYER+1
C        FIND FIBER ANGLE VARIATION FROM ENDO- TO EPICARDIUM IE. FROM-H
      DO 10 I=1,NZIT
      FWT = (I-1)*DFWT-0.5
      AFWT(I) = FWT
      AZETA(I) = 4*ZETAS*FWT*FWT
      IF (FWT.GT.0.0)  AZETA(I) = -AZETA(I)
      ZETA = AZETA(I)
      ZETA2 = 2*ZETA
C        CALCULATE TRIG FUNCTIONS OF ANGLE, ZETA
      SZ = SIN(ZETA)
      ASZSQ(I) = SZ*SZ
      ASZQU(I) = ASZSQ(I)*ASZSQ(I)
      AS2Z(I) = SIN(ZETA2)
      AS2ZSQ(I) = AS2Z(I)*AS2Z(I)
      CZ = COS(ZETA)
      ACZSQ(I) = CZ*CZ
      ACZQU(I) = ACZSQ(I)*ACZSQ(I)
      AC2Z(I) = COS(ZETA2)
      AC2ZSQ(I) = AC2Z(I)*AC2Z(I)
   10 CONTINUE
      RETURN
  100 FORMAT ()
      END
```

```
      SUBROUTINE SPARAM(KS3FF,LA1,NDATA,A,B0,B1,BPHI,HB,D2,D3,PTAIL,
     1   PINC,TINC,RPROP,PI,
     2   PETURB,APHI,ATHETA,AA11,AA12,AA22,AADET,AADDET,
     2   AAI11,AA112,AAI22,AB11,AB12,AB22,AC11,AC12,AC22,
     4   ANORM1,ANORM2,ANORM3,ARHO,ADP,ADT,PHI0)
C        CONTROLS THE COMPUTATION OF THE FIRST, SECOND & THIRD SURFACE
C           FUNDAMENTAL FORMS ARRAYS; THIRD FORM ONLY IF CONTROLLING
C          SWITCH KS3FF=2 (IE ON, 1= OFF)
C     ******************************************************************
C        FOR NOTATION, SEE SUBS CALLED (GCONST,HDERIV,DCONST, H1FF ETC)
C          ADPH,ADTH; ARRAYS OF RADIAL STRAIN
C                THESE ARE DIMENSIONED IN THIS PROGRAMNE
C     ******************************************************************
      DIMENSION APHI(LA1),ATHETA(LA1),AA11(LA1,LA1),AA12(LA1,LA1)
      DIMENSION AA22(LA1,LA1),AADET(LA1,LA1),AADDET(LA1,LA1)
      DIMENSION AAI11(LA1,LA1),AAI12(LA1,LA1),AAI22(LA1,LA1)
      DIMENSION AB11(LA1,LA1),AB12(LA1,LA1),AB22(LA1,LA1)
      DIMENSION AC11(LA1,LA1),AC12(LA1,LA1),AC22(LA1,LA1)
      DIMENSION ANORM1(LA1,LA1),ANORM2(LA1,LA1),ANORM3(LA1,LA1)
      DIMENSION ARHO(LA1,LA1)
      DIMENSION ADP(LA1,LA1),ADT(LA1,LA1)
      DATA/IWR/5/
      DATA /KINITL/0/
      KINITL = KINITL+1
C        COMPUTE NEW VALVULAR RING POSITION
      BAV = (B0+B1)/2
      PHI0 = RPROP*SQRT(A*A+BAV*BAV)
C        COMPUTE COORDINATE INCREMENTS FOR MERIDIONAL VARIABLE
      PINC = (PI-PHI0)/(NDATA-1)
C        EVALUATE VARIABLE ARRAYS & NECESSARY FUNCTIONAL FORMS
C        FOR GIVEN VALUES OF THETA(U2) LOOP THROUGH PHI(U1)
      DO 10 I=1,NDATA
      THETA = TINC*(I-1)
      IF (THETA.GE.0.99*PI) THETA=PI-0.005
      ATHETA(I) = THETA
      DO 10 J=1,NDATA
      PHI = PINC*(J-1)+PHI0
      IF (  PHI.GE.0.99*PI)   PHI=PI-0.005
      APHI(J) = PHI
C        COMPUTE FUNCTIONS OF ANGLES
      CALL GCONST(NDATA,PHI,THETA,
     1   ST,CT,SP,SPSQ,S2P,CP,CPSQ,C2P)
C        COMPUTE NECESSARY DERIVATIVES ABOUT POINT (PHI,THETA) BY
C          PERTURBING +-PETURB
      CALL HDERIV(PETURB,    BPHI,HB,A,B0,B1,D2,D3,PTAIL,PHI,THETA,
     1   PINC,TINC,
     2   DP,DT,DPP,DTT,DPT,RHO)
C        RESET ANGLES THAT MAY HAVE BEEN DISTURBED IN HDERIV.
      PHI = APHI(J)
      THETA = ATHETA(I)
C        FIND PHYSICAL COMPONENTS OF POSITION VECTOR DIFFERENTIALS
      DP = DP/SQRT(A11)
      DT = DT/SQRT(A22)
      DPP = DPP/A11
```

```
      DTT = DTT/A22
      DPT = DPT/SQRT(A11*A22)
C        EVALUATE NECESSARY FUNCTIONAL FORMS
      CALL DCONST(RHO,DP,DT,RHO2,RHO3,RHO4,DPSQ,DTSQ)
C        COMPUTE FIRST FUNDAMENTAL FORM COMPONENTS
      CALL HIFF(LA1,SP,CP,SPSQ,S2P,DP,DT,DPSQ,DTSQ,
     1   RHO,RHO2,RHO3,RHO4,
     3   A11,A12,A22,AI11,AI12,AI22,ADET)
C        COMPUTE SURFACE TO SPACE TRANSFORMATION VECTORS, DX(I)/DU(ALPHA)
C          NOTATION: DX12 ETC.; OTHER  SEE HDERIV,SCONST
      DX11 = (RHO*CP+DP*SP)*CT
      DX12 = (-RHO*ST+DT*CT)*SP
      DX21 = (RHO*CP+DP*SP)*ST
      DX22 = (RHO*CT+DT*ST)*SP
      DX31 = -RHO*SP+DP*CP
      DX32 = DT*CP
C        COMPUTE THE SURFACE UNIT NORMAL AT (PHI,THETA): NOTATION; SEE
C          SUB. HSNORM
      CALL HSNORM(ADET,DX11,DX12,DX21,DX22,DX31,DX32,
     1   VNORM1,VNORM2,VNORM3)
C
C     COMPUTE THE SURFACE PARTIAL DERIVATIVES OF THE AFOVE2SPACE
C          TRANSFORMATIONS: D2X(I)/DU(ALPHA*DU(BETA)
C            NOTATION: D2X112 ETC.; OTHER SEE HDERIV,DCONST
      D2X111 = 2*DP*CP*CT+SP*CT*(DPP-RHO)
      D2X112 = CP*(DT*CT-RHO*ST)+SP*(CT*DPT-DP*ST)
      D2X122 = -2*DT*ST*SP+SP*CT*(DTT-RHO)
      D2X211 = 2*DP*ST*CP+SP*ST*(DPP-RHO)
      D2X212 =CP*(+RHO*CT+DT*ST)+SP*(DP*CT+DPT*ST)
      D2X222 = 2*DT*SP*CT+SP*ST*(DTT-RHO)
      D2X311 = -2*DP*SP+CP*(DPP-RHO)
      D2X322 = DTT*CP
      D2X312 = DPT*CP-DT*SP
C        COMPUTE DERIVATIVES (SURFACE) OF THE COMPONENTS OF THE FIRST
C          FUNDAMENTAL FORM: DA(ALPHA,BETA)/DU(GAMMA)
C            NOTATION: DA12D3 ETC.; OTHER - SEE SUBS HDERIV,GCONST,DCONST
      DA12D1 = DT*DPP+DP*DPT
      DA11D1 = 2*DP*(RHO+DPP)
      DA11D2 = 2*(RHO*DT+DP*DPT)
      DA12D2 = DP*DTT+DT*DPT
      DA22D1 = 2*(RHO*DP*SPSQ+DT*DPT)+RHO2*S2P
      DA22D2 = 2*DT*(RHO*SPSQ+DTT)
C        EVALUATION OF SURFACE CHRISTOFFEL SYMBOLS OF FIRST  KIND
C          NOTATION: C11F1 ETC.  (SYMMETRIC IN NUMERIC POSITIONS 1&2)
CC           OTHERWISE SEE ABOVE
      C11F1 = 0.5*DA11D1
      C11F2 = DA12D1-0.5*DA11D2
      C12F1 = 0.5*DA11D2
      C12F2 = 0.5*DA22D1
      C22F1 = DA12D2-0.5*DA22D1
      C22F2 = 0.5*DA22D2
C        EVALUATION OF SURFACE CHRISTOFFEL SYMBOLS OF SECOND KIND
C          NOTATION: C11S1 ETC.  (SYMMETRIC IN NUMERIC POSITIONS 1&2)
CC           OTHERWISE SEE ABOVE
      C11S1 =  A11*C11F1+ A12*C11F2
      C11S2 =  A12*C11F1+ A22*C11F2
      C12S1 =  A11*C12F1+ A12*C12F2
```

```
      C12S2 =  A12*C12F1+ A22*C12F2
      C22S1 =  A11*C22F1+ A12*C22F2
      C22S2 =  A12*C22F1+ A22*C22F2
C        TENSOR DERIVATIVES OF TENSOR: EVALUATION
C          NOTATION: DX1D23 ETC. (SYMMETRIC IN NUMERIC POSITIONS 2&3)
C            OTHERWISE SEE ABOVE
C        FIRST SPACE COMPONENT
      DX1D11 = D2X111-C11S1*DX11-C11S2*DX12
      DX1D12= D2X112-C12S1*DX11-C12S2*DX12
      DX1D22 = D2Y122-C22S1*DX11-C22S2*DX12
C        SECOND SPACE COMPONENT
      DX2D11 = D2X211-C11S1*DX21-C11S2*DX22
      DX2D12 = D2X212-C12S1*DX21-C12S2*DX22
      DX2D22 = D2X222-C22S1*DX21-C22S2*DX22
C        THIRD SPACE COMPONENT
      DX3D11 = D2X311-C11S1*DX31-C11S2*DX32
      DX3D12 = D2X312-C12S1*DX31-C12S2*DX32
      DX3D22 = D2X322-C22S1*DX31-C22S2*DX32
C        COMPUTE COMPONENTS OF SECOND FUNDAMENTAL FORM
C        NOTATION: B11 ETC. (SYMMETRIC)
      CALL H2FF(LA1,DX1D11,DX1D12,DX1D22,DX2D11,DX2D12,DX2D22,
     1   DX3D11,DX3D12,DX3D22,VNORM1,VNORM2,VNORM3,B11,B12,B22)
      GO TO (11,12), KS3FF
   12 CONTINUE
C        COMPUTE THIRD FUNDAMENTAL FORM
      C11 = 0.0
      C12 = 0.0
      C22 = 0.0
   11 CONTINUE
C        STORE INITIAL VALUE OF METRIC DETERMINANT
      IF (KINITL-1) ,,20
       AADDET(J,I) = ADET
   20 CONTINUE
C        STORE OUTPUT VARIABLES IN ARRAYS, THE POSITIONS BEING (PHI,THETA
      AA11(J,I) = A11
      AA12(J,I) = A12
      AA22(J,I) = A22
      AADET(J,I) = ADET
      AAI11(J,I) = AI11
      AAI12(J,I) = AI12
      AAI22(J,I) = AI22
      AB11(J,I) = B11
      AB12(J,I) = B12
      AB22(J,I) = B22
      AC11(J,I) = C11
      AC12(J,I) = C12
      AC22(J,I) = C22
      ANORM1(J,I) = VNORM1
      ANORM2(J,I) = VNORM2
      ANORM3(J,I) = VNORM3
      ARHO(J,I) = RHO
      ADP(J,I) = DP
      ADT(J,I) = DT
   10 CONTINUE
      RETURN
  100 FORMAT ()
      END
```

```
      SUBROUTINE DCONST(RHO,DP,DT,RHO2,RHO3,RHO4,DPSQ,DTSQ)
C        EVALUATES FACTORS IN COMPUTATION OF SECOND FUNDAMENTAL FORM
C     ******************************************************************
C        NOMENCLATURE:
C          RHO=POSITION VECTOR; P=PHI; T=THETA; D=DIFFERENTIAL; 2/SQ=SQUA
C          4=POWER 4
C     ******************************************************************
C        RHO FACTORS
      RHO2 = RHO*RHO
      RHO3 = RHO*RHO2
      RHO4 = RHO*RHO3
C        DIFFERENTIAL FACTORS
      DPSQ = DP*DP
      DTSQ = DT*DT
      RETURN
      END


      SUBROUTINE GCONST(NDATA,PHI,THETA,
     1   ST,CT,SP,SPSQ,S2P,CP,CPSQ,C2P)
C        EVALUATES ARRAYS OF CONSTANTS ASSOCIATED WITH SURFACE COORDINATE
C        THETA CONSTANTS INDEPENDENT OF ITERATION & SO EVALUATED ON
C     ******************************************************************
C        NOMENCLATURE:
C          S=SIN; C=COS; P=PHI; T=THETA; SQ=SQARED; A=ARRAY
C          2=MULTIPLIED BY 2
C     ******************************************************************
C        THETA CONSTANTS
       ST    = SIN(THETA)
       CT    = COS(THETA)
C        PHI CONSTANTS
      PHI2 = 2*PHI
       SP    = SIN(PHI)
       CP    = COS(PHI)
       S2P    = SIN(PHI2)
       C2P    = COS(PHI2)
       SPSQ    = SP*SP
       CPSQ    = CP*CP
      RETURN
      END
```

```
      SUBROUTINE HDERIV(PETURB,BPHI,HB,A,B0,B1,D2,D3,PTAIL,PHI,THETA,
     1   PINC,TINC,
     2   DP,DT,DPP,DTT,DPT,RHO)
      EXTERNAL FLVS
      EXTERNAL BCALC
C        COMPUTATION OF THE FIRST & SECOND PARTIAL DERIVATIVES WITH RESP
C          TO THE SURFACE COORDINATES OF THE POSITION VECTOR
C        NOTE: FUNCTION FLVS COMPUTES THE MAGNITUDES OF THE POSITION
C          VECTOR
C     ******************************************************************
C        NOMENCLATURE:
C          RHO=POSITION VECTOR; P=PHI/POSITIVE/PERTURBED; T=THETA;
C          N=NEGATIVE; D=DIFFERENTIAL; L=NEGATIVE; U=POSITIVE
C     ******************************************************************
      PI = 22./7.
C        CHECK IF PHI, THETA ARE AT LIMITS OF RANGE
      IF (PHI.LE.0.001) PHI=PHI+PETURB+0.0000001
      IF (THETA.LE.0.001) THETA = THETA+PETURB+0.0000001
      CPHI = PI-PHI
      CTHETA = PI-THETA
      IF (CPHI.LE.0.001) PHI=PHI-PETURB-0.0000001
      IF (CTHETA.LE.0.001) THETA=THETA-PETURB-0.0000001
C        COMPUTE POSITION VECTOR
      B = BCALC(B0,B1,PHI,THETA,PI)
      RHO = FLVS(PHI,THETA,PINC,TINC,BPHI,HB,A,B,D2,D3,PTAIL,PI)
C        NEGATIVE PERTURBATION OF PHI: THETA CONSTANT
      PHIN = PHI-PETURB
      B = BCALC(B0,B1,PHIN,THETA,PI)
      RHOPPN = FLVS(PHIN,THETA,PINC,TINC,BPHI,HB,A,B,D2,D3,PTAIL,PI)
C        POSITIVE PERTURBATION OF PHI: THETA CONSTANT
      PHIP = PHI+PETURB
      B = BCALC(B0,B1,PHIP,THETA,PI)
      RHOPPP = FLVS(PHIP,THETA,PINC,TINC,BPHI,HB,A,B,D2,D3,PTAIL,PI)
C     ******************************************************************
C        NEGATIVE PERTURBATION OF THETA: PHI CONSTANT
      THETAN = THETA-PETURB
      B = BCALC(B0,B1,PHI,THETAN,PI)
      RHOPTN = FLVS(PHI,THETAN,PINC,TINC,BPHI,HB,A,B,D2,D3,PTAIL,PI)
C        POSITIVE PERTURBATION OF THETA: PHI CONSTANT
      THETAP = THETA+PETURB
      B = BCALC(B0,B1,PHI,THETAP,PI)
      RHOPTP = FLVS(PHI,THETAP,PINC,TINC,BPHI,HB,A,B,D2,D3,PTAIL,PI)
C     ******************************************************************
C        NEG PHI; NEG THETA
      B = BCALC(B0,B1,PHIN,THETAN,PI)
      RNN = FLVS(PHIN,THETAN,PINC,TINC,BPHI,HB,A,B,D2,D3,PTAIL,PI)
C        NEG PHI; POS THETA
      B = BCALC(B0,B1,PHIN,THETAP,PI)
      RNP = FLVS(PHIN,THETAP,PINC,TINC,BPHI,HB,A,B,D2,D3,PTAIL,PI)
C        POS PHI;NEGS THETA
      B = BCALC(B0,B1,PHIP,THETAN,PI)
      RPN = FLVS(PHIP,THETAN,PINC,TINC,BPHI,HB,A,B,D2,D3,PTAIL,PI)
C        POS PHI;POSS THETA
      B = BCALC(B0,B1,PHIP,THETAP,PI)
```

```
      RPP = FLVS(PHIP,THETAP,PINC,TINC,BPHI,HB,A,B,D2,D3,PTAIL,PI)
C     ****************************************************************
C        COMPUTATION OF FIRST PARTIAL DERIVATIVES OF RHO WRT:
C          PHI
      DPL = (RHO-RHOPPN)/PETURB
      DPU = (RHOPPP-RHO)/PETURB
      DP = (DPL+DPU)*.5
CC         THETA
      DTL = (RHO-RHOPTN)/PETURB
      DTU = (RHOPTP-RHO)/PETURB
      DT = (DTL+DTU)*.5
C     ****************************************************************
C        COMPUTATION OF SECOND PARTIAL DERIVATIVES OF RHO WRT:
C          PHI,PHI
      DPP = (DPU-DPL)/PETURB
C          THETA,THETA
      DTT = (DTU-DTL)/PETURB
C          PHI,THETA
      DPT = 0.25*(RPP-RNP-RPN+RNN)/(PETURB*PETURB)
C     ****************************************************************
C     ****************************************************************
      RETURN
      END



      SUBROUTINE WTDIST(LA1,NDATA,PI,HPI,HPI2,APHI,AHO)
C        COMPUTES INITIAL DISTRIBUTION OF LV WALL THICKNESS ASSUNING A
C          INCREASE FROM BASE TO APEX WITH MINIMUM AT APEX GIVEN APICAL
C          EQUATORIAL WALL THICKNESS (IE. DEPENDENT ON MERIDIONAL & NO
C          CIRCUMFERENTIAL COORDINATE)
C     ****************************************************************
C        NOMENCLATURE:
C            H=WALL THICKNESS; HO=INITIAL WALL THICKNESS
C            HPI2=WALL H AT EQUATOR(PHI=PI/2); HPI=H AT APEX (PHI=PI)
C            A=ARRAY
C     ****************************************************************
      DIMENSION APHI(LA1),AHO(LA1,LA1)
C        VARY THETA(ETA)
      DO 10 I=1,NDATA
C        VARY PHI(XI)
      DO 10 J=1,NDATA
      PHI = APHI(J)
C        STORE INITIAL WALL THICKNESS
      AHO(I,J) = HPI2+(HPI-HPI2)*ABS(COS(PHI))
   10 CONTINUE
      RETURN
      END
```

```
      SUBROUTINE H1FF(LA1,SP,CP,SPSQ,S2P,DP,DT,DPSQ,DTSQ,
     1   RHO,RHO2,RHO3,RHO4,
     2   A11,A12,A22,AI11,AI12,AI22,ADET)
C        CALCULATES COMPONENTS OF FIRST FUNDAMENTAL FORM & ITS DETERMINA
C     ******************************************************************
C        NOMENCLATURE:
C          OBVIOUS; ALSO SEE SUB. DCONST
C     ******************************************************************
C        COMPONENTS
      A11 = RHO2+DPSQ
      A12 = DP*DT
      A22 = RHO2*SPSQ+DTSQ
C        DETERMINANT
      ADET = RHO4*SPSQ+RHO2*(DTSQ+DPSQ*SPSQ)
Cv       COMPUTE CONTRAVARIANT ASSOCIATE OF A11,AI11 ETC.
      ADETI = 1/ADET
      AI11 = A22*ADETI
      AI12 = A12*ADETI
      AI22 = A11*ADETI
      RETURN
       END
```

```
      SUBROUTINE H2FF(LA1,DX1D11,DX1D12,DX1D22,DX2D11,DX2D12,DX2D22,
     1   DX3D11,DX3D12,DX3D22,VNORM1,VNORM2,VNORM3,B11,B12,B22)
C        CALCULATES COMPONENTS OF SECOND FUNDAMENTAL FORM
C     ******************************************************************
C        NOMENCLATURE:
C            DXIDJK= TENSOR DERIVATIVE OF DXIJ, I IS SPACE & J, K SURFAC
C            B11 ETC.= 2ND FUNDAMENTAL FORM COMPONENTS
C          ALSO SEE SUB. HSNORM
C     ******************************************************************
      B11 = -VNORM1*DX1D11-VNORM2*DX2D11-VNORM3*DX3D11
      B12 = -VNORM1*DX1D12-VNORM2*DX2D12-VNORM3*DX3D12
      B22 = -VNORM1*DX1D22-VNORM2*DX2D22-VNORM3*DX3D22
      RETURN
      END
```

```
      SUBROUTINE HSNORM(ADET,DX11,DX12,DX21,DX22,DX31,DX32,
     1   VNORM1,VNORM2,VNORM3)
C        CALCULATES SPACE COMPONENTS OF UNIT NORMAL SURFACE VECTOR
C     ******************************************************************
C        NOMENCLATURE:
C          VNORM1=COMPONENT OF UNIT NORMAL VECTOR ALONG X1-AXIS ETC.;
C          DXIJ=DIFFERENTIAL OF I-TH SPACE WRT J-TH SURFACE COORDINATE
C          ADET= VALUE OF DETERMINANT OF FIRST FUNDAMENTAL FORM
C     ******************************************************************
      RADET = 1/SQRT(ADET)
      VNORM1 = (DX21*DX32-DX31*DX22)*RADET
      VNORM2 = (DX31*DX12-DX11*DX32)*RADET
      VNORM3 = (DX11*DX22-DX21*DX12)*RADET
      RETURN
      END
```

```
      SUBROUTINE STRAIN(KSTRAN,FWT,DP,DT,DRHOP,DRHOT,ADET,A11,A12,A22,
     1   AI11,AI12,AI22,B11,B12,B22,C11,C12,C22,
     2   AH11,AH12,AH22,ADETH ,GH11,GH12,GH22,
     2   G11,G12,G22,GAM11,GAM12,GAM21,GAM22,GAM13,GAM31,GAM23,
     3   GAM32,GAM33)
C        COMPUTES STRAIN TENSOR, GAMMA, FRO M DIFFERENCE BETWEEN
C          UNDEFORMED (FROM PREVIOUS ITERATION, H) & DEFORMED (FROM
C          PRESENT ITERATION) SURFACE METRIC
C          G(ALPHA,BETA) USED IF KSTRAN=2 (ON) (COMPUTED HERE)
C          A(ALPHA,BETA) USED IF KSTRAN=1(OFF)
C     ******************************************************************
C        NOMENCLATURE:
C            GAM12 ETC; STRAIN TENSOR
C            A11; B11; C11 ETC FUNDAMENTAL FORMS
C            AI11 BI11 CI11 ETC ASSOCIATES OF FUMDAMENTAL FORMS
C            BV11 ETC  BASE VECTORS FOR 2ND RANK TENSOR
C            ADET ; DETERMINANT OF FIRST FUNDAEMENTAL FORM
C            2=MULTIPLIED BY 2; SQ=SQUARED; H=FROM PREVIUOS ITERATION
C            OTHER ; SEE SUBS H1FF,H2FF,H3FF,& FCONST
C     ******************************************************************
C        COMPUTE INVARIANT (UNDER SURFACE TRANSFORMATION) STRAINS
      GAM13  = 0.5*DRHOP
      GAM23  = 0.5*DRHOT
C        COMPUTE NORMAL STRAIN
C        CHECK ON DIVISION BY ZERO
      IF (ADET-0.000001) ,,40
      GAM33 = 0.0
      GO TO 30
   40 CONTINUE
C          CHECK THAT LOG ARGUMENT NOT = 0
      ARGLOG = ADETH/ADET
      IF (ARGLOG) ,30,
      GAM33  = 0.5*ALOG(ARGLOG)
   30 CONTINUE
C        COMPUTE COORDINATE UNIT BASE VECTORS FOR 2ND RANK TENSORS
      BV11 = SQRT(A11*AI11)
      BV12 = SQRT(A11*AI22)
      BV21 = SQRT(A22*AI11)
      BV22 = SQRT(A22*AI22)
C        CHECK WHETHER SURFACE(=1) OR LOCAL STRAIN(=2) TO BE COMPUTED
      GO TO (10,20), KSTRAN
C        SURFACE STRAIN
   10 CONTINUE
      GAM11 = 0.5*(A11-AH11)
      GAM12 = 0.5*(A12-AH12)
      GAM22 = 0.5*(A22-AH22)
C        COMPUTE PHYSICAL COMPONENTS
      GAMP11 = GAM11*BV11
      GAMP12 = GAM12*BV12
      GAMP21 = GAM12*BV21
      GAMP22 = GAM22*BV22
      RETURN
C        LOCAL STRAIN
   20 CONTINUE
```

```
      FWT2 = 2*FWT
      FWTSQ = FWT*FWT
      G11 = A11-FWT2*B11+FWTSQ*C11
      G12 = A12-FWT2*B12+FWTSQ*C12
      G22 = A22-FWT2*B22+FWTSQ*C22
      GDET = G11*G22-G12*G12
C        TENSOR STRAIN COMPONENTS
       GAM11 = 0.5*(G11-GH11)
       GAM12 = 0.5*(G12-GH12)
       GAM22 = 0.5*(G22-GH22)
C        COMPUTE PHYSICAL COMPONENTS
      GAMP11 = GAM11*BV11
      GAMP12 = GAM12*BV12
      GAMP21 = GAM12*BV21
      GAMP22 = GAM22*BV22
      RETURN
      END
```

```
      SUBROUTINE STRESR(LA2,NZIT,FWT,ASP11,ASP12,ASP21,ASP22,
     3   N11,N22,N12,N21)
C        NOMENCLATURE:
C     ***************************************************************
C        COMPUTES STRESS RESULTANTS
C            N11 ETC.: STRESS RESULTANTS
C            Q1,Q2; SHEARING FORCES
C            OTHERWISE SEE SUBS STRESS
C     ***************************************************************
C        NOTE: (1) SIMPSON'S RULE INTEGRATION ROUTINE, QSF, IS USED.
C                  REF: IBM SCIENTIFIC SUBROUTINE PACKAGE
C              (2) DUMMY HAS A FIXED DIMENSION
C     ***************************************************************
      REAL N11,N12,N21,N22
      DIMENSION ASP11(LA2),ASP22(LA2),          ASP12(LA2),ASP21(LA2)
      DIMENSION DUMMY(11)
C        STRESS RESULTANTS
      CALL QSF(FWT,ASP11,DUMMY,LA2)
      N11 = DUMMY(NZIT)
      CALL QSF(FWT,ASP22,DUMMY,LA2)
      N22 = DUMMY(NZIT)
      CALL QSF(FWT,ASP12,DUMMY,LA2)
      N12 = DUMMY(NZIT)
      CALL QSF(FWT,ASP21,DUMMY,LA2)
      N21 = DUMMY(NZIT)
      RETURN
      END
```

```
      SUBROUTINE LVSURF(KSURF,LA1,NDATA,PINC,TINC,APHI,ATHETA,ARHO,AH,
     1   ANORM1,ANORM2,ANORM3,
     2   ARHOIN,ARHOUT)
C        COMPUTES LOCI OF ENDO- & EPICARDIAL SURFACES
CC         RADIAL WALL THICKNESS IF KSURF=1 (OFF)
CC         NORMAL WALL THICKNESS IF KSURF=2 (ON)
C     ******************************************************************
C        NOMENCLATURE:
C            RHOIN, RHOUT; ENDO & EPICARDIAL POSITION VECTORS
C            OTHERS; SEE SUBS HDERIV, HSNORM
C     ******************************************************************
      DIMENSION APHI(LA1),ATHETA(LA1),ARHO(LA1,LA1),AH(LA1,LA1)
      DIMENSION ANORM1(LA1,LA1),ANORM2(LA1,LA1),ANORM3(LA1,LA1)
      DIMENSION ARHOIN(LA1,LA1),ARHOUT(LA1,LA1)
      PI = 22./7.
C        VARY THETA (X1)
      DO 10 I=1,NDATA
      THETA = ATHETA(I)
C        VARY PHI (ETA) - AVOID SINGULARITY AT POLE(APEX; PHI=PI)
      DO 20 J=1,NDATA
       PHI = APHI(J)
      RHO = ARHO(J,I)
      H = AH(J,I)
      GO TO (51,52), KSURF
C        COMPUTE RADIAL WALL THICKNESS
   51 CONTINUE
      ARHOIN(J,I) = RHO-0.5*H
      ARHOUT(J,I) = RHO+0.5*H
      GO TO 20
   52 CONTINUE
C        COMPUTE NORMAL WALL THICKNESS
      VNORM1 = ANORM1(J,I)
      VNORM2 = ANORM2(J,I)
      VNORM3 = ANORM3(J,I)
C        RECTANGULAR COORDINATES OF MID-SURFACE
      X1 = RHO*SIN(PHI)*COS(THETA)
      X2 = RHO*SIN(PHI)*SIN(THETA)
      X3 = RHO*COS(PHI)
C        RECTANGULAR COORDINATES OF ENDOCARDIUM
      XN1 = X1-0.5*H*VNORM1
      XN2 = X2-0.5*H*VNORM2
      XN3 = X3-0.5*H*VNORM3
C        RECTANGULAR COORDINATES OF  EPICARDIUM
      XP1 = X1+0.5*H*VNORM1
      XP2 = X2+0.5*H*VNORM2
      XP3 = X3+0.5*H*VNORM3
C        ENDO- & EPICARDIAL POSITION VECTORS
      DO 23 N=1,2
      GO TO (11,12), N
   11 CONTINUE
      X = XN1
      Y = XN2
      Z = XN3
      GO TO 15
```

```
   12 CONTINUE
      X = XP1
      Y = XP2
      Z = XP3
   15 CONTINUE
C        CALCULATE POSITION VECTOR FROM PYTHAGORAS
      RW = SQRT(X*X+Y*Y+Z*Z)
C        COMPUTE SURFACE CURVILINEAR COORDINATES
      CALL HSPHTR(PI,RW,0.0,X,Y,Z,PHI,THETA,
     1   PHIS,THETAS)
      GO TO (21,22), N
   21 CONTINUE
      ARHOIN(J,I) = RW
      GO TO 23
   22 CONTINUE
      ARHOUT(J,I) = RW
   23 CONTINUE
C        END PHI LOOP
   20 CONTINUE
C         END THETA LOOP
   10 CONTINUE
      RETURN
      END



      SUBROUTINE LVVOL(LA1,NDATA,PINC,TINC,ARHOIN,PHIO,RPROP,
     1   R,PI,PVECT,
     1   VC)
C        COMPUTES LEFT VENTRICULAR VOLUME, VC
C     ******************************************************************
C        NOMENCLATURE:
C            SEE SUB. HDERIV
C     ******************************************************************
C        NOTE: (1) SIMPSON'S RULE INTEGRATION ROUTINE, QSF, IS USED.
C                  REF: IBM SCIENTIFIC SUBROUTINE PACKAGE
C              (2) DUMMY HAS A FIXED DIMENSION
C     ******************************************************************
      DIMENSION ARHOIN(LA1,LA1)
      DIMENSION DUMMY1(20),DUMMY2(20),DUMMY3(20)
C        VARY THETA (X1)
      DO 10 I=1,NDATA
C        VARY PHI (ETA)
       DO 20 J=1,NDATA
      RHOIN = ARHOIN(J,I)
      DUMMY1(J) = RHOIN*RHOIN
   20 CONTINUE
C        INTEGRATE MERIDIANS
      CALL QSF(PINC,DUMMY1,DUMMY2,20)
      DUMMY3(I) = DUMMY2(NDATA)
   10 CONTINUE
C        INTEGRATE CIRCUMFERENCES
      CALL QSF(TINC,DUMMY3,DUMMY2,20)
C        CONE VOLUME
      VCONE = PI*R*R*RPROP*PVECT*COS(PHIO)/3
      VC = DUMMY2(NDATA)+VCONE
      RETURN
      END
```

```
      FUNCTION FLVS(PHI,THETA,PINC,TINC,BPHI,HB,A,B,D2,D3,PTAIL,PI)
C        CONTROL FOR INITIALIZATION
C        COMPUTE SPHERICAL TRANSFORMATION ANGLE, ANU
C        THIS POSITIONS BULGE AT ANGLE PHI=BPHI IN PLANE OF SYMMETRY
      ANU = PI/2-BPHI
      SANU = SIN(ANU)
      CANU = COS(ANU)
   10 CONTINUE
C        PROLATE RADIUS
      RHOM = SQRT((  B*SIN(PHI))**2.+(A*COS(PHI))**2)
      IF (HB-0.01*RHOM) 15,,
C        SPHERICAL - RECTANGULAR
      X = SIN( PHI)*COS( THETA)
      Y = SIN( PHI)*SIN( THETA)
      Z = COS( PHI)
C        PLANE ROTATION THROUGH ANGLE, ANU, ABOUT Y-AXIS
      XT =  X*CANU+Z*SANU
      YT =  Y
      ZT = -X*SANU+Z*CANU
      RW = SQRT(XT*XT+YT*YT+ZT*ZT)
      CALL HSPHTR(PI, RW,ANU,XT,YT,ZT,PHI,THETA,
     1   PHIT,THETAT)
C        GIVE PROPER FUNCTIONAL VALUES TO PHIT
      IF (ANU) ,20,21
      IF (PHI.LT.-ANU) PHIT=-PHIT
      GO TO 20
   21 CONTINUE
       PHIN = PI-ANU
      IF (PHI.GT.PHIN) PHIT=2*PI-PHIT
   20 CONTINUE
      GO TO 30
C     ******************************************************************
C        RECTANGULAR - SPHERICAL TILDA
C
C        ENSURE DENOMINATOR NEVER NEGATIVE
      AXT = ABS(XT)
      IF (AXT-0.000000000001) 40,40,
      SARG1 = YT/XT
      THETAT = ATAN(SARG1)
      GO TO 42
   40 CONTINUE
      IF ( XT.LT.0.0) THETAT=PI
      IF ( XT.GE.0.0) THETAT=0.0
   42 CONTINUE
C        ATAN ONLY IN RANGE '-PI/2 TO PI/2': CHANGE TO '0 TO PI'
      ERR = -PI/100
      IF (THETAT.LT.ERR)    THETAT=PI+THETAT
C
      PHIT = ACOS(ZT)
C        ENSURE THAT THETAT IN CORRECT PHASE IN PLANE OF SYMMETRY
C        ALSO OBTAIN VALUES OF PHIT IN THIS PLANE
      IF (THETA-0.1*TINC) ,,52
      THETAT = 0.0
      IF (ANU) ,,54
```

```
      PT = PHI+ANU
      PHIT = PT
      GO TO 55
   54 CONTINUE
      PT = PI-PHI-ANU
      PHIT = ABS(PHI+ANU)
   55 CONTINUE
      IF (PT) ,52,52
      THETAT = PI
   52 CONTINUE
      DTHETA = ABS(THETA -PI)
      IF (DTHETA-0.1*TINC) ,,50
      THETAT = PI
      IF (ANU) 56,,
      PT = PHI-ANU
      PHIT = ABS(PHI-ANU)
      GO TO 57
   56 CONTINUE
      PT = PI-PHI+ANU
      PHIT = PHI+ANU
   57 CONTINUE
      IF (PT) ,,50
      THETAT = 0.0
   50 CONTINUE
C        CHECK ON PROPER FUNCTION VALUES OF PHI
      IF (PHIT) ,30,30
      IF (XT.GT.0.0) PHIT=-PHIT
      IF (XT.LT.0.0) PHIT=PI+PHIT
   30 CONTINUE
C     ****************************************************************
C        COMPUTE ANGLE MAGNIFICATIONS FOR BULGE
      THETA2 = 100*(PHIT-PI/2)/D3
      THETA3 = 100*THETAT/D3
C*****************************************************************
C        COMPUTE BULGE
      DNP = EXP(-.5*(20000*ALOG(100/PTAIL)*(THETA2**2)/((PI*D2)**2)))
      DNT = EXP(-.5*(20000*ALOG(100/PTAIL)*(THETA3**2)/((PI*D3)**2)))
C*****************************************************************
      RHOB = HB*DNP*DNT
      GO TO 16
   15 CONTINUE
      RHOB = 0.0
   16 CONTINUE
      FLVS = RHOM+RHOB
      RETURN
      END
```

14 NOV 1973

```
      SUBROUTINE FIBRE(T,EP1,EP2,ESE,SDC,AS,GAMAA,GAMAAS,
     1   SAA)
      STR = GAMAA -GAMAAS
      SAA = EP2*STR*STR
      RETURN
      END




C         CALCULATION OF SEMI-MINOR AXIS
      FUNCTION BCALC(B0,B1,PHI,THETA,PI)
      BCALC = B0+16*THETA*PHI*(B1-B0)*(1-.5*THETA/PI)*(1-.5*PHI/PI
     1   (3*PI*PI)
      RETURN
      END



      SUBROUTINE HPRT2(L,NDATA,APR)
C        PRINTS 2-DIMENSIONAL ARRAY
      DIMENSION APR(L,L)
      DATA/IWR/5/
      WRITE (IWR,110)
C        ROWS: CIRCUMFERENCES (THETA)    COLUMNS: MERIDIANS (PHI)
       DO 10 JPR=1,NDATA
      WRITE (IWR,120) (APR(JPR,IPR), IPR=1,NDATA)
   10 CONTINUE
      RETURN
  100 FORMAT()
  120 FORMAT (6(2X,F8.2))
  110 FORMAT(//)
      END
```